

NOS EXPERIMENTAL GALVESTON BAY NOWCAST/FORECAST SYSTEM: STORM SURGE STUDIES

Silver Spring, Maryland
June 2007



noaa National Oceanic and Atmospheric Administration

U.S. DEPARTMENT OF COMMERCE
National Ocean Service
Coast Survey Development Laboratory

**Office of Coast Survey
National Ocean Service
National Oceanic and Atmospheric Administration
U.S. Department of Commerce**

The Office of Coast Survey (OCS) is the Nation's only official chartmaker. As the oldest United States scientific organization, dating from 1807, this office has a long history. Today it promotes safe navigation by managing the National Oceanic and Atmospheric Administration's (NOAA) nautical chart and oceanographic data collection and information programs.

There are four components of OCS:

The Coast Survey Development Laboratory develops new and efficient techniques to accomplish Coast Survey missions and to produce new and improved products and services for the maritime community and other coastal users.

The Marine Chart Division acquires marine navigational data to construct and maintain nautical charts, Coast Pilots, and related marine products for the United States.

The Hydrographic Surveys Division directs programs for ship and shore-based hydrographic survey units and conducts general hydrographic survey operations.

The Navigational Services Division is the focal point for Coast Survey customer service activities, concentrating predominately on charting issues, fast-response hydrographic surveys, and Coast Pilot updates.

**NOS EXPERIMENTAL GALVESTON BAY
NOWCAST/FORECAST SYSTEM:
STORM SURGE STUDIES**

Richard A. Schmalz, Jr.

Office of Coast Survey, Coast Survey Development Laboratory, Silver Spring,
MD

June 2007



noaa National Oceanic and Atmospheric Administration

U. S. DEPARTMENT
OF COMMERCE

Carlos Gutierrez, Secretary

National Oceanic and
Atmospheric Administration

Conrad C. Lautenbacher, Jr.,
VADM USN (Ret.), Under Secretary

National Ocean Service

John H. Dunnigan

Assistant Administrator

Office of Coast Survey
Captain Steven R. Barnum, NOAA

Coast Survey Development Laboratory
Mary Erickson

NOTICE

Mention of a commercial company or product does not constitute an endorsement by NOAA. Use for publicity or advertising purposes of information from this publication concerning proprietary products or the tests of such products is not authorized.

TABLE OF CONTENTS

LIST OF FIGURES	vii
LIST OF TABLES	xiv
BASE MAP	xv
EXECUTIVE SUMMARY	xvi
1. INTRODUCTION	1
2. LONG WAVE HYDRODYNAMIC MODEL	3
2.1. Governing Equations	3
2.2. Model Grids	6
3. SHORT WAVE HYDRODYNAMIC MODEL	11
3.1. Governing Equations	11
3.2. Initial Validation	11
3.3. Joint Computational	14
3.4. Overtopping and Barrier Island Breaching Limitations	14
4. WAVE-CURRENT INTERACTION	15
4.1. Surface Drag Coefficient Adjustment	15
4.2. Bottom Friction Adjustment	15
4.3. Setup and Runup Limitations	16
5. STORM SURGE METHODOLOGY	17
5.1. Rainfall/Runoff	17
5.2. Overland Flooding Scheme	20
5.3. Hurricane Wind and Atmospheric Pressure Fields	22
5.4. Wave Algorithm	25
5.5. Design of the All-Weather Nowcast/Forecast System	26
5.6. Additional Hydrodynamic Model Considerations	27
5.7. Simulation Objectives	27
6. HURRICANE CARLA (1961) STORM SURGE SIMULATIONS	29
6.1. Storm Characteristics	29
6.2. Simulation Set-up Procedures	31
6.3. Experiment One Long Wave Results	32
6.4. Experiment One Short Wave Results	61
6.5. Experiment Two Long and Short Wave Results	79
6.6. Wind and Water Surface Elevation Validation	80
6.7. Surface Salinity, Surface Current, and Inundation Statistics	81
7. HURRICANE ALICIA (1983) STORM SURGE SIMULATIONS	85
7.1. Storm Characteristics	85

7.2. Simulation Set-up Procedures.....	86
7.3. Experiment One Long Wave Results.....	87
7.4. Experiment One Short Wave Results	104
7.5. Experiment Two Long and Short Wave Results.....	116
7.6. Wind and Water Surface Elevation Validation.....	116
7.7. Surface Salinity, Surface Current, and Inundation Statistics.....	117
8. TROPICAL STORM ALLISON (2001) STORM SURGE SIMULATIONS.	129
8.1. Coastal Surge Propagation Event Characteristics.....	129
8.2. Rainfall/Runoff Event Characteristics	130
8.3. Coastal Surge Propagation Event Simulation Set-up Procedures.....	131
8.4. Rainfall/Runoff Event Simulation Set-up Procedures	131
8.5. Coastal Surge Propagation Event Long Wave Results	132
8.6. Coastal Surge Propagation Event Short Wave Results.....	142
8.7. Rainfall/Runoff Event Experiment One Long Wave Results	145
8.8. Rainfall/Runoff Event Experiment Two Long Wave Results	171
8.9. Rainfall/Runoff Event Experiment Short Wave Results	188
9. OPERATIONAL CONSIDERATIONS.....	189
10. CONCLUSIONS AND FUTURE WORK.....	191
ACKNOWLEDGMENTS.....	191
REFERENCES.....	191

LIST OF FIGURES

Figure 1.1. Map showing Galveston Bay and the Houston Ship Channel including PORTS stations.....	2
Figure 2.1. Galveston Bay model grid.....	7
Figure 2.2. Galveston Bay model bathymetry, contours in meters.....	8
Figure 2.3. Galveston Bay model grid in red with Houston Ship Channel model grid in green.....	9
Figure 3.1. Galveston Bay Wave Model vs Observed Wave Parameters at Eagle Point, January 25-30, 1997.....	12
Figure 3.2. Galveston Bay Wave Model vs Observed Wave Parameters at 42035, January 25-30, 1997.....	13
Figure 6.1. Hurricane Carla (1961) Storm Track 3-16 September 1961	29
Figure 6.2. Hurricane Carla GBM Water Levels Experiment One: 9-10 September 1961.....	35
Figure 6.3. Hurricane Carla GBM Water Levels Experiment One: 10-11 September 1961.....	36
Figure 6.4. Hurricane Carla GBM Water Levels Experiment One: 11-12 September 1961.....	37
Figure 6.5. Hurricane Carla HSCM Water Levels and GBM Water Level Residual Experiment One: 9-10 September 1961.....	38
Figure 6.6. Hurricane Carla HSCM Water Levels and GBM Water Level Residual Experiment One: 10-11 September 1961.....	39
Figure 6.7. Hurricane Carla HSCM Water Levels and GBM Water Level Residual Experiment One: 11-12 September 1961.....	40
Figure 6.8. Hurricane Carla GBM Bolivar Roads Currents Experiment One: 9-10 September 1961.....	41
Figure 6.9. Hurricane Carla GBM Bolivar Roads Currents Experiment One: 10-11 September 1961.....	42
Figure 6.10. Hurricane Carla GBM Bolivar Roads Currents Experiment One: 11-12 September 1961.....	43
Figure 6.11. Hurricane Carla GBM Morgans Point Currents Experiment One: 9-10 September 1961.....	44
Figure 6.12. Hurricane Carla GBM Morgans Point Currents Experiment One: 10-11 September 1961.....	45
Figure 6.13. Hurricane Carla GBM Morgans Point Currents Experiment One: 11-12 September 1961.....	46
Figure 6.14. Hurricane Carla GBM Bolivar Roads Temperature and Salinity Experiment One: 9-10 September 1961.....	47
Figure 6.15. Hurricane Carla GBM Bolivar Roads Temperature and Salinity Experiment One: 10-11 September 1961.....	48
Figure 6.16. Hurricane Carla GBM Bolivar Roads Temperature and Salinity Experiment One: 11-12 September 1961.....	49
Figure 6.17. Hurricane Carla HSCM Eagle Point Temperature and Salinity Experiment One: 9-10 September 1961.....	50
Figure 6.18. Hurricane Carla HSCM Eagle Point Temperature and Salinity Experiment One: 10-11 September 1961.....	51

LIST OF FIGURES

Figure 6.19. Hurricane Carla HSCM Eagle Point Temperature and Salinity Experiment One: 11-12 September 1961.....	52
Figure 6.20. Hurricane Carla GBM Water Surface Elevation Field Experiment One: 11 September 1961 18:00 CST.....	53
Figure 6.21. Hurricane Carla GBM Water Surface Elevation Field Experiment One: 12 September 1961 18:00 CST.....	54
Figure 6.22. Hurricane Carla GBM Near Surface Salinity Field Experiment One: 12 September 1961 18:00 CST.....	55
Figure 6.23. Hurricane Carla GBM Near Bottom Salinity Field Experiment One: 12 September 1961 18:00 CST.....	56
Figure 6.24. Hurricane Carla HSCM Water Surface Elevation Field Experiment One: 11 September 1961 18:00 CST.....	57
Figure 6.25. Hurricane Carla HSCM Water Surface Elevation Field Experiment One: 12 September 1961 18:00 CST.....	58
Figure 6.26. Hurricane Carla HSCM Near Surface Salinity Field Experiment One: 12 September 1961 18:00 CST.....	59
Figure 6.27. Hurricane Carla HSCM Near Bottom Salinity Field Experiment One: 12 September 1961 18:00 CST.....	60
Figure 6.28. Hurricane Carla GBM Significant Wave Height Experiment One: 9-10 September 1961.....	63
Figure 6.29. Hurricane Carla GBM Significant Wave Height Experiment One: 10-11 September 1961.....	64
Figure 6.30. Hurricane Carla GBM Significant Wave Height Experiment One: 11-12 September 1961.....	65
Figure 6.31. Hurricane Carla HSCM and GBM 42035 Significant Wave Height. Experiment One: 9-10 September 1961.....	66
Figure 6.32. Hurricane Carla HSCM and GBM 42035 Significant Wave Height Experiment One: 10-11 September 1961.....	67
Figure 6.33. Hurricane Carla HSCM and GBM 42035 Significant Wave Height Experiment One: 11-12 September 1961.....	68
Figure 6.34. Hurricane Carla GBM Significant Wave Period Experiment One: 9-10 September 1961.....	69
Figure 6.35. Hurricane Carla GBM Significant Wave Period Experiment One: 10-11 September 1961.....	70
Figure 6.36. Hurricane Carla GBM Significant Wave Period Experiment One: 11-12 September 1961.....	71
Figure 6.37. Hurricane Carla HSCM and GBM 42035 Significant Wave Period Experiment One: 9-10 September 1961.....	72
Figure 6.38. Hurricane Carla HSCM and GBM 42035 Significant Wave Period Experiment One: 10-11 September 1961.....	73
Figure 6.39. Hurricane Carla HSCM and GBM 42035 Significant Wave Period Experiment One: 11-12 September 1961.....	74
Figure 6.40. Hurricane Carla GBM Significant Wave Height and Direction Experiment One: 11 September 1961 18:00 CST.....	75

LIST OF FIGURES

Figure 6.41. Hurricane Carla GBM Significant Wave Period Experiment One: 11 September 1961 18:00 CST.....	76
Figure 6.42. Hurricane Carla HSCM Significant Wave Height and Direction Experiment One: 11 September 1961 18:00 CST.....	77
Figure 6.43. Hurricane Carla HSCM Significant Wave Period Experiment One: 11 September 1961 18:00 CST.....	78
Figure 6.44. Hurricane Carla GBM Atmospheric Pressure Field Experiment Two: 11 September 1961 18:00 CST	83
Figure 6.45. Hurricane Carla GBM Wind Field Experiment Two: 11 September 1961 18:00 CST.....	84
Figure 7.1. Hurricane Alicia (1983) Storm Track 15-21 August.....	85
Figure 7.2. Hurricane Alicia GBM Water Levels Experiment One: 16-17 August 1983.....	89
Figure 7.3. Hurricane Alicia GBM Water Levels Experiment One: 17-18 August 1983.....	90
Figure 7.4. Hurricane Alicia HSCM Water Levels and GBM Water Level Residual Experiment One: 16-17 August 1983.....	91
Figure 7.5. Hurricane Alicia HSCM Water Levels and GBM Water Level Residual Experiment One: 17-18 August 1983.....	92
Figure 7.6. Hurricane Alicia GBM Bolivar Roads Currents Experiment One: 16-17 August 1983.....	93
Figure 7.7. Hurricane Alicia GBM Bolivar Roads Currents Experiment One: 17-18 August 1983.....	94
Figure 7.8. Hurricane Alicia GBM Morgans Point Currents Experiment One: 16-17 August 1983.....	95
Figure 7.9. Hurricane Alicia GBM Morgans Point Currents Experiment One: 17-18 August 1983.....	96
Figure 7.10. Hurricane Alicia GBM Bolivar Roads Temperature and Salinity Experiment One: 16-17 August 1983.....	97
Figure 7.11. Hurricane Alicia GBM Bolivar Roads Temperature and Salinity Experiment One: 17-18 August 1983.....	98
Figure 7.12. Hurricane Alicia HSCM Eagle Point Temperature and Salinity Experiment One: 16-17 August 1983.....	99
Figure 7.13. Hurricane Alicia HSCM Eagle Point Temperature and Salinity Experiment One: 17-18 August 1983.....	100
Figure 7.14. Hurricane Alicia GBM Water Surface Elevation Field Experiment One: 18 August 1983 18:00 CST.....	101
Figure 7.15. Hurricane Alicia GBM Near Surface Salinity Field Experiment One: 18 August 1983 18:00 CST.....	102
Figure 7.16. Hurricane Alicia GBM Near Bottom Salinity Field Experiment One: 18 August 1983 18:00 CST.....	103
Figure 7.17. Hurricane Alicia GBM Significant Wave Height Experiment One: 16-17 August 1983.....	106
Figure 7.18. Hurricane Alicia GBM Significant Wave Height Experiment One: 17-18 August 1983.....	107

LIST OF FIGURES

Figure 7.19. Hurricane Alicia HSCM and GBM 42035 Significant Wave Height Experiment One: 16-17 August 1983.....	108
Figure 7.20. Hurricane Alicia HSCM and GBM 42035 Significant Wave Height Experiment One: 17-18 August 1983.....	109
Figure 7.21. Hurricane Alicia GBM Significant Wave Period Experiment One: 16-17 August 1983.....	110
Figure 7.22. Hurricane Alicia GBM Significant Wave Period Experiment One: 17-18 August 1983.....	111
Figure 7.23. Hurricane Alicia HSCM and GBM 42035 Significant Wave Period Experiment One: 16-17 August 1983.....	112
Figure 7.24. Hurricane Alicia HSCM and GBM 42035 Significant Wave Period Experiment One: 17-18 August 1983.....	113
Figure 7.25. Hurricane Alicia GBM Significant Wave Height and Direction Experiment One: 18 August 1983 18:00 CST.....	114
Figure 7.26. Hurricane Alicia GBM Significant Wave Period Experiment One: 18 August 1983 18:00 CST.....	115
Figure 7.27. Hurricane Alicia GBM Water Levels Experiment Two: 16-17 August 1983.....	119
Figure 7.28. Hurricane Alicia GBM Water Levels Experiment Two: 17-18 August 1983.....	120
Figure 7.29. Hurricane Alicia HSCM Water Levels and GBM Water Level Residual Experiment Two: 16-17 August 1983.....	121
Figure 7.30. Hurricane Alicia HSCM Water Levels and GBM Water Level Residual Experiment Two: 17-18 August 1983.....	122
Figure 7.31. Hurricane Alicia Wind and Atmospheric Pressure at Morgans Point Experiment Two: 16-17 August 1983.....	123
Figure 7.32. Hurricane Alicia Wind and Atmospheric Pressure at Morgans Point Experiment Two: 17-18 August 1983.....	124
Figure 7.33. Hurricane Alicia GBM Atmospheric Pressure Field Experiment Two: 17 August 1983 18:00 CST.....	125
Figure 7.34. Hurricane Alicia GBM Atmospheric Pressure Field Experiment Two: 18 August 1983 18:00 CST.....	127
Figure 7.35. Hurricane Alicia GBM Wind Field Experiment Two: 17 August 1983 18:00 CST	127
Figure 7.36. Hurricane Alicia GBM Wind Field Experiment Two: 18 August 1983 18:00 CST.....	128
Figure 8.1. Tropical Storm Allison Storm Track 5-6 June 2001.....	130
Figure 8.2. Tropical Storm Allison GBM Water Levels: 5 June 2001 Nowcast/Forecast Cycle.....	134
Figure 8.3. Tropical Storm Allison GBM Water Levels: 6 June 2001 Nowcast/Forecast Cycle.....	135
Figure 8.4. Tropical Storm Allison HSCM Water Levels and GBM Water Level Residual: 5 June 2001 Nowcast/Forecast Cycle.....	136

LIST OF FIGURES

Figure 8.5. Tropical Storm Allison HSCM Water Levels and GBM Water Level Residual: 6 June 2001 Nowcast/Forecast Cycle.....	137
Figure 8.6. Tropical Storm Allison HSCM Morgans Point Temperature and Salinity: 5 June 2001 Nowcast/Forecast Cycle.....	138
Figure 8.7. Tropical Storm Allison HSCM Morgans Point Temperature and Salinity: 6 June 2001 Nowcast/Forecast Cycle.....	139
Figure 8.8. Tropical Storm Allison HSCM Morgans Point Wind and Atmospheric Pressure: 5 June 2001 Nowcast/Forecast Cycle.....	140
Figure 8.9. Tropical Storm Allison HSCM Morgans Point Wind and Atmospheric Pressure: 6 June 2001 Nowcast/Forecast Cycle.....	141
Figure 8.10. Tropical Storm Allison GBM Significant Wave Height: 5 June 2001 Nowcast/Forecast Cycle.....	143
Figure 8.11. Tropical Storm Allison HSCM and GBM 42035 Significant Wave Height: 5 June 2001 Nowcast/Forecast Cycle.....	144
Figure 8.12. Tropical Storm Allison Standard Inflows Experiment One: 10 June 2001 Nowcast/Forecast Cycle.....	147
Figure 8.13. Tropical Storm Allison Standard Inflows Experiment One: 11 June 2001 Nowcast/Forecast Cycle.....	148
Figure 8.14. Tropical Storm Allison GBM Water Levels Experiment One: 10 June 2001 Nowcast/Forecast Cycle.....	149
Figure 8.15. Tropical Storm Allison GBM Water Levels Experiment One: 11 June 2001 Nowcast/Forecast Cycle.....	150
Figure 8.16. Tropical Storm Allison HSCM Water Levels and GBM Water Level Residual Experiment One: 10 June 2001 Nowcast/Forecast Cycle.....	151
Figure 8.17. Tropical Storm Allison HSCM Water Levels and GBM Water Level Residual Experiment One: 11 June 2001 Nowcast/Forecast Cycle.....	152
Figure 8.18. Tropical Storm Allison GBM Bolivar Roads Currents Experiment One: 10 June 2001 Nowcast/Forecast Cycle.....	153
Figure 8.19. Tropical Storm Allison GBM Bolivar Roads Currents Experiment One: 11 June 2001 Nowcast/Forecast Cycle.....	154
Figure 8.20. Tropical Storm Allison GBM Redfish Bar Currents Experiment One: 10 June 2001 Nowcast/Forecast Cycle.....	155
Figure 8.21. Tropical Storm Allison GBM Redfish Bar Currents Experiment One: 11 June 2001 Nowcast/Forecast Cycle.....	156
Figure 8.22. Tropical Storm Allison GBM Morgans Point Currents Experiment One: 10 June 2001 Nowcast/Forecast Cycle.....	157
Figure 8.23. Tropical Storm Allison GBM Morgans Point Currents Experiment One: 11 June 2001 Nowcast/Forecast Cycle.....	158
Figure 8.24. Tropical Storm Allison GBM Bolivar Roads Temperature and Salinity Experiment One: 10 June 2001 Nowcast/Forecast Cycle.....	159
Figure 8.25. Tropical Storm Allison GBM Bolivar Roads Temperature and Salinity Experiment One: 11 June 2001 Nowcast/Forecast Cycle.....	160
Figure 8.26. Tropical Storm Allison HSCM Eagle Point Temperature and Salinity Experiment One: 10 June 2001 Nowcast/Forecast Cycle.....	161

LIST OF FIGURES

Figure 8.27. Tropical Storm Allison HSCM Eagle Point Temperature and Salinity Experiment One: 11 June 2001 Nowcast/Forecast Cycle.....	162
Figure 8.28. Tropical Storm Allison HSCM Morgans Point Temperature and Salinity Experiment One: 10 June 2001 Nowcast/Forecast Cycle.....	163
Figure 8.29. Tropical Storm Allison HSCM Morgans Point Temperature and Salinity Experiment One: 11 June 2001 Nowcast/Forecast Cycle.....	164
Figure 8.30. Tropical Storm Allison Wind and Atmospheric Pressure at Morgans Point Experiment One: 10 June 2001 Nowcast/Forecast Cycle.....	165
Figure 8.31. Tropical Storm Allison Wind and Atmospheric Pressure at Morgans Point Experiment One: 11 June 2001 Nowcast/Forecast Cycle.....	166
Figure 8.32. Tropical Storm Allison HSCM Near Surface Salinity Field Experiment One: 11 June 2001 Nowcast End.....	167
Figure 8.33. Tropical Storm Allison HSCM Near Bottom Salinity Field Experiment One: 11 June 2001 Nowcast End.....	168
Figure 8.34. Tropical Storm Allison HSCM Near Surface Salinity Field Experiment One: 11 June 2001 Forecast End.....	169
Figure 8.35. Tropical Storm Allison HSCM Near Bottom Salinity Field Experiment One: 11 June 2001 Forecast End.....	170
Figure 8.36. Tropical Storm Allison City of Houston Inflow Set One Experiment Two: 10 June 2001 Nowcast/Forecast Cycle.....	172
Figure 8.37. Tropical Storm Allison City of Houston Inflow Set One Experiment Two: 11 June 2001 Nowcast/Forecast Cycle.....	173
Figure 8.38. Tropical Storm Allison City of Houston Inflow Set Two Experiment Two: 10 June 2001 Nowcast/Forecast Cycle.....	174
Figure 8.39. Tropical Storm Allison City of Houston Inflow Set Two Experiment Two: 11 June 2001 Nowcast/Forecast Cycle.....	175
Figure 8.40. Tropical Storm Allison HSCM Water Levels and GBM Water Level Residual Experiment Two: 10 June 2001 Nowcast/Forecast Cycle.....	176
Figure 8.41. Tropical Storm Allison HSCM Water Levels and GBM Water Level Residual Experiment Two: 11 June 2001 Nowcast/Forecast Cycle.....	177
Figure 8.42. Tropical Storm Allison HSCM Morgans Point Currents Experiment Two: 10 June 2001 Nowcast/Forecast Cycle.....	178
Figure 8.43. Tropical Storm Allison HSCM Morgans Point Currents Experiment Two: 11 June 2001 Nowcast/Forecast Cycle.....	179
Figure 8.44. Tropical Storm Allison HSCM Eagle Point Temperature and Salinity Experiment Two: 10 June 2001 Nowcast/Forecast Cycle.....	180
Figure 8.45. Tropical Storm Allison HSCM Eagle Point Temperature and Salinity Experiment Two: 11 June 2001 Nowcast/Forecast Cycle.....	181
Figure 8.46. Tropical Storm Allison HSCM Morgans Point Temperature and Salinity Experiment Two: 10 June 2001 Nowcast/Forecast Cycle.....	182
Figure 8.47. Tropical Storm Allison HSCM Morgans Point Temperature and Salinity Experiment Two: 11 June 2001 Nowcast/Forecast Cycle.....	183
Figure 8.48. Tropical Storm Allison HSCM Near Surface Salinity Field Experiment Two: 10 June 2001 Nowcast End.....	184

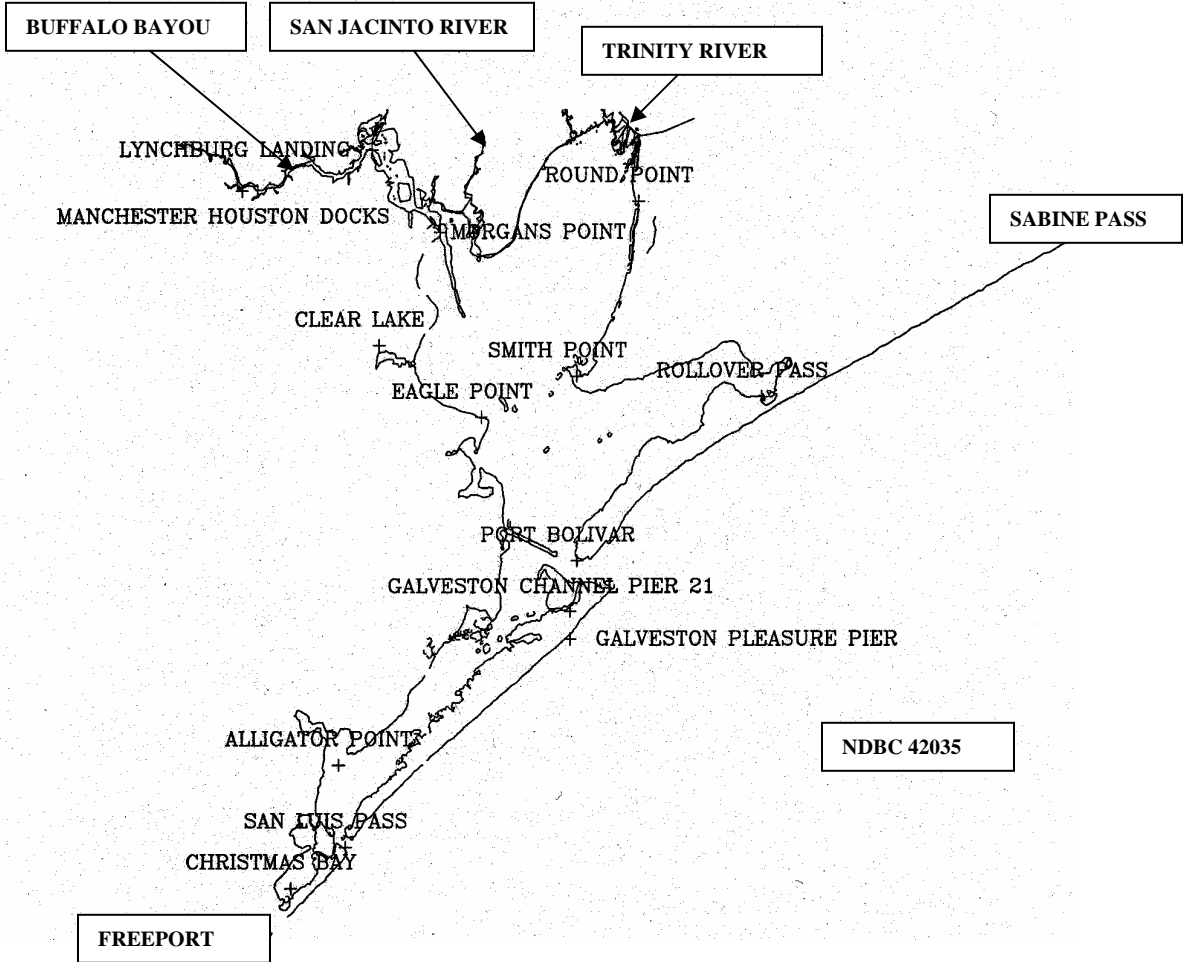
LIST OF FIGURES

Figure 8.49. Tropical Storm Allison HSCM Near Bottom Salinity Field Experiment Two: 10 June 2001 Nowcast End.....	185
Figure 8.50. Tropical Storm Allison HSCM Near Surface Salinity Field Experiment Two: 11 June 2001 Forecast End.....	186
Figure 8.51. Tropical Storm Allison HSCM Near Bottom Salinity Field Experiment Two: 11 June 2001 Forecast End.....	187

LIST OF TABLES

Table 5.1. Major Runoff Descriptors for Use in USGS Rainfall/Runoff Regression Relations.....	17
Table 5.2. Basin Characteristics for Major Runoff in the City of Houston.....	18
Table 5.3. USGS Runoff Characteristic Regression Equations from Liscum (2001).....	19
Table 5.4. Average Daily Flow (cfs) Comparison June 3-12, 2001 during Tropical Storm Allison.....	20
Table 5.5. Empirical Reduction Factors for Large Rainfall Events.....	20
Table 5.6. Test Topography Based on Cell-Centered Distance from mid-Bay (29.4°N,95.0°N).....	22
Table 5.7. Test Storm Surge Specifications Based Upon Hurricane Carla (1961) and Alicia (1983) Surge Levels.....	22
Table 5.8. Simulated Mean Water Surface Elevation (m) JD 249.75-250.75 Nowcast Cycle with Test Storm Surge.....	22
Table 5.9. Hurricane and Pressure Fields For An Arbitrary Storm Based On SPH, Tetra Tech, and Holland Methods.....	24
Table 5.10. Major Storm Characteristics for Galveston Bay, Texas.....	27
Table 6.1. Hurricane Carla Storm Characteristics 3-16 September 1961.....	30
Table 6.2. Hurricane Carla (1961) Windspeed Validation.....	80
Table 6.3. Hurricane Carla (1961) GBM Storm Surge Validation.....	81
Table 6.4. Hurricane Carla (1961) GBM Minimum Surface Salinity. and Maximum Surface Current Speeds.....	81
Table 6.5. Hurricane Carla (1961) Inundation Statistics.....	82
Table 7.1. Hurricane Alicia Storm Characteristics 15-21 August 1983.....	86
Table 7.2. Hurricane Alicia (1983) Windspeed Validation.....	117
Table 7.3. Hurricane Alicia (1983) GBM Storm Surge Validation.....	117
Table 7.4. Hurricane Alicia (1983) GBM Minimum Surface Salinity. and Maximum Surface Current Speeds.....	118
Table 7.5. Hurricane Alicia (1983) Inundation Statistics.....	118
Table 8.1. Tropical Storm Allison Storm Characteristics 5-6 June 2001.....	130
Table 9.1. Hurricane Carla (1961) Long and Short Wave Computational Time.....	189
Table 9.2. Hurricane Alicia (1983) Long and Short Wave Computational Time.....	189
Table 9.3. Tropical Storm Allison (2001) Coastal Surge Propagation Event Long and Short Wave Computational Time.....	190
Table 9.4. Tropical Storm Allison (2001) Rainfall/Runoff Event Long and Short Wave Computational Time.....	190

GALVESTON BAY BASE MAP



Galveston Bay Base Map

EXECUTIVE SUMMARY

Since the transfer of the NOS Galveston Bay Experimental Nowcast/Forecast System (GBEFS) to operational status in June 2004, the experimental system has continued to be run and enhanced. This report documents the work to extend the modeling system to consider storm surge within the context of an all-weather nowcast/forecast capability. The long wave and short surface gravity wave equations are developed. Some initial approaches to wave current interaction are outlined but are not considered in the computations, nor are wave runup, overtopping, and barrier island breaching, which all represent areas for additional research.

Overland flooding, rainfall/runoff, and blended hurricane wind and pressure field forcing have been incorporated within the system. In addition, surface gravity wave algorithms have been incorporated in both hydrodynamic models to simulate hurricane wave conditions. Simulations of Hurricane Carla (1961), Hurricane Alicia (1983), and Tropical Storm Allison (2001) are presented with results compared to observations. Operational considerations are also addressed and recommendations for further improvements are presented.

1. INTRODUCTION

To assess the feasibility of including storm surge computations within the NOS Galveston Bay Experiment Nowcast/Forecast System thereby moving towards an all weather capability, the following processes have been considered: 1) rainfall/runoff inflows from four major basins within the City of Houston, 2) overland flooding, 3) tropical storm and hurricane wind and pressure fields, and 4) surface gravity waves. The governing long wave and short surface gravity wave equations are developed in Chapters 2 and 3, respectively and wave-current interaction is discussed in Chapter 4 as further development. The algorithms used to describe each of the above processes are presented in Chapter 5 followed by the design of the all weather nowcast/forecast system. Simulations of Hurricane Carla (1961), Alicia (1983), and Tropical Storm Allison (2001) are considered in Chapters 6, 7, and 8, respectively. Tropical Storm Allison consists of a storm surge event on 5-6 June and a rainfall/runoff event on 10-11 June. Results for each event are presented. Operational considerations are discussed in Chapter 9, while conclusions and recommendations for future work are outlined in Chapter 10.

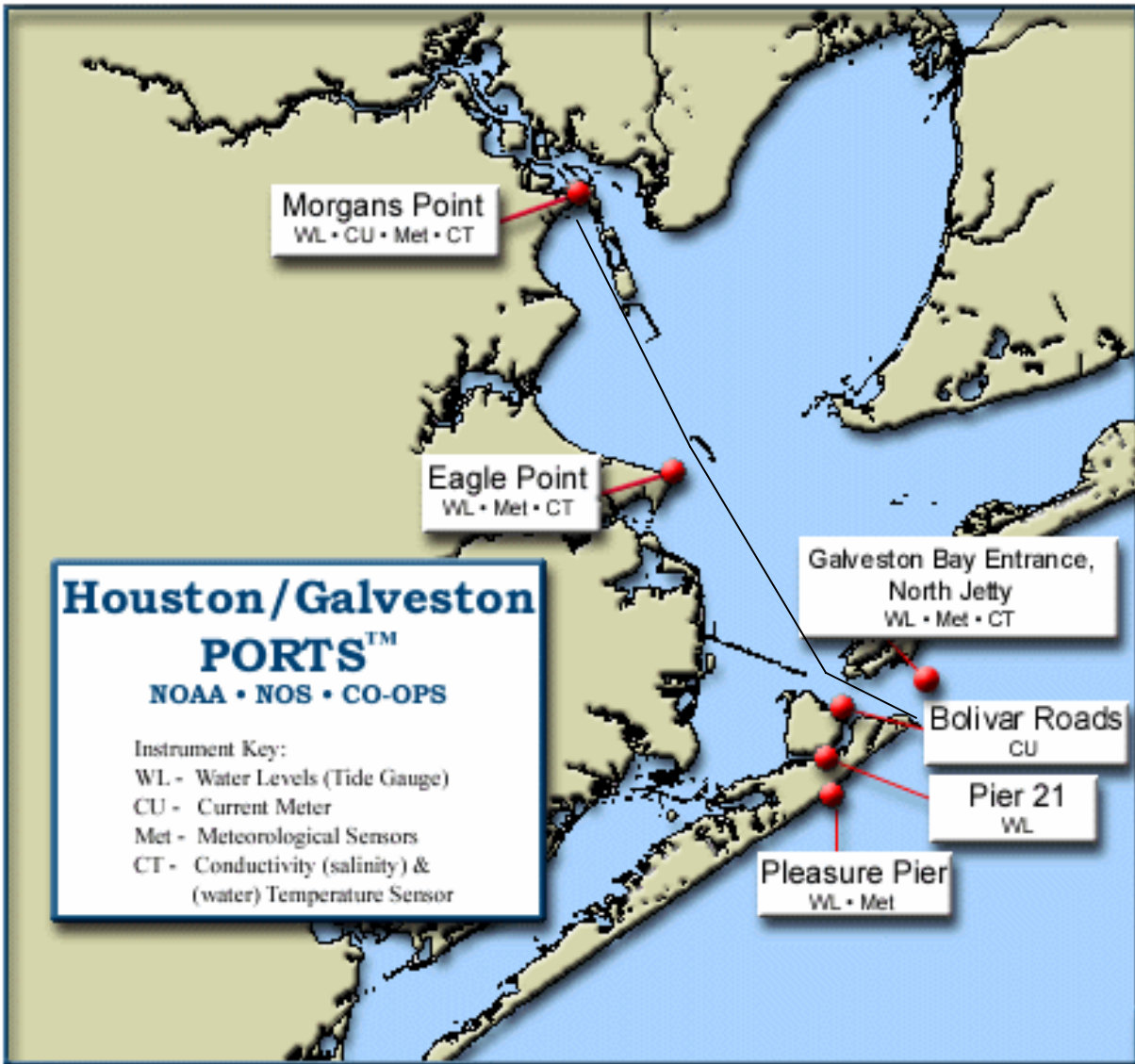


Figure 1.1. Map showing Galveston Bay and the Houston Ship Channel including PORTS stations.

2. LONG WAVE HYDRODYNAMIC MODEL

2.1. Governing Equations

A three-dimensional sigma coordinate Galveston Bay and near shelf model (GBM) has been developed (Schmalz, 1996) based on a version of the Princeton Ocean Model (POM) developed by Blumberg and Mellor (1987) extended to orthogonal curvilinear coordinates. GBM is a three-dimensional baroclinic circulation model for simulating water levels, current velocities, and density. The model is forced with: water levels at the near shore open boundaries based on observed levels at Galveston Pleasure Pier; freshwater inflows from the Buffalo Bayou, San Jacinto, and Trinity Rivers; and surface winds. In addition, a high resolution Houston Ship Channel model (HSCM) has been incorporated to provide finer spatial resolution along the channel (Schmalz, 1998a; 2000a; 2000c). The governing equations in a vertical sigma coordinate are briefly given as follows. Detailed formulation is contained in Blumberg and Mellor (1987), Mellor (2003b), and Schmalz (2001).

$$\mathfrak{I}(1) = 0, \quad (2.1)$$

$$\mathfrak{I}(U) - fDV + gD \frac{\partial(\eta + P_a)}{\partial x} = \frac{\partial}{\partial \sigma} \left[\frac{K_M}{D} \frac{\partial U}{\partial \sigma} \right] - \frac{gD^2}{\rho_0} \int_{\sigma}^0 \frac{\partial \rho}{\partial x} d\sigma + \frac{gD}{\rho_0} \frac{\partial D}{\partial x} \int_{\sigma}^0 \sigma \frac{\partial \rho}{\partial \sigma} d\sigma + F_x, \quad (2.2)$$

$$\mathfrak{I}(V) + fDU + gD \frac{\partial(\eta + P_a)}{\partial y} = \frac{\partial}{\partial \sigma} \left[\frac{K_M}{D} \frac{\partial V}{\partial \sigma} \right] - \frac{gD^2}{\rho_0} \int_{\sigma}^0 \frac{\partial \rho}{\partial y} d\sigma + \frac{gD}{\rho_0} \frac{\partial D}{\partial y} \int_{\sigma}^0 \sigma \frac{\partial \rho}{\partial \sigma} d\sigma + F_y, \quad (2.3)$$

$$\mathfrak{I}(T) = \frac{\partial}{\partial \sigma} \left[\frac{K_H}{D} \frac{\partial T}{\partial \sigma} \right] + F_T, \quad (2.4)$$

$$\mathfrak{I}(S) = \frac{\partial}{\partial \sigma} \left[\frac{K_H}{D} \frac{\partial S}{\partial \sigma} \right] + F_S, \quad (2.5)$$

$$\mathfrak{I}(q^2) = \frac{\partial}{\partial \sigma} \left[\frac{K_q}{D} \frac{\partial q^2}{\partial \sigma} \right] + \frac{2K_M}{D} \left[\left(\frac{\partial U}{\partial \sigma} \right)^2 + \left(\frac{\partial V}{\partial \sigma} \right)^2 \right] + \frac{2gK_H}{\rho_0} \frac{\partial \rho}{\partial \sigma} - \frac{2Dq^3}{B_1 l} + F_q, \quad (2.6)$$

$$\mathfrak{I}(q^2 l) = \frac{\partial}{\partial \sigma} \left[\frac{K_q}{D} \frac{\partial (q^2 l)}{\partial \sigma} \right] + E_1 l \left[\frac{K_M}{D} \left(\left(\frac{\partial U}{\partial \sigma} \right)^2 + \left(\frac{\partial V}{\partial \sigma} \right)^2 \right) + \frac{E_3 g}{\rho_0} K_H \frac{\partial \rho}{\partial \sigma} \right] - \frac{Dq^3}{B_1} \tilde{W} + F_l, \quad (2.7)$$

where $\mathfrak{I}(\ast) = \frac{\partial D \ast}{\partial t} + \frac{\partial UD \ast}{\partial x} + \frac{\partial VD \ast}{\partial y} + \frac{\partial \omega \ast}{\partial \sigma}$ and $\sigma = (z - \eta)/(H + \eta)$. Here (x, y, z, t) are the Cartesian

spatial and temporal coordinates and $D = H + \eta$ is the total water depth with H the depth and η the water surface elevation with respect to model datum. P_{atm} is the sea level atmospheric pressure in

millibars with $P_a = \frac{100 P_{atm}}{\rho_0 g}$, U and V horizontal velocities, S and T salinity and temperature, K_M

and K_H the vertical kinematic viscosity and diffusivity, respectively, K_q the vertical turbulence mixing coefficient, q^2 twice the turbulence kinetic energy, and l is the turbulence length scale.

Note $\tilde{W} = 1 + E_2 \left(\frac{l}{\kappa L} \right)^2$, $\kappa = 0.4$ is the von Karman constant with $L^{-1} = (\eta - z)^{-1} + (H + z)^{-1}$, and B_1 , E_1 ,

E_2 , and E_3 are constants. g is the acceleration due to gravity, f is the Coriolis parameter, $\rho = \rho(S, T)$

is the water density, and ω is the transformed vertical velocity normal to a sigma surface. The relation of ω ($Hd\sigma/dt$) to the Cartesian vertical velocity w is

$$w = \omega + U \left[\sigma \frac{\partial D}{\partial x} + \frac{\partial \eta}{\partial x} \right] + V \left[\sigma \frac{\partial D}{\partial y} + \frac{\partial \eta}{\partial y} \right] + \sigma \frac{\partial D}{\partial t} + \frac{\partial \eta}{\partial t}. \quad (2.8)$$

The horizontal viscosity F_x and F_y , and diffusion terms F^* are defined as

$$F_x = \frac{\partial}{\partial x} \left[2DA_M \frac{\partial U}{\partial x} \right] + \frac{\partial}{\partial y} \left[DA_M \left(\frac{\partial U}{\partial y} + \frac{\partial V}{\partial x} \right) \right] \quad (2.9)$$

$$F_y = \frac{\partial}{\partial y} \left[2DA_M \frac{\partial V}{\partial y} \right] + \frac{\partial}{\partial x} \left[DA_M \left(\frac{\partial U}{\partial y} + \frac{\partial V}{\partial x} \right) \right], \quad (2.10)$$

$$F^* = \frac{\partial}{\partial x} \left[DA_H \frac{\partial^*}{\partial x} \right] + \frac{\partial}{\partial y} \left[DA_H \left(\frac{\partial^*}{\partial y} \right) \right], \text{ with } *=(T,S,q,l,C) \quad (2.11)$$

where $A_M = A_H$ are the horizontal eddy viscosity and diffusivity, defined by the Smagorinsky formula (1963)

$$A_M = C_N \Delta x \Delta y \left[\left(\frac{\partial U}{\partial x} \right)^2 + 0.5 \left(\frac{\partial U}{\partial y} + \frac{\partial V}{\partial x} \right)^2 + \left(\frac{\partial V}{\partial y} \right)^2 \right]^{0.5}, \quad (2.12)$$

with C_N being a non-dimensional parameter.

For the passive tracer sulfur hexafluoride (SF_6), the concentration equation is

$$\mathfrak{I}(C) = \frac{\partial}{\partial \sigma} \left[\frac{K_H}{D} \frac{\partial C}{\partial \sigma} \right] + F_C \quad (2.13)$$

where C is the concentration of SF_6 .

Boundary conditions at the free surface ($\sigma=0$) are as follows:

$$\omega = 0, \rho \frac{K_M}{H} \left(\frac{\partial U}{\partial \sigma}, \frac{\partial V}{\partial \sigma} \right) = (\tau_{sx}, \tau_{sy}), \rho \frac{K_H}{H} \left(\frac{\partial S}{\partial \sigma}, \frac{\partial T}{\partial \sigma}, \frac{\partial C}{\partial \sigma} \right) = (\tilde{S}, \tilde{T}, \tilde{C}), l=0, q^2 = B_1^{2/3} u_s^* \quad (2.14)$$

Boundary conditions at the bottom ($\sigma=-1$) are as follows:

$$\omega = 0, \rho \frac{K_M}{H} \left(\frac{\partial U}{\partial \sigma}, \frac{\partial V}{\partial \sigma} \right) = (\tau_{bx}, \tau_{by}), \rho \frac{K_H}{H} \left(\frac{\partial S}{\partial \sigma}, \frac{\partial T}{\partial \sigma}, \frac{\partial C}{\partial \sigma} \right) = (0,0,0), l=0, q^2 = B_1^{2/3} u_b^* \quad (2.15)$$

where τ_s and τ_b are the wind stress and bottom friction and $(\tilde{S}, \tilde{T}, \tilde{C})$ are surface fluxes.

The above equation set is transformed into orthogonal horizontal coordinates after Blumberg and Herring (1987) with

$$dx = h_1 d\varepsilon_1, dy = h_2 d\varepsilon_2, ds^2 = dx^2 + dy^2 = h_1^2 d\varepsilon_1^2 + h_2^2 d\varepsilon_2^2 \text{ and } U_1 = h_1 \frac{d\varepsilon_1}{dt}, U_2 = h_2 \frac{d\varepsilon_2}{dt}. \quad (2.16)$$

$$\mathfrak{I}(1) = 0$$

$$\mathfrak{I}(U_1) - \tilde{f} DU_2 + \frac{gD}{h_2} \frac{\partial(\eta + P_a)}{h_1 \partial \varepsilon_1} = \frac{K_M}{D} \frac{\partial}{\partial \sigma} \left[K_M \frac{\partial U_1}{\partial \sigma} \right] - \frac{gD}{\rho_0} \left[D \int_{\sigma}^0 \frac{\partial \rho}{h_1 \partial \varepsilon_1} d\sigma + \frac{\partial D}{h_1 \partial \varepsilon_1} \int_{\sigma}^0 \sigma \frac{\partial \rho}{\partial \sigma} d\sigma \right] + F_{12} \quad (2.17)$$

$$\mathfrak{I}(U_2) + \tilde{f} DU_1 + \frac{gD}{h_1} \frac{\partial(\eta + P_a)}{h_2 \partial \varepsilon_2} = \frac{K_M}{D} \frac{\partial}{\partial \sigma} \left[K_M \frac{\partial U_2}{\partial \sigma} \right] - \frac{gD}{\rho_0} \left[D \int_{\sigma}^0 \frac{\partial \rho}{h_2 \partial \varepsilon_2} d\sigma + \frac{\partial D}{h_2 \partial \varepsilon_2} \int_{\sigma}^0 \sigma \frac{\partial \rho}{\partial \sigma} d\sigma \right] + F_{21} \quad (2.18)$$

$$\mathfrak{I}(T) = \frac{\partial}{\partial \sigma} \left[\frac{K_H}{D} \frac{\partial T}{\partial \sigma} \right] + F_T \quad (2.19)$$

$$\mathfrak{I}(S) = \frac{\partial}{\partial \sigma} \left[\frac{K_H}{D} \frac{\partial S}{\partial \sigma} \right] + F_S \quad (2.20)$$

$$\mathfrak{I}(q^2) = \frac{\partial}{\partial \sigma} \left[\frac{K_q}{D} \frac{\partial q^2}{\partial \sigma} \right] + \frac{2K_M}{D} \left[\left(\frac{\partial U_1}{\partial \sigma} \right)^2 + \left(\frac{\partial U_2}{\partial \sigma} \right)^2 \right] + \frac{2gK_H}{\rho_0} \frac{\partial \rho}{\partial \sigma} - \frac{2Dq^3}{B_1 l} + F_q \quad (2.21)$$

$$\mathfrak{I}(q^2 l) = \frac{\partial}{\partial \sigma} \left[\frac{K_q}{D} \frac{\partial (q^2 l)}{\partial \sigma} \right] + E_1 l \left[\frac{K_M}{D} \left(\left(\frac{\partial U_1}{\partial \sigma} \right)^2 + \left(\frac{\partial U_2}{\partial \sigma} \right)^2 \right) + \frac{E_3 g}{\rho} K_H \frac{\partial \rho}{\partial \sigma} \right] - \frac{Dq^3}{B_1} \tilde{W} + F_l \quad (2.22)$$

where $\mathfrak{I}^* = \frac{\partial(D^*)}{\partial t} + \frac{\partial(h_2 U_1 D^*)}{h_1 h_2 \partial \varepsilon_1} + \frac{\partial(h_1 U_2 D^*)}{h_1 h_2 \partial \varepsilon_2} + \frac{\partial(\omega^*)}{\partial \sigma}$

$$\tilde{f} = f + \frac{U_2}{h_1 h_2} \frac{\partial h_2}{\partial \varepsilon_1} - \frac{U_1}{h_1 h_2} \frac{\partial h_1}{\partial \varepsilon_2}$$

The relationship of ω with the Cartesian vertical velocity w is

$$w = \omega + \frac{U_1}{h_2} \left[\sigma \frac{\partial D}{\partial \varepsilon_1} + \frac{\partial \eta}{\partial \varepsilon_1} \right] + \frac{U_2}{h_1} \left[\sigma \frac{\partial D}{\partial \varepsilon_2} + \frac{\partial \eta}{\partial \varepsilon_2} \right] + \sigma \frac{\partial D}{\partial t} + \frac{\partial \eta}{\partial t}. \quad (2.23)$$

The horizontal viscosity F_{ij} and diffusion terms F^* are defined as

$$F_{ij} = \frac{1}{h_i h_j} \left(\frac{\partial}{\partial \varepsilon_i} \left[2DA_M \frac{h_j \partial U_i}{h_i \partial \varepsilon_i} \right] + \frac{\partial}{\partial \varepsilon_j} \left[DA_M \left(\frac{h_i \partial U_i}{h_j \partial \varepsilon_j} + \frac{h_j \partial U_j}{h_i \partial \varepsilon_i} \right) \right] \right) \quad (2.24)$$

$$F^* = \frac{1}{h_1 h_2} \left(\frac{\partial}{\partial \varepsilon_1} \left[DA_H \frac{h_2 \partial^*}{h_1 \partial \varepsilon_1} \right] + \frac{\partial}{\partial \varepsilon_2} \left[DA_H \left(\frac{h_1 \partial^*}{h_2 \partial \varepsilon_2} \right) \right] \right), \text{ with } * = (T, S, q, l, C) \quad (2.25)$$

where

$$A_M = A_H = C_N h_1 h_2 \left[\left(\frac{\partial U_1}{\partial \varepsilon_1} \right)^2 + 0.5 \left(\frac{\partial U_1}{\partial \varepsilon_2} + \frac{\partial U_2}{\partial \varepsilon_1} \right)^2 + \left(\frac{\partial U_2}{\partial \varepsilon_2} \right)^2 \right]^{0.5}, \quad (2.26)$$

where C_N , a non-dimensional parameter, is set to be 0.005 for both Bay and Channel models.

For the passive tracer SF_6 , the concentration equation is

$$\mathfrak{S}(C) = \frac{\partial}{\partial \sigma} \left[\frac{K_H}{D} \frac{\partial C}{\partial \sigma} \right] + F_C \quad (2.27)$$

where C is the concentration of SF_6 .

Boundary conditions at the free surface ($\sigma=0$) and at the bottom ($\sigma=-1$) remain as given above, while the concentration lateral open boundary condition during the outflow is specified with one-dimensional advection, $\frac{\partial(DC)}{\partial t} + \frac{\partial(DCU_i)}{h_i \partial \varepsilon_i} = 0$, where U_i is the velocity in the normal direction to

the boundary while the following gradient condition is used for inflow, $\frac{\partial(DC)}{\partial t} = \frac{\partial(DCU_i)}{h_i \partial \varepsilon_i} = 0$.

2.2. Model Grids

The GBM computational grid as shown in Figure 2.1 consists of 181x101 horizontal cells ($dx = 254\text{-}2482\text{m}$, $dy = 580\text{-}3502\text{m}$) with 5 levels in the vertical. GBM water depths range from 1 m in the shallows to 20m along the shelf boundary (Figure 2.2). The HSCM grid shown in Figure 2.3 was developed in three sections. Each grid section was linked in order to develop the final composite channel grid consisting of 71 x 211 horizontal cells ($dx=63\text{-}1007\text{m}$, $dy=133\text{-}1268\text{m}$) with the same 5 sigma levels as in the GBM. Note navigation channel depths are order 14m. The HSCM was then nested inside the GBM using a one-way coupling scheme, wherein GBM water surface elevation, salinity, temperature, turbulent kinetic energy, and turbulent length scale time histories were saved at 6-minute intervals to provide boundary conditions to drive the HSCM. For salinity, temperature, turbulent kinetic energy, and turbulent length scale, a one-dimensional (normal to the boundary) advection equation is used. On inflow GBM values are advected into the HSCM domain, while on outflow HSCM internal values are advected through the boundary.

GALVESTON BAY MODEL GRID

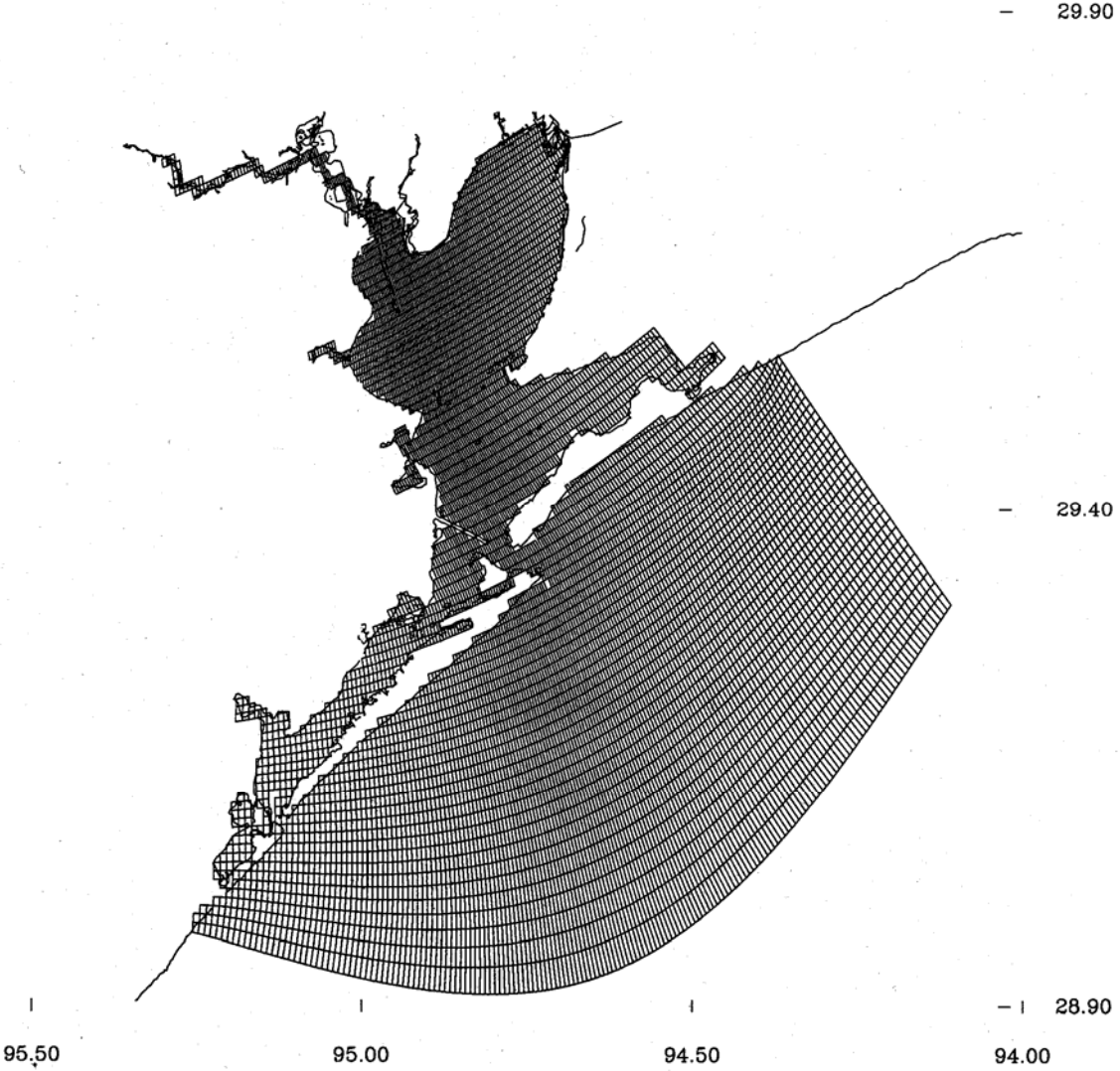


Figure 2.1. Galveston Bay model grid.

GALVESTON BAY TOPOGRAPHY

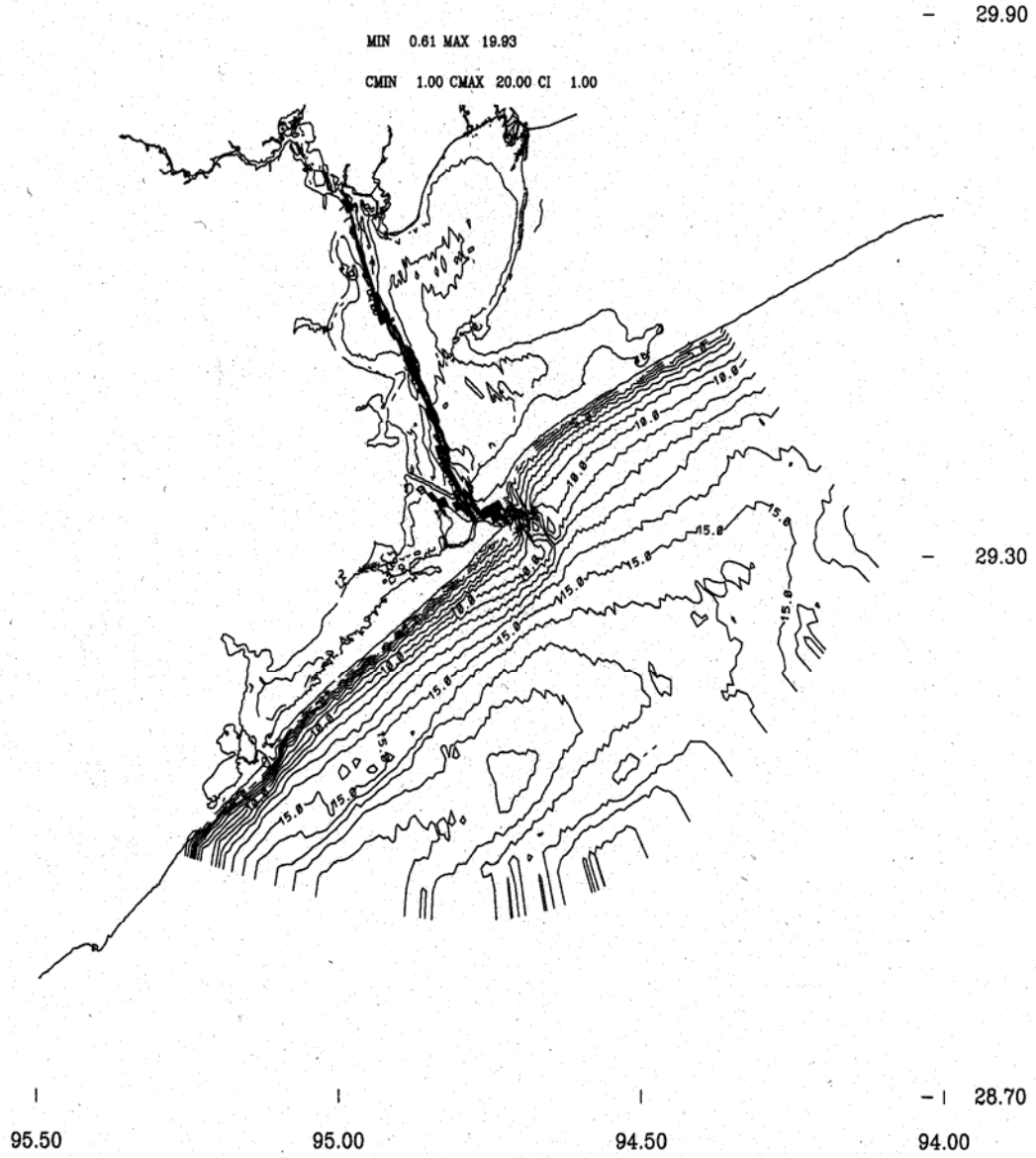


Figure 2.2. Galveston Bay model bathymetry, contours in meters.

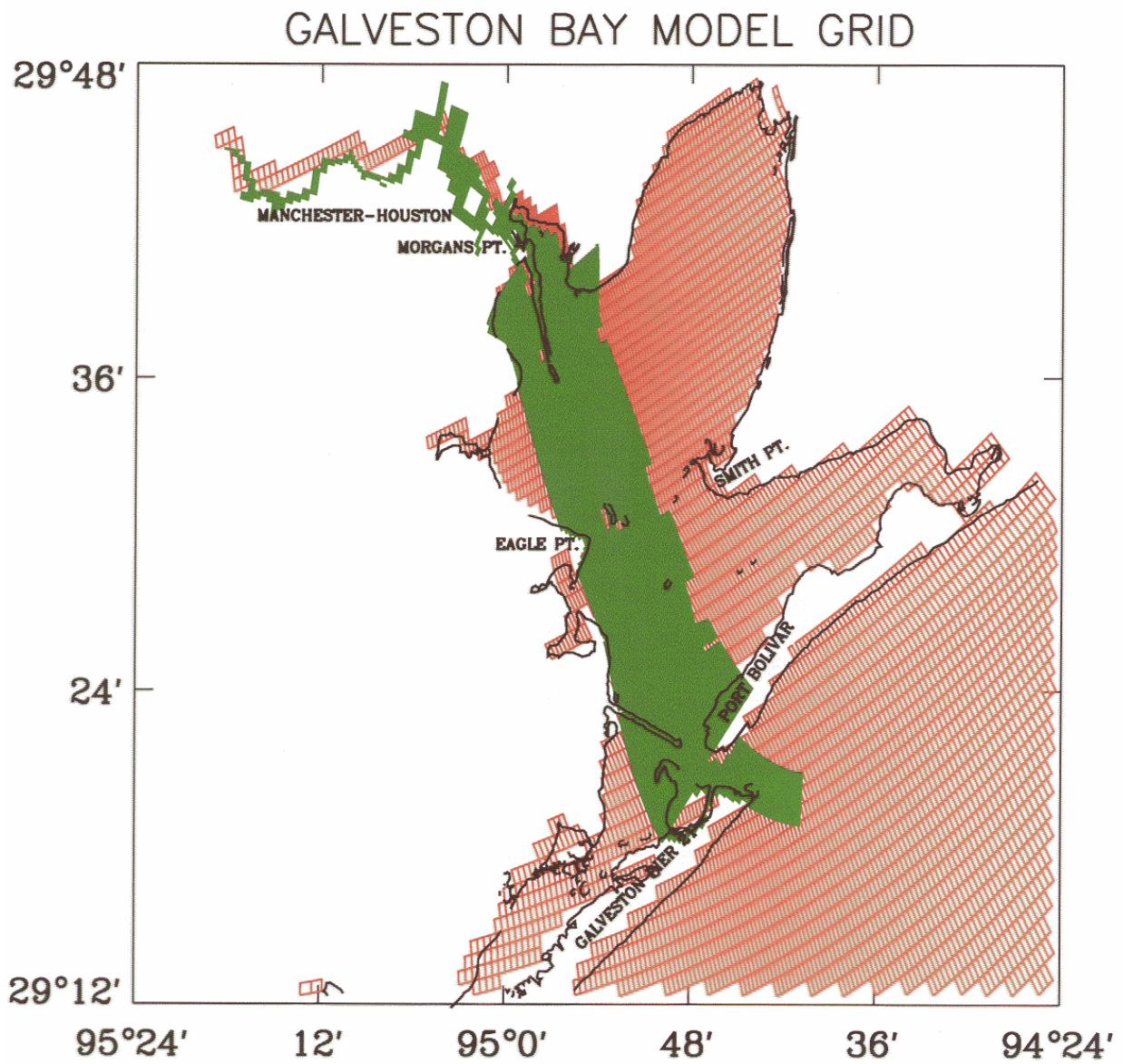


Figure 2.3. Galveston Bay model grid in red with Houston Ship Channel grid shown in green.

3. SHORT WAVE HYDRODYNAMIC MODEL

Schmalz (2003) has compared two USACE parametric wave models (CETN-I-6, 1981; Project CW-167, 1955) with the finite difference based Donelan (1977) wave model for wind events over Galveston Bay. The two parametric models were run on the same grid employed for the Bay circulation model (Figure 2.1), while a uniform square grid was used for the Donelan model. Further details on the Donelan (1977) wave model may be found in Schwab et al. (1984). Details of the initial testing may be found in Schmalz (2003). Best results were achieved by the mixture of the two parametric models as presented in the governing equations below and described in section 3.2.

3.1. Governing Equations

CETN-I-6 (1981) significant wave height, H_s (ft):

$$\frac{gH_s}{U_A^2} = 0.283 \tanh[0.530[gD/U_A^2]^{0.75}] \tanh\left[\frac{0.00565[gF/U_A^2]^{0.5}}{\tanh[0.530[gD/U_A^2]^{0.75}]}\right] \quad (3.1)$$

CW-167 (Project CW-167, 1955): significant wave period, T_s (sec):

$$T_s = 6.262 \frac{U_A}{g} \left(\frac{gD}{U_A^2}\right)^{0.4507} \quad (3.2)$$

using the following notation:

g = Gravitational acceleration (32.2 ft/sec²)

U_A = Windspeed (kts)

F = Fetch (nm)

D = Total water depth (ft)

3.2. Initial Validation

The January 25-30, 1997 time period was studied due to the availability of USACE wave measurements off Eagle Point. Application of the models to this period revealed that best results were achieved by using a combination of the two simpler parametric wave models, even though the finite difference based Donelan model incorporated the shallow water effects by using a linear reduction in transfer of wind to wave momentum as described in Schmalz (2003). Total significant wave height was computed as the sum of the CETN-I-6 results plus the swell, which was determined at the open boundary from the NDBC Buoy 42035 measurements. The total significant wave period was taken as equal to the CW-167 result alone. Results for January 25-30, 1997 are shown in Figure 3.1 at Eagle Point and in Figure 3.2 at NDBC Buoy 42035, respectively. Note, the peak at Eagle Point is no longer delayed relative to the observations as experienced using the Donelan model with the shallow water adjustment (results not shown) and the peak at NDBC Buoy 42035 is well reproduced.

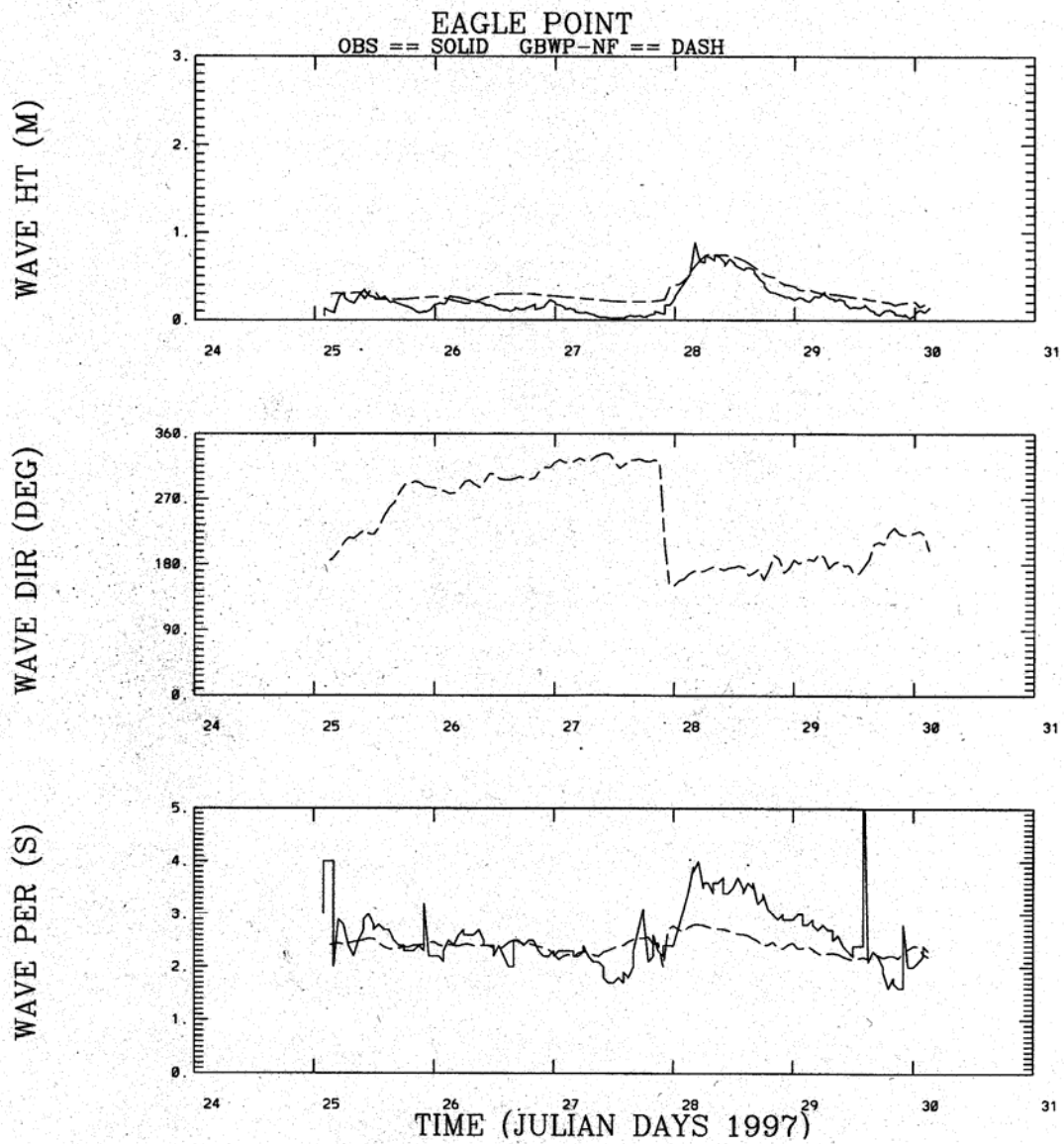


Figure 3.1. Galveston Bay Wave Model vs Observed Wave Parameters at Eagle Point, January 25-30 1997.

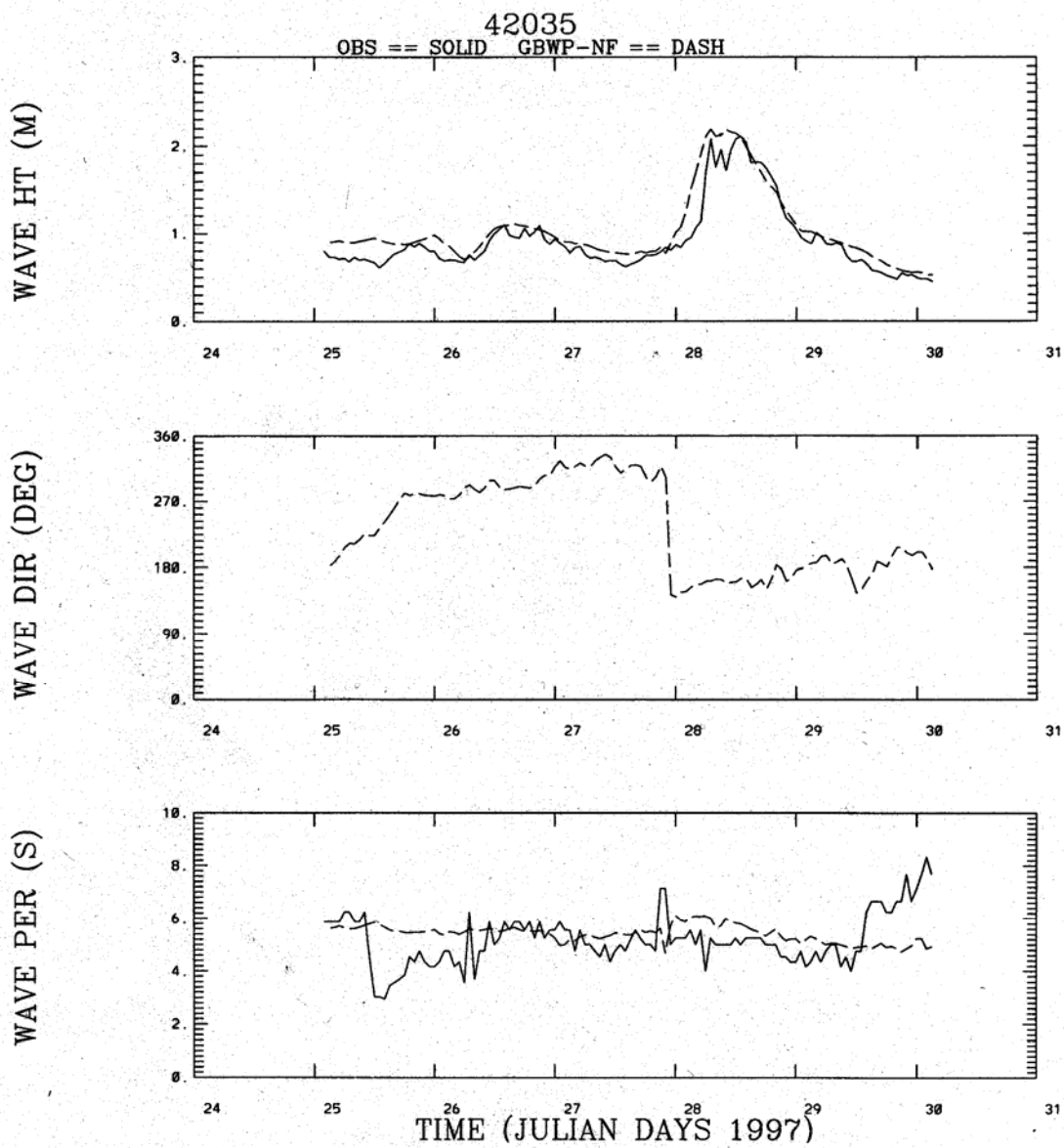


Figure 3.2. Galveston Bay Wave Model vs Observed Wave Parameters at 42035, January 25-30 1997.

3.3 Joint Computation

The mixed parametric wave model has been included as a subroutine within both the Bay and Channel long wave models and uses the same wind field. The waves are computed every six-minutes. In the Bay model, fetch data are specified for each octant of wind direction at 25 locations surrounding the Bay. An inverse distance squared interpolation is performed to determine the fetch distribution over the Bay for each wave computation. The long wave model provides the updated total water depth. At each wave computation in the Bay model, the swell height and fetch at each boundary point required by the Channel model are written on the transfer file in addition to the one-way coupled long wave information. Swell effects in the Bay model are input as a boundary condition and are reduced from the offshore boundary by a inverse distance squared interpolation of empirical reduction factors supplied at the above 25 locations around the Bay.

3.4. Overtopping and Barrier Island Breaching Limitations

Several effects associated with milder waves, such as refraction due to changes in bathymetry are not specifically treated. The wave field is represented here by a single frequency, height, and direction rather than a continuous spectrum. Thus no wave-wave interaction is considered. Wave diffraction around breakwaters and jetties and wave reflection are also not included.

The erosion of the barrier island system and breaching of the barrier islands are not considered. This would involve the description of the stress and the nature of the barrier island soil structure as well as the prediction of soil pressure and sediment transport mechanics. The islands may be and are during Hurricane Carla (1961) overtopped by overland flooding.

4. WAVE-CURRENT INTERACTION MECHANICS

We consider a wave field with significant wave height, H_s , dominant period, C , and wave direction, ϕ . The wave direction is assumed to be in the direction of the wind. To determine the wave age, it is necessary to compute the wave phase speed, $C_p = \frac{\omega}{k}$, where

$$\omega = \frac{2\pi}{C}, \quad \text{and} \quad k = \frac{\omega^2}{g \tanh(rk)}, \quad \text{with} \quad rk = \begin{cases} S(1 + 2e^{-2S} - 12e^{-4S}) & S > 2 \\ S^{0.5}(1 + 0.169S + 0.031S^2) & S \leq 2 \end{cases},$$

where $S = D\omega^2 / g$ with D and g as defined previously as reported at http://web.mit.edu/fluids-modules/www/potential_flows/Lectures.

The friction velocity, u_* , is then computed as $u_* = U_{10N} \sqrt{C_{D10}}$, and the wave age is formed as the ratio of C_p to u_* .

4.1. Surface Drag Coefficient Adjustment

In the presence of waves, the surface drag coefficient is increased. Following Drennan et al. (2003), we employ their Figure 10 in which the drag coefficient, C_{D10N} , and wind speed, U_{10N} , are given versus inverse wave age, u_*/C_p . Wind speed ranges are from 5 to 20 m/s. The following relationships are used in the algorithm to define the adjustment factor of the surface drag, F , based the ratio of measured C_{D10N} with respect to inverse wave age to the Smith (1980) relationship.

$$\begin{aligned} F &= 1. - (0.16)(U_{10N} - 5)/15 & u_*/C_p \leq 0.06, \\ F &= 1.16 - (0.13)(U_{10N} - 5)/15 & 0.06 < u_*/C_p \leq 0.08, \\ F &= 1.27 - (0.07)(U_{10N} - 5)/15 & 0.08 < u_*/C_p \leq 0.10, \\ F &= 1.38 - (0.05)(U_{10N} - 5)/15 & 0.10 < u_*/C_p \end{aligned} \quad (3.3)$$

The effective surface drag coefficient, is given as the product of the adjustment factor, F , and the Large and Pond (1981) surface drag relation:

$$C_{D10N} \times 10^3 = \begin{cases} 1.2 & U_{10N} \leq 11 \text{ m/s} \\ (0.49 + 0.065U_{10N}) & U_{10N} > 11 \text{ m/s} \end{cases} \quad (3.4)$$

$$C_{eff} = FC_{D10N}$$

Note with no wave current interaction, $F=1.0$.

4.2. Bottom Friction Adjustment

In the presence of waves, the near bottom wave orbital velocity based on linear wave theory, U_o is first computed as $U_o = \frac{0.5H_s\omega}{\sinh(kD)}$ after Signell et al. (1990). The near bottom excursion amplitude, a_b , and effective roughness, k_b , are then determined as

$a_b = \frac{U_o}{\omega}$ and $k_b = 30z_0$, with z_0 the bottom roughness. The wave friction velocity, u_{*w} , is determined based on $S_b = k_b / a_b$ in the relationship reported by Grant and Madsen (1982) in the following manner:

$$f_w = \left\{ \begin{array}{ll} 0.13S_b^{0.40} & S_b < 0.08 \\ 0.23S_b^{0.62} & 0.08 \leq S_b \leq 1.0 \\ 0.23 & S_b > 1.0 \end{array} \right\}, \text{ with } u_{*w} = \sqrt{0.5f_w U_o^2} \quad (3.5)$$

Next the current friction velocity, u_{*c} , is determined based on the model horizontal velocity components (U_b, V_b), at the level nearest the bed as follows (see Davies and Lawrence, 1995):

$$f_c = 2[\kappa / \ln(0.1/z_0)]^2, \text{ with } u_{*c} = \sqrt{0.5f_c (U_b^2 + V_b^2)} \quad (3.6)$$

The total friction velocity is then determined based on the current friction velocity and the wave friction velocity in the direction of the current as follows:

$u_{*T} = \sqrt{u_{*c}^2 + (u_{*w} \cos(\theta_{wc}))^2}$, where θ_{wc} , is the angle between the wave and wind directions (refer to Grant and Madsen, 1979). A roughness adjustment is determined as $F_p = \frac{24u_{*T}}{U_o} (S_b)^{1 - \frac{u_{*c}}{u_{*T}}}$ as reported by Signell (1990). The bottom friction adjustment

factor, F_{pb} , is given by $F_{pb} = \left[\frac{\ln(h_b / z_0)}{\ln(h_b / F_p z_0)} \right]^2$. In the present study, F_{pb} cannot exceed 2.

The effective bottom roughness is the product of the bottom roughness and this adjustment factor. Note in this approach, wave and current effects are considered independently (z_0 is never altered) and are then combined to determine the adjustment factor. In theory, an iterative approach on z_0 is desired.

4.3. Setup and Runup Limitations

Wave setup and the associated runup at the shoreline due to breaking waves are not considered. These effects were considered by Schmalz (1986) in Lake Okeechobee by using empirical relations. In general, the radiation stresses induced by the waves must be included as an additional stress in the long wave model. This has been accomplished by Mastenbroek et al. (1992) within a two-dimensional vertically integrated model. Recently, Mellor (2003; 2005) has developed the radiation stress relations in three dimensions and initial work has been reported by Mellor and Donelan (2006) on coupling a short wave and three-dimensional long wave model including the radiation stresses.

5. STORM SURGE METHODOLOGY

Storm surge is considered as a rise in water levels associated with either the propagation of the offshore storm surge or from the associated river and basin flooding generated by the storm rain/runoff. To be able to account for this phenomena within the nowcast/forecast system, algorithms for the rainfall/runoff, overland flooding, hurricane wind and pressure fields, and surface gravity waves are discussed in Sections 5.1 – 5.4, respectively. Next the design of the all-weather nowcast/forecast system is presented in Section 5.5. In section 5.6 additional hydrodynamic model considerations are presented followed by the discussion of the storm surge simulation objectives.

5.1. Rainfall/Runoff

In conjunction with the Houston Urban Runoff Program, the USGS has obtained streamflow and rainfall data for major drainage basins throughout the City of Houston during 1964 to 1989. In an effort to characterize the influence of development on drainage characteristics, sets of regression equations for basins north (based on 408 storms) and south (based on 331 storms) of Buffalo Bayou have been developed by Liscum (2001) for the major descriptors of the runoff as given in Table 5.1. To apply these relations to the City of Houston, four major basins are considered with basin characteristics given in Table 5.2.

Table 5.1. Major Runoff Descriptors for Use in USGS Rainfall/Runoff Regression Relations.

Stormwater Runoff Characteristics

QPEAK = Peak flow (cfs)

RODUR= Runoff duration (hrs)

TRISE=Time of rise from base flow to QPEAK (hrs)

Q75DUR=Duration of flow that equals or exceeds 75 percent of QPEAK (hrs)

Q50DUR=Duration of flow that equals or exceeds 50 percent of QPEAK (hrs)

TRECES=Time of recession from QPEAK to base flow (hrs)

BLAG=Duration from centroid of storm rainfall to centroid of direct runoff (hrs)

Rainfall Event Characteristics

RTOT=Total rainfall (in)

R60MAX=Maximum 60-minute rainfall (in)

RDUR=Rainfall duration (hrs)

R85DUR=Shortest 85 percent RDUR (hrs)

RI=Antecedent rainfall index (in)

Table 5.2. Basin Characteristics for Major Runoff in City of Houston. Note Region 1 is located North and Region 2 South of Buffalo Bayou.

Characteristic	Greens Bayou	Brays Bayou	Sims Bayou	Hunting Bayou
USGS Gage No.	08076700	08074760	08075500	08075770
Region	1	2	2	1
Total Basin Drainage Area (DA) (mi ²)	182.0	94.9	20.2	16.1
Gage Drainage Area (DA) (mi ²)	182.0	94.9	64.0	16.1
Basin Development Factor (BDF) (0-12)	7	8	8	8
Basin Slope (SL) (ft/(ft/mi) ^{0.5})	4.5	3.9	3.9	3.9
Base flow (cfs)	0.0	0.0	0.0	0.0

Daily hyetographs are separated into *nevent*, rainfall events by specifying a no rainfall minimum duration of 12 hours between events. Then for each event, the rainfall event characteristics in Table 5.1 are computed for use in the regression equations given in Table 5.3.

The antecedent rainfall index is a key parameter and is determined at the start of each event based on the hourly rainfall of the previous 5 days using the following relation:

$$RI_t = RI_{t-1}k^{\Delta t} + r_{\Delta t} \quad t = 1, \dots, n \quad (5.1)$$

where

RI_0 =Initial value (inches)

RI_t =Reduced value of the index t hours later (inches)

k =Recession factor set to 0.9 after Linsley et al. (1982)

$\Delta t = T_t - T_{t-1}$ (hrs)

$r_{\Delta t}$ =Rainfall during Δt

For each $t=1, \dots, n$, the event flows Q_t^i for $i=1, nevents$ are summed to obtain the basin hydrograph.

Table 5.3. USGS Runoff Characteristic Regression Equations from Liscum (2001).

Region	Equation	R ² (percent)
1	$QPEAK=312 DA^{0.728} (13-BDF)^{-1.04} RTOT^{0.984} RI^{0.135}$	87
2	$QPEAK=312 DA^{0.735} (13-BDF)^{-1.07} RTOT^{0.837} RI^{0.093}$	87
1	$RODUR=13.7 DA^{0.199} (13-BDF)^{0.227} RTOT^{0.298} R85DUR^{0.154}$	67
2	$RODUR=10.7 SL^{0.410} (13-BDF)^{0.439} RTOT^{0.274} R85DUR^{0.117}$	66
1	$TRISE=1.93 DA^{0.199} RTOT^{0.741} R60MAX^{-0.519} R85DUR^{0.255}$	55
2	$TRISE=1.63 DA^{0.278} RTOT^{0.501} R60MAX^{-0.357} R85DUR^{0.266}$	50
1	$Q75DUR=0.374 DA^{0.294} (13-BDF)^{0.678} RTOT^{0.678} R60MAX^{-0.425}$	77
2	$Q75DUR=0.367 DA^{0.274} (13-BDF)^{0.646} RTOT^{0.682} R60MAX^{-0.431}$	55
1	$Q50DUR=0.665 DA^{0.287} (13-BDF)^{0.723} RTOT^{0.625} R60MAX^{-0.454}$	80
2	$Q50DUR=0.624 DA^{0.271} (13-BDF)^{0.711} RTOT^{0.665} R60MAX^{-0.471}$	57
1	$TRECES=9.50 DA^{0.223} (13-BDF)^{0.337} RTOT^{0.282} R85DUR^{0.084}$	62
2	$TRECES=9.17 SL^{0.435} (13-BDF)^{0.473} RTOT^{0.314} RI^{0.091}$	58
1	$BLAG=0.720 DA^{0.333} (13-BDF)^{0.781} RTOT^{0.126} R85DUR^{0.106}$	77
2	$BLAG=0.693 SL^{0.481} (13-BDF)^{0.969} RTOT^{0.296} RI^{0.110}$	62

To test the scheme, basin rainfall records were obtained from 3-12 June 2001 during Tropical Storm Allison from the Harris County Flood Control District. Computed average daily runoff flows using the above method were compared with the USGS records as shown in Table 5.4.

Results given in Table 5.4 were computed by applying the reduction factors based on event rainfall totals to TRISE, TRECES, BLAG, Q50DUR, and Q75DUR given in Table 5.3. This was necessary to improve the timing of the runoff flows, since the regression equations were developed for rainfall events of less than 5 inches.

Table 5.4. Average Daily Flow (cfs) Comparison June 3-12, 2001 during Tropical Storm Allison. Note Pred=Prediction, Obs=Observation, and e following observation denotes an estimated value.

Date 2001	Greens Bayou		Brays Bayou		Sims Bayou		Hunting Bayou	
	Pred	Obs	Pred	Obs	Pred	Obs	Pred	Obs
June 3	0	-	0	107	0	8.8	0	4.8
June 4	0	-	0	106	0	7.3	0	5.5
June 5	0		166		32		0	
	1110		3100		862		378	
June 6	6438		4927		876		866	
	13500		960		809		1290	
June 7	5520		2013		476		787	
	2540		5560		3210		332	
June 8	2938		1001		200		257	
	2380		3000		939		601	
June 9	37609		12377		1021		4172	
	59300e		14000e		4650		2950	
June 10	17886		4839		358		405	
	41100e		530e		109		1320	
June 11	1240		210		110		17	
	4240e		210		27		103	
June 12	54		9		5		1	
	702		137		17		45	
Total Rainfall(in)	34.07		21.07		12.90		24.11	
Total Pred Runoff (in)	13.82		9.49		5.39		14.06	
Ratio 1	0.406		0.450		0.418		0.583	
Ratio 2	0.352		0.655		0.479		-	

Ratio 1== Total Predicted Runoff/Total Rainfall June 3-12, 2001; Ratio 2==Average Yearly Runoff/Average Yearly Rainfall with averages computed over 1965-1989.

Table 5.5. Empirical Reductions Factors for Large Rainfall Events

Rainfall total (in)	5	10	15	20	25	50
Reduction factor	1.	0.5	0.25	0.33	0.29	0.2

5.2. Overland Flooding Scheme

The scheme was developed to supplement the drying/wetting scheme previously developed (Schmalz, 1998a; 2001). The original scheme allowed water areas to dry and subsequently wet (tidal flat problem) but did not allow land areas to flood. To accommodate this feature, a digital elevation model or test topography is used in which

land elevations are set to a maximum of -1 m. Along the grid border, land elevations are set to -100 m. Since it is necessary to perform computations over dry grid cells, a minimum water depth, $dflood$, is specified. Subsequent cell and cell face flags properly mask any undesired results. For surface temperature specification, a value $tflood=29.5^{\circ}\text{C}$ is used for the overland flood cells. The flood scheme is actuated each internal mode time step and consists of the following check for a typical u-velocity face to see if it should be activated. Activation is based on the water level in the wet cell exceeding the dry cell bed elevation by a critical depth, $dcrit$, equal to $10dflood$ plus the depth needed to account for the water initially placed on the dry cell as given in the relation below, following Mellor's (2003) notation:

If $dum_{i,j} = 0$, $fsm_{i,j} = 0$, and $fsm_{i-1,j} = 1$, then we compute

$$dil = dflood * art_{i,j} / art_{i-1,j}$$

If $el_{i-1,j}^m + h_{i,j} > dcrit + dil$ and $d_{i-1,j}^m > 2dcrit$ then

(5.2)

$fsm_{i,j} = iover_{i,j} = dum_{i,j} = 1$ and the cell face is activated

$$\text{and } F_{i,j,k}^m = F_{i-1,j,k}^m, \quad F_{i,j,k}^{m-1} = F_{i-1,j,k}^{m-1}, \quad k = 1, \dots, kbm1, \text{ where } F == (T, S, Q^2, Q^2l)$$

A similar procedure is used for the case, $dum_{i,j}=0$, $fsm_{i,j}=1$, and $fsm_{i-1,j}=0$ and for the v-cell face. Once both u and v faces have been activated, the potential exists on a u-face for both $fsm_{i,j}=fsm_{i-1,j}=1$ with $dum_{i,j}=0$. If this occurs, the average u-cell face water depth, $dbar$, is computed as $dbar = 0.5(el_{i,j}^m + el_{i-1,j}^m + h_{i,j} + h_{i-1,j})$. If $dbar > dcrit + dflood$ then $dum_{i,j}=1$. An analogous procedure is used for the v-face. To monitor the computations and determine the areal extent of overland flooding, the following procedures were implemented. First an additional cell mask, $imask_{i,j}$, was created and set to 1. If the cell bed elevation becomes negative, $imask_{i,j}=-1$. If overland flooding occurs, $iover_{i,j}=1$ and $imask_{i,j}=0$. This allows water depths over the complete water area, or over just the overland flooded portions of the grid, to be printed/plotted.

Two test applications were employed in which $dflood=25\text{mm}$ and $dcrit=25\text{cm}$. In the first application a test topography was specified based on the cell's distance from mid-Bay as given in Table 5.6. In the second application, the USGS 3-arc second DEM for Houston-West and Houston-East was used to specify the overland topography. In both applications, the 8 Sept 1999 JD 251 24-hour nowcast cycle (249.75-250.75) was simulated with the test surge given in Table 5.7 imposed. Model mean water surface elevations at three locations are given in Table 5.8 for each case. While the model mean and maximum water surface elevations were very close at the stations in Table 5.8, the areal extent of the flooding was vastly different. For the test topography, only order 10 grid cells in the lower eastern portion of the Bay mean sea level boundary were inundated with flood depth levels of order 0.5m. For the DEM topography, order 1000 grid cells over major portions of the Bay east and west mean sea level boundaries were inundated with flood depth levels of order 2.2m. The river input flow cells were surrounded by floodwater.

One should also note that salinity computations are performed over the flooded areas and as the water recede the flooded cells become inactive (they do not communicate with the Bay grid cells) and retain the values of salinity that were present when they were active during the surge propagation phase of the storm.

Table 5.6. Test Topography based on Cell-Centered Distance from mid-Bay (29.4°N, 95.0°W).

Distance (km)	0	5	10	15	20	25	30	35	40	45	50
Bed elevation (m)	-2.	-2.5	-3.0	-4.0	-5.0	-6.0	-7.0	-8.0	-10.0	-12.0	-15.0

Table 5.7. Test Storm Surge Specification based upon Hurricane Carla and Alicia surge levels.

Elapsed Time (Hours)	0	6	12	48	72
Surge Level (m)	0.	2.5	3.5	2.0	1.0

Table 5.8. Simulated Mean Water Surface Elevation (m) JD 249.75-250.75 Nowcast Cycle with Test Storm Surge.

Case	Galveston Pleasure Pier	Port Bolivar	Galveston Pier 21
Test Topography	3.07	2.23	2.60
DEM Topography	3.05	2.51	2.66

5.3. Hurricane Windfield and Atmospheric Pressure Algorithms

Initially, the work of Schmalz (1986a,b,c) was reviewed to consider the Standard Project Hurricane (SPH) and the Tetra Tech (1979) models. A more recent parametric model developed by Holland (1980) and further modified by Sinha and Mandal (1999) was also considered. Each is outlined below and was studied using a hypothetical storm track and parameter set (R = radius to maximum winds, P_o =far field atmospheric pressure, and ΔP = atmospheric pressure deficit). Each approach uses an inflow angle, α , as given by Graham and Nunn (1959) in the following relationship:

$$\alpha = \left\{ \begin{array}{ll} 10d/R & d \leq R \\ 10 + 15(d - R)/1.2R & R < d < 1.2R \\ 25 & d \geq 1.2R \end{array} \right\} \quad (5.3)$$

where d =Distance from the storm center

Each approach also uses the Schwerdt et al. (1979) asymmetry factor to account for storm forward speed as follows:

$$\begin{aligned}
\theta_{\max} &= \theta_h + 90 + \alpha \\
\theta_a &= \theta_s - \theta_{\max} \\
V_a &= 1.5V_f^{1.63} \cos \theta_a
\end{aligned} \tag{5.4}$$

where

θ_h =Storm direction bearing θ_{\max} =Bearing of maximum wind
 α =Inflow angle θ_a =Asymmetry angle
 θ_s =Storm center bearing V_a =Asymmetry speed adjustment
 V_f =Storm forward speed

For the Standard Project Hurricane (SPH), the maximum gradient windspeed is determined from the following relation:

$$V_{gx} = 67\Delta P^{1/2} - 1800\Omega R \tag{5.5}$$

where

ΔP =Central pressure deficit
 Ω =Earth rotation

The maximum sustained windspeed at 10m, is then determined by $V_{max}=0.9V_{gx}$. Next a reduction factor, f_r is determined by fits to observed radial wind profiles in Schwerdt et al. (1979) and is given by:

$$f_r = \begin{cases} (d/R)^3 & d \leq R \\ e^{-(d/7R+1/7)} & d > R \end{cases} \tag{5.6}$$

where d and R are as previously defined. The complete windspeed, V , including asymmetry effects and Schloemer (1954) pressure profile, P , are given by:

$$\begin{aligned}
V &= f_r V_{\max} + V_a \\
P &= P_0 + \Delta P(e^{-R/d} - 1)
\end{aligned} \tag{5.7}$$

where quantities on the right hand sides have been previously defined.

For the Tetra Tech approach, the algorithm is the same as the SPH algorithm with the exception of the relation for f_r , which is replaced by the following relation developed by Collins and Viehman (1971).

$$f_r = \begin{cases} 0 & 0 < d \leq R/3 \\ 3/2(d/R - 1/3) & R/3 < d \leq R \\ 1/c_1 d^k \log(R/c_2 d^m) & d > R \end{cases} \tag{5.8}$$

where $c_1 = 3.354$, $c_2 = 1.265 \times 10^{-3}$, $k = -0.15128$, $m = 1.607$.

For the Holland approach, the storm category, k_{cat} , is first determined based on the central pressure deficit using the following relation:

$$k_{cat} = \left\{ \begin{array}{ll} 1 & \Delta P \leq 30 \\ 2 & 30 < \Delta P \leq 50 \\ 3 & 50 < \Delta P \leq 70 \\ 4 & \Delta P > 70 \end{array} \right\} \quad (5.9)$$

$$\begin{aligned} R_1^m &= 28. & R_2^m &= 26. & R_3^m &= 22. & R_4^m &= 18. \\ b_1 &= 1.0 & b_2 &= 1.1 & b_3 &= 1.2 & b_4 &= 1.3 \\ pf_1 &= 1.6 & pf_2 &= 3.1 & pf_3 &= 1.3 \end{aligned} \quad (5.10)$$

Next the Coriolis parameter, f , is determined based on the hurricane latitude, λ_h , by:

$$\begin{aligned} f &= 2\Omega \sin \lambda_h \\ a_{kcat} &= Rb_{kcat} \end{aligned} \quad (5.11)$$

Note a_{kcat} is determined from b_{kcat} rather than independently specified. The complete windfield and pressure description is then determined as:

$$\begin{aligned} V_{gx} &= (a_{kcat} b_{kcat} \Delta P e^{-a_{kcat}/d^{b_{kcat}}} / \rho_{air} d^{b_{kcat}} - d^2 f^2 / 4)^{1/2} - df / 2 \\ f_r &= 0.65 pf_1 + e^{-(pf_2 R / R_{kcat}^m + pf_3 b_{kcat}^m / R)} \\ P &= P_0 + \Delta P (e^{-a_{kcat}/d^{b_{kcat}}} - 1) \end{aligned} \quad (5.12)$$

The three approaches are contrasted in Table 5.9 for a storm moving due North over (29.4°N, 95°W) with a constant radius to maximum winds of 25 nm and central pressure deficit of 25 mb.

Table 5.9. Hurricane Wind and Pressure Fields for an Arbitrary Storm based on SPH, Tetra Tech, and Holland Methods. Note longitude of the storm track is constant at 95°W, radius to maximum winds is 25nm, and central pressure deficit is 25mb with a far field pressure of 1013mb. Note f=all weather nowcast/forecast system, 1=SPH, 2=Tetra Tech, and 3=Holland.

Track Index	Location (lat °N)	Distance (nm)	Forward Speed (kts)	Windspeed (kts) Method				Wind Direction (oT)	Sea Level Pressure (mb)
				f	1	2	3		
1	28.0	84	3.5	32.5	30.1	30.7	21.7	-115	1007.7
2	28.35	63	3.5	36.9	35.2	34.9	27.7	-115	1006.2
3	28.7	42	3.5	42.4	41.2	40.2	36.1	-115	1003.5
4	29.05	21	3.5	50.8	48.8	48.2	49.8	-101	997.6
5	29.4	0	3.5	3.3	3.3	3.3	3.3	0	988.0
6	29.65	15	3.25	33.2	21.4	31.5	55.1	83	994.6
7	29.9	30	3.0	49.0	47.6	46.6	45.3	65	1000.8
8	30.15	45	2.75	45.1	42.8	41.9	37.0	65	1004.0
9	30.4	60	2.5	40.1	38.5	38.1	30.8	65	1005.9

A slightly modified approach was selected for incorporation within the all weather nowcast/forecast system in which for the Holland method, V_{gx} is evaluated for $d=R$ and f_r is based on the Collins and Viehman (1971) method used by Tetra Tech (1979) to determine the reduction factor. The Holland (1980) pressure profile is used.

5.4. Wave Algorithms

The previously described algorithm used in the tracer studies is a robust and computationally efficient scheme, which can also be extended to hurricane conditions with minor modification. At present no distinction is made between a flooded cell and a cell which is always wet in the wave computation method. It should be noted that in the present approach wave conditions are computed for all water cells using the same method. The same curvilinear grid used by the Galveston Bay circulation model and the same windfield are used.

The algorithm has been incorporated as a separate subroutine within the circulation model as was done by Schmalz (1986) for Lake Okeechobee, which allowed for further experimentation with wave-current interaction in the tracer studies. This has not been pursued in the storm surge studies.

Since no wave data are available during historical hindcasts, the following relations were used to specify representative wave conditions along the open boundary:

$$\begin{aligned} H_S &= \max(0.5, 1.0 + wl) \\ T_S &= 1.2H_S + 4.0 \\ \theta_S &= 315. + 5.0(wl - 4.0) \end{aligned} \tag{5.13}$$

Where H_S , T_S , θ_S , and wl represent significant wave height (m), significant wave period (s), significant wave direction (deg T), and observed water level at Galveston Pleasure Pier (ft relative to MLLW).

Data resources are required on nowcast and forecast. For the nowcast, data from NDBC Buoy 42035 may be obtained from the Texas Automated Buoy System (TABS) Project sponsored by the Texas General Land Office (TGLO) at:

http://tabs.gerg.tamu.edu/Tglo/DailyData/Data/42035_met.shtml.

For the forecast, the NWS Wavewatch III model forecast results at 42035 can be utilized at: ftp://polar.wwb.noaa.gov/pub/waves/latest_run/wna.42035.bull

Note with the present three-dimensional long wave modeling approach, the effect of return flows can be simulated and the potential exists for more accurate surge prediction with the wave effects included as well. Since in the present experimental nowcast/forecast system both GBM and HSCM are executed, we have also performed wave computations using the HSCM with the GBM results providing boundary conditions.

5.5. Design of the All Weather Nowcast/Forecast System

The NOS experimental all weather nowcast/forecast system uses the separate nowcast/forecast set-up program to establish hydrodynamic model nowcast and forecast inputs with minor modifications (indicated by * and italics in the list below). The modified set-up program utilizes the following twelve-step procedure, where the steps 1-10 constitute the original procedure:

- *1) Setup 24 hour nowcast and 36 hour forecast time periods and grid parameters,
- 2) Predict astronomical tide,
- 3) Predict astronomical currents,
- 4) Read PUFFF files and develop station time series,
- 5) Develop GBM subtidal water level signal,
- 6) Assimilate PORTS salinity and temperature data into GBM and HSCM initial conditions,
- *7) Establish GBM and HSCM salinity and temperature boundary conditions,
- 8) Establish GBM and HSCM SST forcing,
- *9) Establish USGS observed and NWS/WGRFC forecast freshwater inflows,
- *10) Establish PORTS based and NWS/Aviation Model wind and pressure fields,
- 11) Establish rainfall/runoff for City of Houston inflows, and*
- 12) Establish wave swell characteristics*

Step 1 was modified to include the grid modifications to incorporate the four additional City of Houston inflows. Step 7 was modified to include salinity and temperature specification for these inflows. Step 9 was modified to set the City of Houston inflows to zero for no rainfall/runoff. Note if rainfall/runoff occurs (storm track file specified) these flows are determined in Step 11. In Step 10, hurricane wind and pressure fields are developed if the storm track file exists. If a storm track file does not exist, the set-up program skips to Step 12. Otherwise, the wind and pressure fields are then blended into the NWS Aviation Model (now called the Global Forecast System Model) far fields over a distance from the storm center of five times the radius to maximum winds. In Step 11, the rainfall/runoff is developed if a storm track file is present. A 2-5 day antecedent rainfall description is used to determine the rainfall moisture index. A Quantitative Precipitation Forecast (QPF) will be used to provide the rainfall input over the forecast period. In Step 12, the open boundary wave swell height, direction, and period are specified based on measurements at Buoy 42035 and the NCEP Wavewatch forecast at Buoy 42035.

The GBM is modified to incorporate the overland flooding algorithm and includes the four additional freshwater inflows. The combined parametric wave model is included as a subroutine and uses the same wind fields. An open boundary swell condition is applied to incorporate Gulf of Mexico wave swell conditions. The fetch along the HSCM boundary is written to a transfer file for input to the HSCM. The HSCM modifications are similar. The overland flooding algorithm is included and the wave algorithm appears as a separate subroutine. The fetch from the GBM boundary and additional fetch specification within

the Port of Houston is interpolated over the grid for input to the wave subroutine. The City of Houston inflows are incorporated as in the GBM.

5.6. Additional Hydrodynamic Model Considerations

To isolate the standard freshwater inflows from flooding, it was necessary to extend the river channels to the grid boundary and to further surround them with a land elevation of 100m. In addition four other inflow channels were inserted in both the GBM and HSCM grids to model the Greens, Brays, Sims, and Hunting Bayou inflows. These inflow channels were extended to the grid boundaries as was done for the standard inflows. Note the Galveston sea wall was not directly included in the computations.

Additional modifications were required in the restart mechanics to allow for the continuation of overland flood events during restarts between subsequent nowcast/forecast cycles. The status of the flooded cells needed to be retained from simulation to simulation. Additional modifications to the IDL field plot programs were required to allow for the moving land/water boundaries.

5.7. Simulation Objectives

The storms shown in Table 5.10 are used to test the all-weather nowcast/forecast system first on a hindcast basis for two historical hurricanes and then on a nowcast/forecast cycle basis for Tropical Storm Allison. Separate storm track files were constructed and the modified set-up program exercised to provide forcing for the hydrodynamic models. Both long wave and short wave hydrodynamic computations were made using the GBM as well as the HSCM. The wave-current option outlined in Chapter 4 was not used in these initial computations.

Table 5.10. Major Storm Characteristics for Galveston Bay, Texas.

Storm/ Source	Central Pressure (mb)	Windspeed (kts)	Radius to Max Winds (nm)	Rainfall (in)	Storm Surge (ft)
Carla 3-15 Sept 1961/ Dunn and staff (1962)	970-975	75-80	30	5.0-10.0	8.8-9.3
Alicia 15-21 Aug 1983/ Case and Gerrish (1984)	963-965	80-100	30	7.8-10.7	8.9
Allison 9-11 June 2000/ NWS(2001); Stewart (2002)	990	20-30	30	9.8-35.1	1.8-2.1

Hurricanes Carla and Alicia were simulated and wind and water level validation were performed to assess the ability to replicate the effects of severe storms. The focus is not only on peak storm surge prediction ability but also on the complete hydrograph. Inundation statistics are computed to assess overland flooding. To utilize the three-dimensional capability, salinity and temperature responses will also be addressed.

Tropical Storm Allison is simulated using the experimental nowcast/forecast system. During the rainfall/runoff event, water level and current predictions will be compared to available data to assess the impact of including additional rainfall/runoff flows from the City of Houston.

While no short wave data are available to compare with simulation results, significant wave height and period are assessed for representativeness of hurricane conditions assuming no wave-current interaction.

6. HURRICANE CARLA (1961) SIMULATION

Three 24-hour hindcasts for September 9-11, 1961 were performed with the calculations restarted after each daily hindcast. No NCEP forecasts of surface winds and pressure fields or of storm surge were available. In experiment one, no wind and atmospheric pressure forcing were used while the open boundary storm surge was based on the nontidal water level at Galveston Pleasure. In experiment two, the parametric hurricane wind and atmospheric pressure forcing were applied with the same open boundary surge as in experiment one. The wind and atmospheric pressure forcing were mild over the Galveston Bay region, since the track of Hurricane Carla was well to the south of Galveston Bay (see Figure 6.1). As a result the results from experiment one and two are very similar with the results of experiment one presented below. Long wave results are given in terms of water surface elevation, prediction depth current (4.57m below MLLW), near surface salinity, and near surface temperature time series as well as field plots of water surface elevation and salinity. Short wave results are given in terms of significant wave height, period, and direction as well as field plots of significant wave height and period. Summary statistics are presented for flood inundation, maximum water surface elevation and maximum significant wave height.

6.1. Storm Characteristics

The track of Hurricane Carla is shown in Figure 6.1 with storm parameters given in Table 6.1. The storm made landfall at Port O'Connor, Texas at 1400 CST on the afternoon of September 11.

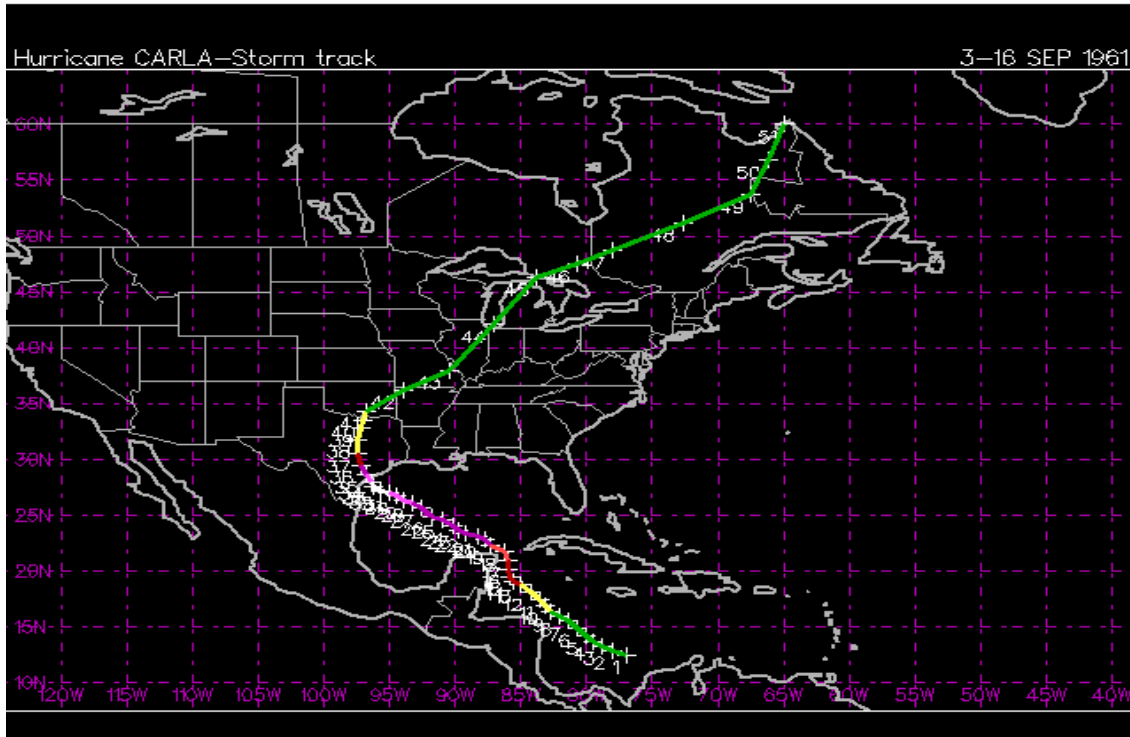


Figure 6.1. Hurricane Carla (1961) Storm Track 3-16 September.

Table 6.1. Hurricane Carla Storm Characteristics 3-16 September 1961.

ADV	LAT	LON	TIME	WIND	PR	STAT
	Deg N	Deg W	GMT	MPH	MB	Saffir-Simpson Scale
1	12.50	-77.00	09/03/12Z	25	-	TROPICAL DEPRESSION
2	12.90	-78.00	09/03/18Z	25	-	TROPICAL DEPRESSION
3	13.30	-78.80	09/04/00Z	25	-	TROPICAL DEPRESSION
4	13.70	-79.50	09/04/06Z	25	1007	TROPICAL DEPRESSION
5	14.20	-80.10	09/04/12Z	25	1006	TROPICAL DEPRESSION
6	14.90	-80.70	09/04/18Z	25	1005	TROPICAL DEPRESSION
7	15.50	-81.40	09/05/00Z	30	1002	TROPICAL DEPRESSION
8	15.90	-82.10	09/05/06Z	30	999	TROPICAL DEPRESSION
9	16.30	-82.70	09/05/12Z	40	997	TROPICAL STORM
10	16.90	-83.10	09/05/18Z	45	993	TROPICAL STORM
11	17.40	-83.60	09/06/00Z	50	990	TROPICAL STORM
12	18.10	-84.30	09/06/06Z	55	987	TROPICAL STORM
13	18.80	-85.10	09/06/12Z	65	984	HURRICANE-1
14	19.10	-85.60	09/06/18Z	70	981	HURRICANE-1
15	19.50	-85.90	09/07/00Z	75	978	HURRICANE-1
16	20.20	-86.00	09/07/06Z	80	975	HURRICANE-1
17	20.90	-86.00	09/07/12Z	85	973	HURRICANE-2
18	21.70	-86.30	09/07/18Z	95	970	HURRICANE-2
19	22.30	-87.30	09/08/00Z	100	968	HURRICANE-3
20	22.80	-87.80	09/08/06Z	105	966	HURRICANE-3
21	23.10	-88.30	09/08/12Z	110	965	HURRICANE-3
22	23.40	-89.20	09/08/18Z	110	962	HURRICANE-3
23	23.70	-89.80	09/09/00Z	110	959	HURRICANE-3
24	24.00	-90.20	09/09/06Z	110	956	HURRICANE-3
25	24.60	-91.00	09/09/12Z	110	953	HURRICANE-3
26	24.90	-91.80	09/09/18Z	110	948	HURRICANE-3
27	25.60	-92.60	09/10/00Z	110	944	HURRICANE-3
28	26.10	-93.30	09/10/06Z	115	940	HURRICANE-4
29	26.30	-93.90	09/10/12Z	120	937	HURRICANE-4
30	26.70	-94.50	09/10/18Z	130	936	HURRICANE-4
31	27.00	-95.00	09/11/00Z	140	936	HURRICANE-5
32	27.20	-95.70	09/11/06Z	150	936	HURRICANE-5
33	27.60	-96.20	09/11/12Z	145	935	HURRICANE-5
34	28.00	-96.40	09/11/18Z	125	931	HURRICANE-4---Landfall 21z
35	28.60	-96.80	09/12/00Z	100	940	HURRICANE-3
36	29.50	-97.20	09/12/06Z	80	955	HURRICANE-1
37	30.50	-97.40	09/12/12Z	60	975	TROPICAL STORM
38	31.80	-97.40	09/12/18Z	45	979	TROPICAL STORM
39	32.80	-97.20	09/13/00Z	40	980	TROPICAL STORM
40	33.50	-97.00	09/13/06Z	35	-	TROPICAL STORM
41	34.30	-96.80	09/13/12Z	30	-	EXTRATROPICAL DEPRESSION
42	36.20	-94.00	09/13/18Z	30	-	EXTRATROPICAL DEPRESSION
43	38.00	-90.50	09/14/00Z	30	-	EXTRATROPICAL DEPRESSION
44	42.10	-87.10	09/14/06Z	30	-	EXTRATROPICAL DEPRESSION
45	46.30	-83.80	09/14/12Z	30	-	EXTRATROPICAL DEPRESSION
46	47.50	-80.70	09/14/18Z	30	-	EXTRATROPICAL DEPRESSION
47	48.70	-78.00	09/15/00Z	30	-	EXTRATROPICAL DEPRESSION
48	51.20	-72.70	09/15/06Z	30	-	EXTRATROPICAL DEPRESSION
49	53.70	-67.50	09/15/12Z	30	-	EXTRATROPICAL DEPRESSION
50	56.80	-66.20	09/15/18Z	30	-	EXTRATROPICAL DEPRESSION
51	60.00	-65.00	09/16/00Z	30	-	EXTRATROPICAL DEPRESSION

In the simulations, the radius to maximum winds was estimated at approximately 15 nm around the time of landfall and subsequently increased to 25 nm over the next 12 hours. Hourly rainfall information was obtained at Station 413430 Galveston, Texas for use in the rainfall/runoff computations and totaled 16.23 inches. Cooperman and Sumner (1961) note that the crest elevation of the barrier islands from Port Aransas to Galveston is generally less than 10 feet MSL and for much of the distance it is less than 5 feet. Since the peak surge elevation at Galveston Pleasure Pier was 9.3 feet relative to NGVD 1929 (which differs by a few tenths of a foot from local MSL), much of the barrier islands were inundated.

6.2 Simulation Set-up Procedures

The first hindcast covers the period June 9 18:00 CST to June 10 18:00 CST. Water surface elevations and velocities are started from rest. The initial salinity and temperature fields are determined based on climatology. Since no PORTS data are available, no adjustment of these fields is made. Open boundary conditions for the GBM for water surface elevation are computed by adding the observed nontidal water level at Galveston Pleasure Pier to the predicted astronomical tide. Salinity and temperature values along the open boundary are based on climatology. Sea surface temperature is specified by using the top layer of the temperature field and is held constant in time. River inflows for the San Jacinto, Buffalo Bayou, and Trinity Rivers are based on USGS daily observed values. Since no wave data are available, the relationships used in Equation 6.13 were used to prescribe the wave conditions along the GBM open boundary.

For the subsequent two daily hindcasts over the periods June 10 18:00 CST to June 11 18:00 CST and June 11 18:00 CST to June 12 18:00 CST, conditions are restarted from the end of the previous hindcast. No adjustment of the salinity and temperature fields is made. Boundary forcing and river inflows are set up the same way as aforementioned. Note the HSCM is directly driven from information saved from the GBM in a one-way coupling scheme. See Schmalz (2000c; 2001) for details.

Two experiments are run using the above conditions but with different meteorological forcing. In experiment one, the observed surge level at Galveston Pleasure Pier is propagated into the Bay and the water level, current, and density response is investigated in the absence of wind and atmospheric pressure forcing. Results are presented for both the long wave and short surface gravity wave cases. Experiment two results with the parametric hurricane model wind and atmospheric pressure field forcing applied are next presented and contrasted.

6.3 Experiment One Long Wave Results

Simulated water surface elevations for each of the three hindcasts are shown for Galveston Pleasure Pier, Bolivar Roads, and Galveston Pier 21 in Figures 6.2–6.4. GBM simulated water levels are in excellent agreement (order 35 cm maximum discrepancy) with the observations at Galveston Pleasure Pier and at Galveston Pier 21. One notes the prolonged duration of elevated water levels and the potential for overland flooding and overtopping of the barrier islands. In Figures 6.5–6.7, HSCM simulated water surface elevations are shown for each hindcast for Eagle Point and Morgans Point. Unfortunately, no water level gages were in operation during this storm at these locations. In the third panel of these figures, the water level residual (surge at Galveston Pleasure Pier) is given. This water level residual is applied uniformly in space over the entire GBM open water boundary. The storm surge at Freeport was order 3.3m, which is considerably larger than the surge at Galveston Pleasure Pier. Since Freeport is immediately south of the lower boundary, it may be more appropriate to use the Freeport surge level along a portion of the lower GBM open boundary. This suggests that for the storm surge case, Freeport, Galveston Pleasure Pier, and Sabine Pass water level residuals be examined and that a procedure using all three of these residuals be developed for the GBM open boundary nontidal water level specification. However, in this case, since the water level stations are near Galveston Pleasure Pier, using the Galveston Pleasure Pier value only, results in good water level comparisons at these two stations.

Simulated currents are examined in three panel figures for current speed, current direction, and principal component direction with flood considered positive. Simulated Bolivar Roads currents are shown in Figures 6.8- 6.10 for each hindcast. One notes the complete absence of ebb flow until near the end of the second hindcast period around 10:45 CST on September 11. This ebb flow is followed by only a four hour duration flood and then a prolonged ebb flow over most of the third hindcast. Peak current strengths on both flood and ebb are order 150 cm/s (~3 kts). Simulated currents at Redfish Bar, mid-way up the Bay, show a similar behavior in the ebb-flood structure to simulated currents at Bolivar Roads; however, the peak current strengths are reduced to order 75 cm/s (~1.5 kts). At Morgans Point, the simulated currents in Figures 6.11- 6.13, exhibit a similar ebb-flood structure, but a second flood current is present during the third hindcast. The peak current strengths on ebb and flood are on the order of 50 cm/s (~1 kt). Additional rainfall/runoff flows have not been included and inflows from the Buffalo Bayou, San Jacinto River, and Trinity River were negligible.

Simulated surface temperature, temperature stratification (absolute difference between simulated surface and bottom temperatures) and surface salinity are examined in three panels at Bolivar Roads in Figures 6.14-6.16 and at Morgans Point in Figures 6.17-6.19, respectively. One notes the increase in salinity at Bolivar Roads from 30 to 35 psu during the surge propagation phase during hindcasts one and two and subsequent gradual decrease to 30 psu over the third hindcast during which the surge recedes. While the simulated surface temperature remains constant, there is an increase in stratification to order 2.5 °C as the cooler shelf water moves in over the bottom layers during the surge propagation phase of the storm. At Eagle Point the simulated surface salinity increases

from 17 psu to a maximum of 32 psu and then returns to 22.5 psu. The maximum simulated temperature stratification is over 5 °C during the initial phase of the third hindcast. At Morgans Point the simulated surface salinity increase is less dramatic than at Eagle Point going from 18 psu to 24 psu and then returning to 18 psu. The maximum simulated temperature stratification is order 2.5 °C as noted in hindcast three.

GBM simulated water surface elevation contours relative to MTL model datum at the end of hindcast two in Figure 6.20 and at the end of hindcast three in Figure 6.21. Water surface elevations are initiated at rest. One day later at the end of the first hindcast the barrier islands have been overtopped and flooding has occurred. At the end of the second hindcast in Figure 6.20, the flooding has progressed further inland, while at the end of the third hindcast in Figure 6.21, some of the flooded areas have dried. It should be noted that in the present flooding algorithm, no drainage or seepage flows are computed and as result, there is no mechanism for the water to be removed from the majority of flooded grid cells.

Next GBM simulated near surface and near bottom salinity contours are shown at the end of hindcast three in Figures 6.22 and 6.23. One notes the penetration of the shelf salinity into the Bay during the surge propagation phase in both the surface and bottom layers and the subsequent relaxation and seaward propagation of the increased salinity levels in the surface layer during the third hindcast. Note the simulated bottom layer salinity is still elevated and has not returned to prestorm values at the end of the third hindcast. One should also note that salinity computations are performed over the flooded areas and as the water recedes the flooded cells become inactive (they do not communicate with the Bay grid cells) and retain the values of salinity that were present when they were active during the surge propagation phase of the storm. As a result, there are discontinuities in salinity levels between active Bay cells and inactive previously flooded cells as noted at the end of the third hindcast.

Since in the present experimental nowcast/forecast system both GBM and HSCM are executed, we have also performed storm surge computations using the HSCM with the GBM results providing boundary conditions. One should note that the areas, over which the water may flood in the HSCM are limited to the upstream reaches above Morgans Point and to the barrier island system, which is fictitiously extended to regions beyond the jetties extending into the Gulf. HSCM simulated water surface elevation contours relative to MTL model datum are shown at the end of hindcast two in Figure 6.24 and at the end of hindcast three in Figure 6.25. Again water surface elevations are initiated at rest. One day later at the end of the first hindcast the barrier islands have been overtopped and flooding has occurred. At the end of the second hindcast in Figure 6.24, the flooding has progressed further inland, while at the end of the third hindcast in Figure 6.25, some of the flooded areas have dried. It should be noted that also in the HSCM, no drainage or seepage flows are computed and as result, there is no mechanism for the water to be removed from the majority of flooded grid cells.

Next HSCM simulated near surface and near bottom salinity contours are shown in Figures 6.26 and 6.27 at the end of hindcast three. One notes the penetration of the shelf

salinity up the Houston Ship Channel during the surge propagation phase in both the surface and bottom layers and the subsequent relaxation and seaward propagation of the salinity in the surface layer during the third hindcast. Note the simulated bottom layer salinity is still elevated and has not returned to prestorm values at the end of the third hindcast. One should also note that similarly in the HSCM salinity computations are performed over the flooded areas and as the water recedes the flooded cells become inactive and retain the values of salinity that were present when they were active during the surge propagation phase of the storm. As a result, there are discontinuities in salinity levels between active cells and inactive previously flooded cells as noted at the end of the third hindcast.

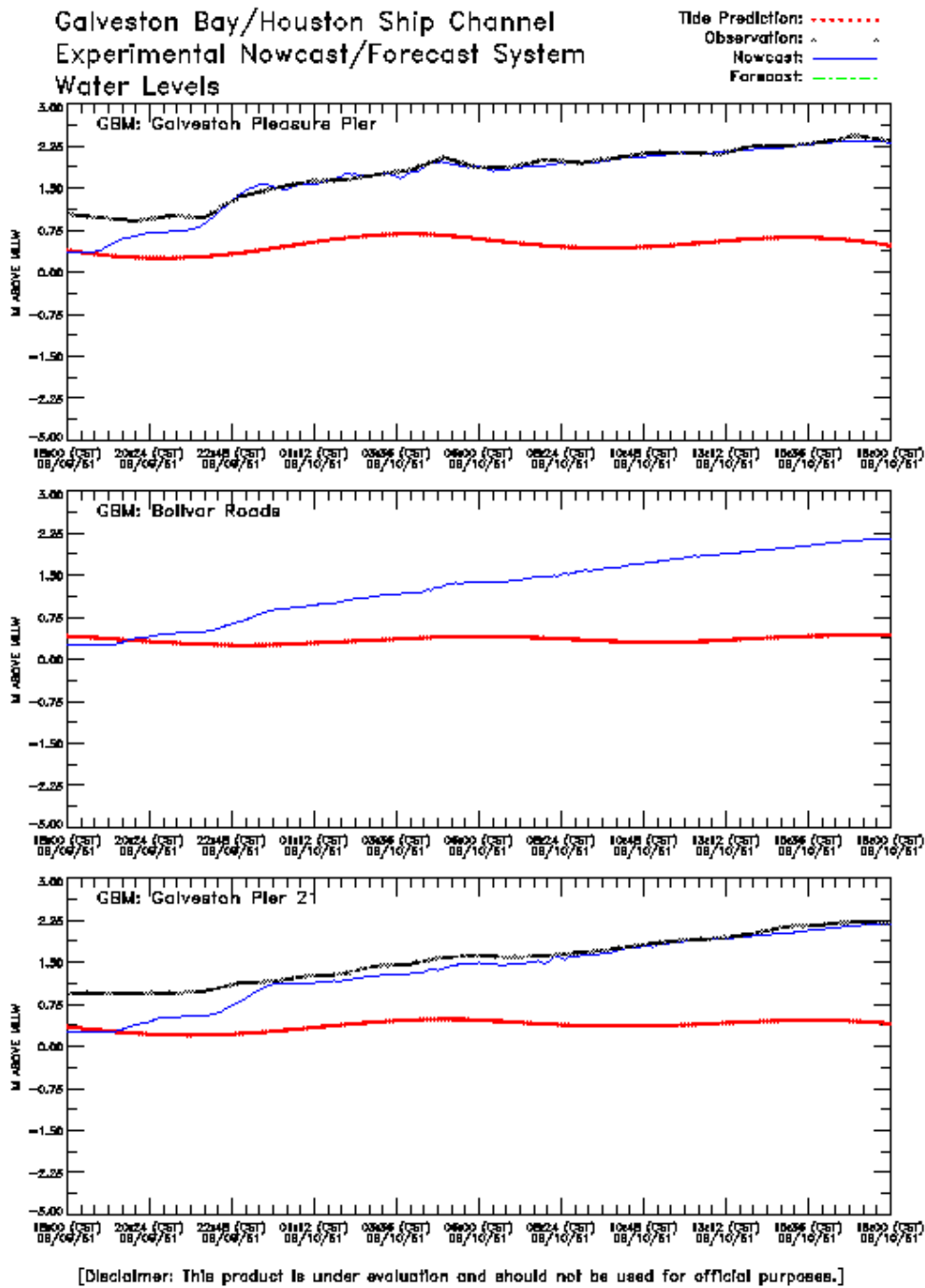


Figure 6.2. Hurricane Carla GBM Water Levels Experiment One: 9-10 September 1961

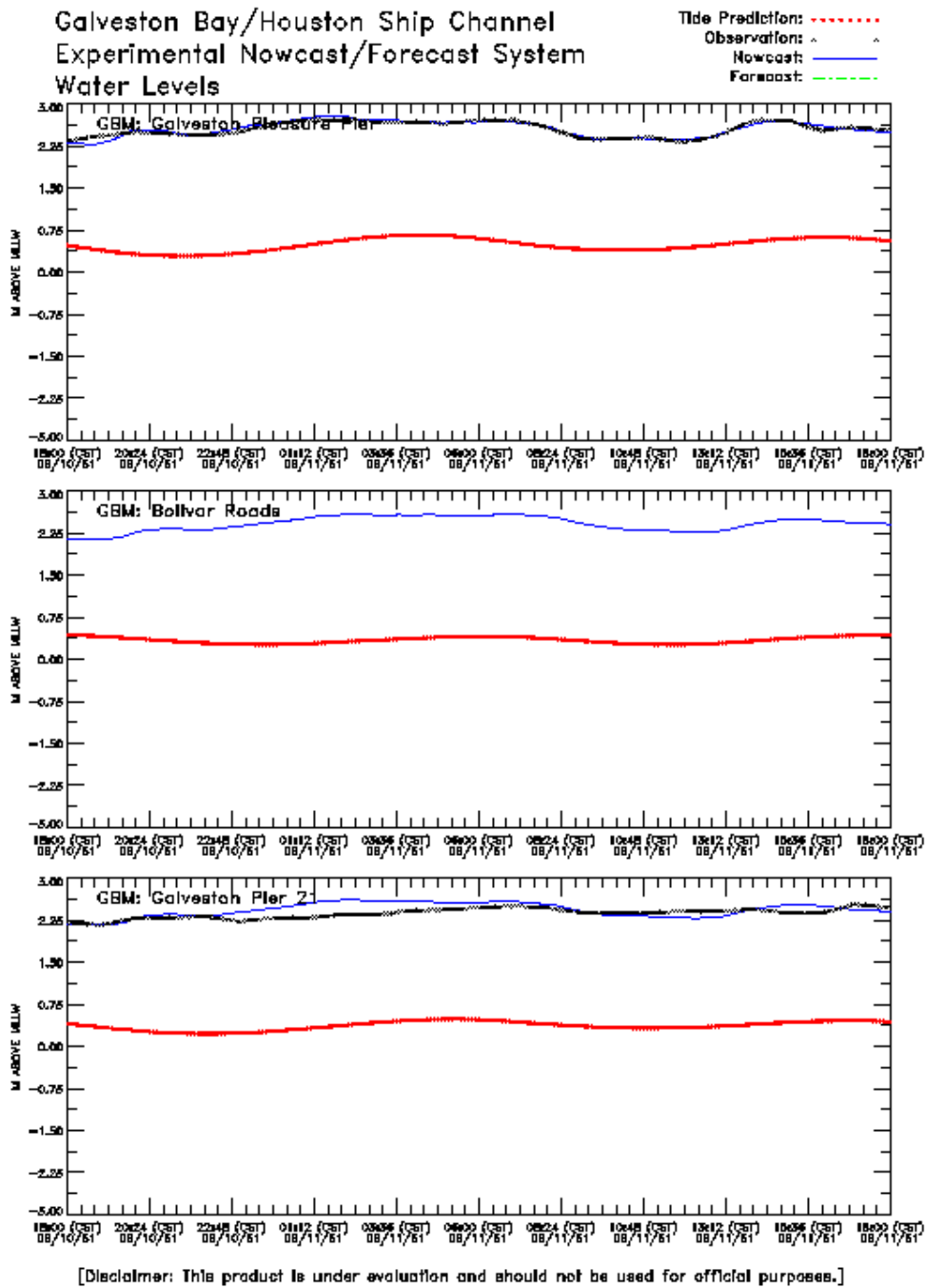


Figure 6.3. Hurricane Carla GBM Water Levels Experiment One: 10-11 September 1961

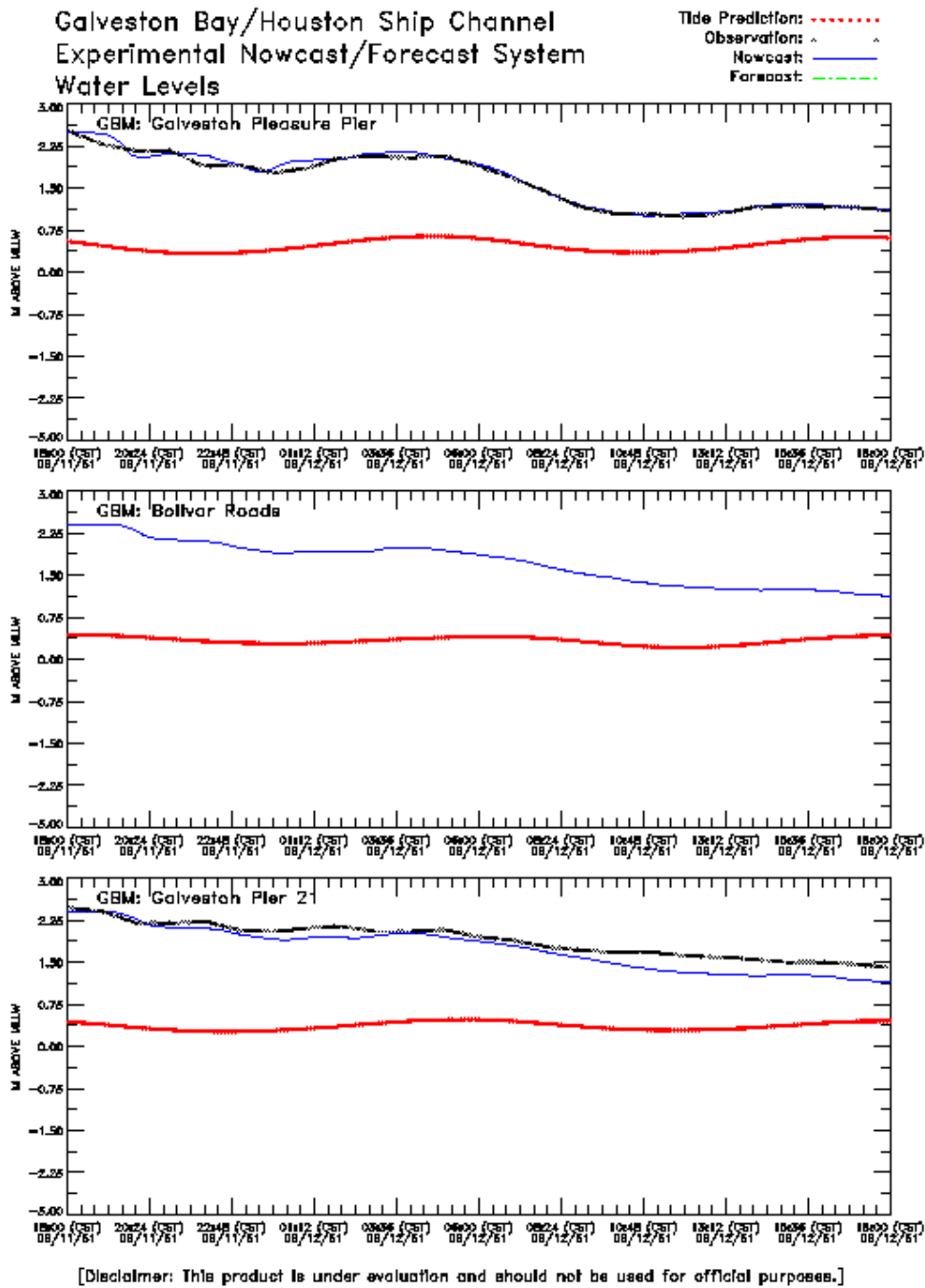


Figure 6.4. Hurricane Carla GBM Water Levels Experiment One: 11-12 September 1961

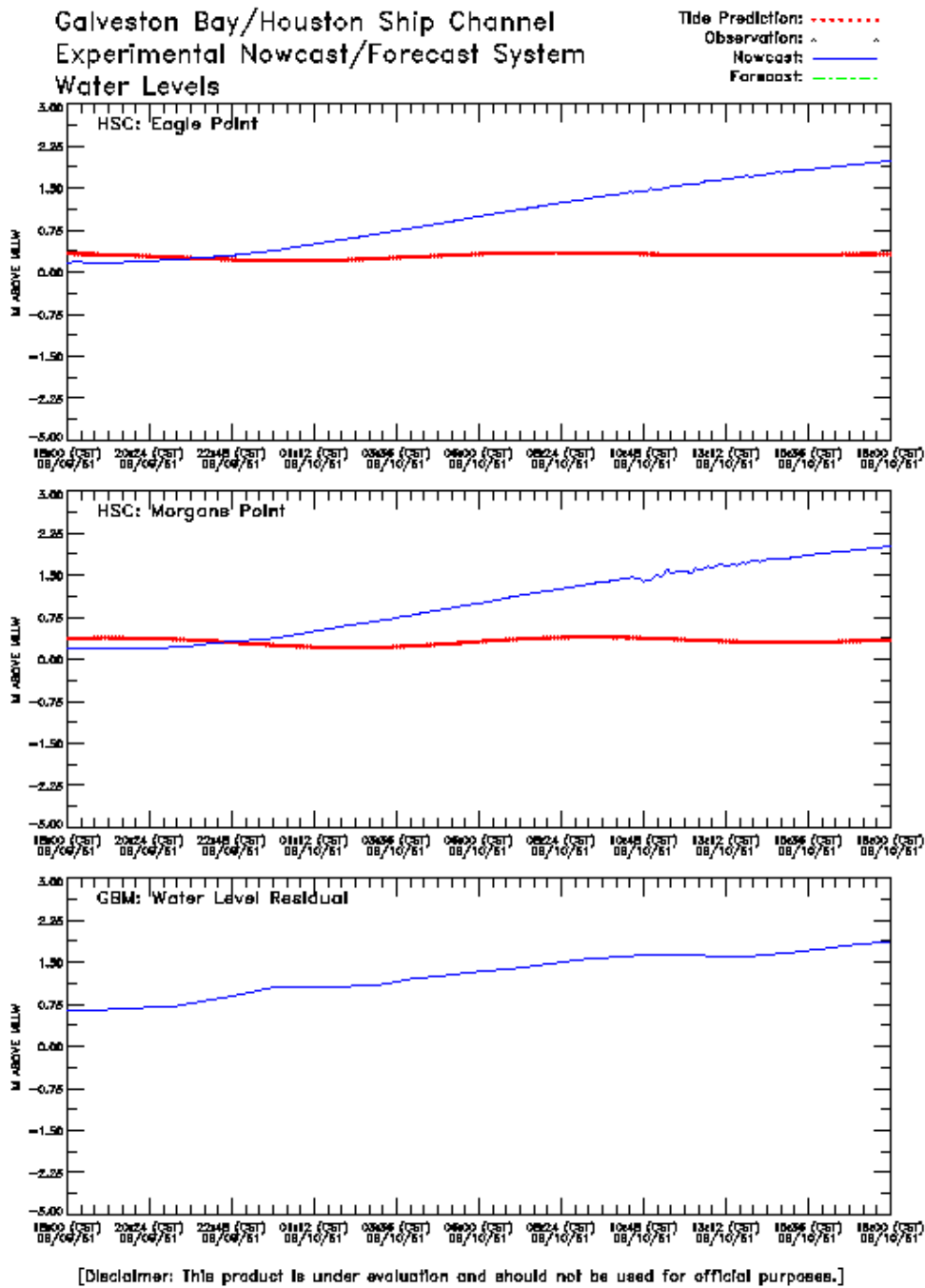


Figure 6.5. Hurricane Carla HSCM Water Levels and GBM Water Level Residual Experiment One: 9-10 September 1961

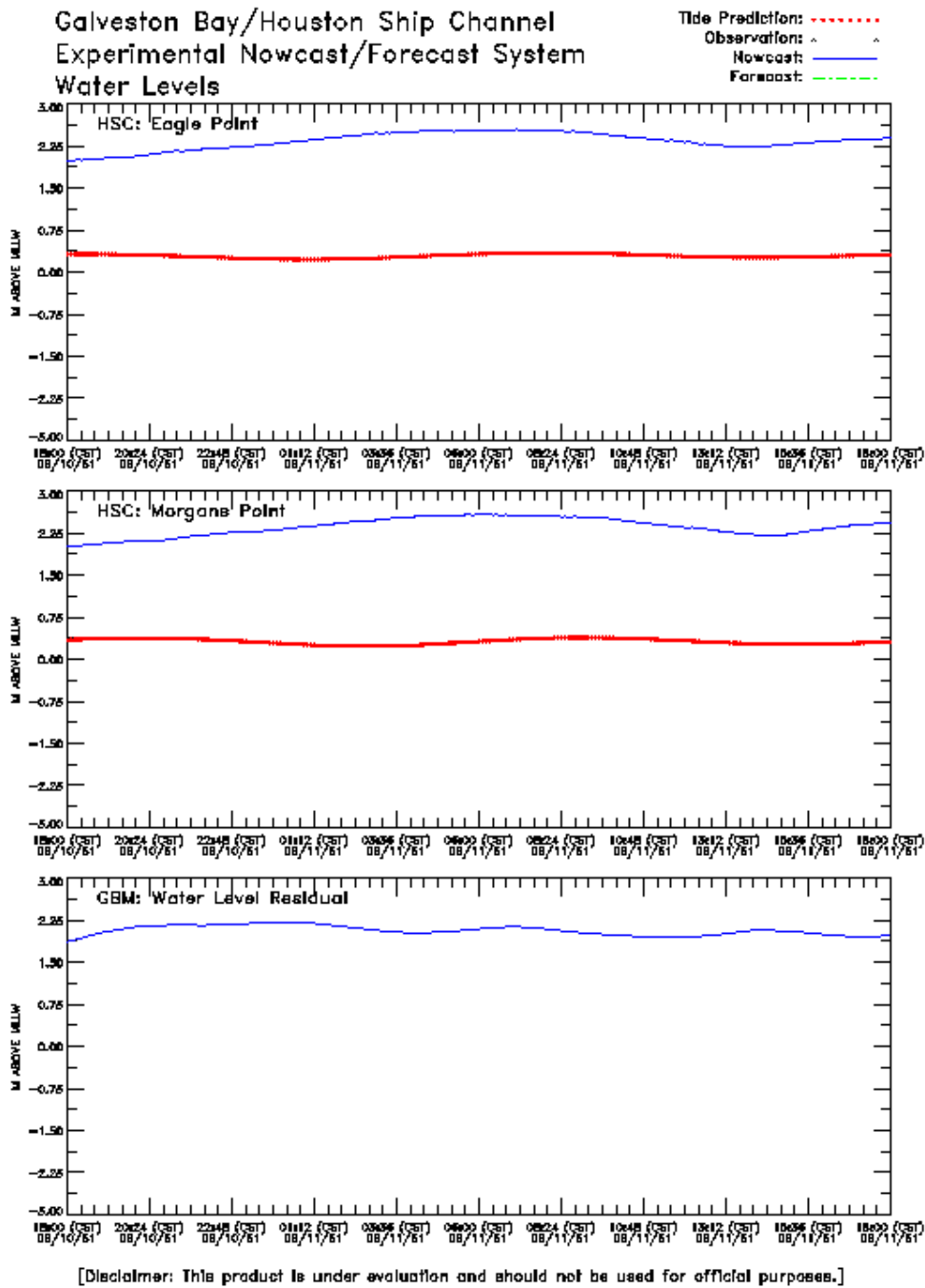


Figure 6.6. Hurricane Carla HSCM Water Levels and GBM Water Level Residual Experiment One: 10-11 September 1961

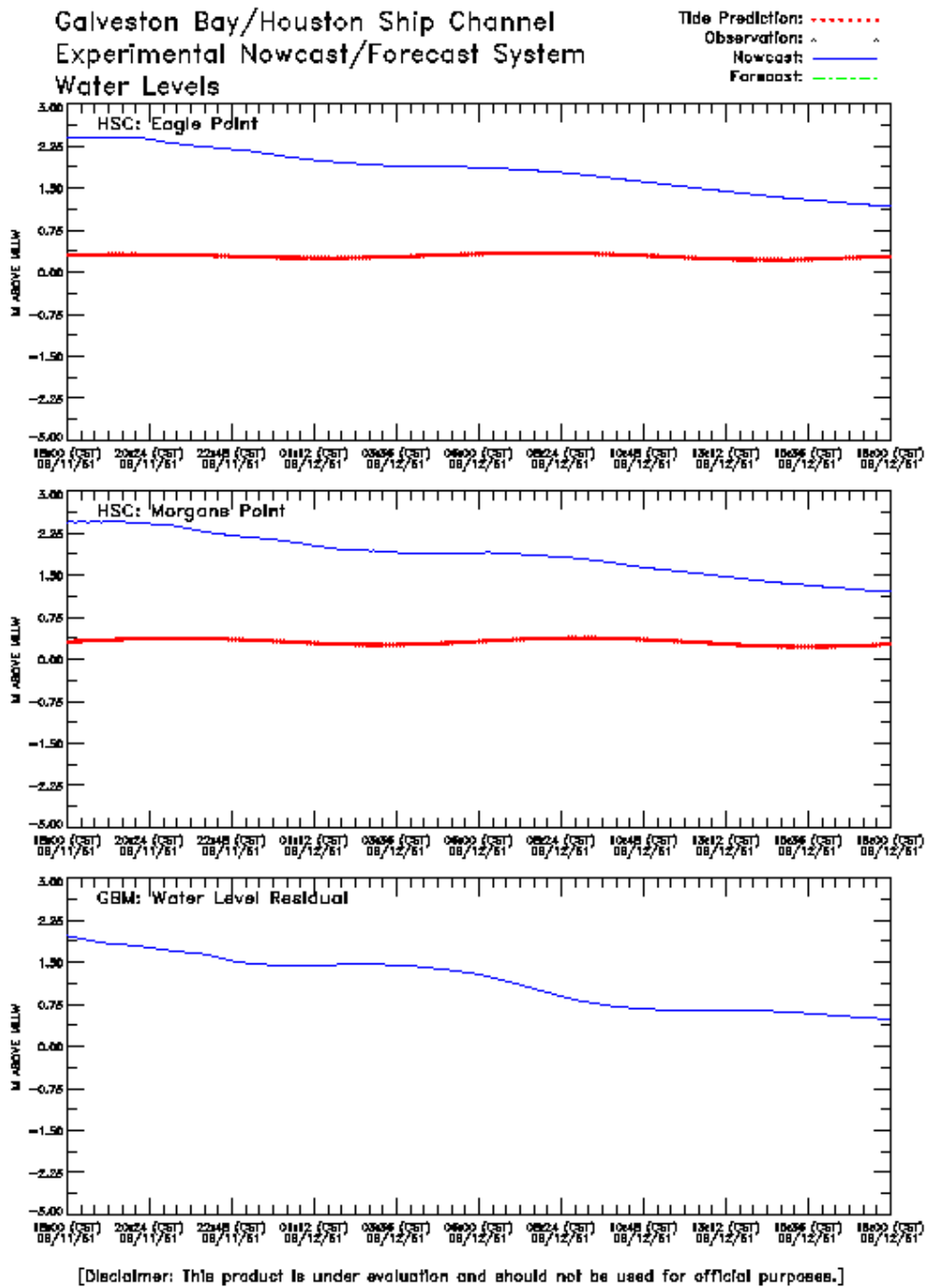


Figure 6.7. Hurricane Carla HSCM Water Levels and GBM Water Level Residual Experiment One: 11-12 September 1961

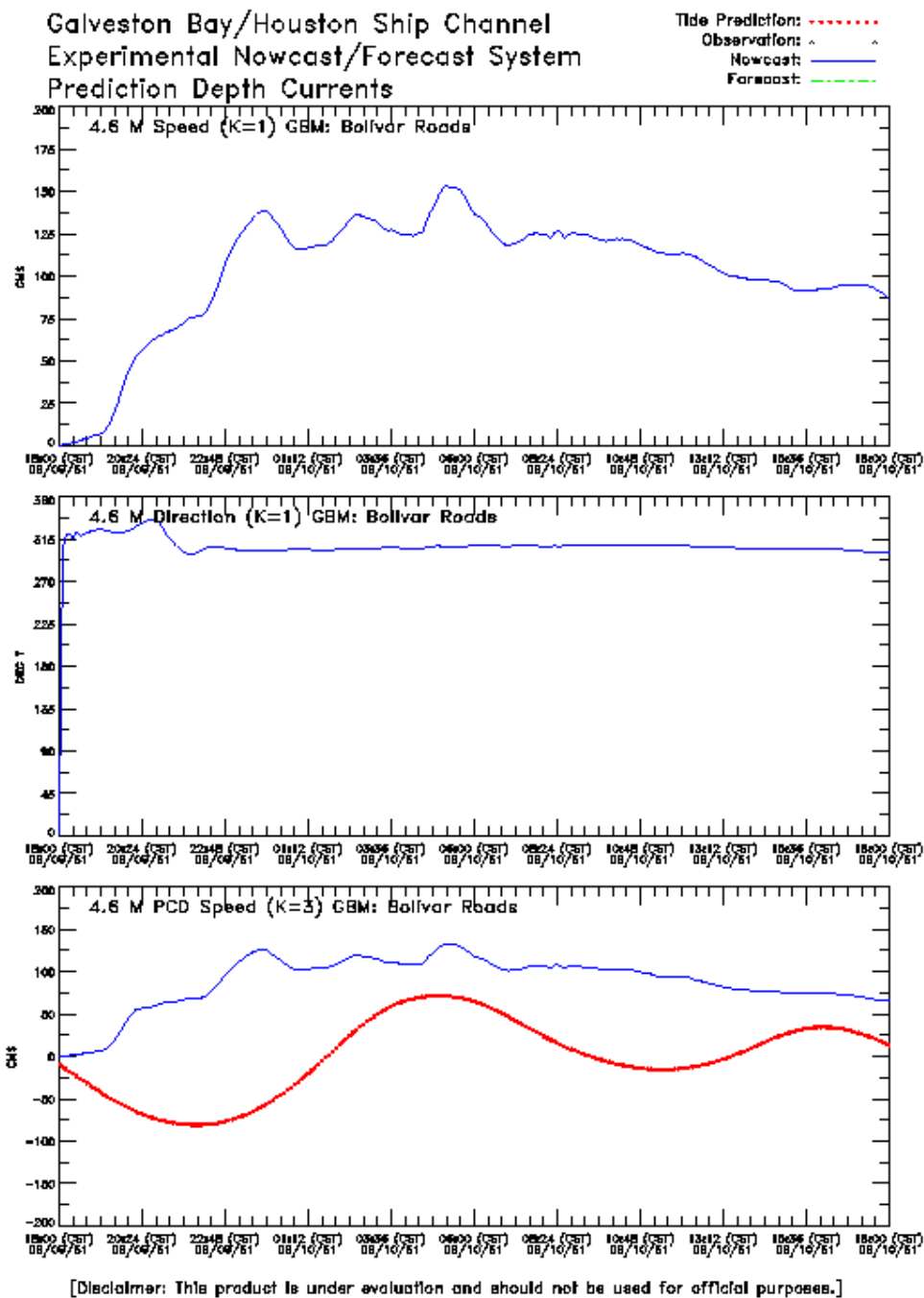


Figure 6.8. Hurricane Carla GBM Bolivar Roads Currents Experiment One: 9-10 September 1961

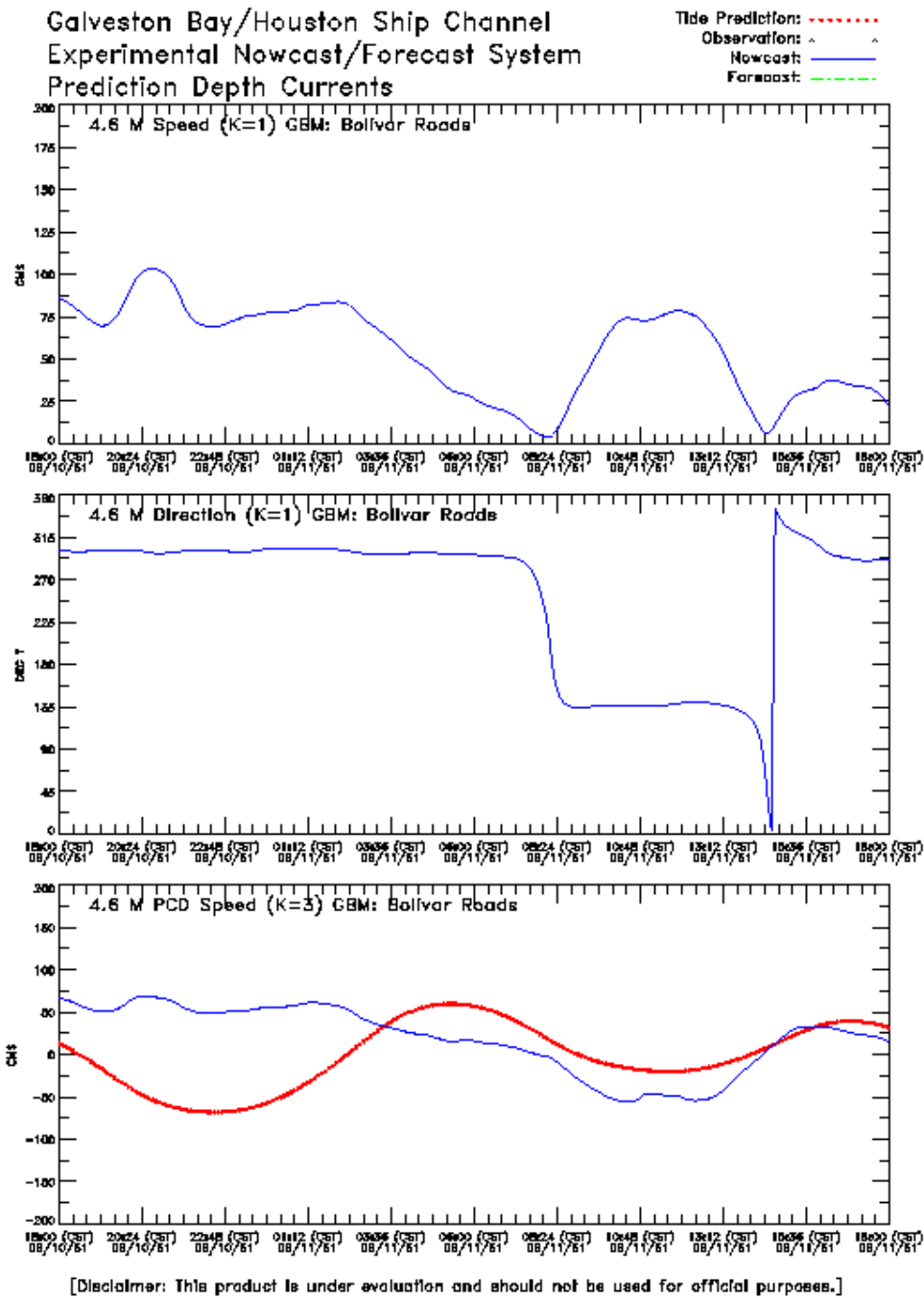


Figure 6.9. Hurricane Carla GBM Bolivar Roads Currents Experiment One: 10-11 September 1961

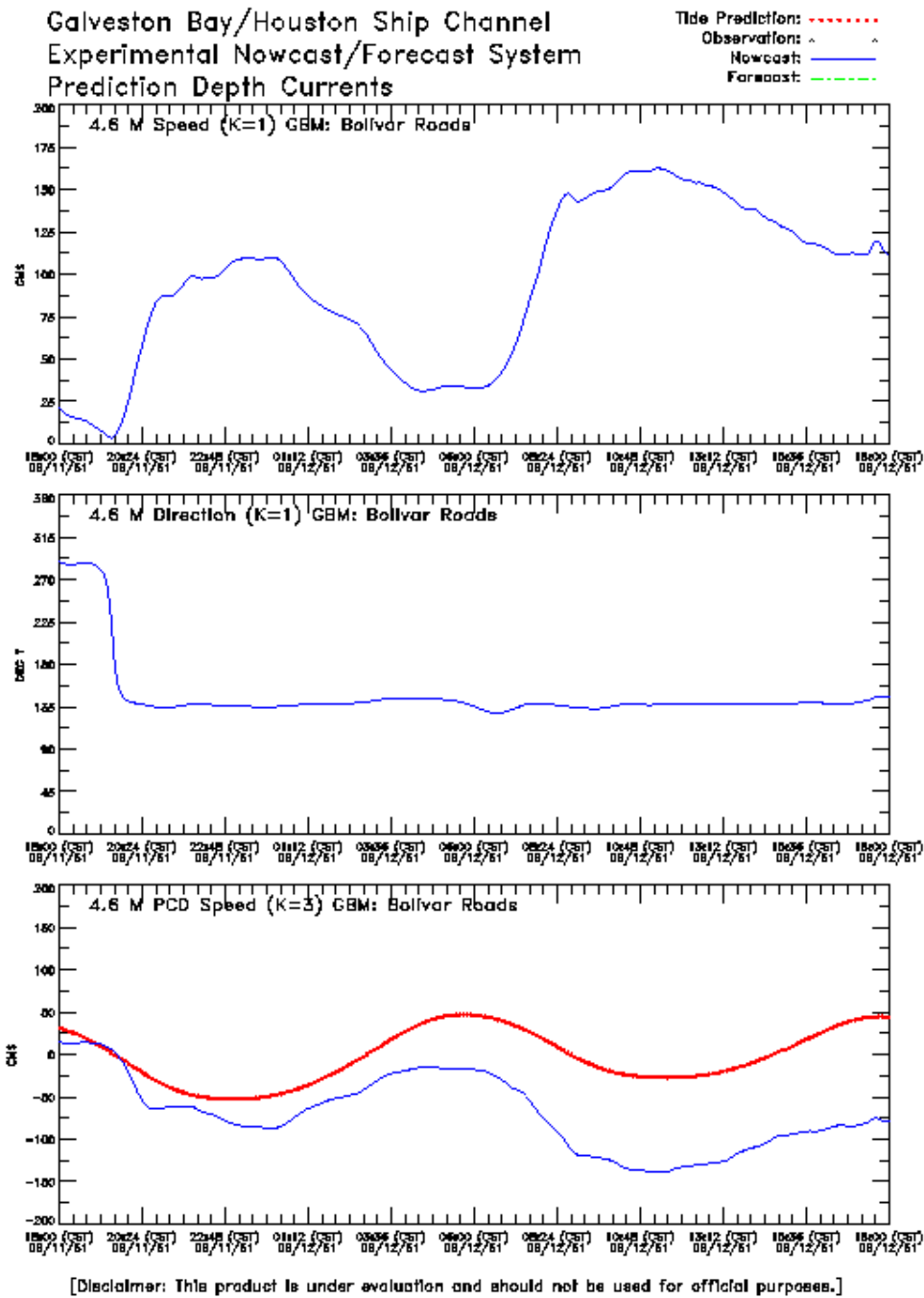


Figure 6.10. Hurricane Carla GBM Bolivar Roads Currents Experiment One: 11-12 September 1961

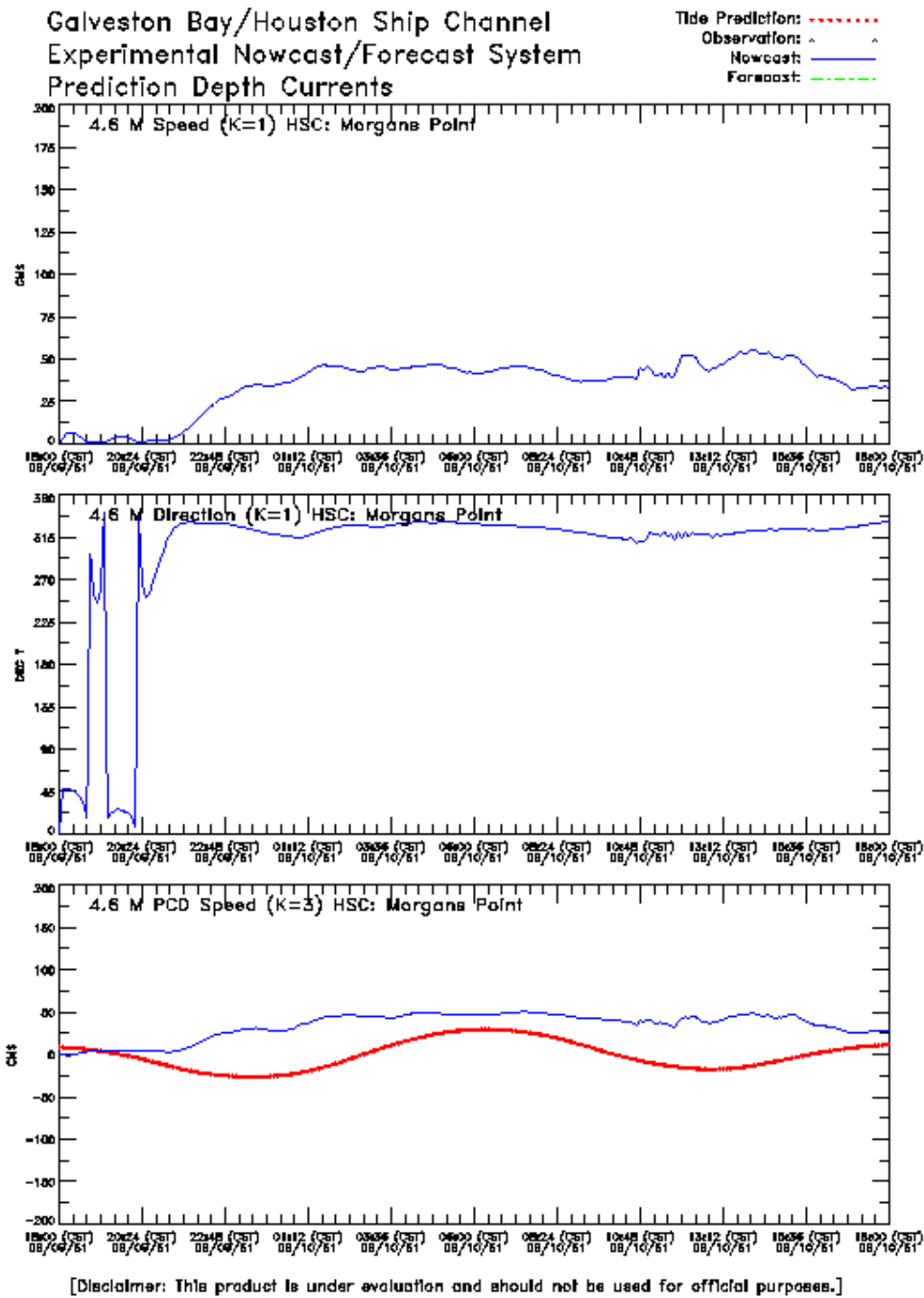


Figure 6.11. Hurricane Carla GBM Morgans Point Currents Experiment One: 9-10 September 1961

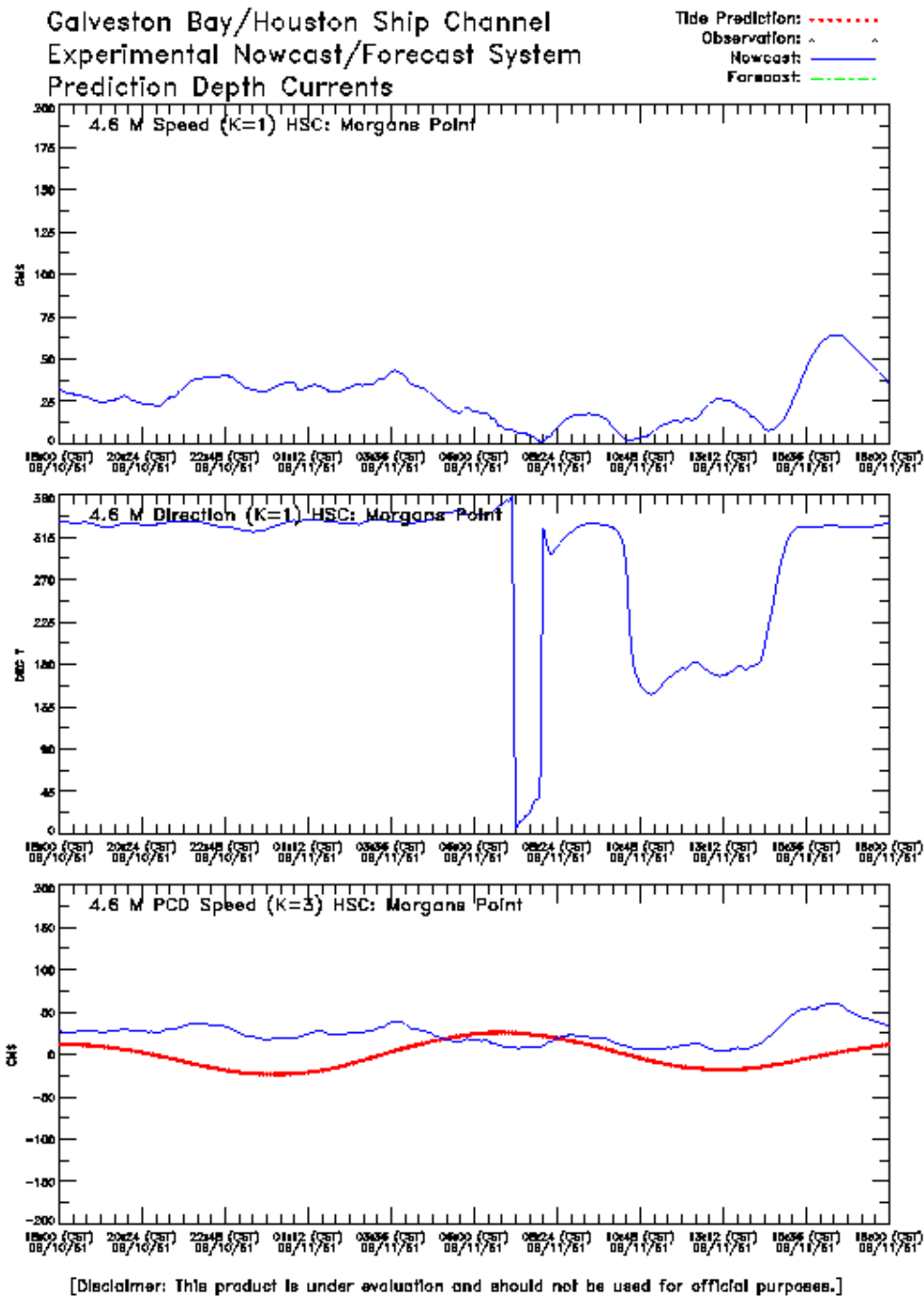


Figure 6.12. Hurricane Carla GBM Morgans Point Currents Experiment One: 10-11 September 1961

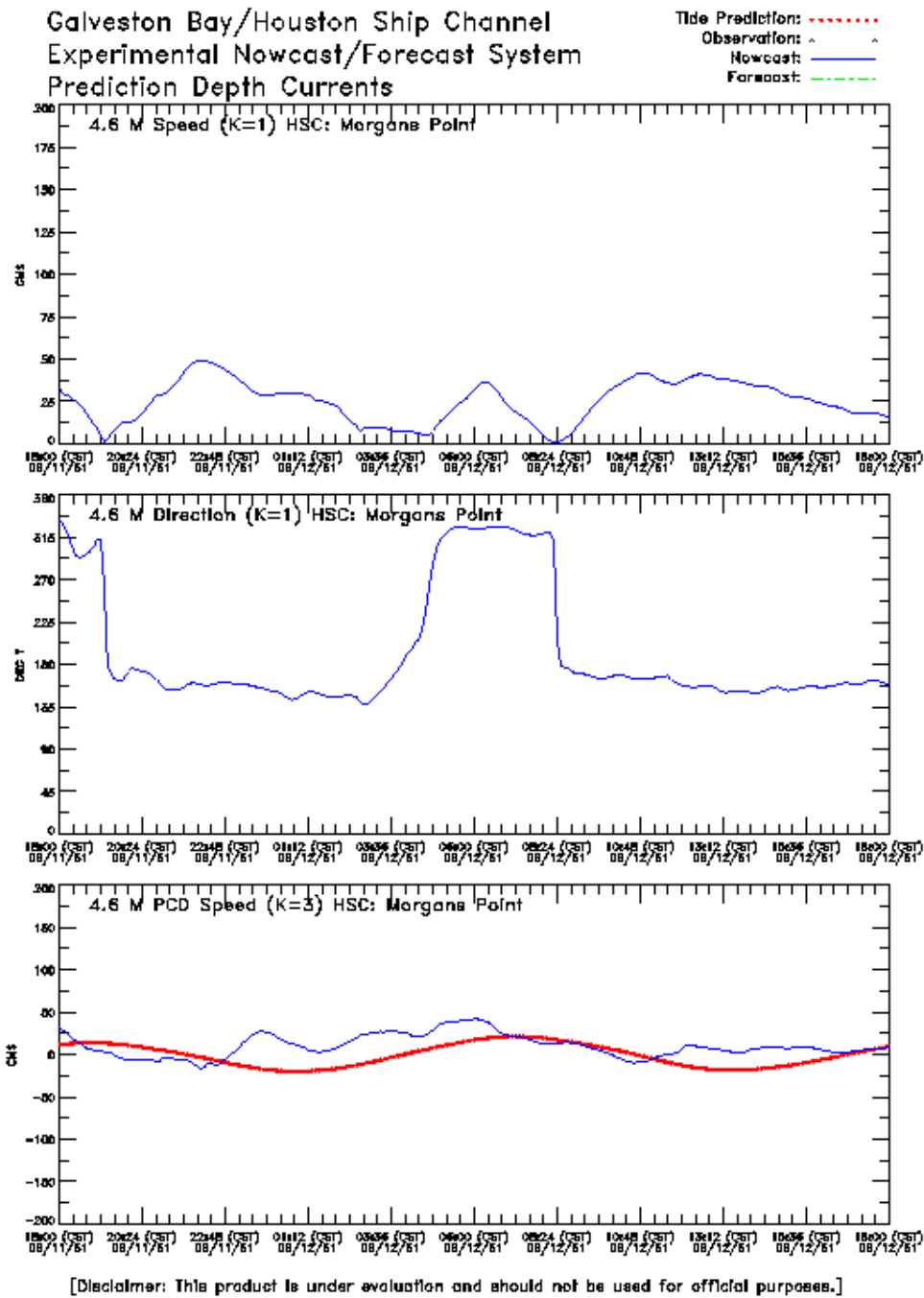


Figure 6.13. Hurricane Carla GBM Morgans Point Currents Experiment One: 11-12 September 1961

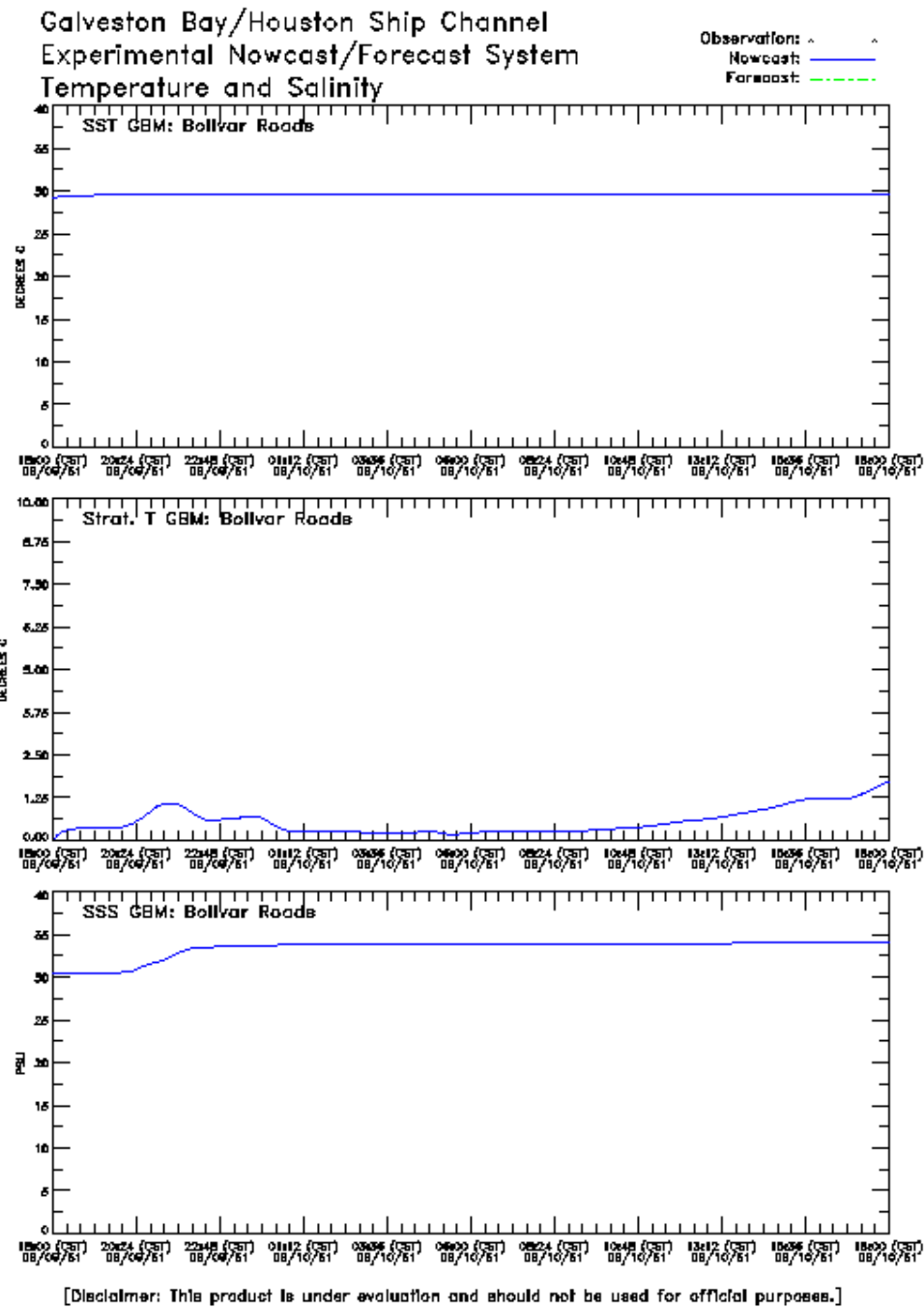


Figure 6.14. Hurricane Carla GBM Bolivar Roads Temperature and Salinity Experiment One: 9-10 September 1961

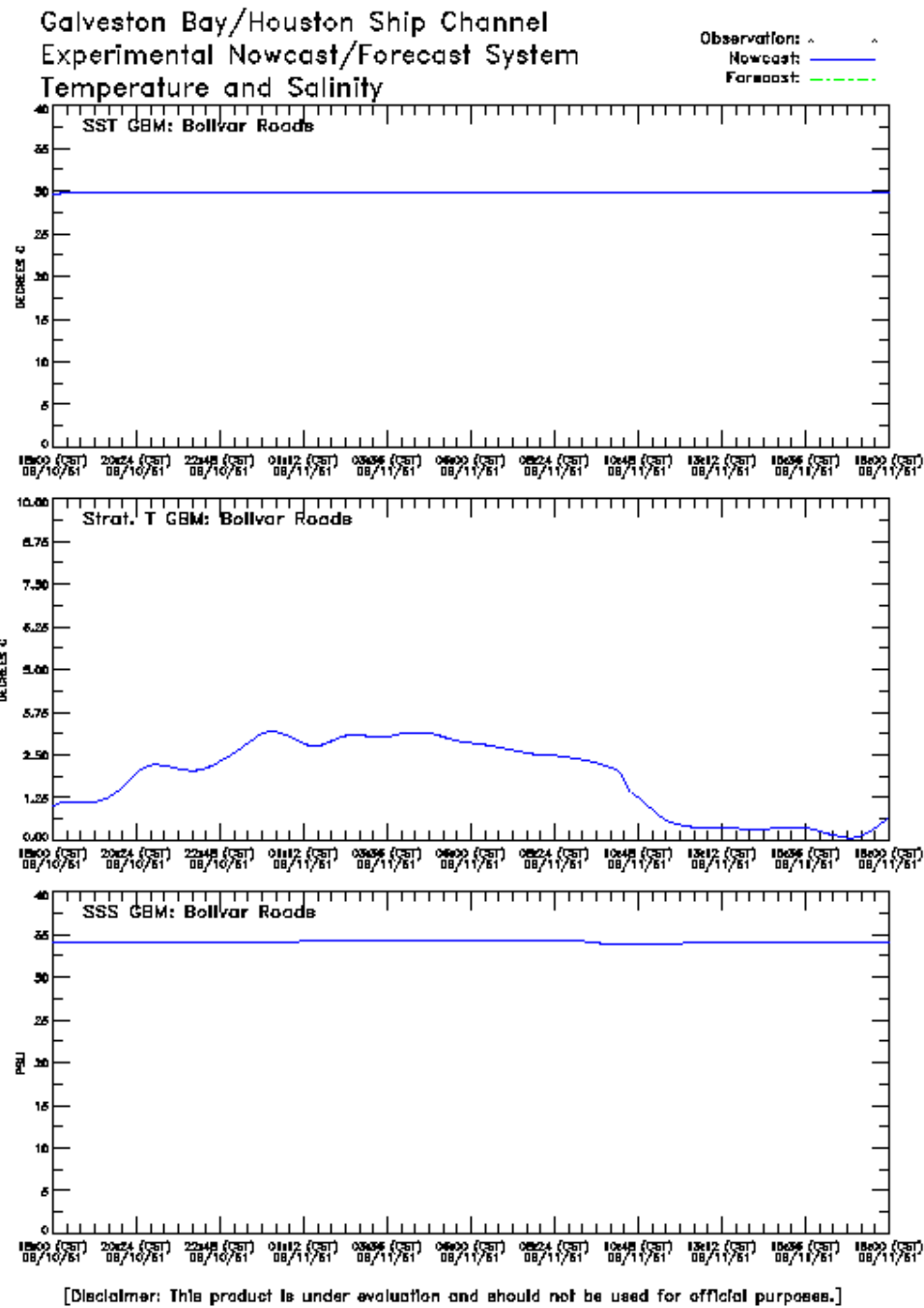


Figure 6.15. Hurricane Carla GBM Bolivar Roads Temperature and Salinity Experiment One: 10-11 September 1961

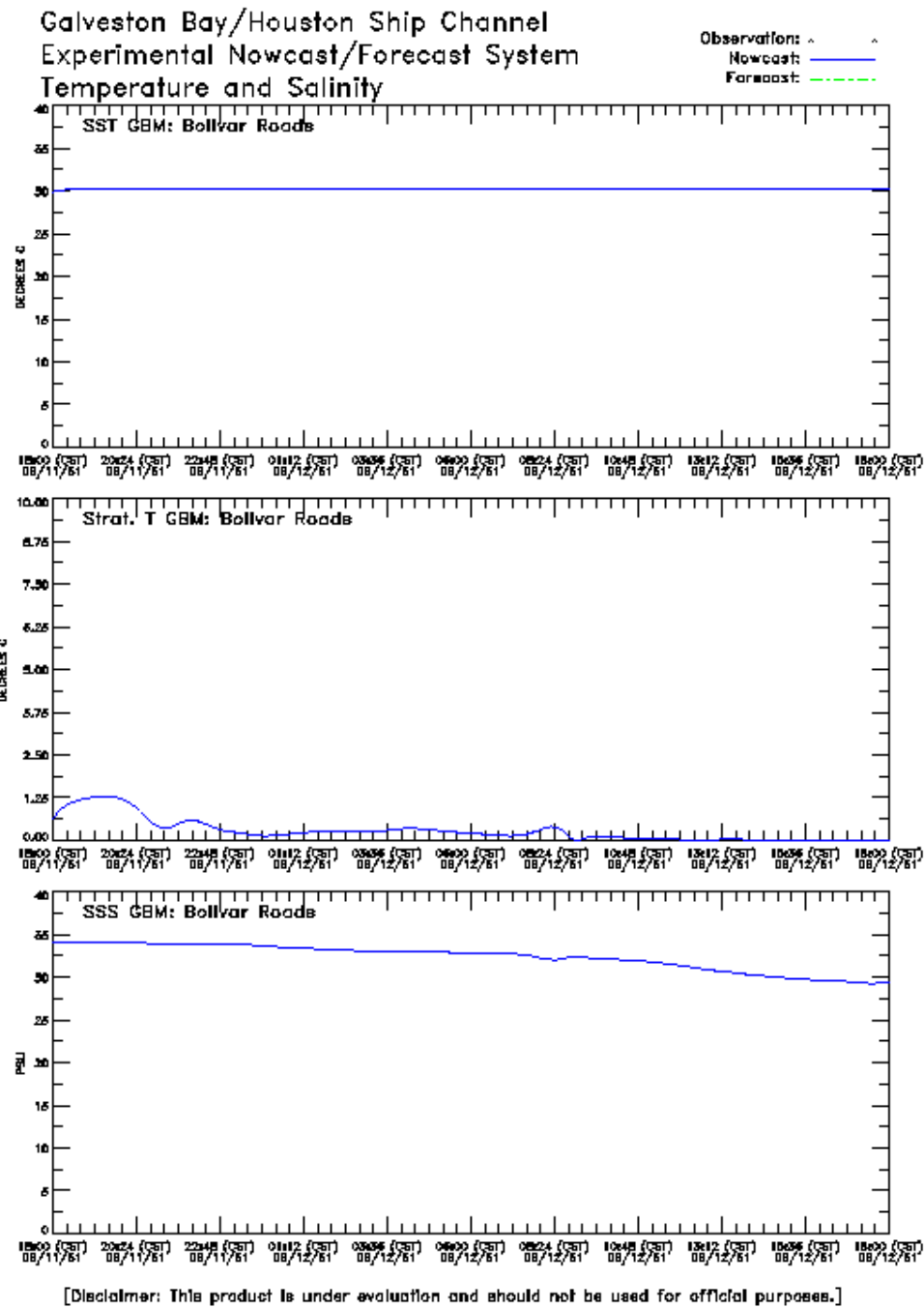


Figure 6.16. Hurricane Carla GBM Bolivar Roads Temperature and Salinity
Experiment One: 11-12 September 1961

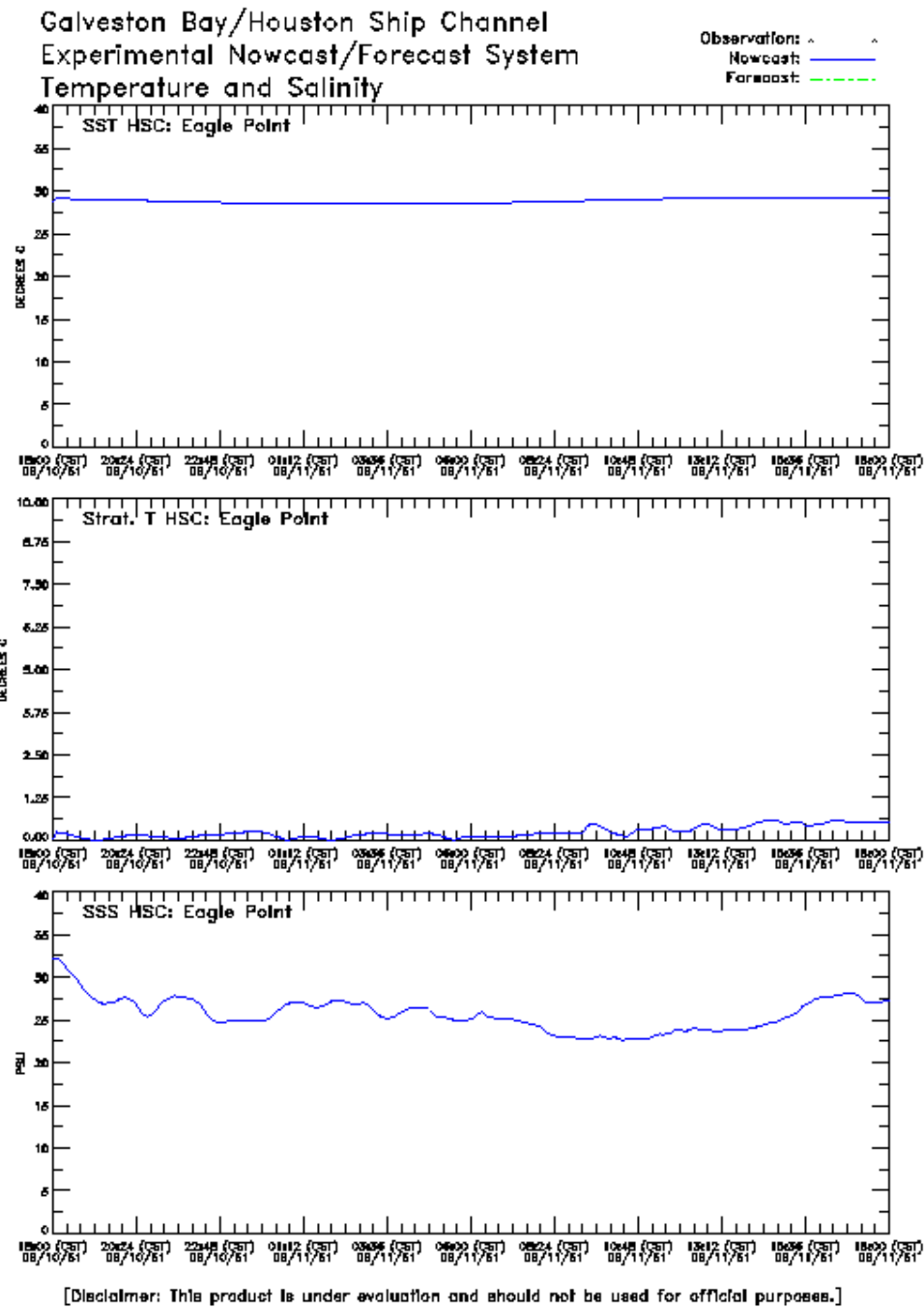


Figure 6.18. Hurricane Carla HSCM Eagle Point Temperature and Salinity
Experiment One: 10-11 September 1961

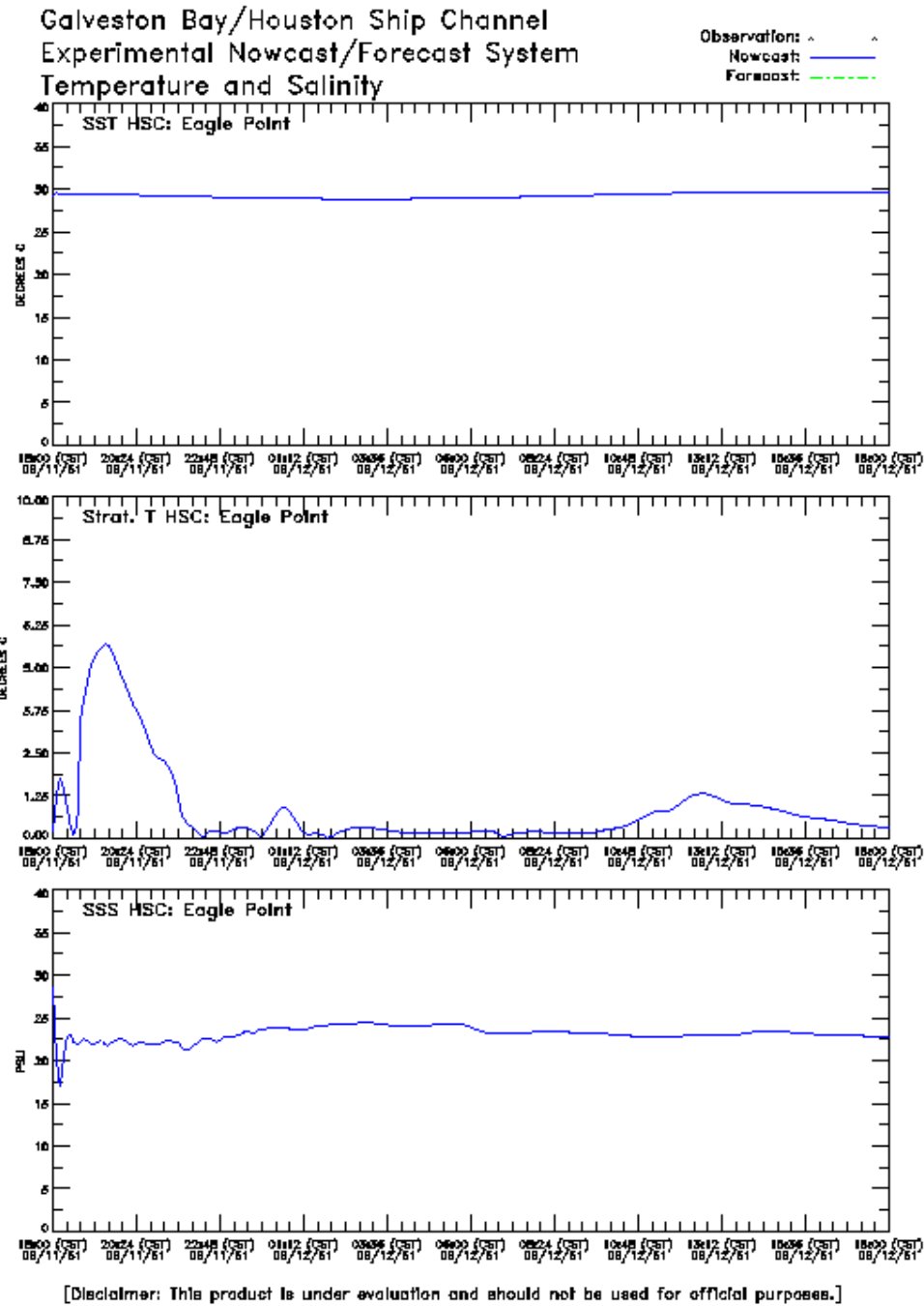


Figure 6.19. Hurricane Carla HSCM Eagle Point Temperature and Salinity Experiment One: 11-12 September 1961

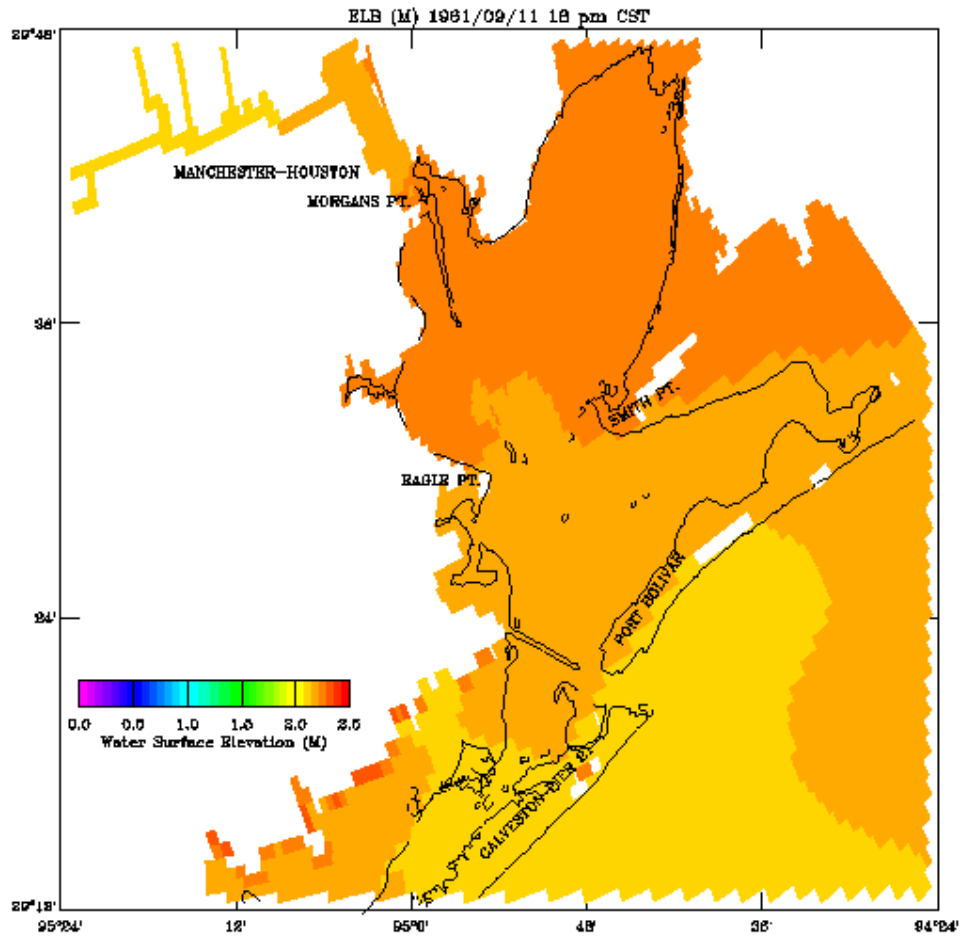


Figure 6.20. Hurricane Carla GBM Water Surface Elevation Field
Experiment One: 11 September 1961 18:00 CST

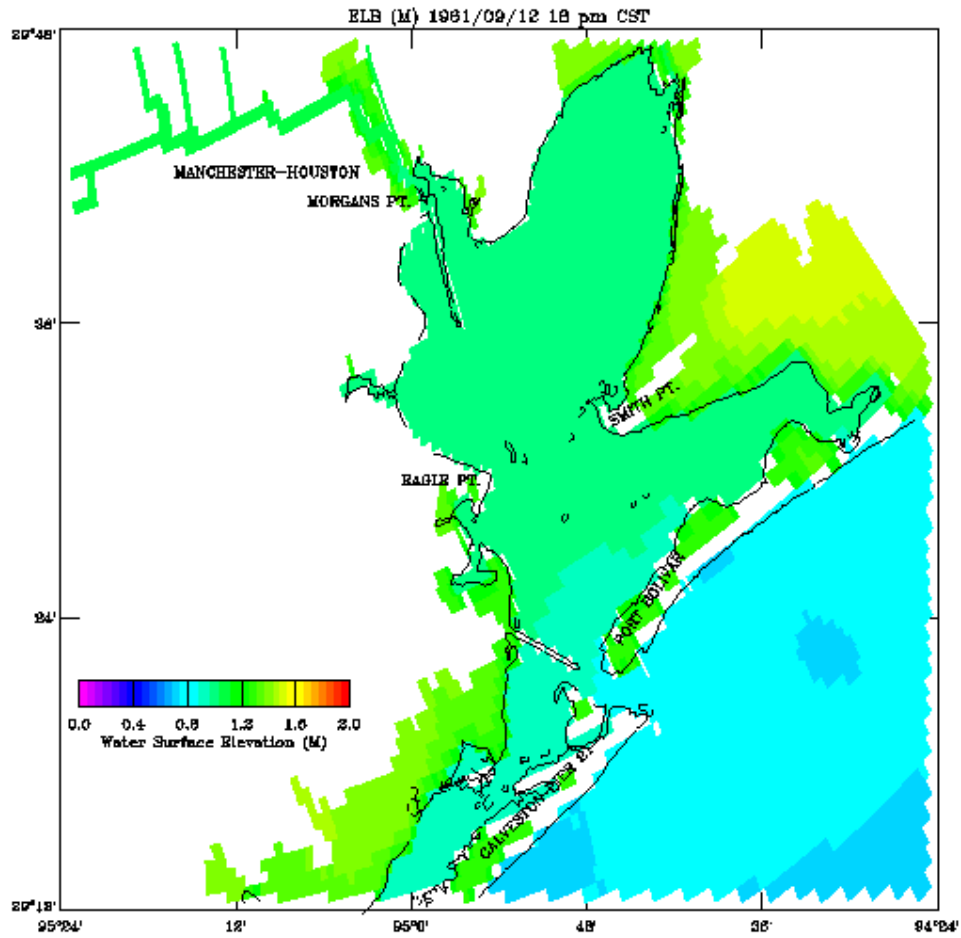


Figure 6.21. Hurricane Carla GBM Water Surface Elevation Field
Experiment One: 12 September 1961 18:00 CST

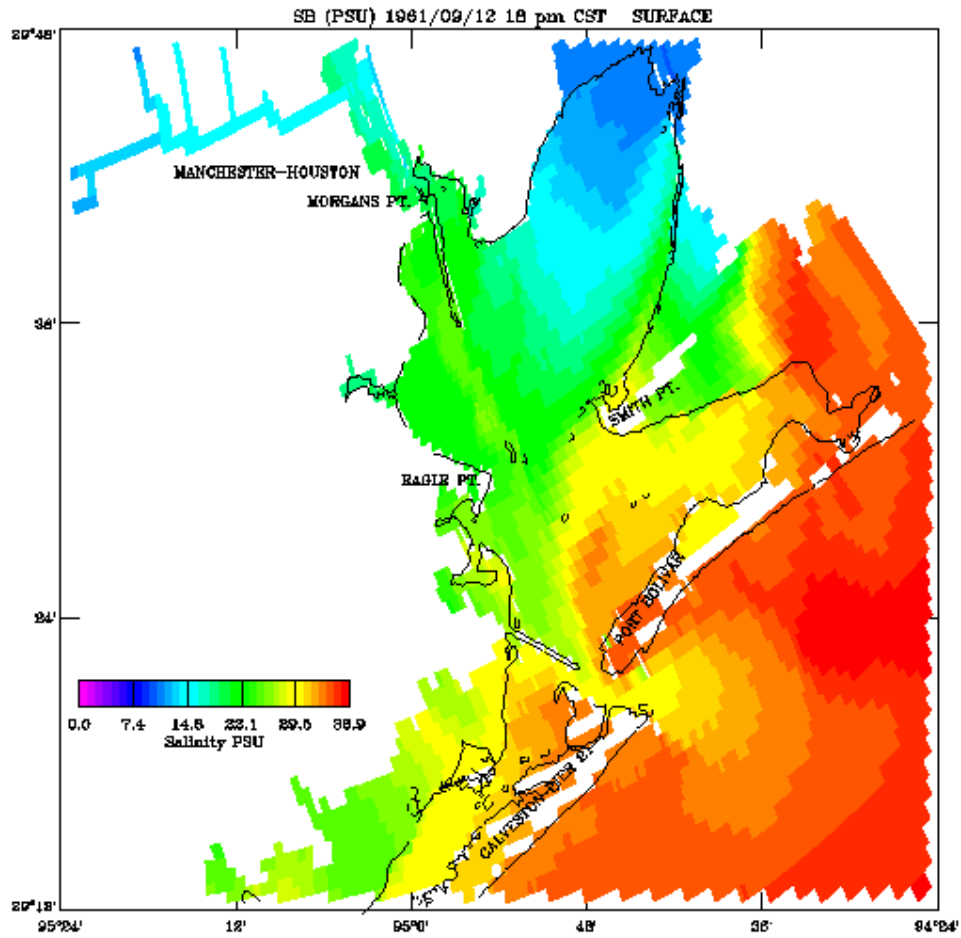


Figure 6.22. Hurricane Carla GBM Near Surface Salinity Field
 Experiment One: 12 September 1961 18:00 CST

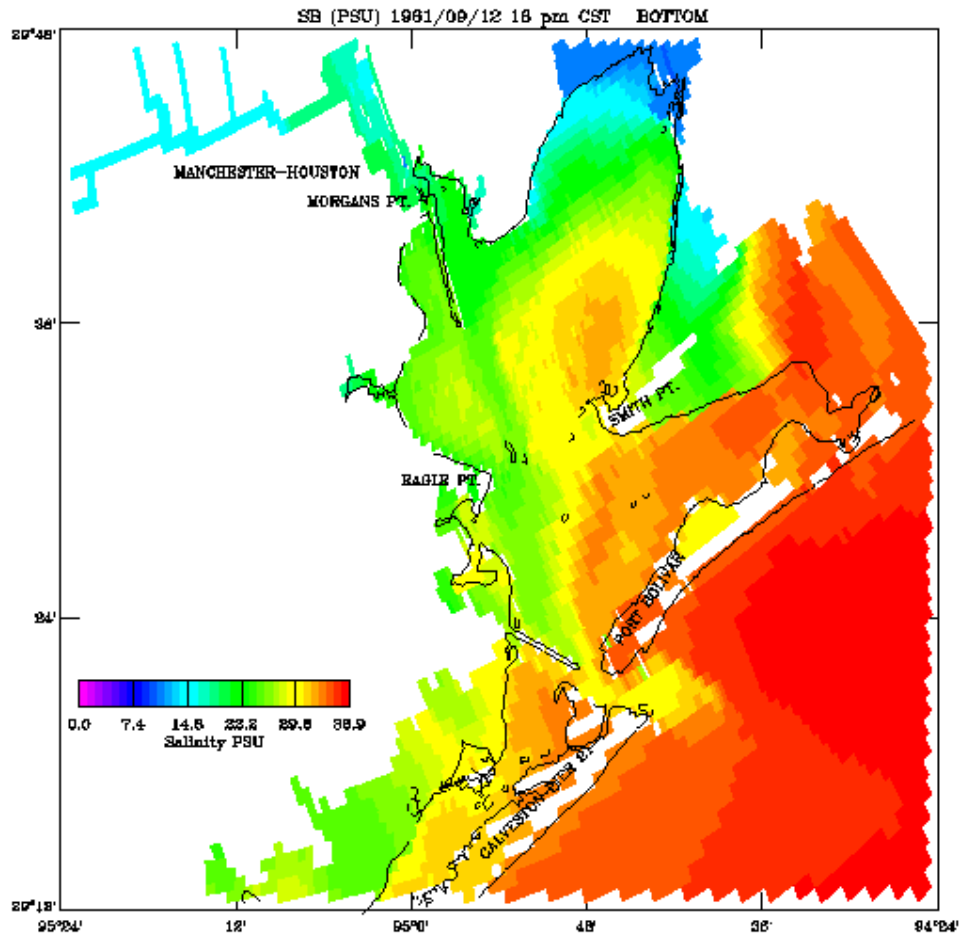


Figure 6.23. Hurricane Carla GBM Near Bottom Salinity Field
Experiment One: 12 September 1961 18:00 CST

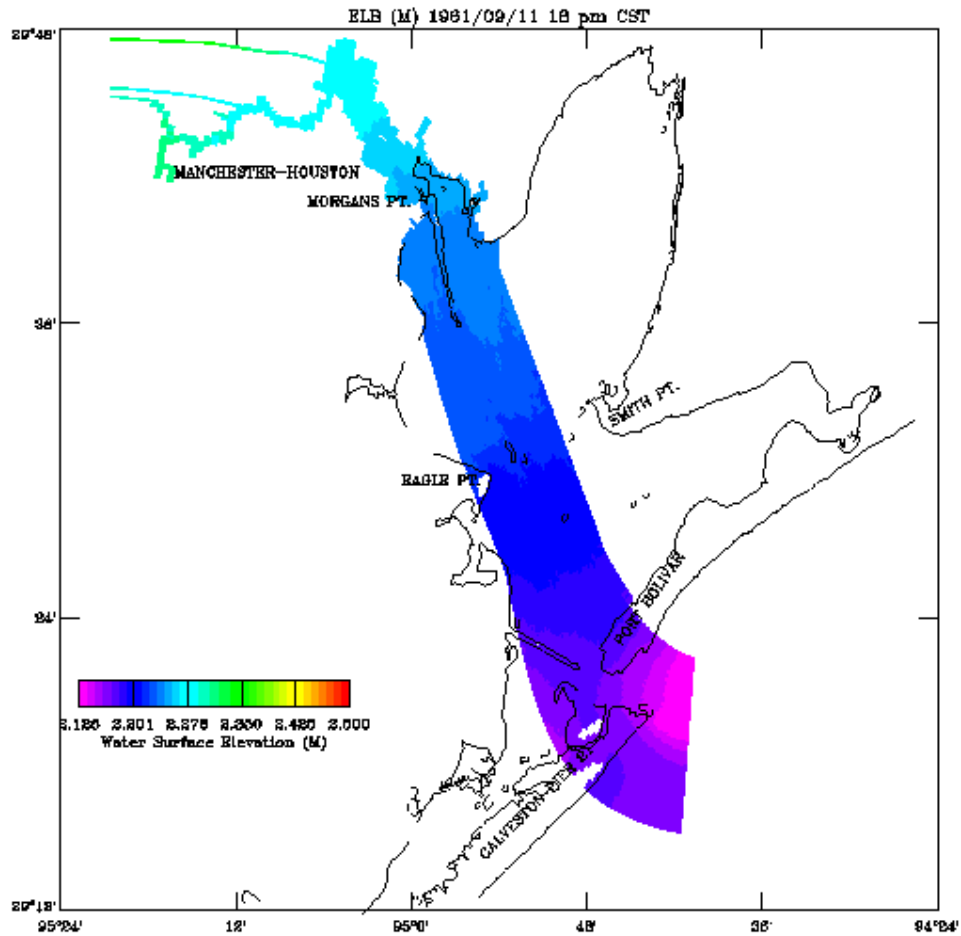


Figure 6.24. Hurricane Carla HSCM Water Surface Elevation Field
Experiment One: 11 September 1961 18:00 CST

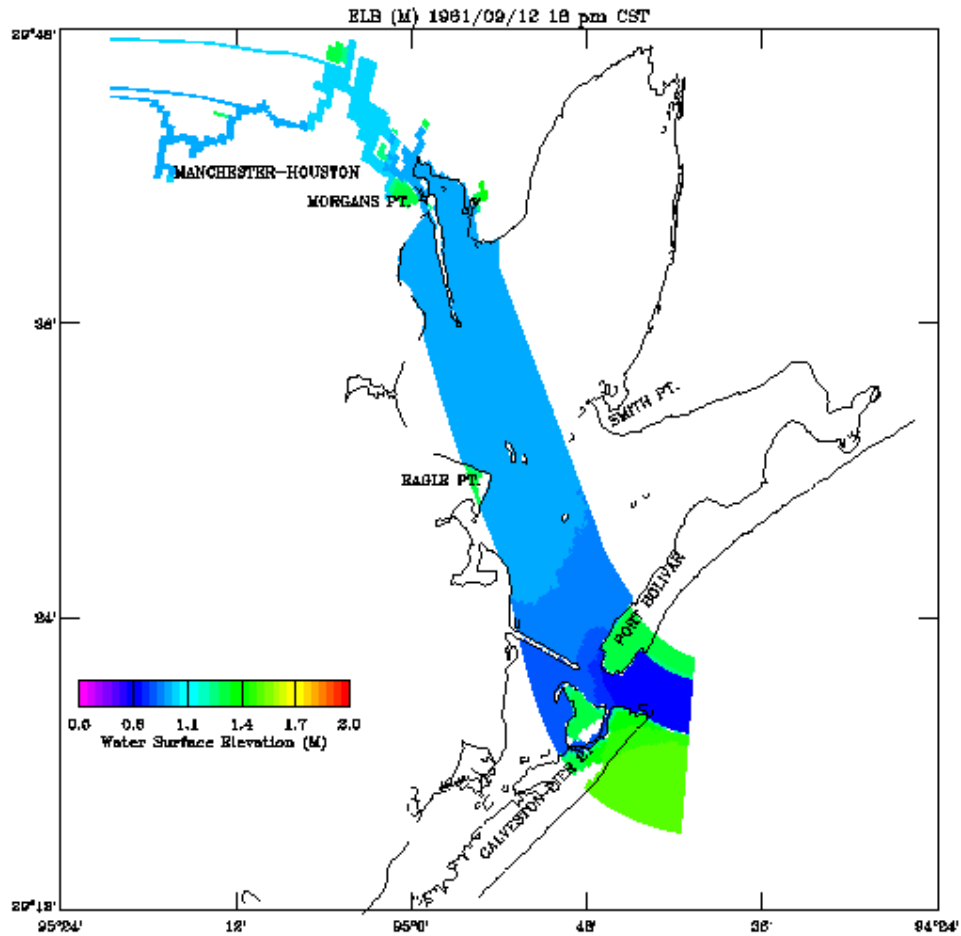


Figure 6.25. Hurricane Carla HSCM Water Surface Elevation Field
Experiment One: 12 September 1961 18:00 CST

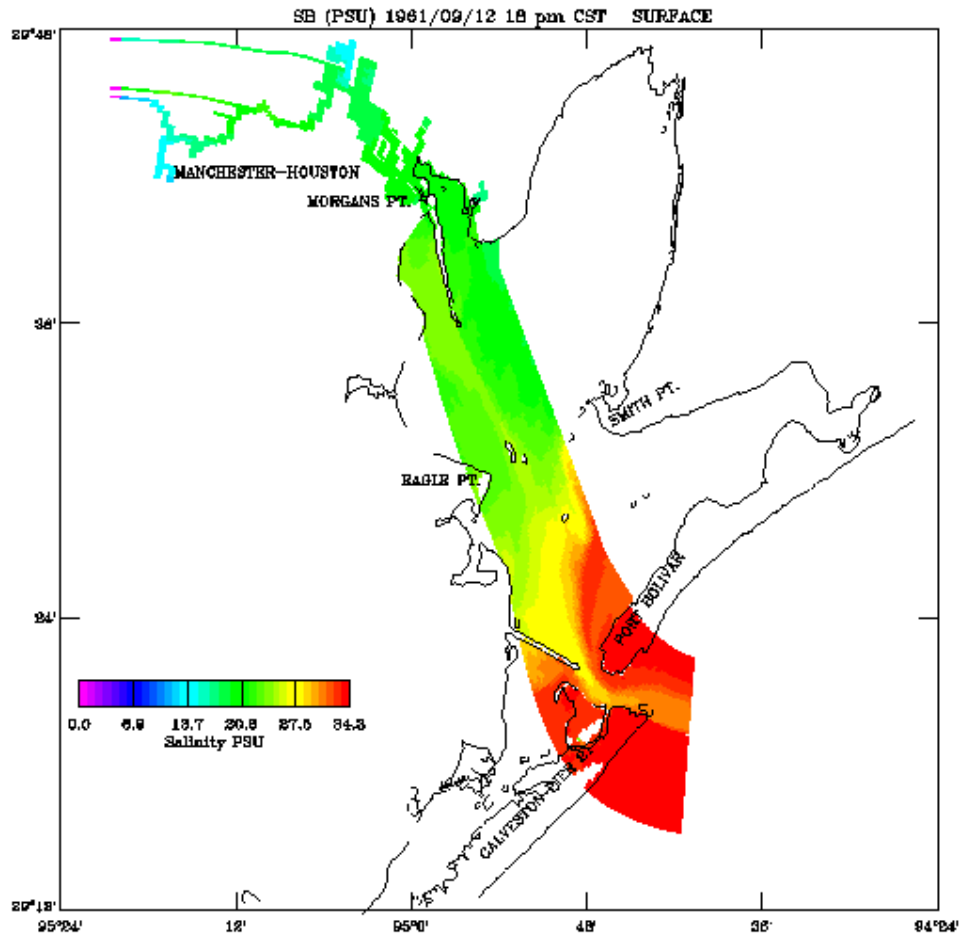


Figure 6.26. Hurricane Carla HSCM Near Surface Salinity Field
Experiment One: 12 September 1961 18:00 CST

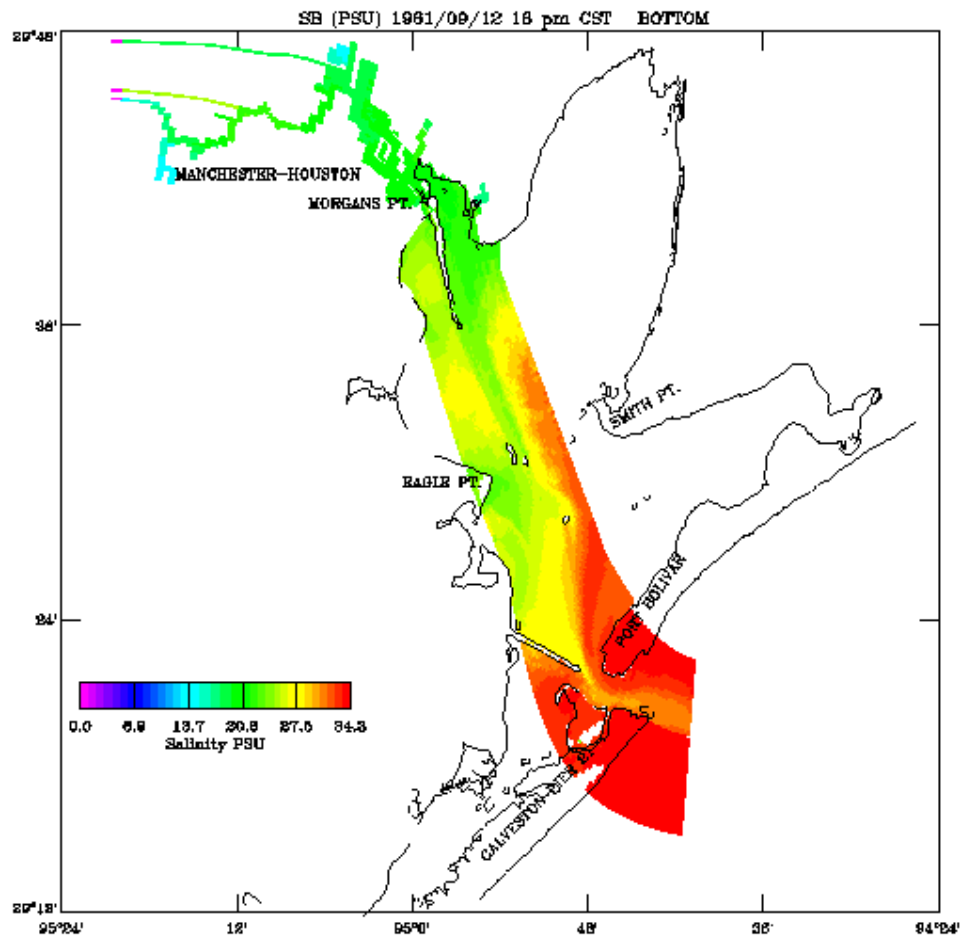


Figure 6.27. Hurricane Carla HSCM Near Bottom Salinity Field
Experiment One: 12 September 1961 18:00 CST

6.4. Experiment One Short Wave Results

Unfortunately, no wave information was available and the results must be judged as being representative of hurricane wave conditions. Since in this experiment, no wind forcing was applied, the results contain no wind generation effects and only use an empirical reduction formula to reduce the offshore boundary wave condition generated using Equation 5.13.

Simulated significant wave height for each of the three hindcasts is shown at Galveston Pleasure Pier, Bolivar Roads, and Galveston Pier 21 in Figures 6.28 – 6.30. One notes the prolonged duration of elevated simulated wave heights on top of the simulated elevated water levels noted in the long wave results and the potential for overland flooding and overtopping of the barrier islands with accompanying large waves order 5m. In Figures 6.31 – 6.33, HSCM simulated significant wave heights are shown for each hindcast at Eagle Point and Morgans Point with maximum significant wave heights of 2.7m and 2.5m, respectively. In the third panel of these figures, the simulated significant wave height at NDBC buoy 42035 is given, which represents the GBM open boundary wave condition. This significant wave height is applied uniformly in space over the entire GBM open water boundary. Note the maximum simulated significant wave heights are order 10m.

Simulated significant wave direction for each of the three hindcasts were considered at Galveston Pleasure Pier, Bolivar Roads, and Galveston Pier 21 in the GBM and for the HSCM at Eagle Point and Morgans Point, respectively. The simulated significant wave direction at NDBC buoy 42035 represents the GBM open boundary wave condition. This significant wave direction is applied uniformly in space over the entire GBM open water boundary. Note in the case of no wind generation, the significant wave direction is equal to the offshore boundary condition in all interior grid cells and varies in time based on the relation given in Equation 5.13. As a result, wave directions are the same for all of the above stations and are near 315 degrees True.

Simulated significant wave period for each of the three hindcasts are shown at Galveston Pleasure Pier, Bolivar Roads, and Galveston Pier 21 in Figures 6.34–6.36. In Figures 6.37-6.39, HSCM simulated significant wave periods are shown for each hindcast at Eagle Point and Morgans Point, respectively. In the third panel of these figures, the simulated significant wave period at NDBC buoy 42035 is given, which represents the GBM open boundary wave condition. This significant wave period is applied uniformly in space over the entire GBM open water boundary. Note in the case of no wind generation, the significant wave period as given in Equation 5.13 is a function of significant wave height, which is based on empirical reduction. As a result, wave periods are the similar in form for all of the above stations. Note the maximum simulated significant wave periods are order 18s.

GBM simulated significant wave height and direction vectors are shown at the end of hindcast two in Figure 6.40. At the end of the first hindcast the barrier islands have been

overtopped and that flooding has occurred and wave computations have been performed over the flooded cells. At present no distinction is made between a flooded cell and a cell which is always wet in the wave computation method. At the end of the second hindcast in Figure 6.40, the flooding has progressed further inland, while at the end of the third hindcast some of the flooded areas have dried. It should be noted that in the present model, no drainage or seepage flows are computed and as result, there is no mechanism for the water to be removed from the majority of flooded grid cells. For all water cells, wave conditions are computed. Simulated significant wave heights are in the range from 1 m in upper Trinity Bay to 10m near the offshore boundary. Note in the present case of no wind generation, simulated significant wave directions are near 315 deg True for all grid cells.

Next GBM simulated significant wave period contours are shown in Figure 6.41 at the end of hindcast two. One should note that wave computations are performed over the flooded areas and as the water recedes, while the flooded cells become inactive in the long wave computations, wave computations continue to be performed over these grid cells. Simulated significant wave periods range from below 1s in upper Trinity Bay to over 14s near the offshore boundary.

HSCM simulated significant wave height and direction at the end of hindcast two in Figure 6.42. Simulated significant wave heights are in the range of 1 to 5 m consistent with those computed in the GBM. Note in the present case of no wind generation, significant wave directions are near 315 deg True for all grid cells as determined in the GBM.

Next HSCM simulated significant wave period contours are shown in Figure 6.43 at the end of hindcast two. One should note that wave computations are performed over the flooded areas and as the water recedes, while the flooded cells become inactive in the long wave computations, wave computations continue to be performed over these grid cells. Simulated significant wave periods are in the range of 1 to 7s consistent with those computed over the GBM.

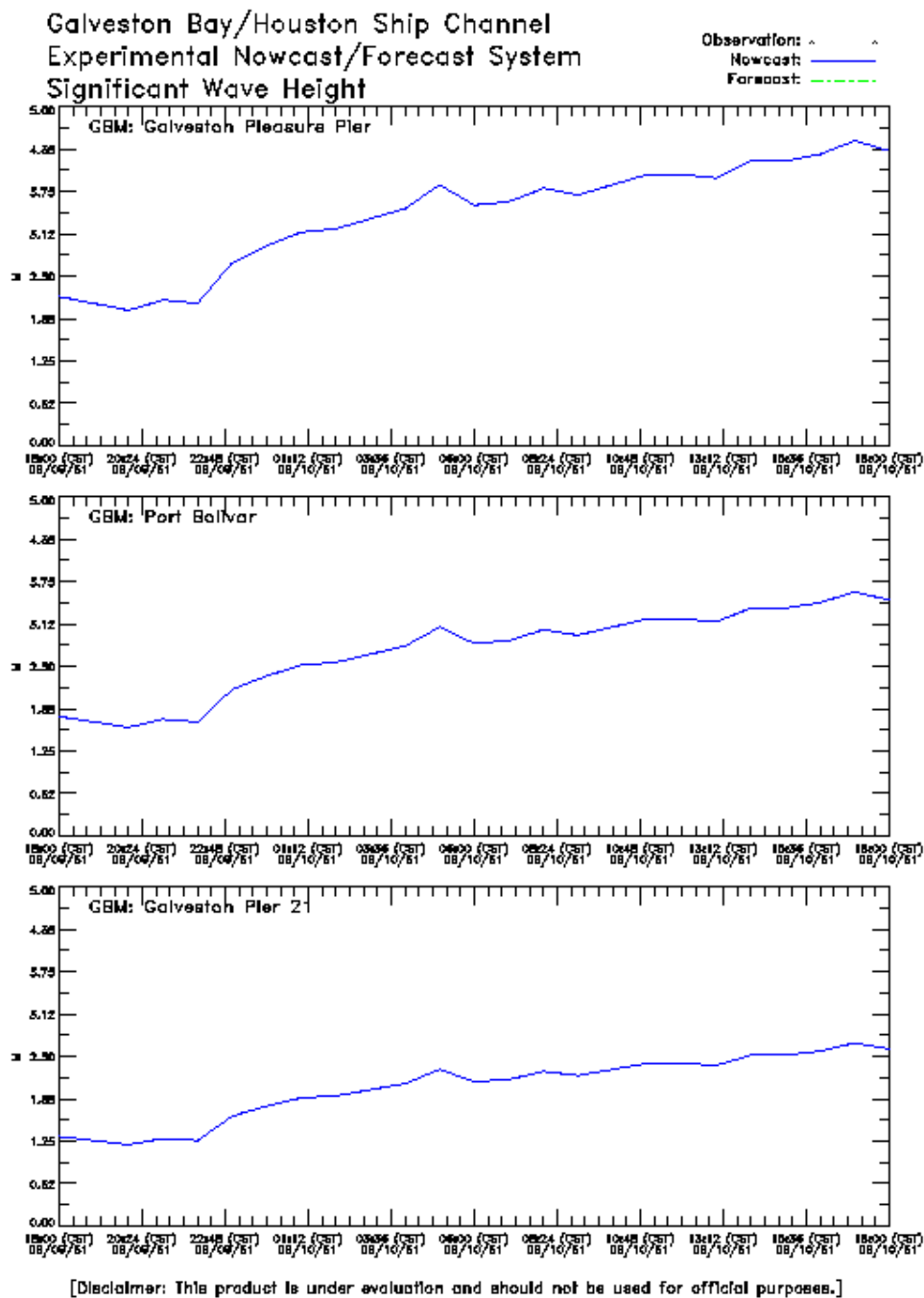


Figure 6.28. Hurricane Carla GBM Significant Wave Height Experiment One:
9-10 September 1961

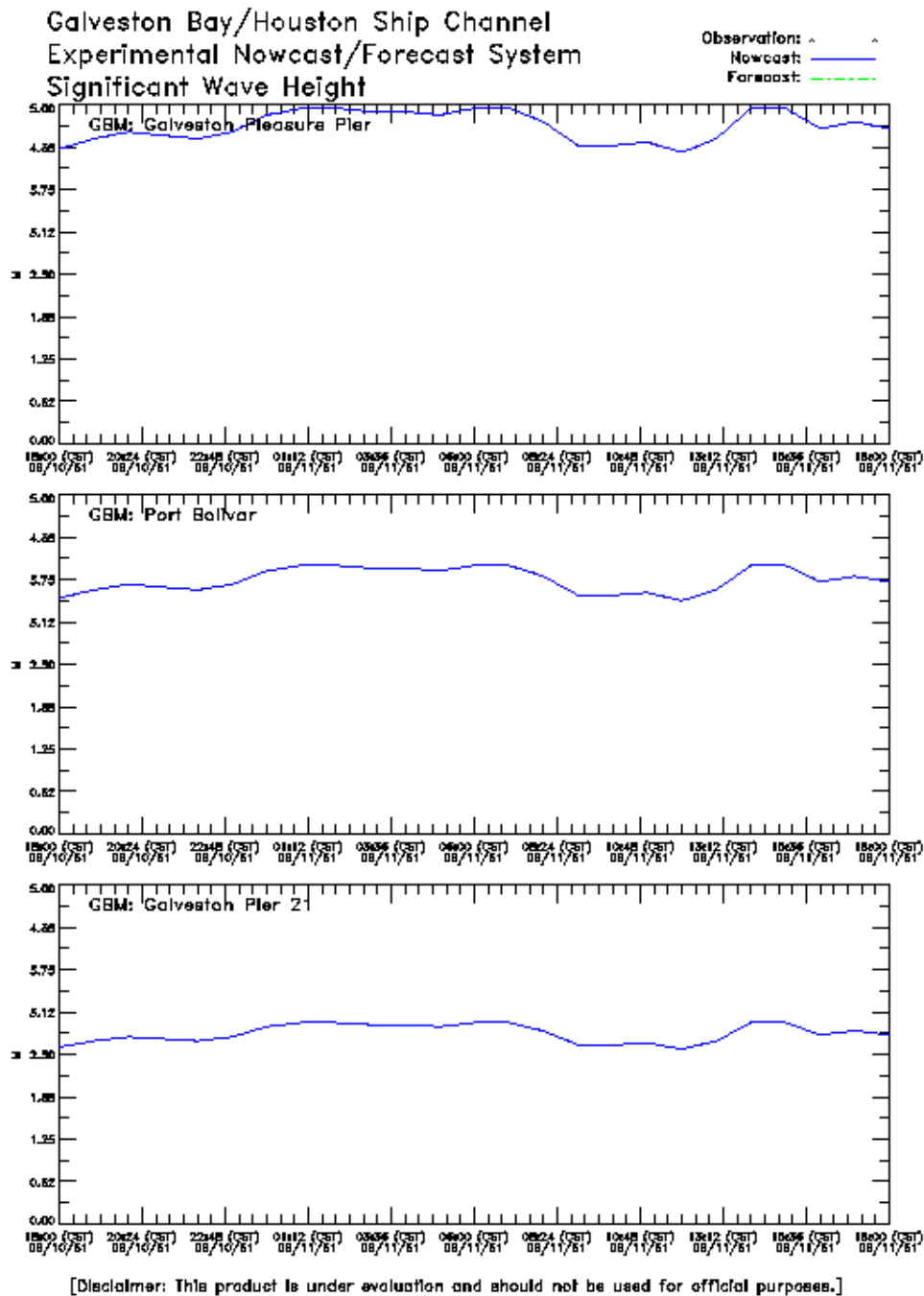


Figure 6.29. Hurricane Carla GBM Significant Wave Height Experiment One: 10-11 September 1961

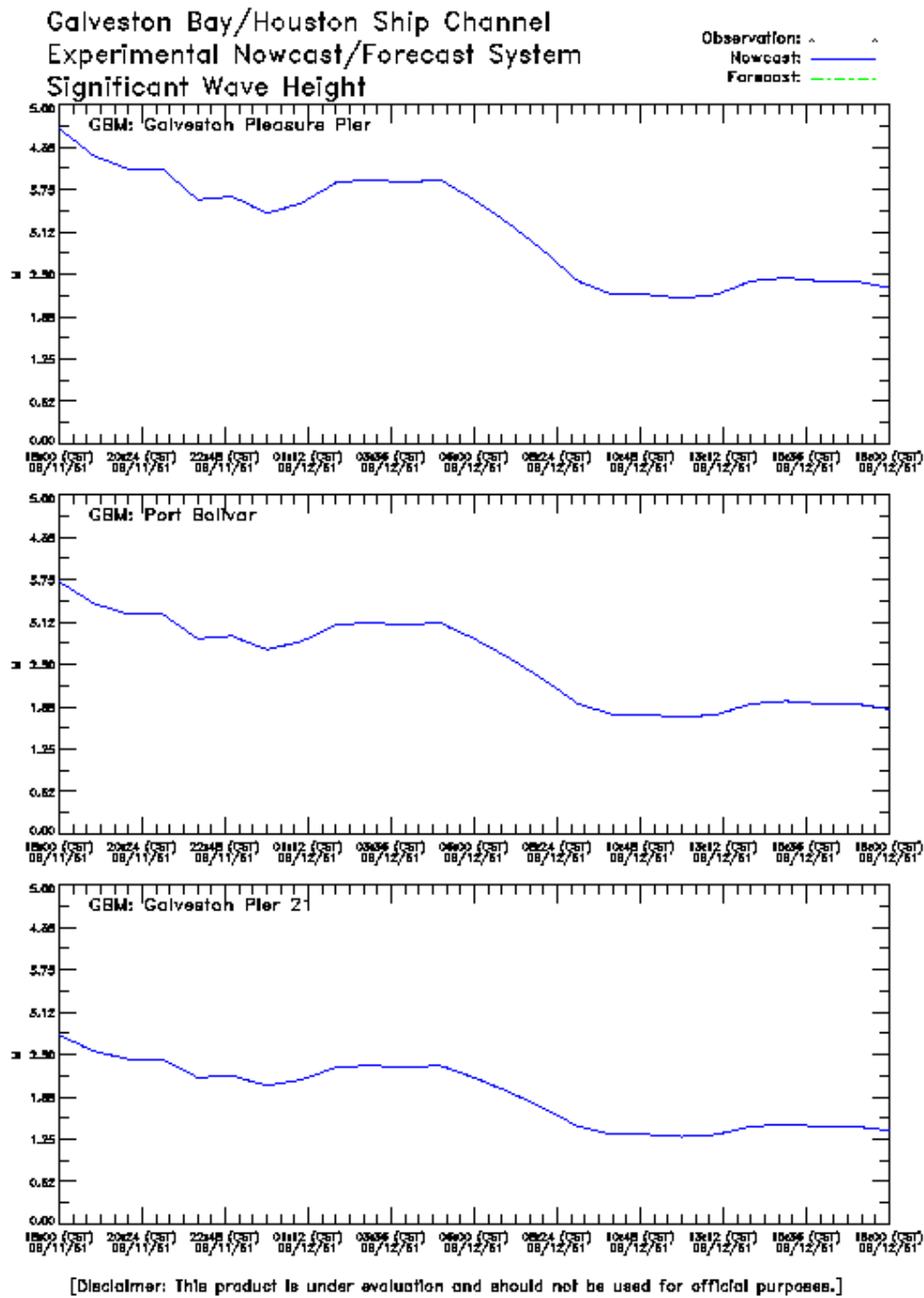


Figure 6.30. Hurricane Carla GBM Significant Wave Height Experiment One: 11-12 September 1961

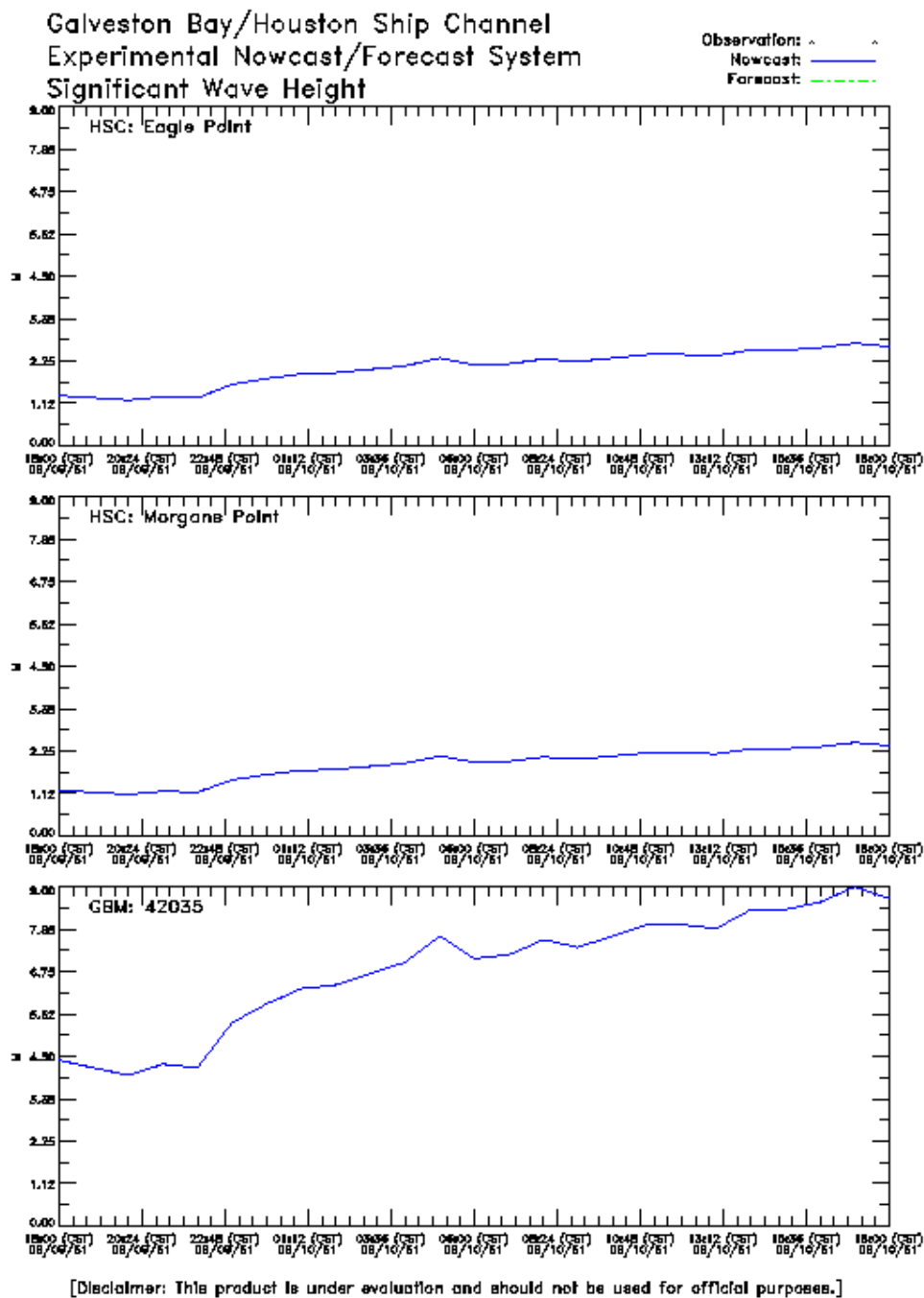


Figure 6.31. Hurricane Carla HSCM and GBM 42035 Significant Wave Height Experiment One: 9-10 September 1961

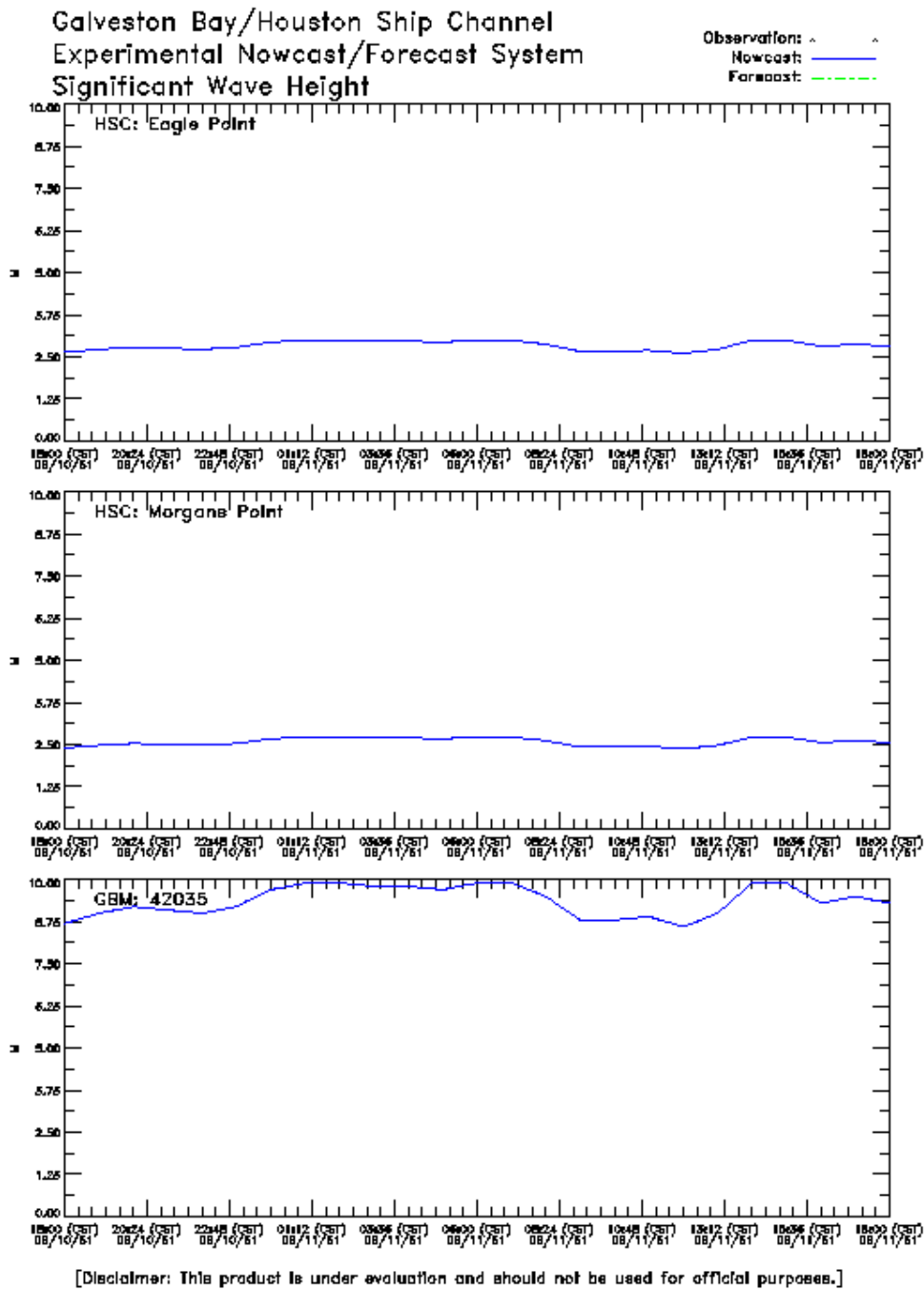


Figure 6.32. Hurricane Carla HSCM and GBM 42035 Significant Wave Height Experiment One: 10-11 September 1961

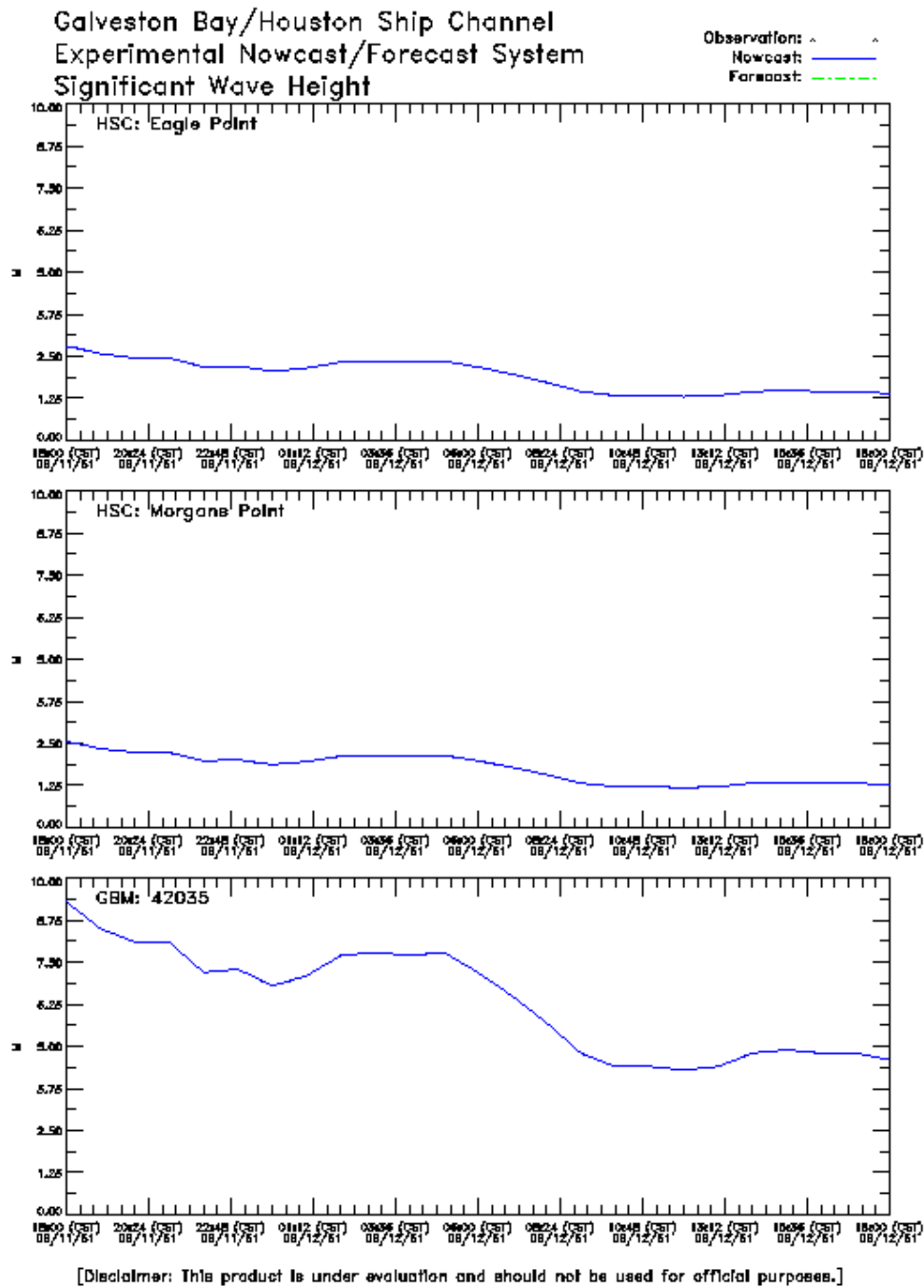


Figure 6.33. Hurricane Carla HSCM and GBM 42035 Significant Wave Height Experiment One: 11-12 September 1961

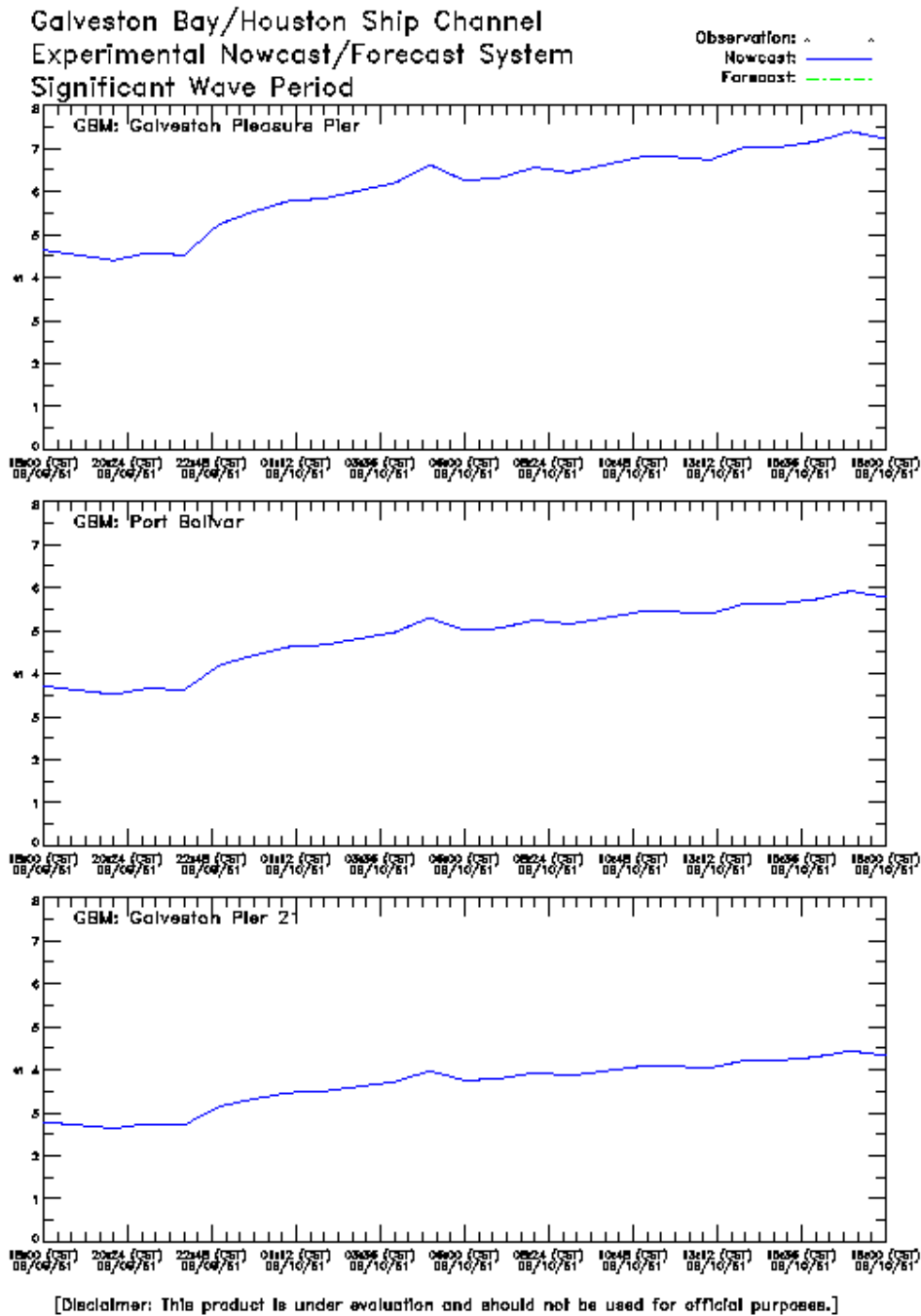


Figure 6.34. Hurricane Carla GBM Significant Wave Period Experiment One: 9-10 September 1961

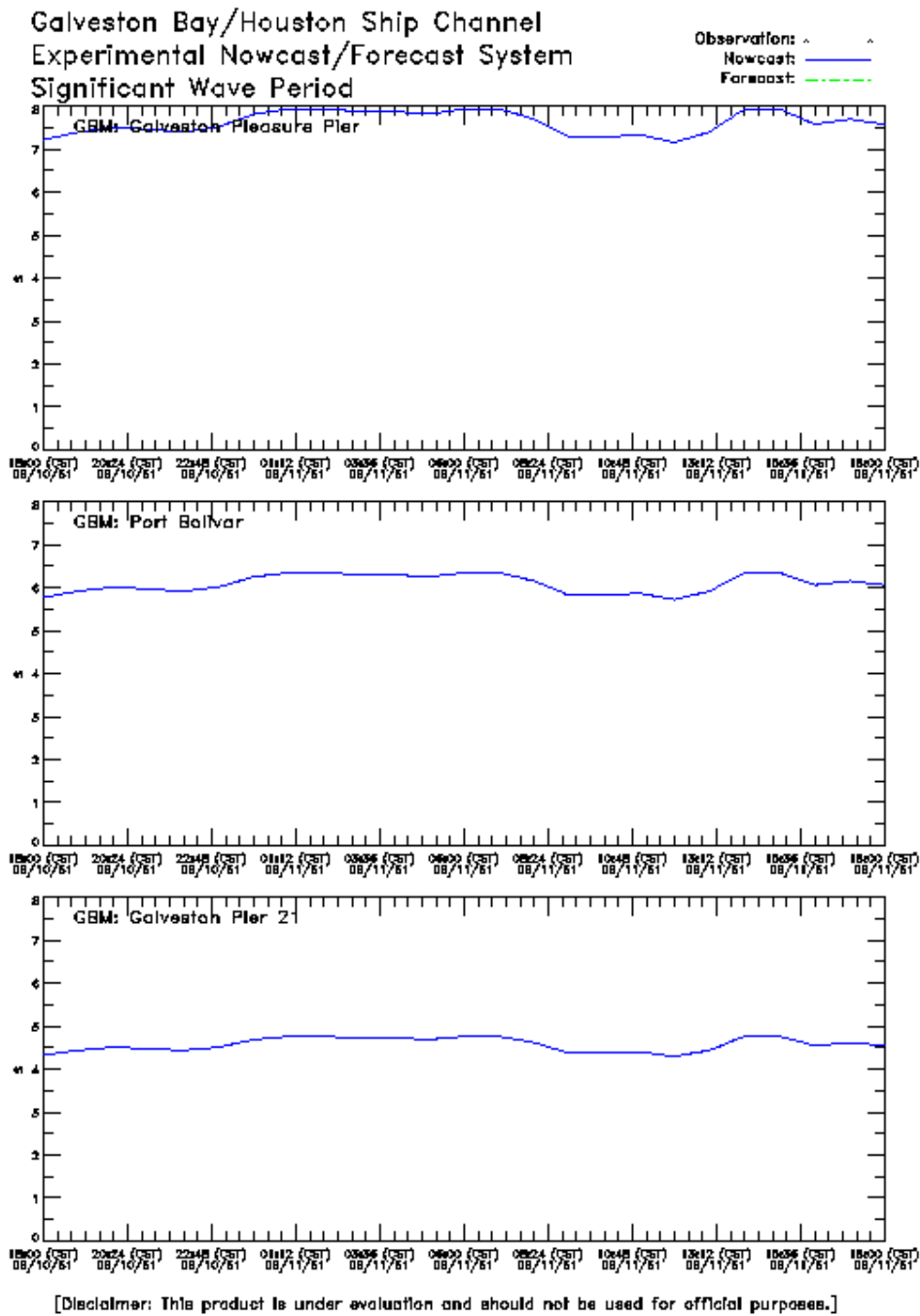


Figure 6.35. Hurricane Carla GBM Significant Wave Period Experiment One: 10-11 September 1961

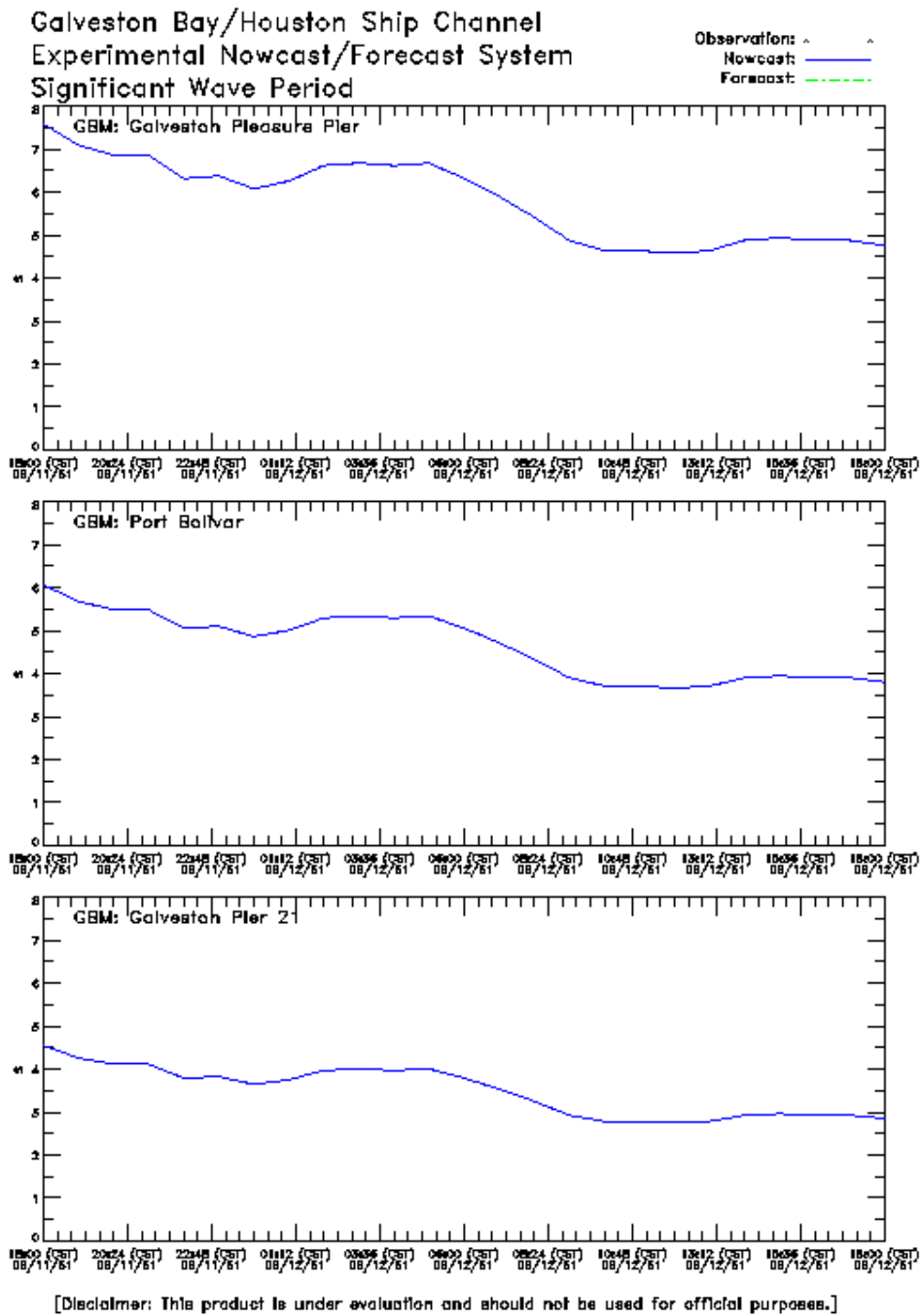


Figure 6.36. Hurricane Carla GBM Significant Wave Period Experiment One:
11-12 September 1961

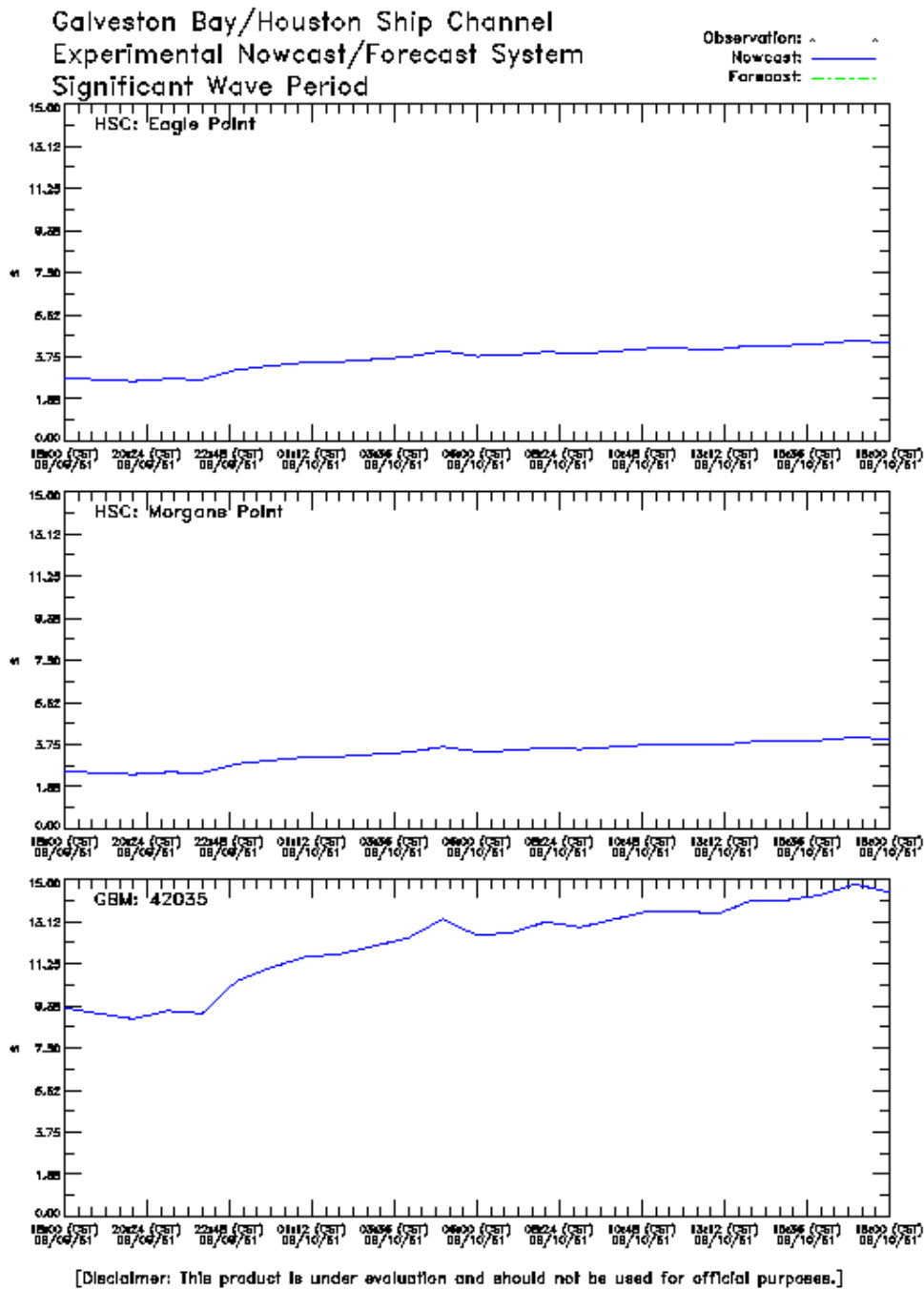


Figure 6.37. Hurricane Carla HSCM and GBM 42035 Significant Wave Period Experiment One: 9-10 September 1961

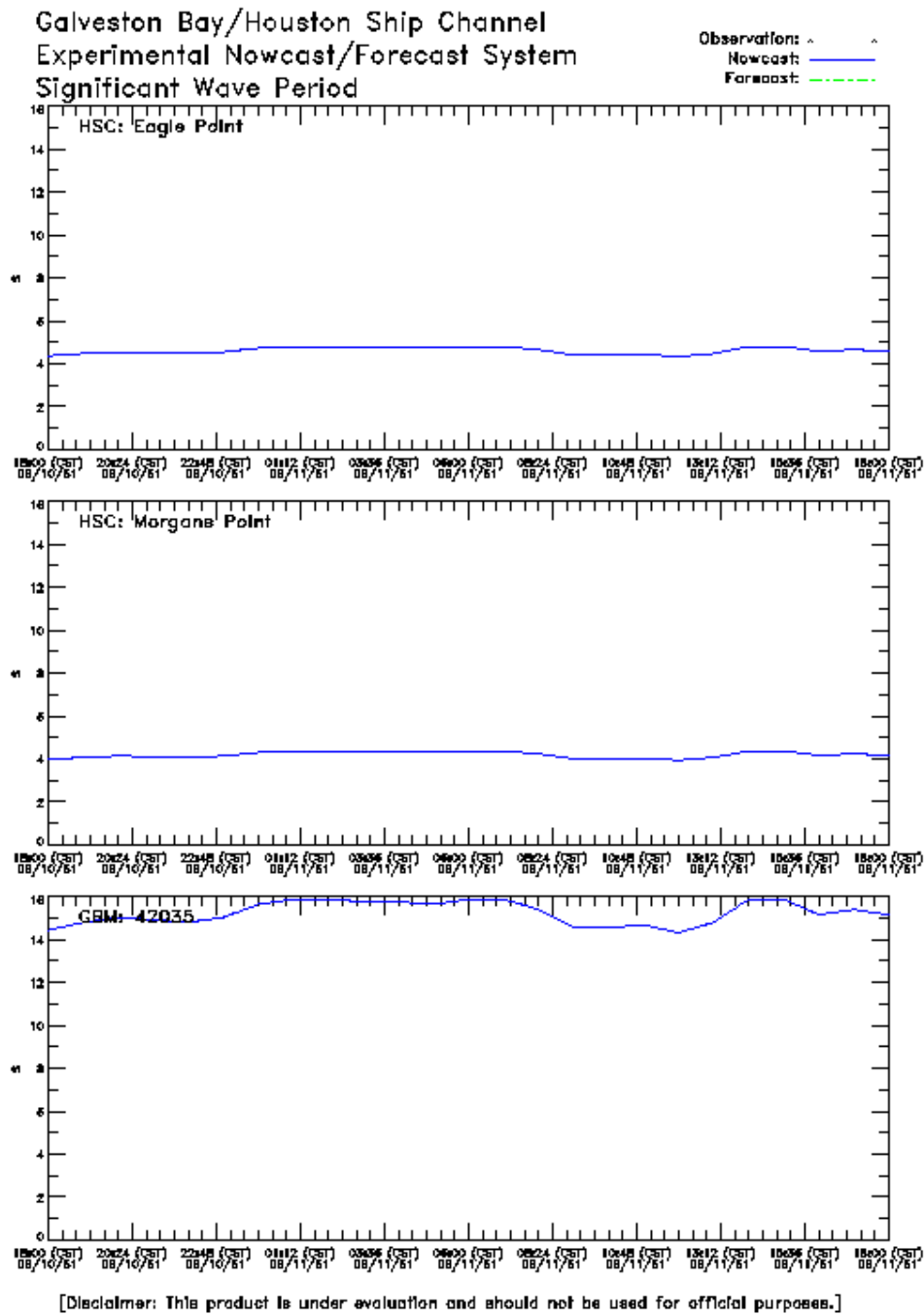


Figure 6.38. Hurricane Carla HSCM and GBM 42035 Significant Wave Period Experiment One: 10-11 September 1961

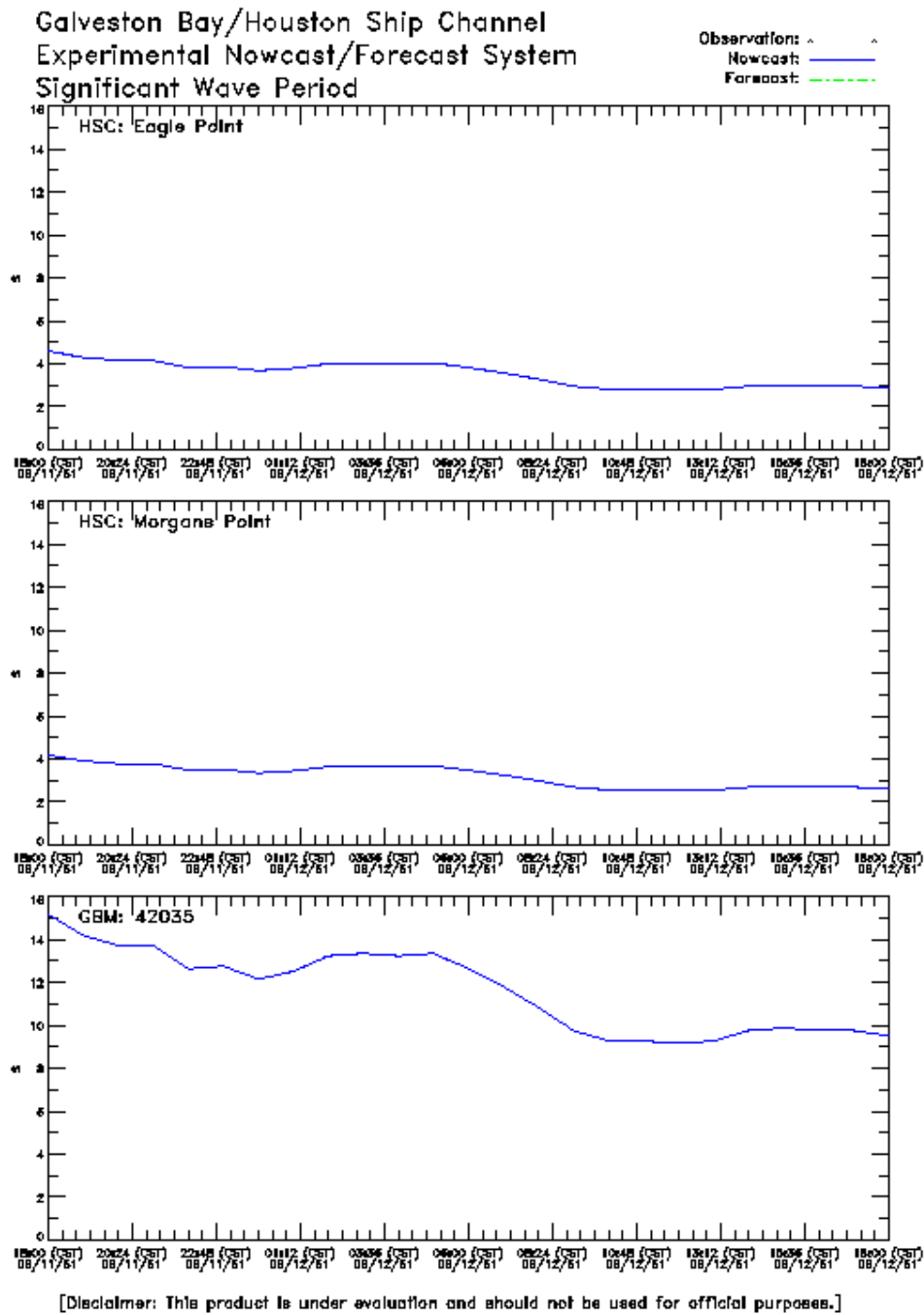


Figure 6.39. Hurricane Carla HSCM and GBM 42035 Significant Wave Period Experiment One: 11-12 September 1961

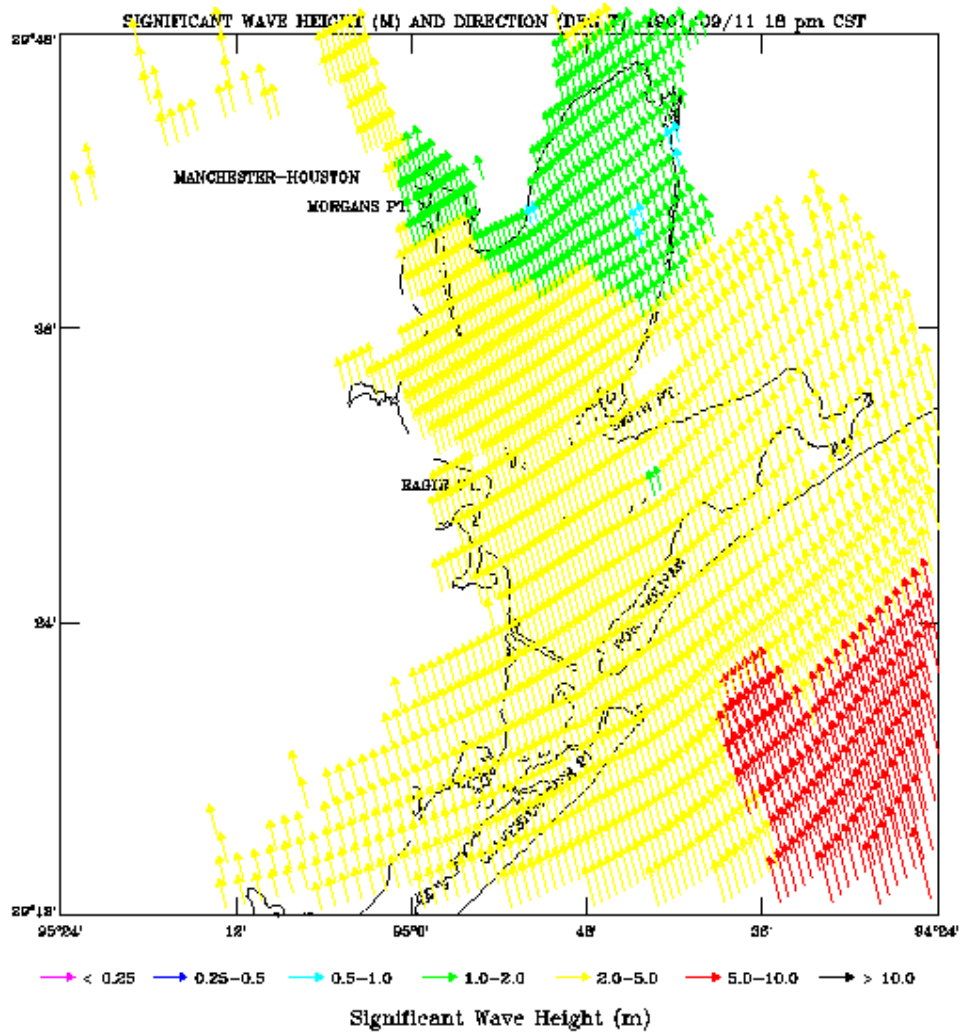


Figure 6.40. Hurricane Carla GBM Significant Wave Height and Direction
Experiment One: 11 September 1961 18:00 CST

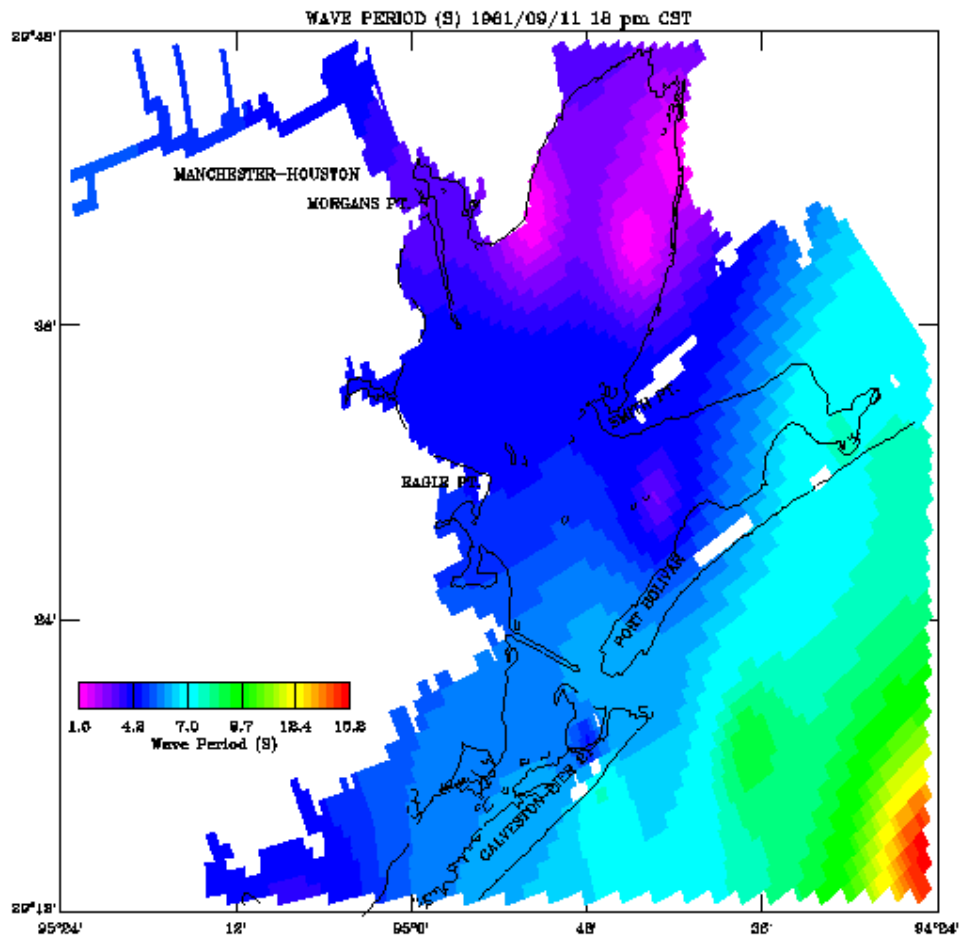


Figure 6.41. Hurricane Carla GBM Significant Wave Period Experiment One: 11 September 1961 18:00 CST

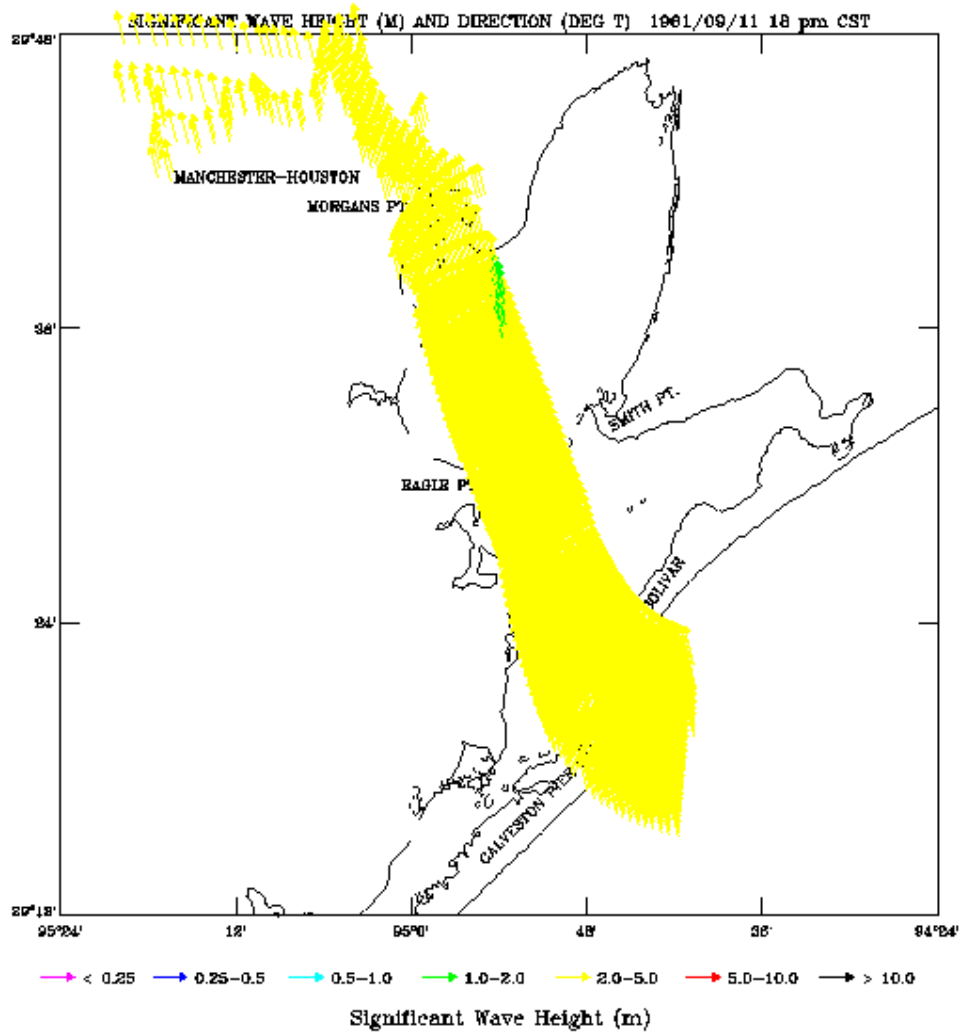


Figure 6.42. Hurricane Carla HSCM Significant Wave Height and Direction Experiment One: 11 September 1961 18:00 CST

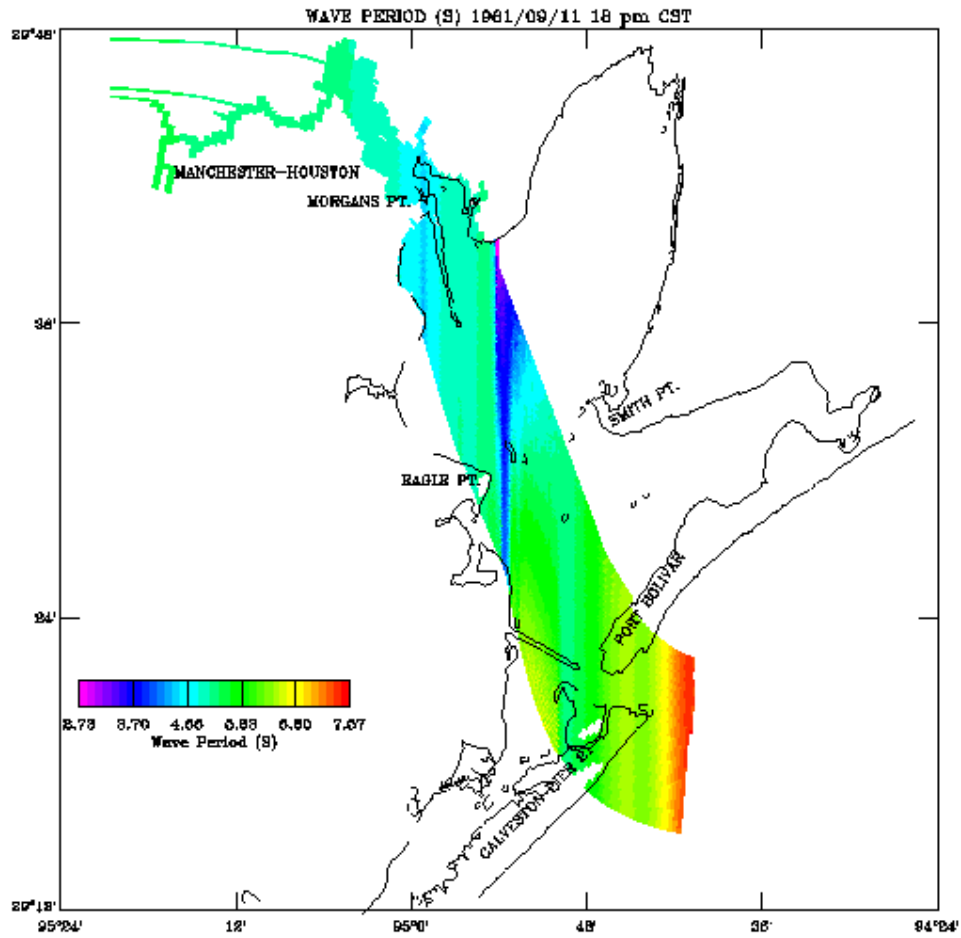


Figure 6.43. Hurricane Carla HSCM Significant Wave Period Experiment One: 11 September 1961 18:00 CST

6.5. Experiment Two Long and Short Wave Results

In this experiment, the parametric hurricane wind and atmospheric pressure algorithm in Section 5.3 is used to provide the meteorological forcing. It should be noted that the present procedure does not allow for a reduction of windspeed due to overland friction effects directly. The central pressure deficit of the storm is reduced based on observed overland weakening, but the windfields computed based on the reduced pressure deficit are not further reduced.

GBM simulated water surface elevations for each of the three hindcasts at Galveston Pleasure Pier, Bolivar Roads, and Galveston Pier 21 and HSCM simulated water surface elevations at Eagle Point and Morgans Point are in good agreement with the available observations and are very near those obtained in experiment one.

Simulated peak windspeeds are approximately 13 m/s at Galveston Pleasure Pier and Eagle Point, and are over 25 m/s at Morgans Point for a few hours during hindcast three. The simulated atmospheric pressure is constant at around 1010 mb at all three stations but drops to 1008 mb at Morgans Point during the period of maximum winds in hindcast three. The wind and atmospheric pressure forcing are from the far field of the hurricane.

The simulated atmospheric pressure field snapshot on 11 September 1961 at 18:00 CST shown in Figure 6.44 indicates the radial structure of the hurricane atmospheric pressure field. The corresponding snapshots of the simulated windfield at the same time shown in Figure 6.45 show a slight tendency for outflow rather than inflow to the radial structure of the pressure field at the end of hindcast two. This result needs further investigation.

In this experiment, simulated significant wave heights follow the same general pattern as in experiment one and are largely determined by the GBM offshore wave conditions. Wind generation increases wave heights by order 0.25m at all stations in each of the three hindcasts, except at Galveston Pier 21, which is sheltered and exhibits no wind generation growth. Wave directions are in the direction of the wind and move from near 315 deg T to a range of 225 to 250 deg T at all stations during hindcast one, to near 0 deg T in the lower Bay to a range from 250 to 300 deg T at Eagle and Morgans Point during hindcast two, and to 45 to 135 deg T in the lower Bay to near 0 deg T in the upper Bay in hindcast three.

In contrast to experiment one, simulated significant wave periods are reduced at Galveston Pleasure Pier from 7s to 5s during hindcast one and are slightly increased at the Bay by less than 1s. During hindcast two, simulated wave periods are reduced at Galveston Pleasure Pier from 8 to 6s, while at all Bay stations the differences in wave periods are less than 1s. During hindcast three, simulated wave periods are reduced at Galveston Pleasure Pier by at most 1.5s, while at the other Bay stations results are less than 1s from those obtained in experiment one.

It should be noted that in experiment two for wind generation, the wave period is

computed directly from the wind wave and the offshore swell period is not used in the wave period computations. This method yielded the best results for the limited one month calibration period for non-hurricane conditions. It might be useful to revisit this procedure for hurricane conditions.

6.6. Wind and Water Surface Elevation Validation

In Table 6.2 peak windspeeds over the GBM grid are compared with fastest mile observations reported by Cooperman and Cumner (1961). Wind speeds computed used the parametric hurricane model in Section 6.3 are in general agreement with these observations.

Table 6.2. Hurricane Carla (1961) Windspeed Validation. Note simulated GBM peak corresponds to results obtained in Experiment Two with parametric hurricane model wind and atmospheric pressure forcing.

Station Location	ID	Simulated GBM Peak (m/s)	Observed Fastest Mile (m/s)
Galveston	12923	14.7	22.8
Ellington AFB	12906	29.4	-
Hobby Airport	12918	30.2	23.3

In Table 6.3, GBM peak simulated water levels and simulated significant wave heights are compared with observed peak water levels reported by Dunn and staff (1961) and Cooperman and Cumner (1961). The observed peak water levels are reported with respect to NGVD-1929 whereas the GBM simulated water levels are with respect to the MTL model datum. Peak water levels from high water marks, particularly at Morgans Point may include surface gravity wave effects. One should note that at two Galveston water level gauges, the level of agreement shown in Figures 6.2-6.4 for experiment one are in close agreement and are both based on a MLLW datum. MSL stands 5 mm and 3 mm lower than MTL at Galveston Pleasure Pier based on the 1960-1978 and 1983-2001 tidal epochs, respectively. At Galveston Pier 21 MSL stands 4 mm and 3 mm higher than MTL for the corresponding tidal epochs. Therefore we can assume that MSL and MTL are approximately equivalent at the coast. At Morgan's Point, MSL is higher by 12 mm and 9 mm than MTL based on the above epochs, respectively. Therefore throughout Galveston Bay MSL and MTL are nearly equivalent differing by at most 1 cm. At Galveston Pleasure Pier and Galveston Pier 21, NGVD-29 stands .201m below MTL. The corrections at the inland stations in Table 6.3 are not known precisely but are probably larger due to subsidence effects induced by groundwater pumping and oil extraction. These effects would tend to elevate the observed peak water levels as would possible surface gravity wave effects in the high water marks, making the direct comparison at the inland stations more problematical.

Table 6.3. Hurricane Carla (1961) GBM Storm Surge Validation.

Note + indicates high water mark. Exp1==Experiment One with no wind and atmospheric forcing, while Exp 2==Experiment Two with parametric hurricane model wind and atmospheric pressure forcing.

Station Location	Simulated Peak Water Level (m-MTL)		Simulated Peak Significant Wave Height (m)		Observed Peak Water Level (m-NGVD-1929)
	Exp 1	Exp 2	Exp 1	Exp2	
Galveston Pl. Pier	2.43	2.44	4.95	5.23	2.8
Galveston Pier 21	2.37	2.38	2.97	2.97	2.7
Eagle Point	2.38	2.39	2.97	3.18	3.35+
Smith Point	2.36	2.39	2.97	3.16	4.27+
Morgans Point	2.39	2.44	1.98	2.25	4.51,5.0+
Round Point	2.39	2.49	0.99	1.13	3.51 +

6.7. Surface Salinity, Surface Current, and Inundation Statistics

In Table 6.4, GBM simulated surface minimum salinity and simulated maximum surface current strengths are given for stations proceeding northward up Galveston Bay are compared between experiment one and two. The added wind forcing adjust the salinity structure and increase the maximum currents only slightly, due to the distance to the center of the storm.

Table 6.4. Hurricane Carla (1961) GBM Minimum Surface Salinity and Maximum Current Speeds. Exp1==Experiment One with no wind and atmospheric forcing, while Exp 2==Experiment Two with parametric hurricane model wind and atmospheric pressure forcing.

Station Location	Minimum Salinity (PSU)		Maximum Current (m/s)	
	Exp 1	Exp 2	Exp 1	Exp 2
Galveston Pl. Pier	33.7	33.6	0.23	0.56
Galveston Pier 21	33.7	33.6	0.74	0.67
Eagle Point	21.9	25.6	0.52	0.51
Smith Point	28.7	28.4	0.57	0.43
Morgans Point	21.5	21.7	0.44	0.30
Round Point	11.1	11.1	0.23	0.37

Inundation statistics for both experiments are presented in Table 6.5 in terms of the time and areal extent of the maximum flooding. Average and maximum flood depths are also determined. Experiment 2 values are slightly elevated over those of experiment 1 due the influence of the wind and atmospheric pressure forcing, which are modest due to the distance to the storm center.

Table 6.5. Hurricane Carla (1961) Inundation Statistics.

Note the first line corresponds to results from Experiment 1 with no wind and atmospheric pressure forcing. The second line presents results from Experiment 2 with parametric hurricane wind and atmospheric pressure forcing.

Hindcast No.	Simulation Dates	Time of Maximum Flood (JD)	Maximum Flooded Area (km ²)	Average Flood Depth (m)	Maximum Flood Depth (m)
1	9/9-9/10	253.75	1113	0.793	1.053
		253.75	1117	0.813	1.052
2	9/10-9/11	254.64	1463	1.112	1.471
		254.50	1462	1.044	1.605
3	9/11-9/12	254.754	1463	1.102	1.297
		255.483	1463	0.402	1.525

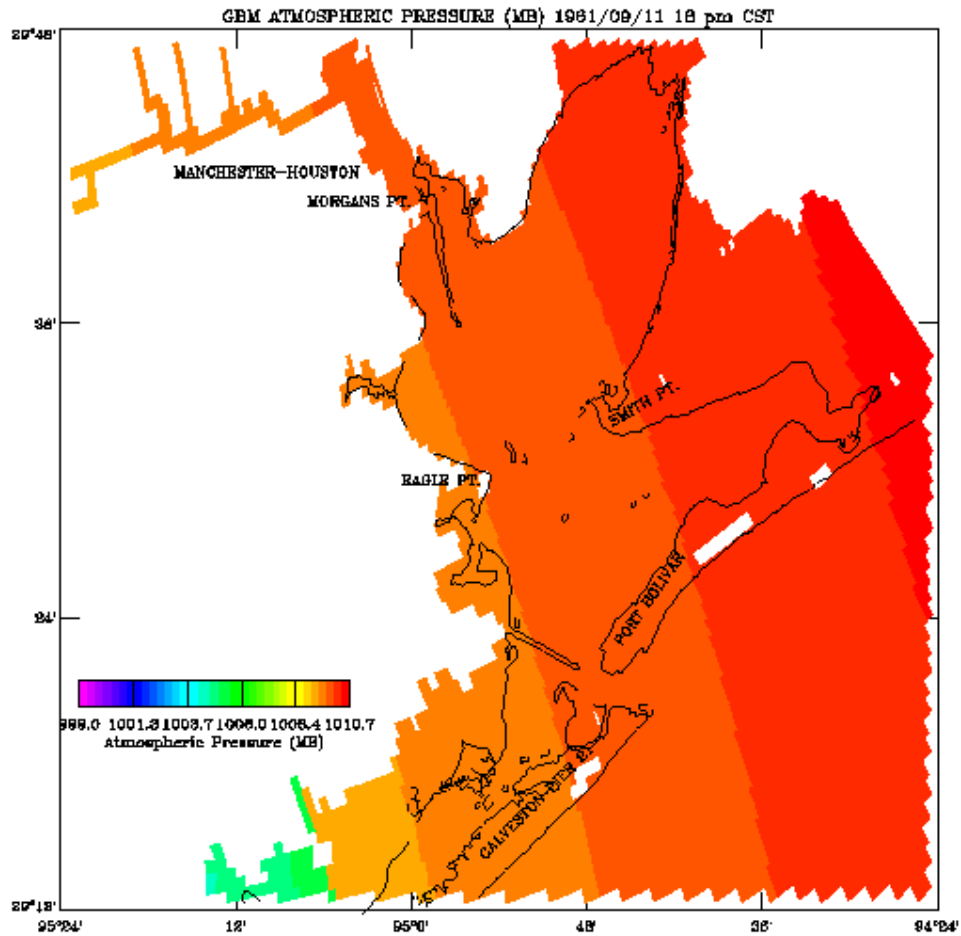


Figure 6.44. Hurricane Carla GBM Atmospheric Pressure Field Experiment Two: 11 September 1961 18:00 CST

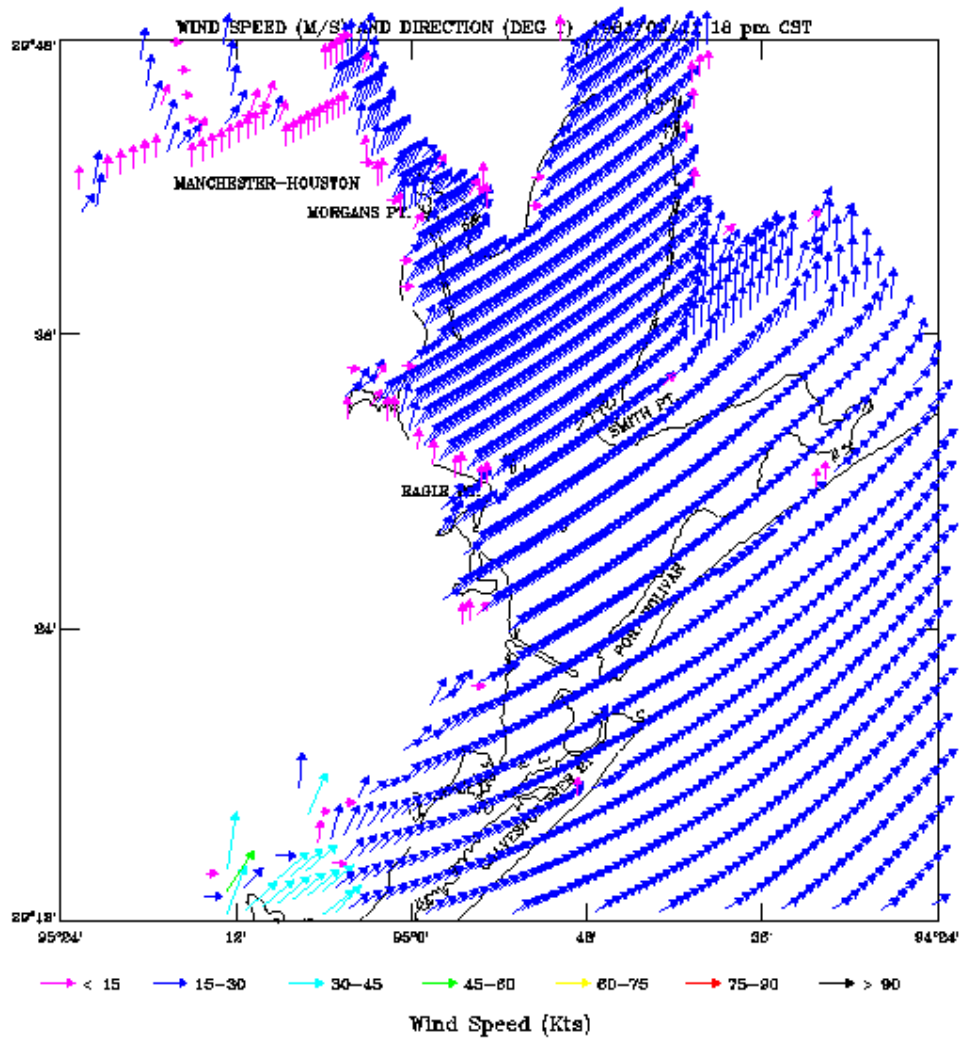


Figure 6.45. Hurricane Carla GBM Wind Field Experiment Two: 11 September 1961 18:00 CST

7. HURRICANE ALICIA (1983) SIMULATION

Two 24-hour hindcasts for August 16-18 were performed with the calculations restarted for the second daily hindcast from results at the end of the first hindcast. No NCEP forecasts of surface winds and atmospheric pressure fields or of storm surge were available. Two separate experiments were performed. In experiment one, no wind and atmospheric pressure forcing were used while the open boundary storm surge was based on the nontidal water level at Galveston Pleasure Pier. In experiment two, the parametric hurricane wind and atmospheric pressure forcing were applied with the same open boundary surge as in experiment one. The wind and atmospheric pressure forcing were severe over the Galveston Bay region, since the track of Hurricane Alicia passed just west of the City of Houston (see Figure 7.1). The results from experiment one are first presented below. Long wave results are given in terms of water surface elevation, current, salinity, and temperature time series as well as field plots of water surface elevation and salinity. Short wave results are given in terms of significant wave height, period, and direction as well as vector plots of significant wave height and direction and contour plots of significant wave period. Next, experiment two results are given in the same format. Wind and water surface elevation validation are presented followed by surface salinity, surface current, and inundation summary statistics.

7.1. Storm Characteristics

The track of Hurricane Alicia is shown in Figure 7.1 with storm parameters given in

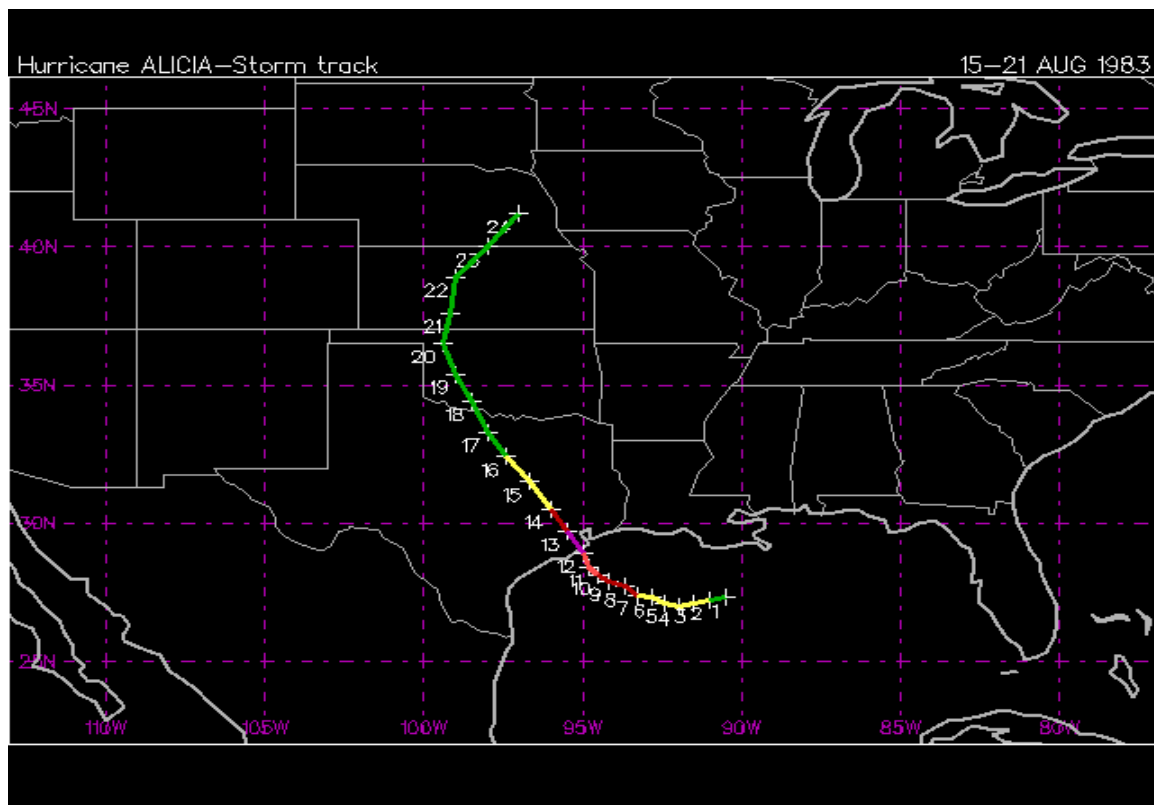


Figure 7.1. Hurricane Alicia (1983) Storm Track 15-21 August.

Table 7.1. The storm made landfall along the Texas coast 40 km southwest of Galveston at San Luis Pass, Texas at 0800 CST on the morning of August 18.

In the simulations, the radius to maximum winds was estimated at approximately 18 nm around the time of landfall and subsequently increased to 31 nm over the next 12 hours. Hourly rainfall information was obtained at Station 414300 Houston International Airport, Texas for use in the rainfall/runoff computations and totaled over 17 inches. Case and Gerrish (1984) note that the peak water surface elevations relative to MSL range from 3.9 m at San Luis Pass to 2.7 m at Galveston Pleasure Pier and that peak water levels within Galveston Bay increase to 3.5 m at Morgans Point.

Table 7.1. Hurricane Alicia Storm Characteristics 15-21 August 1983.

ADV	LAT	LON	TIME	WIND	PR	STAT
1	28.30	-90.50	08/15/12Z	30	1009	TROPICAL DEPRESSION
2	28.20	-91.00	08/15/18Z	40	1006	TROPICAL STORM
3	28.10	-91.50	08/16/00Z	45	1005	TROPICAL STORM
4	28.00	-92.00	08/16/06Z	50	1004	TROPICAL STORM
5	28.10	-92.40	08/16/12Z	55	1002	TROPICAL STORM
6	28.30	-92.80	08/16/18Z	60	998	TROPICAL STORM
7	28.40	-93.30	08/17/00Z	65	991	HURRICANE-1
8	28.70	-93.70	08/17/06Z	70	987	HURRICANE-1
9	28.90	-94.20	08/17/12Z	75	983	HURRICANE-1
10	28.10	-94.50	08/17/18Z	90	974	HURRICANE-2
11	28.40	-94.80	08/18/00Z	95	969	HURRICANE-2
12	28.90	-95.00	08/18/06Z	100	963	HURRICANE-3
13	29.70	-95.50	08/18/12Z	80	965	HURRICANE-1 ----Landfall 15 GMT
14	30.50	-96.00	08/18/18Z	40	990	TROPICAL STORM
15	31.50	-96.70	08/19/00Z	35	998	TROPICAL STORM
16	32.40	-98.40	08/19/06Z	30	1003	TROPICAL DEPRESSION
17	33.30	-98.00	08/19/12Z	25	1006	TROPICAL DEPRESSION
18	34.40	-98.50	08/19/18Z	25	1009	TROPICAL DEPRESSION
19	35.40	-99.00	08/20/00Z	20	1010	TROPICAL DEPRESSION
20	36.50	-99.40	08/20/06Z	20	1011	EXTRATROPICAL DEPRESSION
21	38.60	-99.20	08/20/12Z	20	1011	EXTRATROPICAL DEPRESSION
22	38.90	-99.00	08/20/18Z	20	1011	EXTRATROPICAL DEPRESSION
23	40.00	-98.00	08/21/00Z	20	1010	EXTRATROPICAL DEPRESSION
24	41.20	-98.00	08/21/06Z	20	1010	EXTRATROPICAL DEPRESSION

7.2. Simulation Set-up Procedures

The first hindcast covers the period August 16 18:00 CST to August 17 18:00 CST. Water surface elevations and velocities are started from rest. The initial salinity and temperature fields are determined based on climatology. Since no PORTS data are available, no adjustment of these fields is made. Open boundary conditions for the GBM for water surface elevation are computed based on adding the observed nontidal water level at Galveston Pleasure Pier to the predicted astronomical tide. Salinity and temperature values along the open boundary are based on climatology. Sea surface temperature is specified by using the top level of the initial temperature field and is held constant in time. River inflows for the San Jacinto, Buffalo Bayou, and Trinity Rivers are based on USGS daily observed values. Since no available wave data are available, the

relations in Equation 5.13 were used to specify representative wave conditions along the GBM open boundary.

For the subsequent daily hindcast over the period August 17 18:00 CST to August 18 18:00 CST, conditions are restarted from the end of the previous hindcast. No adjustments of the salinity and temperature fields are made. Open boundary conditions for water surface elevation, salinity, and temperature are specified using the same technique as described above for the first hindcast. Similarly, sea surface temperature, river inflows for the San Jacinto, Buffalo Bayou, and Trinity Rivers, and the wave conditions along the open boundary are specified as above. Note the HSCM is directly driven from information saved from the GBM using the same one-way coupling scheme mentioned previously.

Two experiments are run using the above conditions but with different meteorological forcing. In experiment one, the observed surge level at Galveston Pleasure Pier is propagated into the Bay and the water level, current, and density response is investigated in the absence of wind and atmospheric pressure forcing. Results are presented for both the long wave and short surface gravity wave cases. Experiment two results with the parametric hurricane model wind and atmospheric pressure field forcing applied are next considered.

7.3. Experiment One Long Wave Results

Simulated water surface elevations for each of the two hindcasts are shown at Galveston Pleasure Pier, Bolivar Roads, and Galveston Pier 21 in Figures 7.2–7.3. GBM simulated water levels are in excellent agreement with the observations at Galveston Pleasure Pier and at Galveston Pier 21. The maximum discrepancy is 35 cm. One notes the rapid rise in water levels and the potential for overland flooding and overtopping of the barrier islands during the second hindcast. In Figures 7.4–7.5, HSCM simulated water surface elevations are shown for each hindcast at Eagle Point and Morgans Point. Unfortunately, no water level gages were in operation during this storm at these locations. In the third panel of these figures, the water level residual (surge at Galveston Pleasure Pier) is given. This water level residual is applied uniformly in space over the entire GBM open water boundary. As noted previously, the storm surge at San Luis Pass was order 3.9 m, which is considerably larger than the surge at Galveston Pleasure Pier. Since San Luis Pass is at the lower boundary, it may be more appropriate to use the San Luis Pass surge level along a portion of the lower GBM open boundary.

Simulated currents are examined in three-panel figures for current speed, current direction, and principal component direction with flood considered positive. Simulated Bolivar Roads currents are shown in Figures 7.6- 7.7 for each hindcast. One notes the strong persistent flood flow at the beginning of the first hindcast. This flood flow is followed by a weak ebb flow of 70 cm/s and then a very strong flood flow of over 200 cm/s during the second hindcast. Simulated currents at Redfish Bar, mid-way up the Bay, show a similar behavior in the ebb-flood structure to simulated currents at Bolivar Roads; however, the peak flood current strength during the second hindcast is reduced to order

125 cm/s. At Morgans Point, the simulated currents in Figures 7.8-7.9, exhibit a similar ebb-flood structure. The peak current strengths on ebb and flood are on the order of 70 cm/s. Additional rainfall/runoff flows have not been included and inflows from the Buffalo Bayou, San Jacinto River, and Trinity River were small.

Simulated surface temperature, temperature stratification (absolute difference between simulated surface and bottom temperatures) and surface salinity are examined in three panels at Bolivar Roads in Figures 7.10-7.11 and at Eagle Point in Figures 7.12-7.13, respectively. One notes the increase in salinity at Bolivar Roads from 30 to 34 psu during the surge propagation phase and gradual decrease to 30 psu in the second hindcast during which the surge recedes. While the simulated surface temperature remains constant, there is increase in stratification to order 0.75 °C as the cooler shelf water moves in over the bottom layers during the surge propagation phase of the storm. At Eagle Point the simulated surface salinity increases from 17 psu to a maximum of 27 psu and then returns to 22.5 psu. The maximum simulated temperature stratification is only 0.5 °C. At Morgans Point the surface salinity remains nearly constant at 20 psu with a maximum simulated temperature stratification of order 1.25 °C.

GBM simulated water surface elevation contours relative to MTL model datum are shown at the end of hindcast two in Figure 7.14. Water surface elevations are initiated at rest. One day later at the end of the first hindcast no flooding has occurred. At the end of the second hindcast in Figure 7.14, the barrier islands have been overtopped and areas have been flooded.

Next GBM simulated near surface and near bottom salinity contours are shown in Figures 7.15 and 7.16 at the end of hindcast two. One notes the penetration of the shelf salinity into the Bay during the surge propagation phase at both the surface and bottom. Note that both the surface and bottom layer simulated salinities are still elevated and have not returned to prestorm values at the end of the second hindcast.

HSCM simulated water surface elevation contours relative to MTL model datum and simulated near surface and near bottom salinity contours are consistent with GBM results and are not shown here.

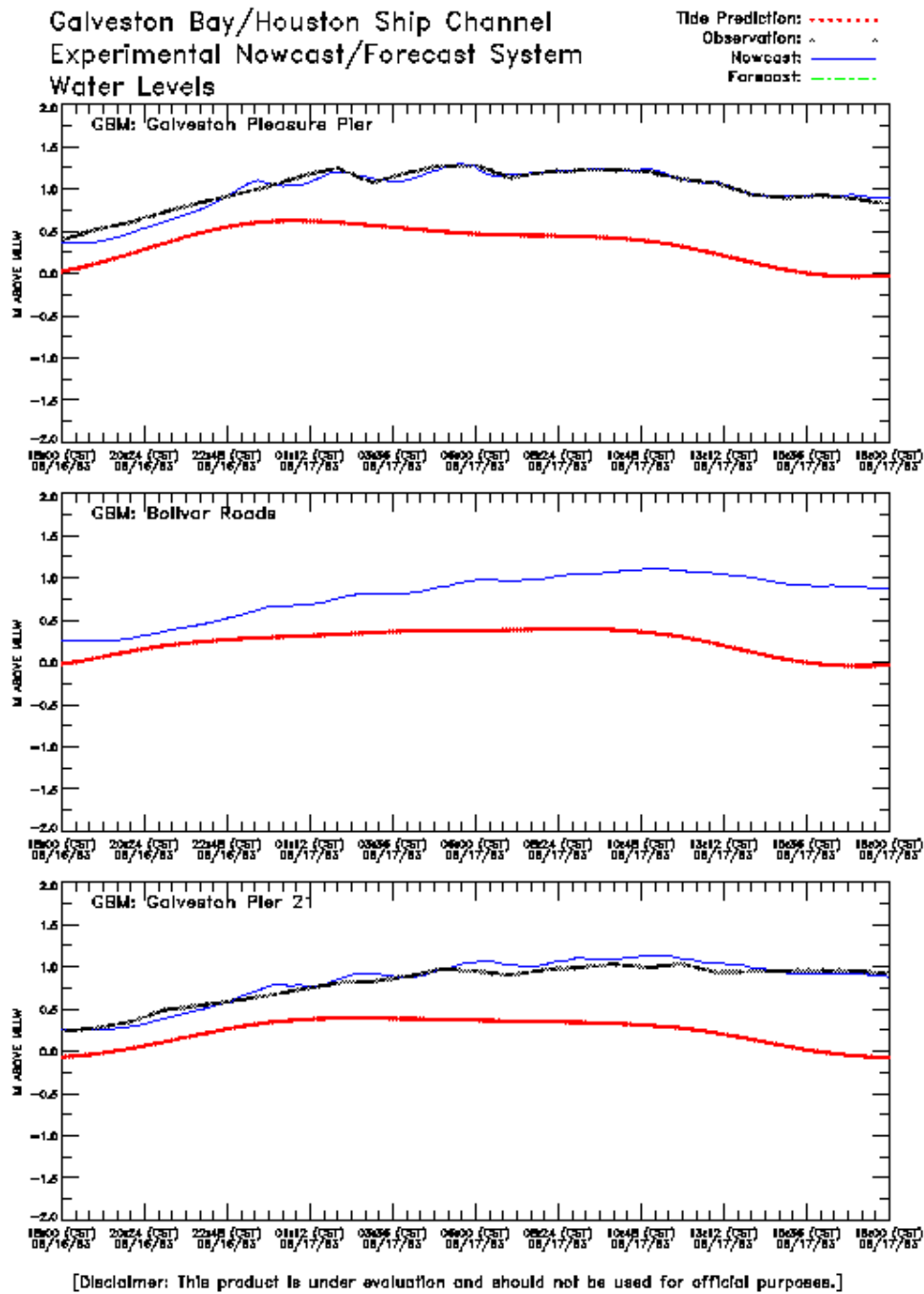


Figure 7.2. Hurricane Alicia GBM Water Levels Experiment One: 16-17 August 1983
September 1961

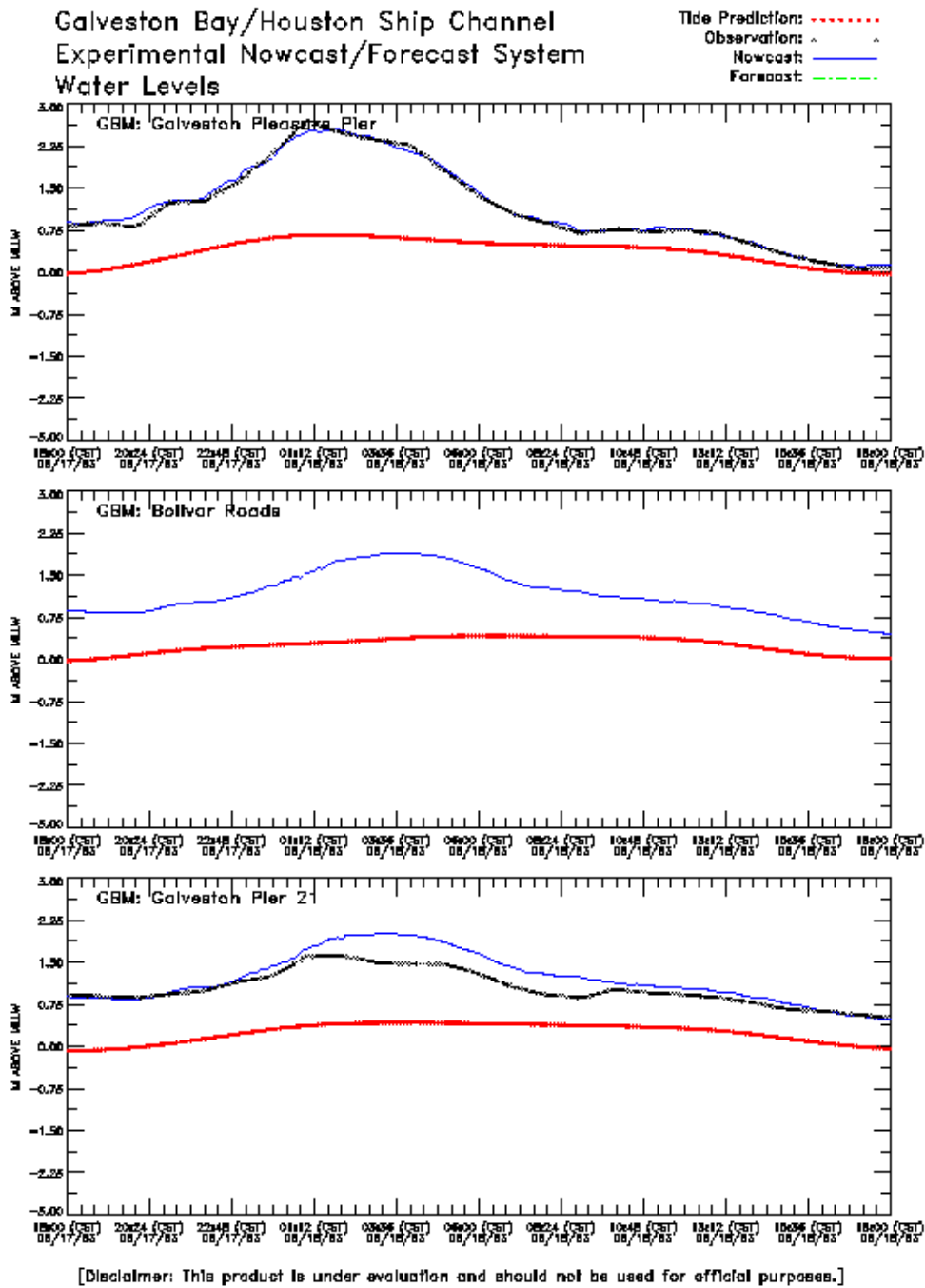


Figure 7.3. Hurricane Alicia GBM Water Levels Experiment One: 17-18 August 1983

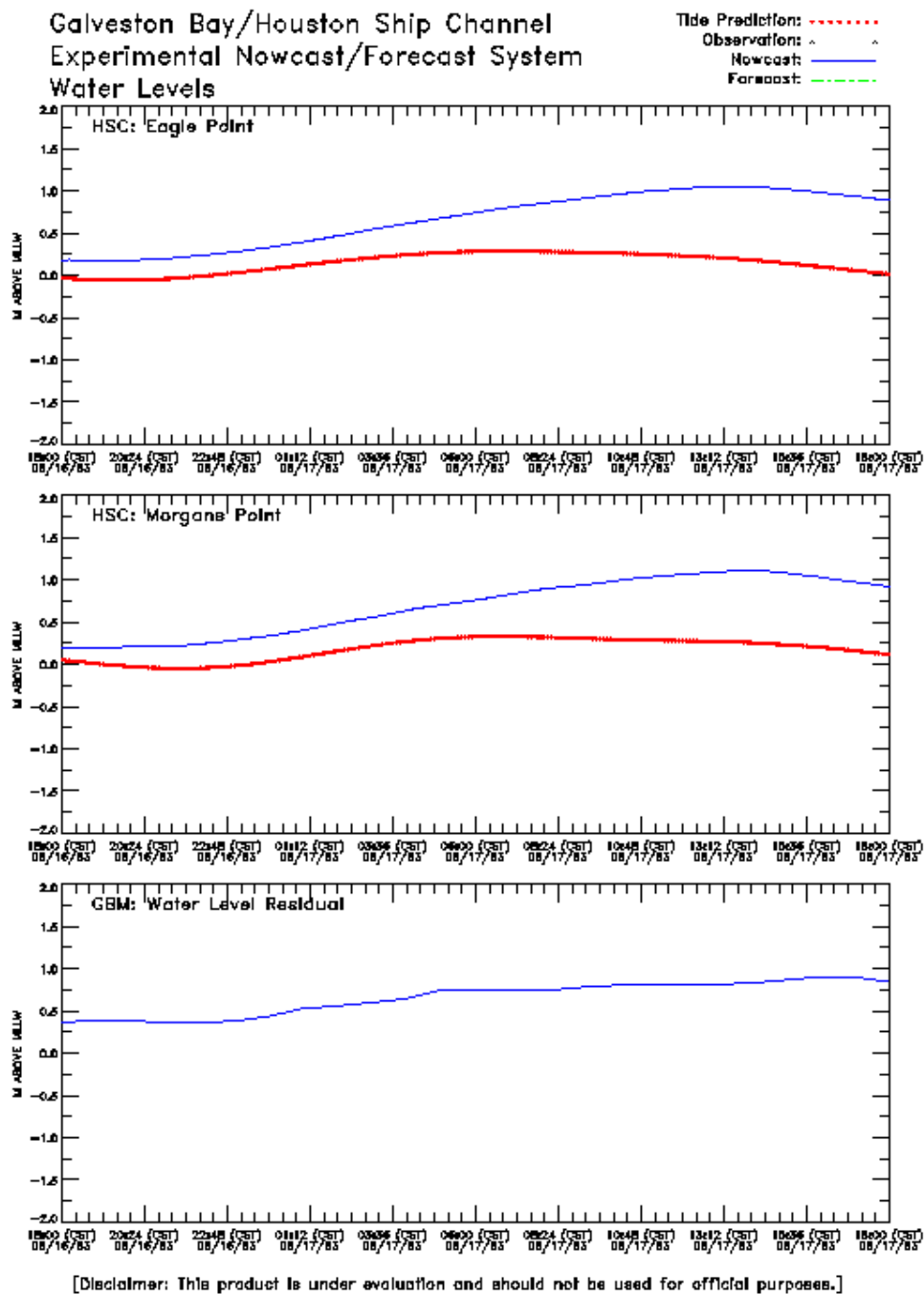


Figure 7.4. Hurricane Alicia HSCM Water Levels and GBM Water Level Residual Experiment One: 16-17 August 1983

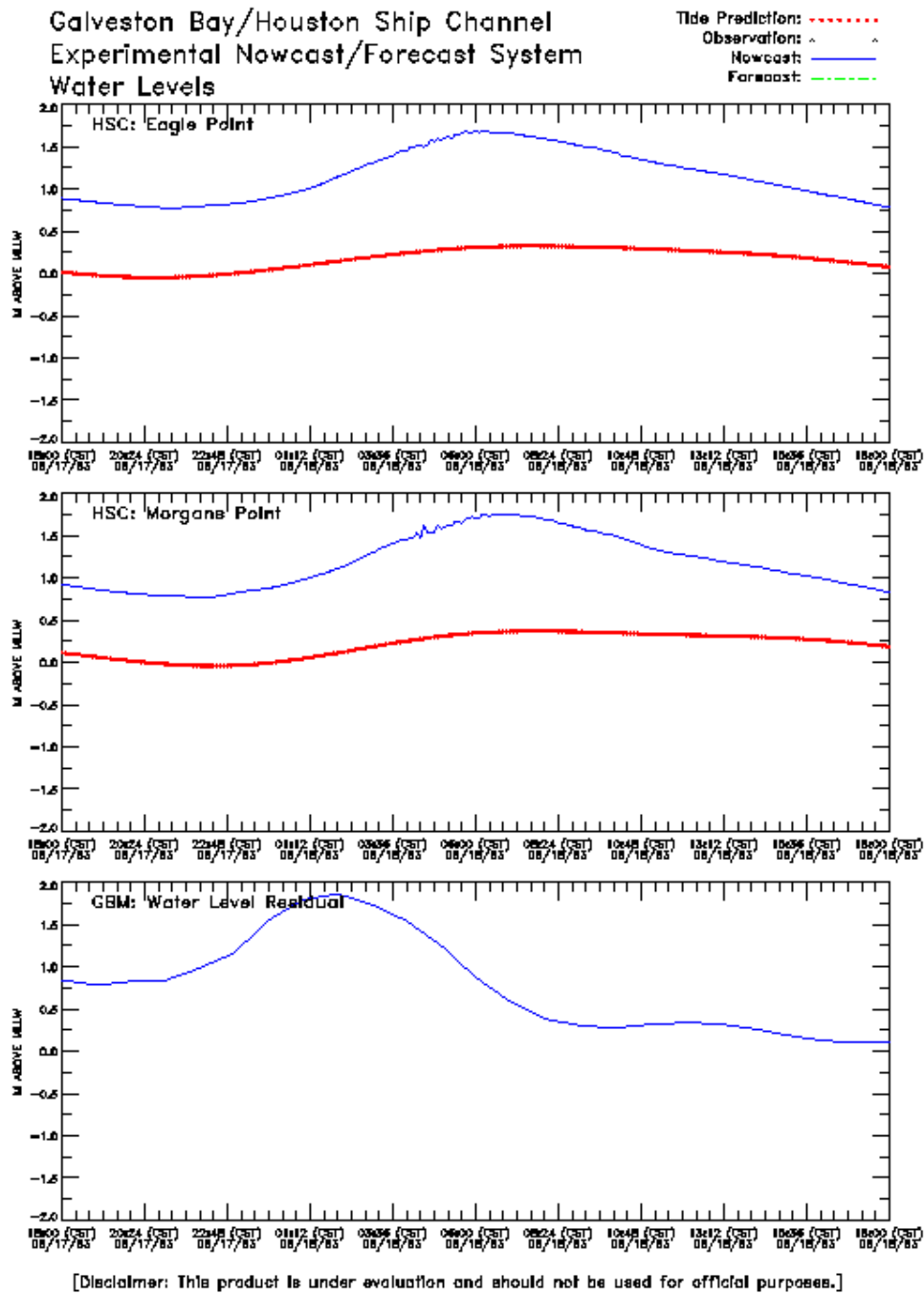


Figure 7.5. Hurricane Alicia HSCM Water Levels and GBM Water Level Residual Experiment One: 17-18 August 1983

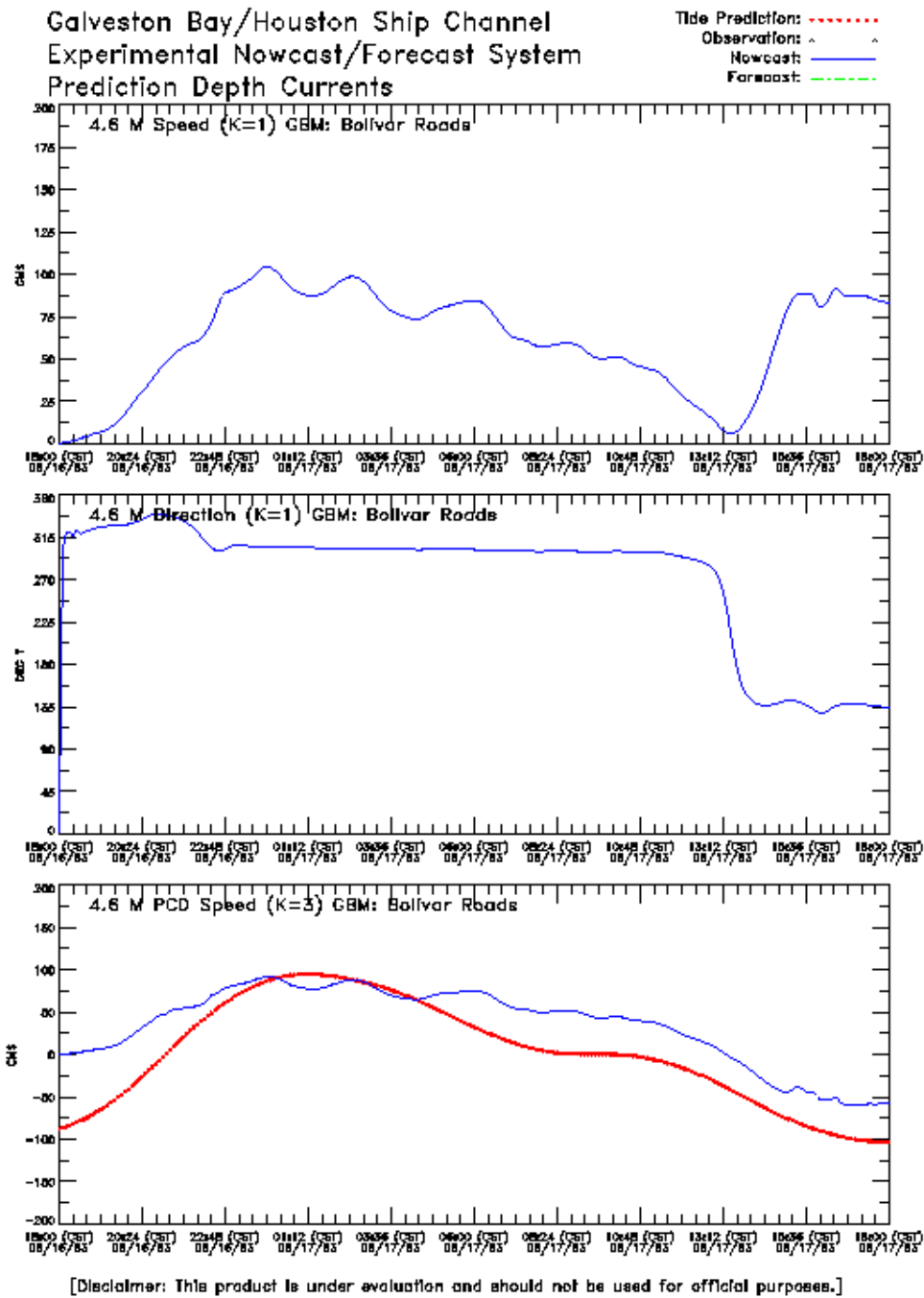


Figure 7.6. Hurricane Alicia GBM Bolivar Roads Currents Experiment One: 16-17 August 1983

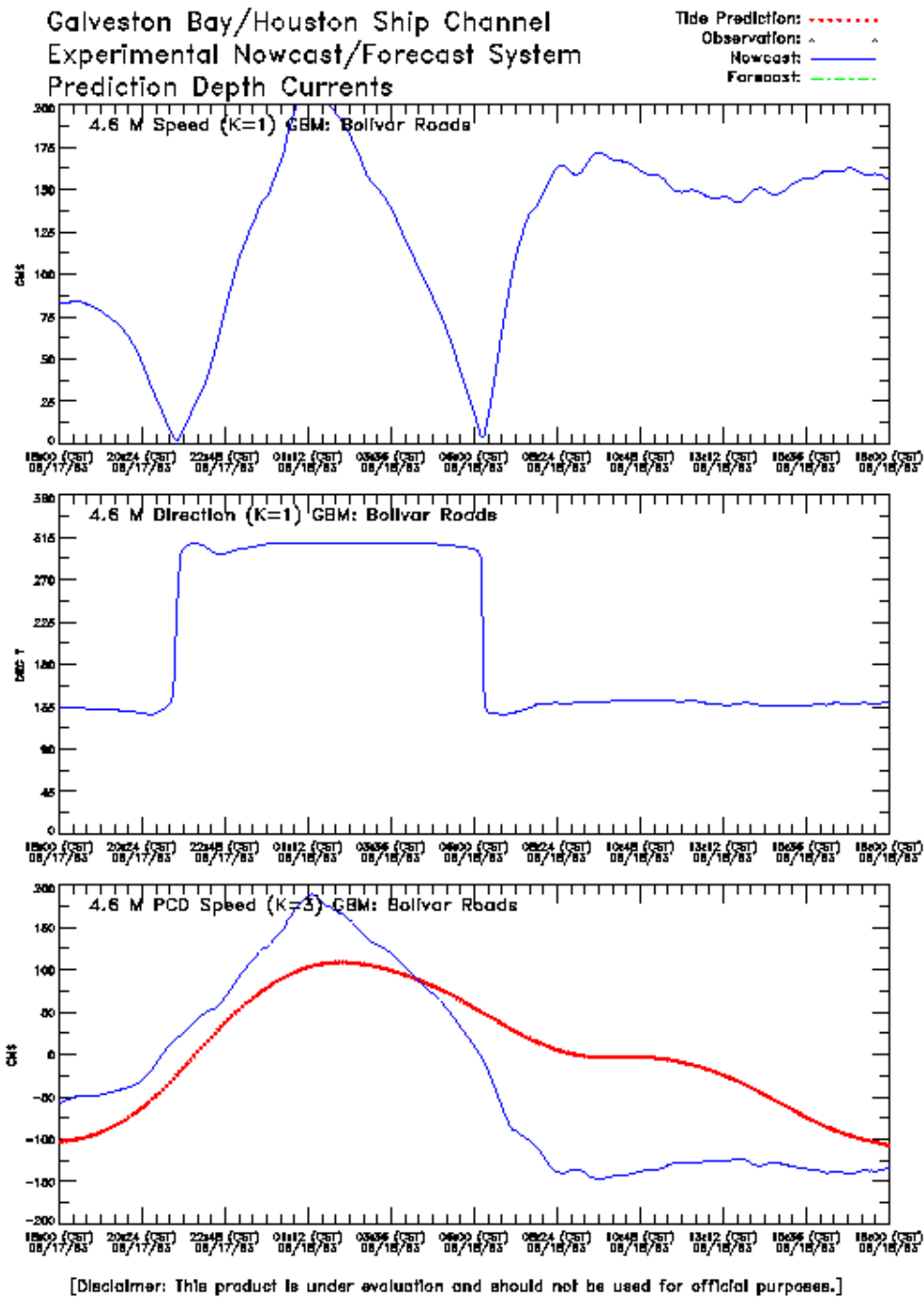


Figure 7.7. Hurricane Alicia GBM Bolivar Roads Currents Experiment One: 17-18 August 1983

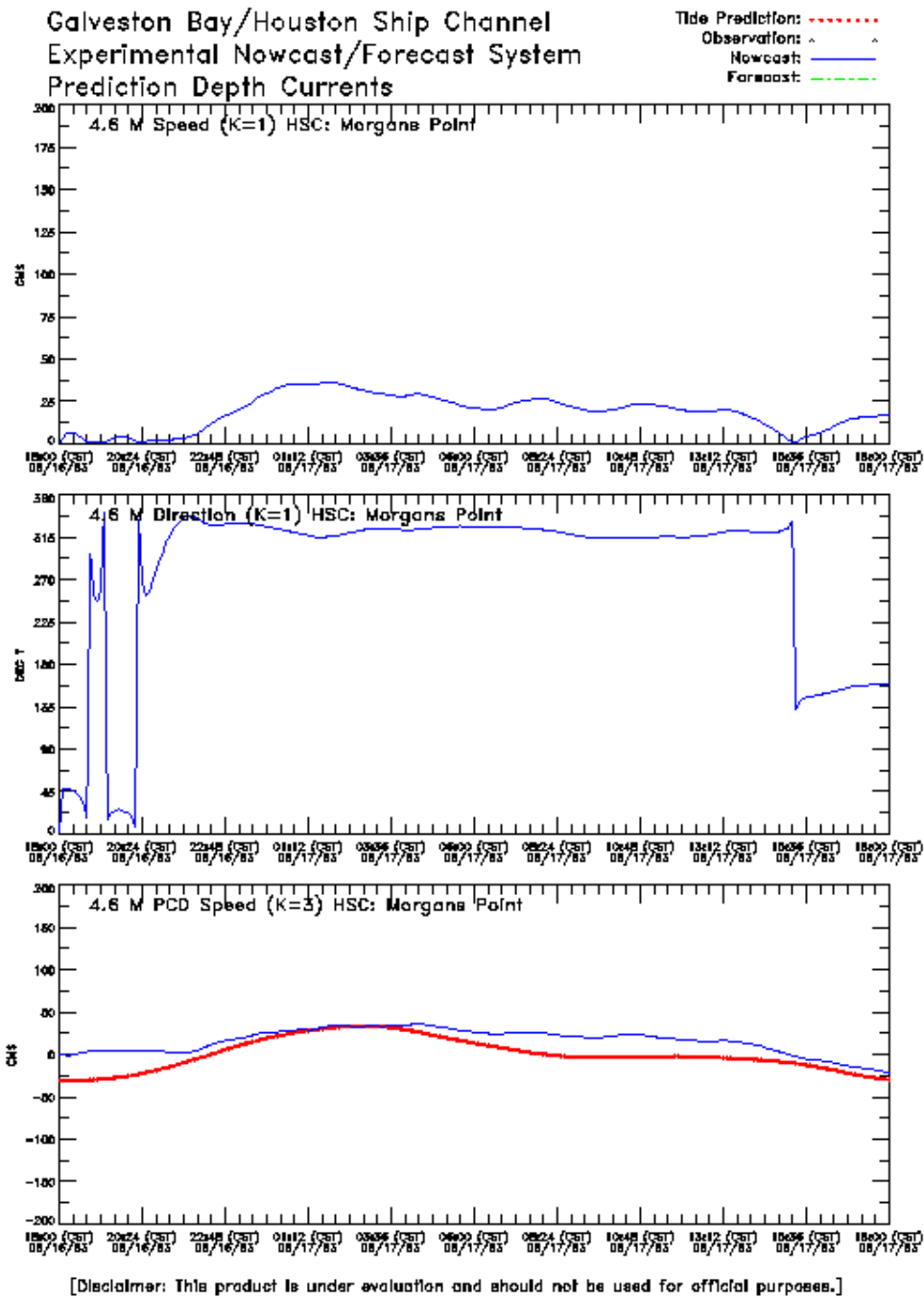


Figure 7.8. Hurricane Alicia GBM Morgans Point Currents Experiment One: 16-17 August 1983

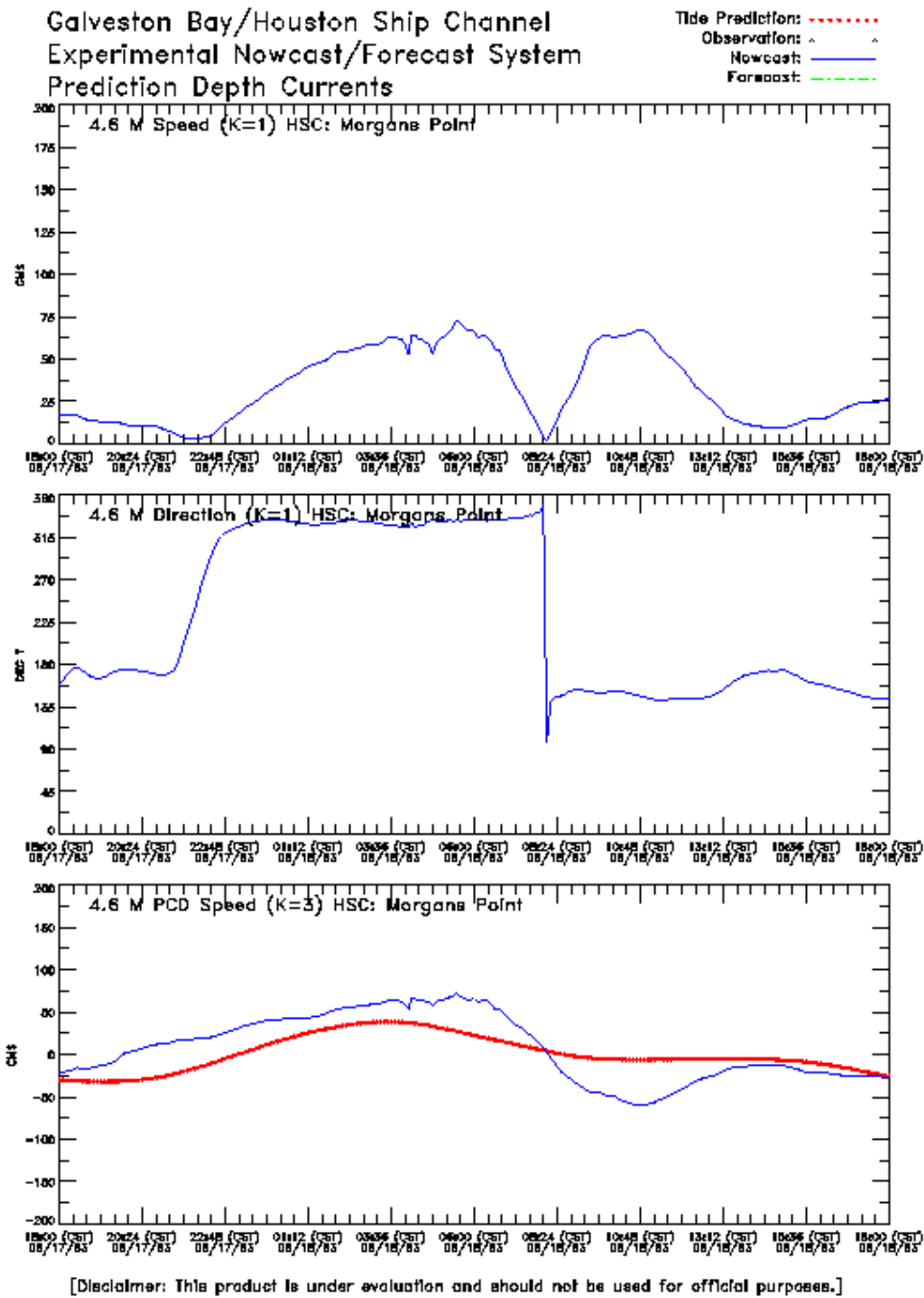


Figure 7.9. Hurricane Alicia GBM Morgans Point Currents Experiment One: 17-18 August 1983

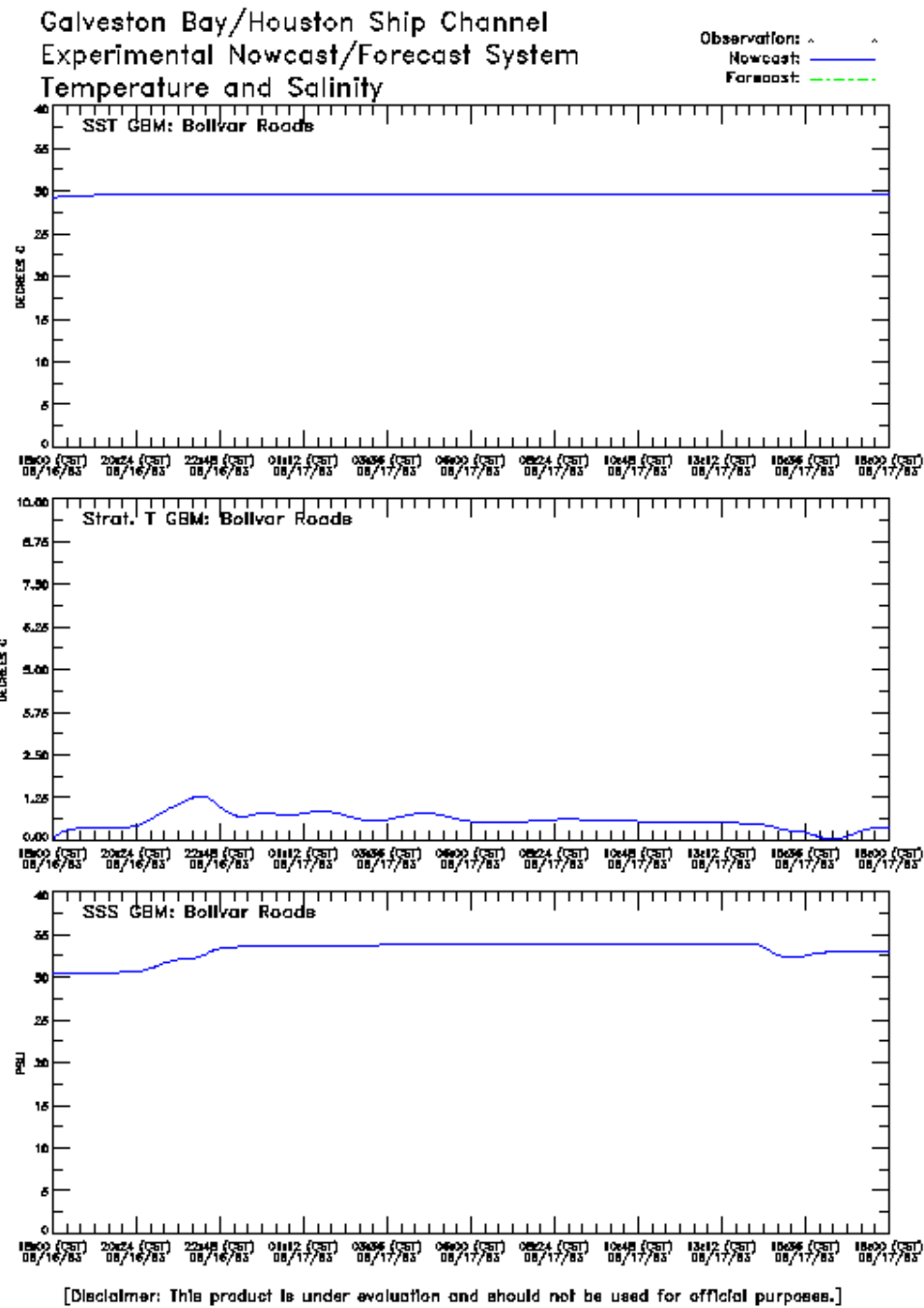


Figure 7.10. Hurricane Alicia GBM Bolivar Roads Temperature and Salinity Experiment One: 16-17 August 1983

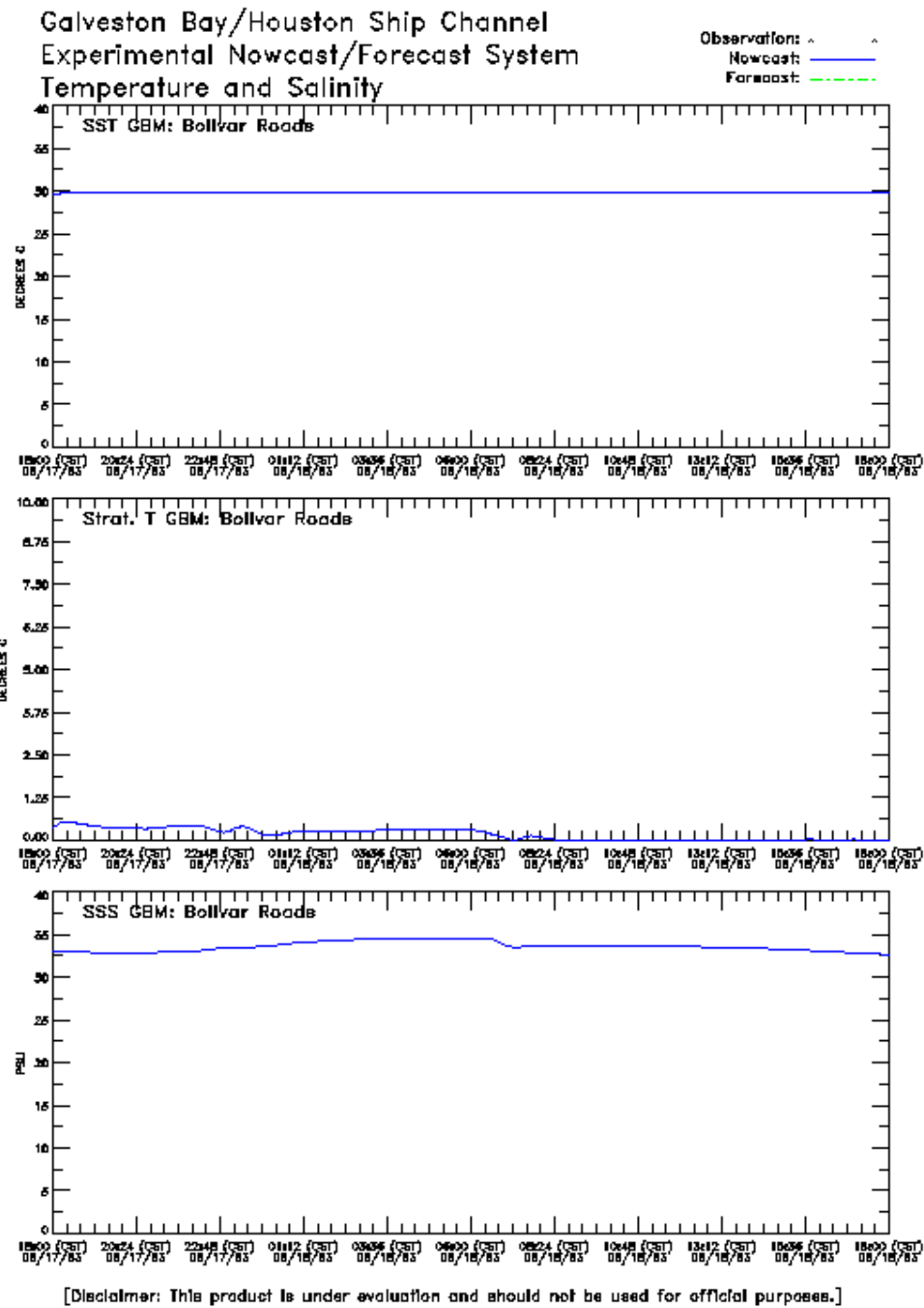


Figure 7.11. Hurricane Alicia GBM Bolivar Roads Temperature and Salinity
Experiment One: 17-18 August 1983

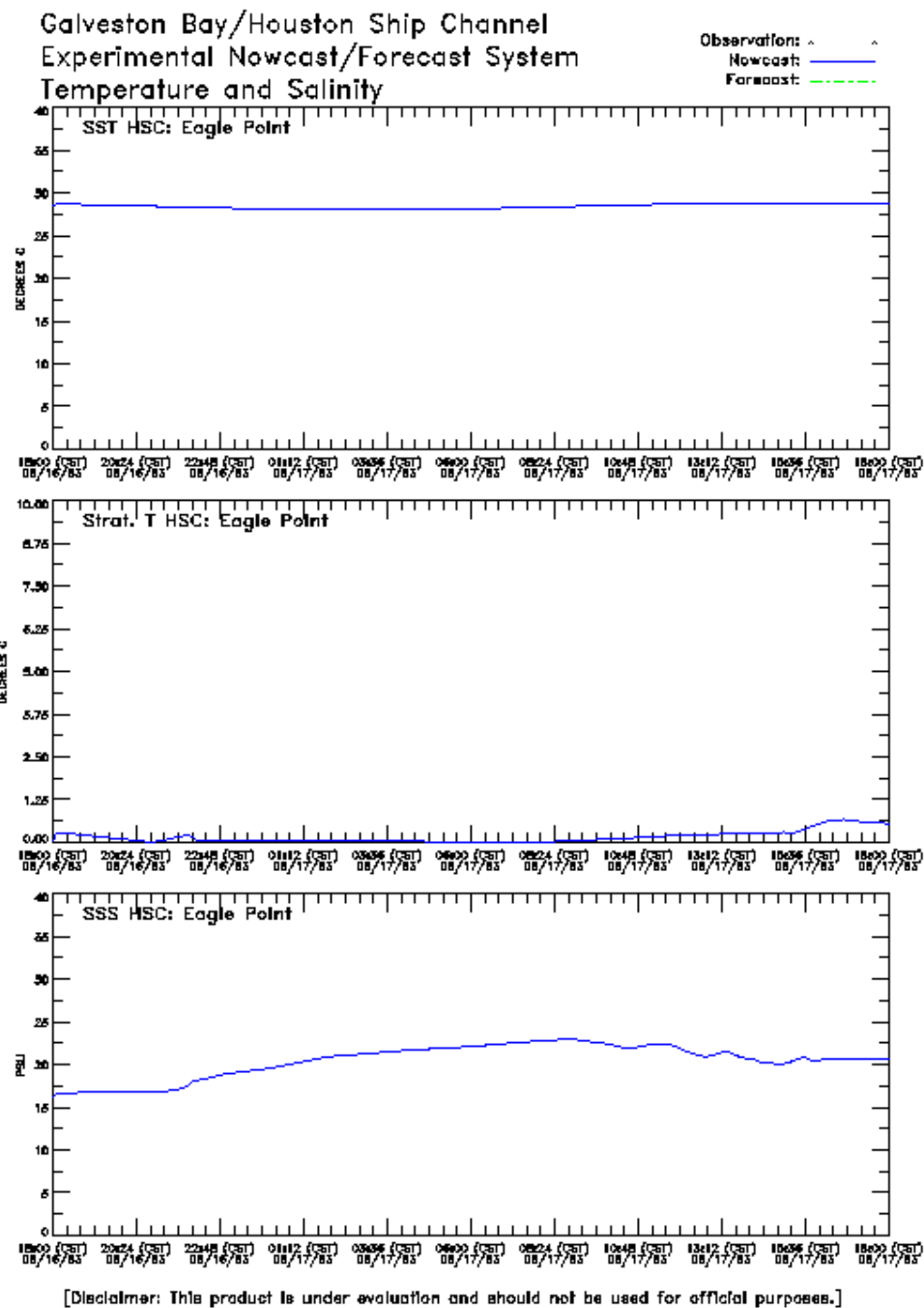


Figure 7.12. Hurricane Alicia HSCM Eagle Point Temperature and Salinity Experiment One: 16-17 August 1983

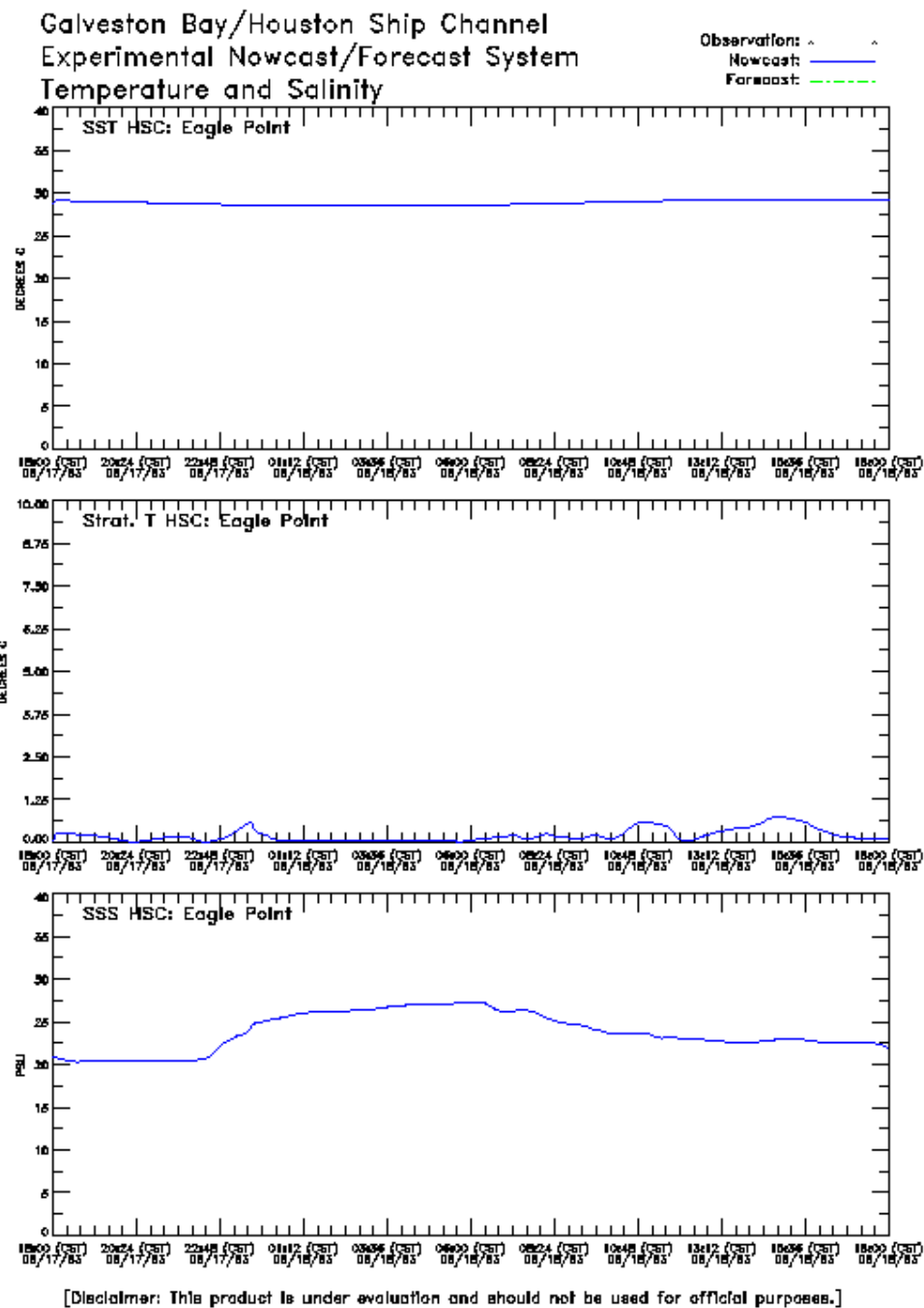


Figure 7.13. Hurricane Alicia HSCM Eagle Point Temperature and Salinity Experiment One: 17-18 August 1983

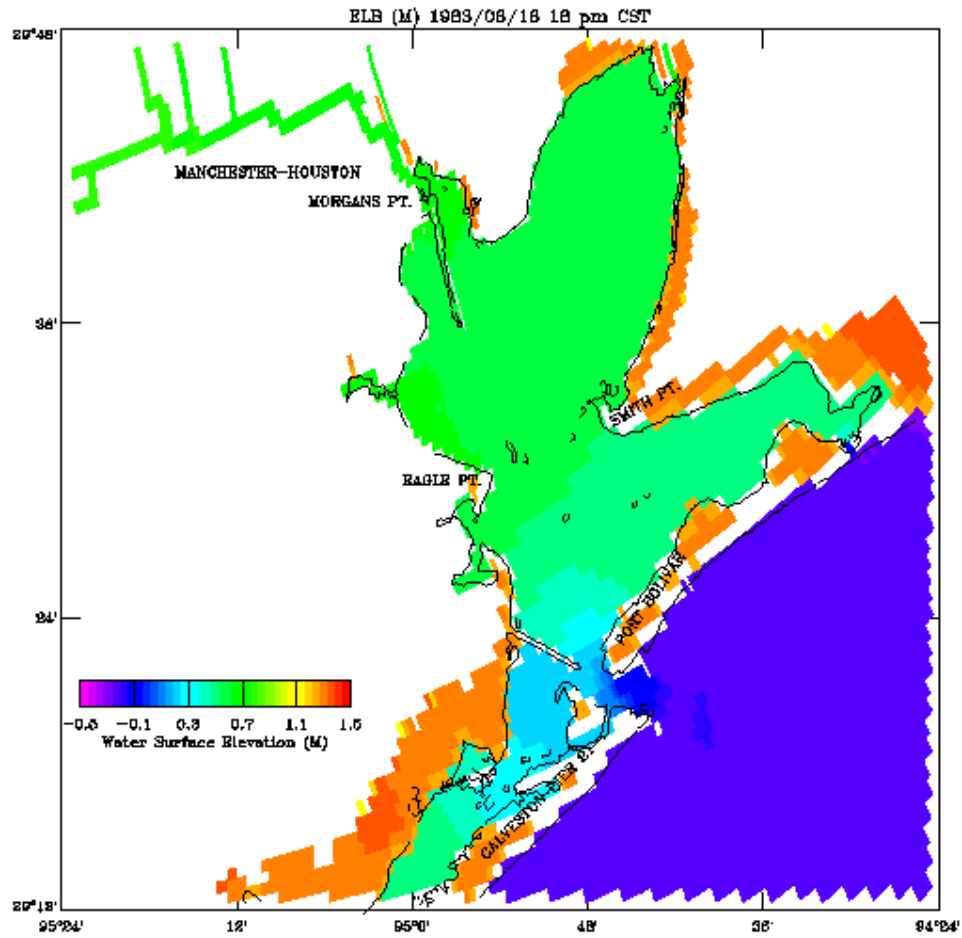


Figure 7.14. Hurricane Alicia GBM Water Surface Elevation Field
Experiment One: 18 August 1983 18:00 CST

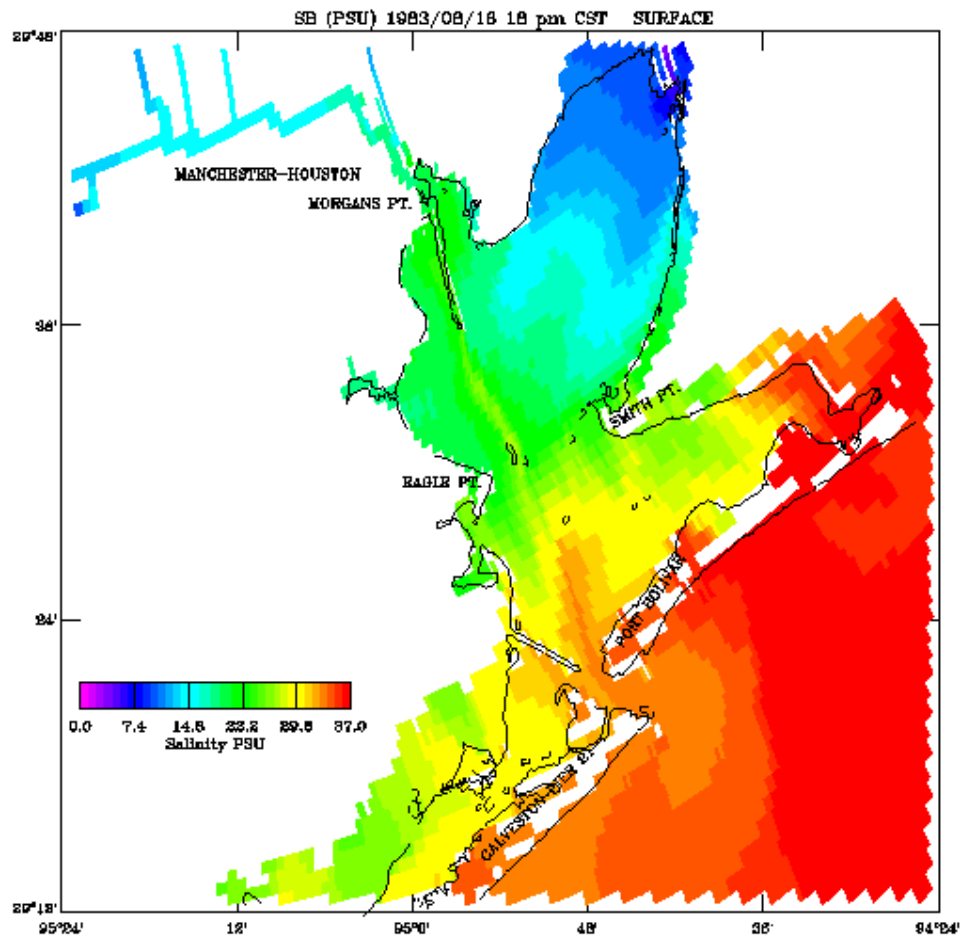


Figure 7.15. Hurricane Alicia GBM Near Surface Salinity Field
Experiment One: 18 August 1983 18:00 CST

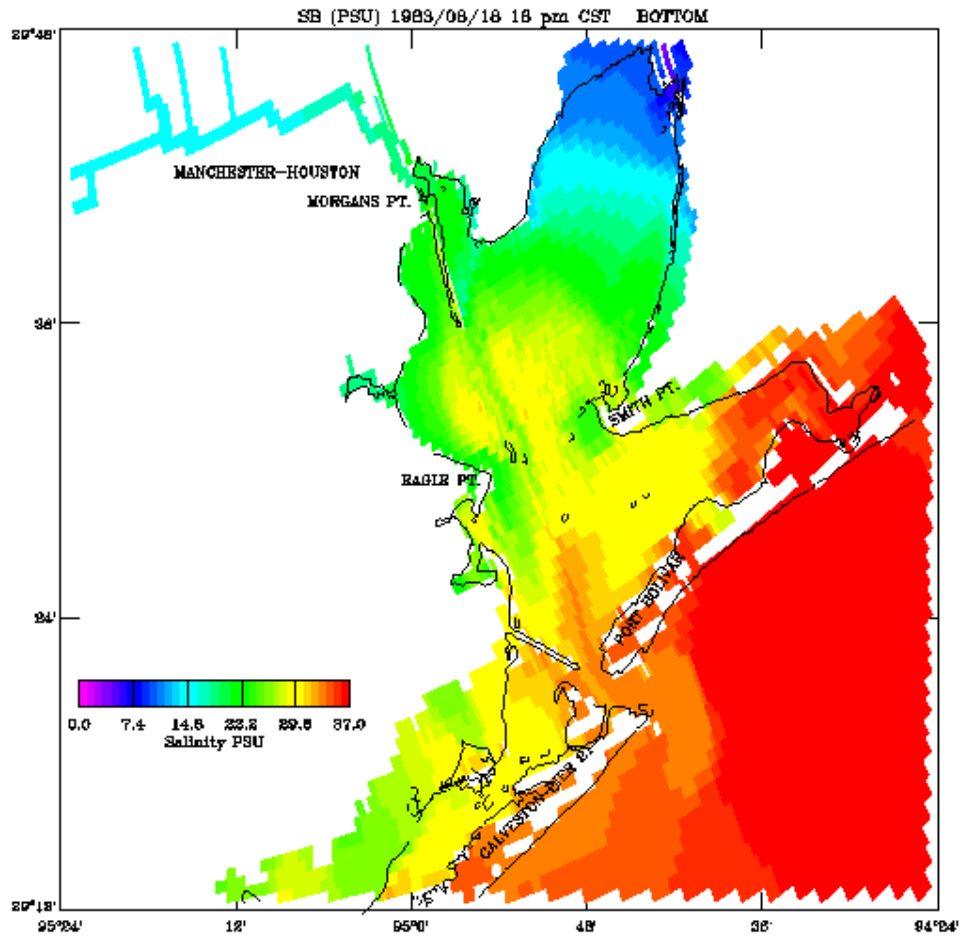


Figure 7.16. Hurricane Alicia GBM Near Bottom Salinity Field
Experiment One: 18 August 1983 18:00 CST

7.4. Experiment One Short Wave Results

Unfortunately, no wave information was available and the results must be judged as being representative of hurricane wave conditions. In experiment one, no wind forcing was applied. An empirical reduction formula is used to reduce the offshore boundary wave condition generated using Equation 5.13 over the interior grid cells.

Simulated significant wave height for each of the two hindcasts is shown at Galveston Pleasure Pier, Bolivar Roads, and Galveston Pier 21 in Figures 7.17-7.18. One notes the period of elevated simulated wave heights on top of the elevated simulated water levels noted in the long wave results and the potential for overland flooding and overtopping of the barrier islands with accompanying large waves order 5m. In Figures 7.19-7.20, HSCM simulated significant wave heights are shown for each hindcast at Eagle Point and Morgans Point with maximum significant wave heights of 2.6m and 2.5m, respectively. In the third panel of these figures, the simulated significant wave height at NDBC buoy 42035 is given, which represents the GBM open boundary wave condition. This significant wave height is applied uniformly in space over the entire GBM open water boundary. Note the maximum simulated significant wave heights are order 10m.

Note in this experiment with no wind generation, the significant wave direction is equal to the offshore boundary swell condition in all interior grid cells and varies in time based on the relation given in Equation 5.13. As a result, wave directions are the same for all of the above stations and are near 315 degrees True.

GBM simulated significant wave periods for each of the hindcasts are shown at Galveston Pleasure Pier, Bolivar Roads, and Galveston Pier 21 in Figures 7.21-7.22. In Figures 7.23-7.24, HSCM simulated significant wave periods are shown for each hindcast at Eagle Point and Morgans Point, respectively. Maximum simulated significant wave periods range from 4 to 8s. In the third panel of these figures, the simulated significant wave period range from 11 to 18s at NDBC buoy 42035, which represents the GBM open boundary wave condition. This significant wave period is applied uniformly in space over the entire GBM open water boundary. Note in the case of no wind generation, the significant wave period as given in Equation 5.13 is a function of significant wave height, which is based on empirical reduction. As a result, wave periods are the similar in form at all of the above stations.

GBM simulated significant wave height and direction vectors are shown at the end of hindcast two in Figure 7.25. At the end of the second hindcast in Figure 7.25 one notes that the barrier islands have been overtopped and that flooding has occurred and that wave computations have been performed over the flooded cells. Simulated significant wave heights are in the range from 1 m in upper Trinity Bay to 10m near the offshore boundary. Note in the present case of no wind generation, simulated significant wave directions are near 315 deg True for all grid cells.

Next GBM simulated significant wave period contours are shown in Figure 7.26 at the end of hindcast two. Simulated significant wave periods range from below 1s in upper Trinity Bay to over 10s near the offshore boundary.

HSCM simulated significant wave height and direction vectors and wave period contours are consistent with those of the GBM. Simulated significant wave periods are in the range of 1 to 7s consistent with those computed over the GBM.

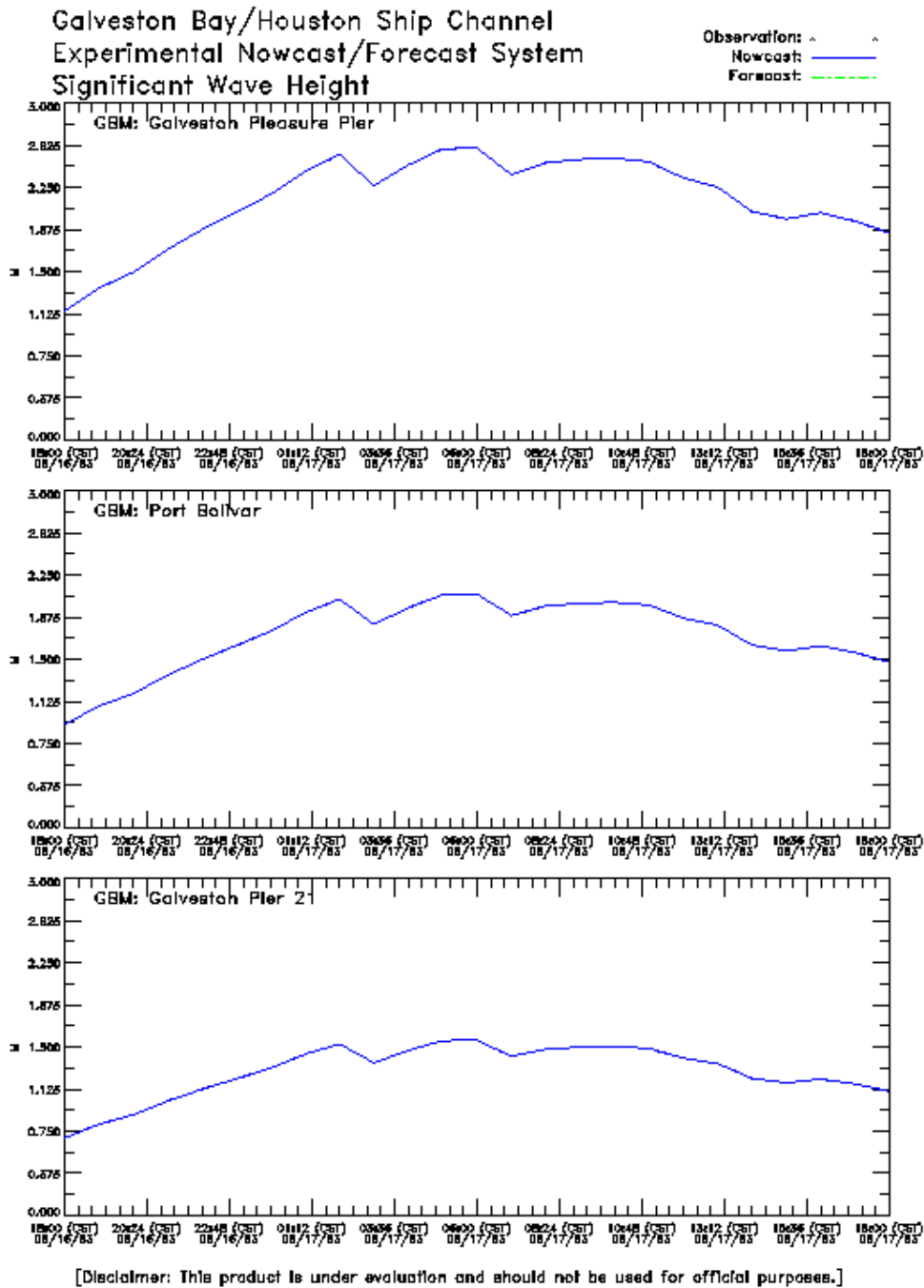


Figure 7.17. Hurricane Alicia GBM Significant Wave Height Experiment One: 16-17 August 1983

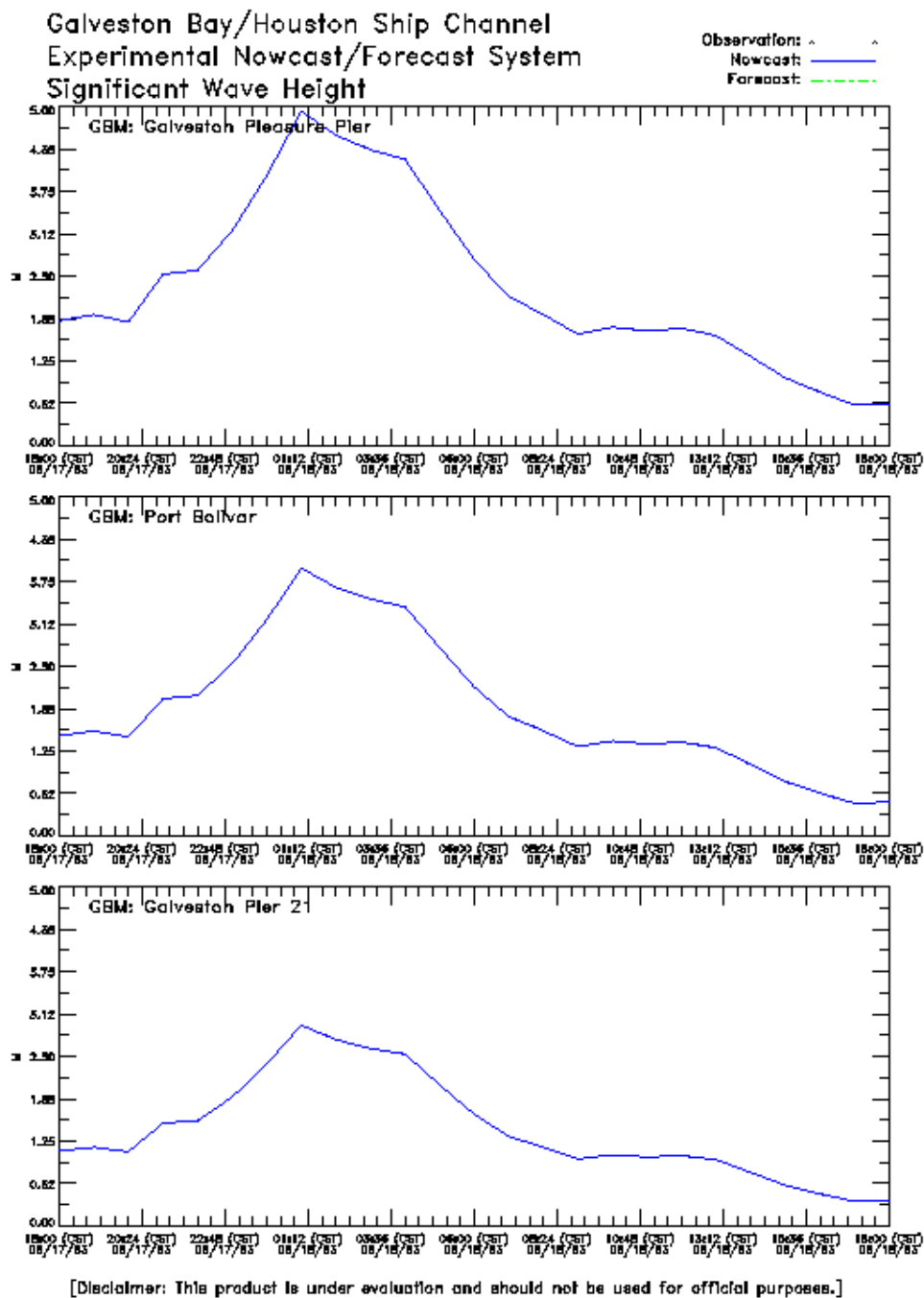


Figure 7.18. Hurricane Alicia GBM Significant Wave Height Experiment One: 17-18 August 1983

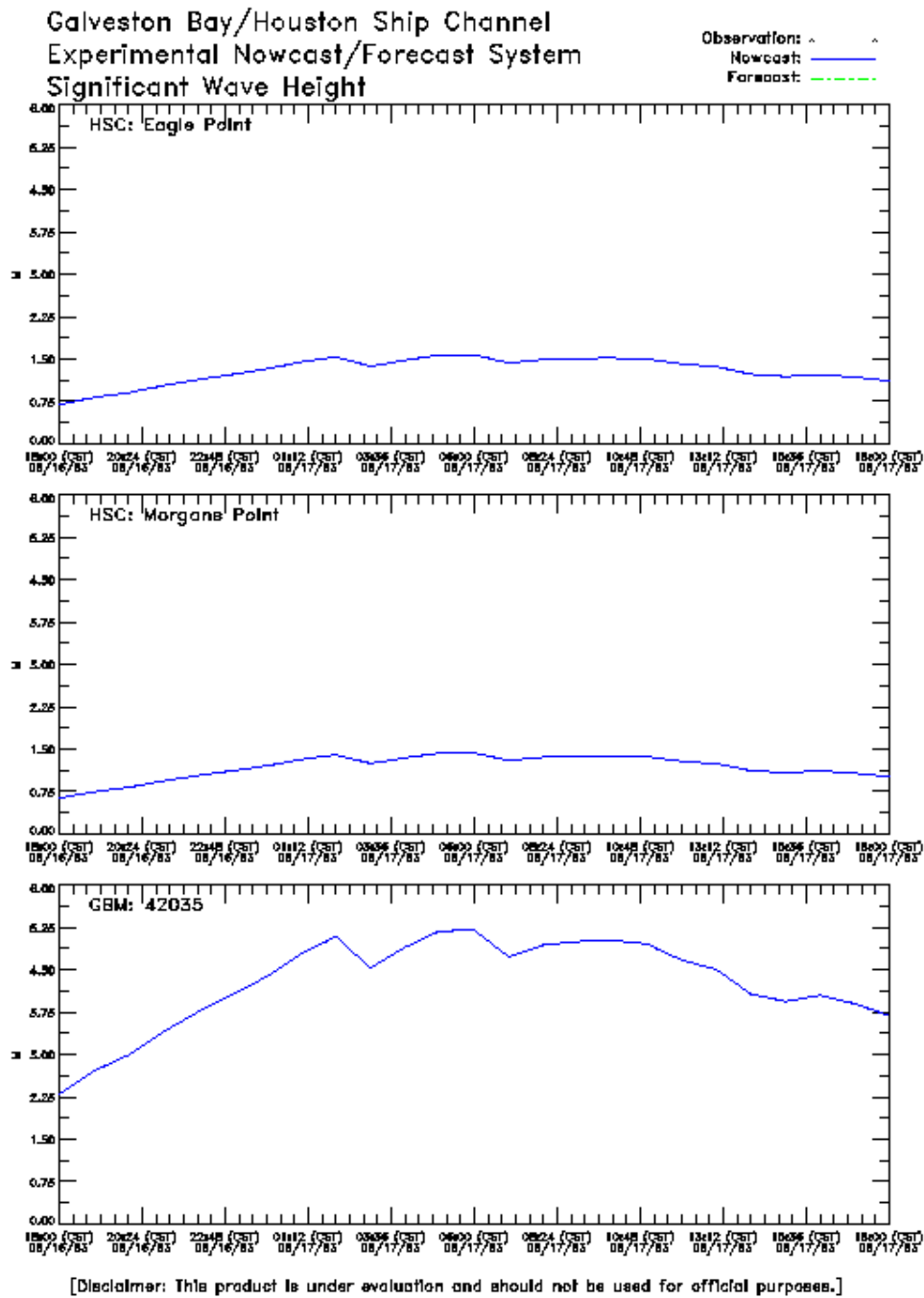


Figure 7.19. Hurricane Alicia HSCM and GBM 42035 Significant Wave Height Experiment One: 16-17 August 1983

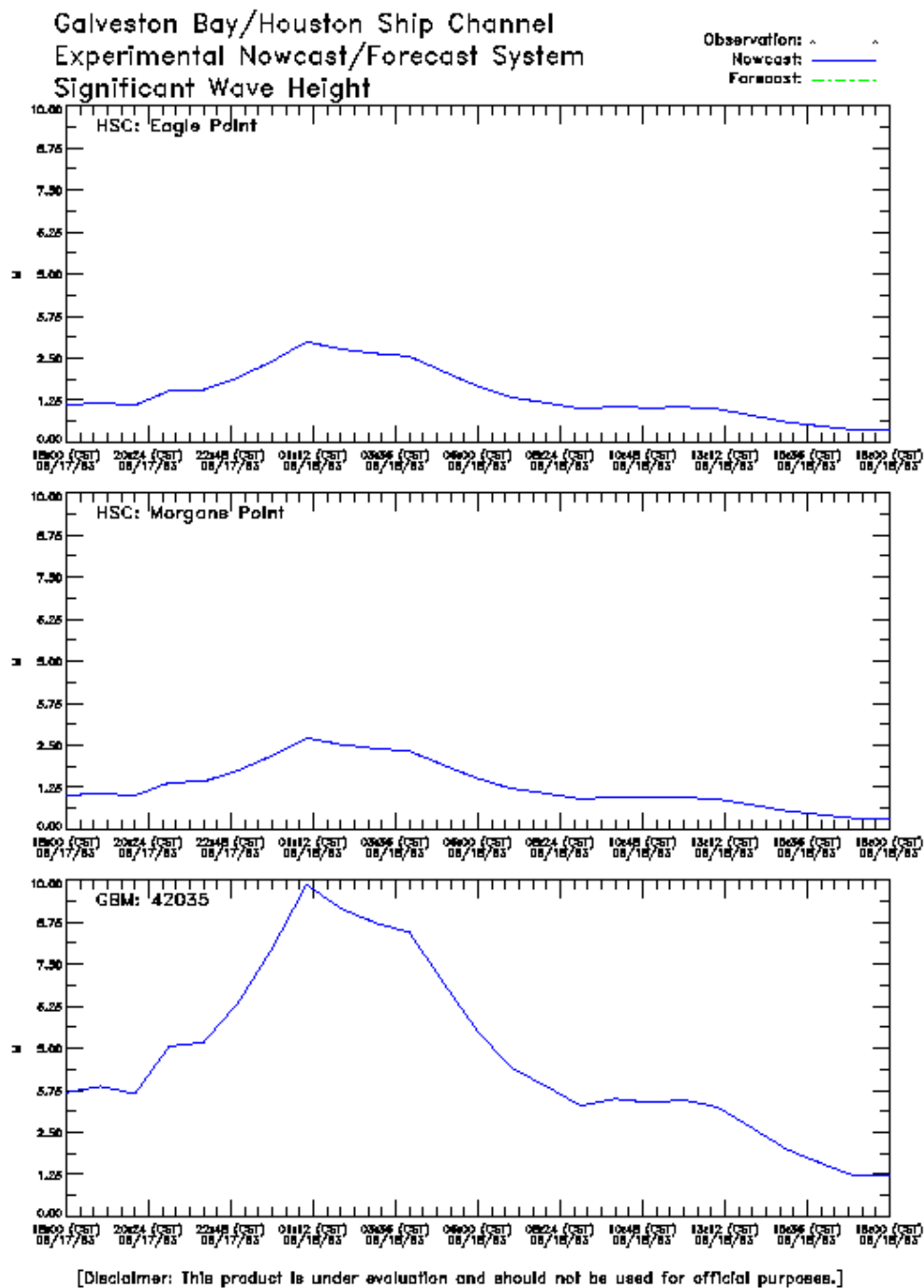


Figure 7.20. Hurricane Alicia HSCM and GBM 42035 Significant Wave Height Experiment One: 17-18 August 1983

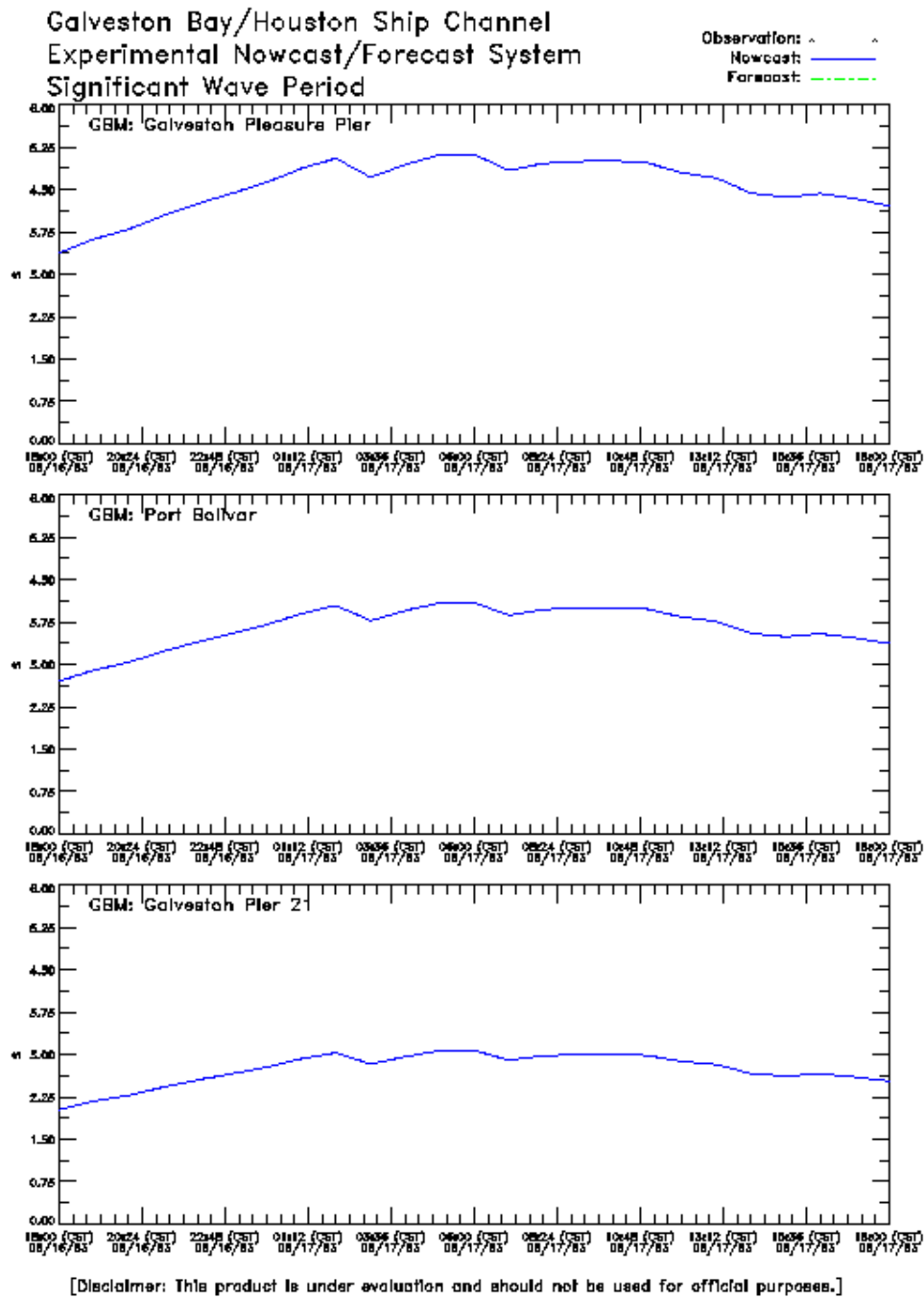


Figure 7.21. Hurricane Alicia GBM Significant Wave Period Experiment One: 16-17 August 1983

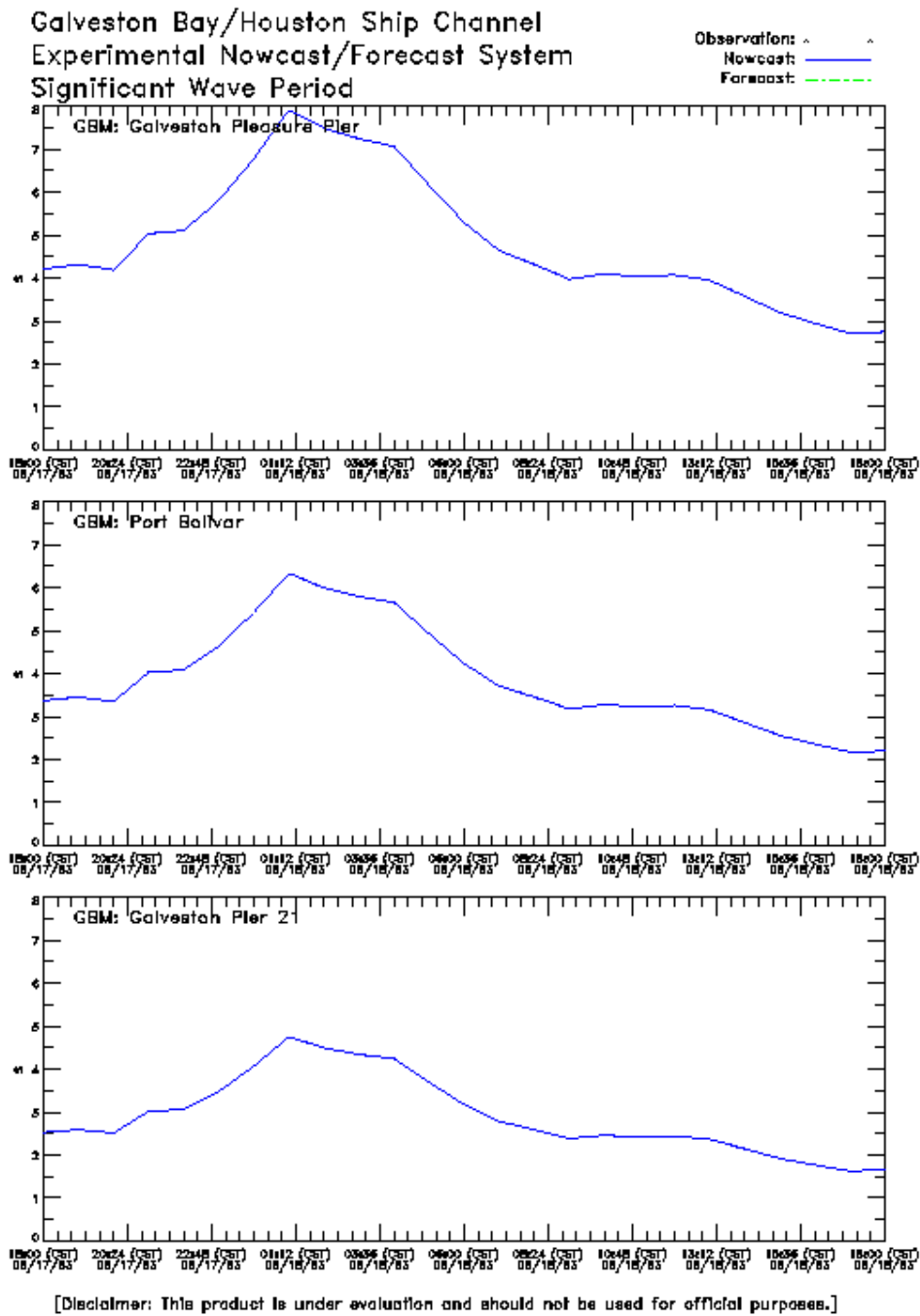


Figure 7.22. Hurricane Alicia GBM Significant Wave Period Experiment One: 17-18 August 1983

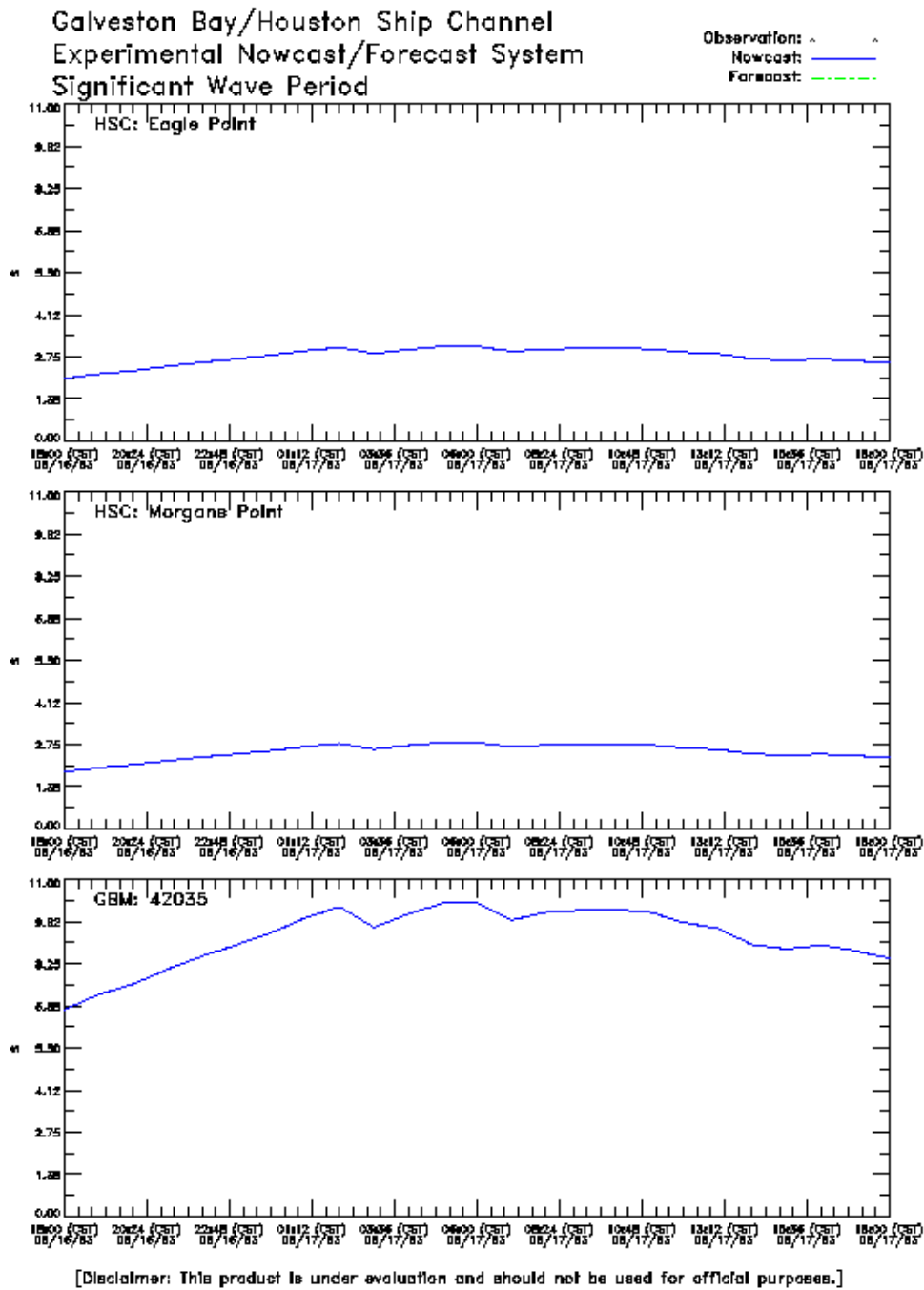


Figure 7.23. Hurricane Alicia HSCM and GBM 42035 Significant Wave Period Experiment One: 16-17 August 1983

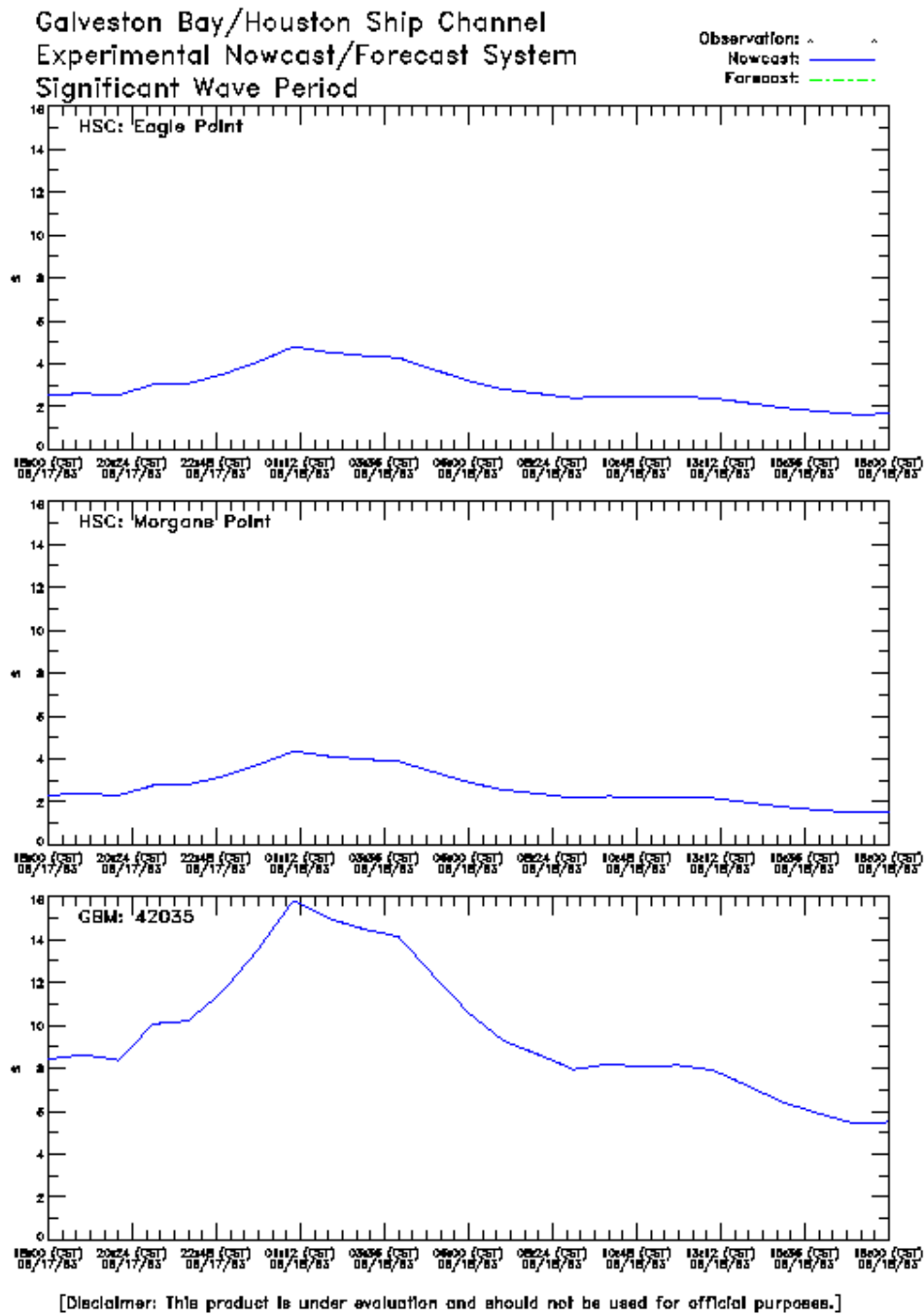


Figure 7.24. Hurricane Alicia HSCM and GBM 42035 Significant Wave Period Experiment One: 17-18 August 1983

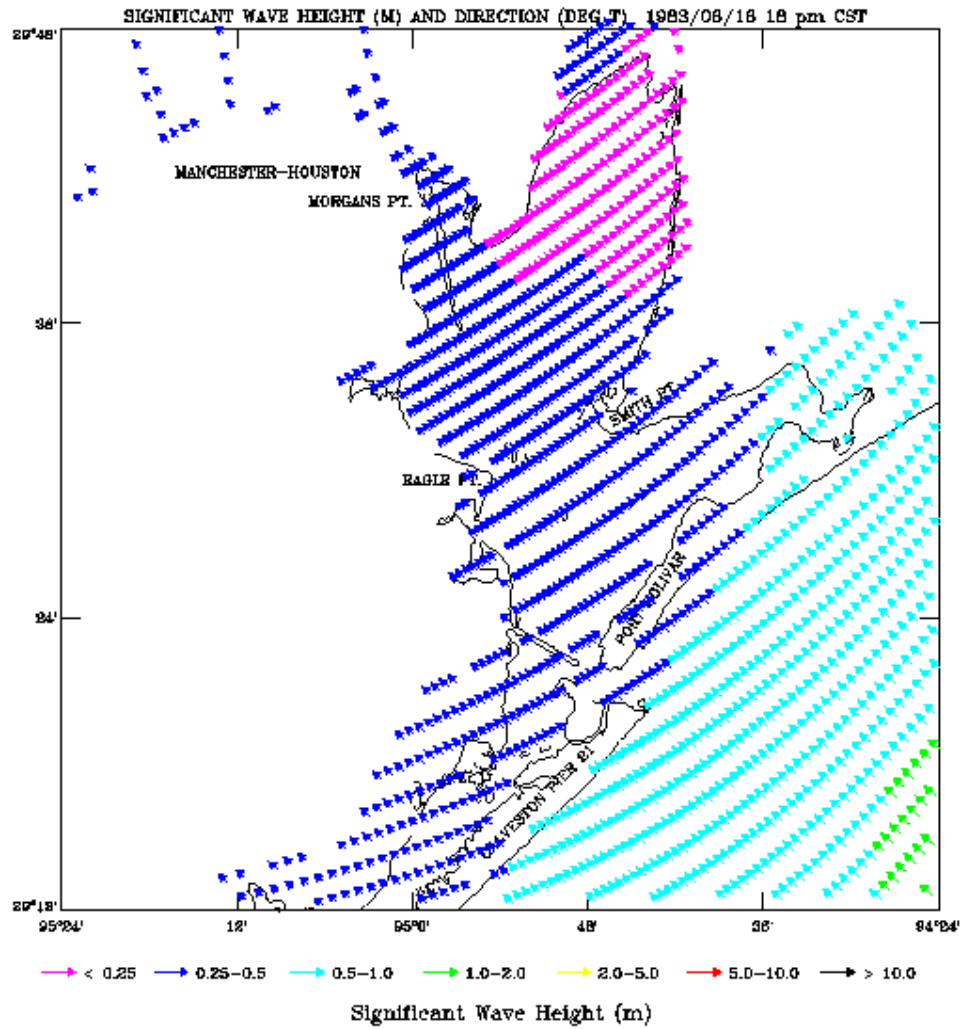


Figure 7.25. Hurricane Alicia GBM Significant Wave Height and Direction
 Experiment One: 18 August 1983 18:00 CST

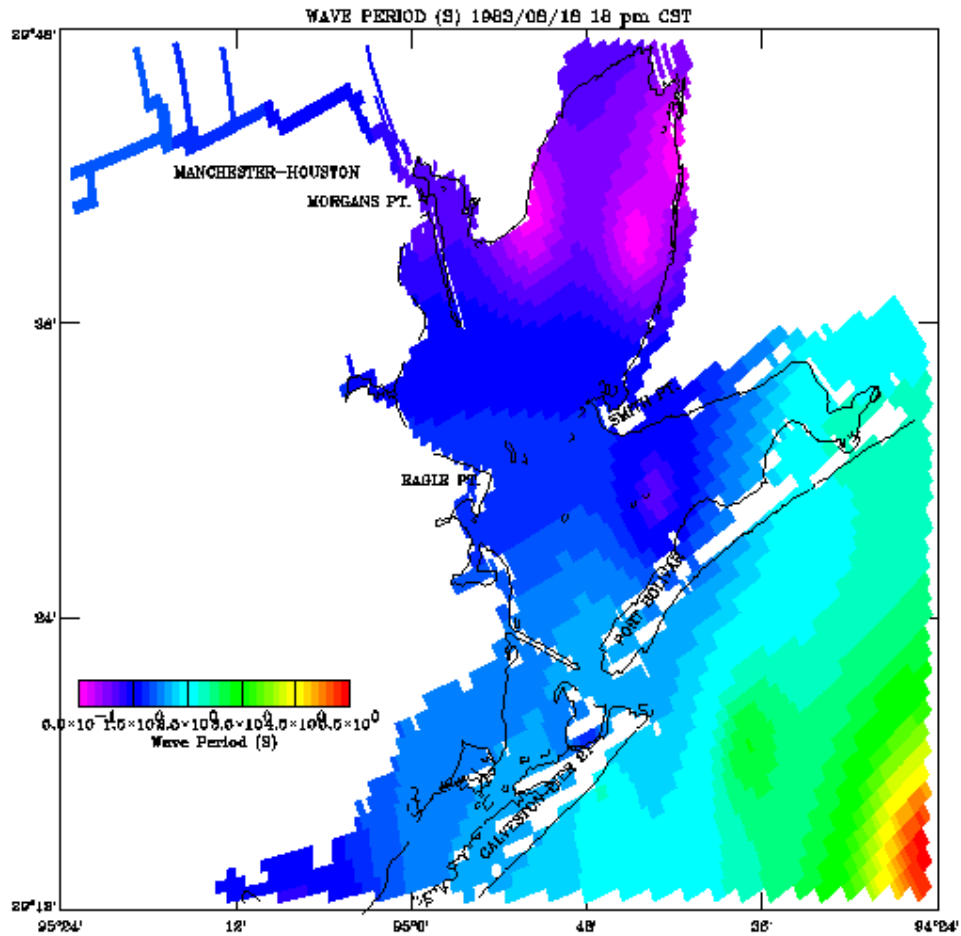


Figure 7.26. Hurricane Alicia GBM Significant Wave Period Experiment One: 18 August 1983 18:00 CST

7.5. Experiment Two Long and Short Wave Results

In experiment two, the parametric hurricane wind and atmospheric pressure model is used to provide the meteorological forcing. It should be noted that the present procedure does not allow for a reduction of windspeed due to overland friction effects directly. The central pressure deficit of the storm is reduced based on observed overland weakening, but the windfields computed based on the reduced pressure deficit are not further reduced.

GBM simulated water surface elevations for each of the two hindcasts are shown at Galveston Pleasure Pier, Bolivar Roads, and Galveston Pier 21 in Figures 7.27-7.28. In Figures 7.29-7.30, HSCM simulated water surface elevations are shown for each hindcast at Eagle Point and Morgans Point. Simulated water levels exceed those of experiment one and are above the available observations by over 1 m, indicating the influence of local wind and atmospheric pressure forcing.

These forcing are shown in Figures 7.31-7.32 at Morgans Point. Simulated peak windspeeds are approximately 40 m/s at Galveston Pleasure Pier, Eagle Point, and Morgans Point. The simulated atmospheric pressure drops sharply from 1008 mb to 985 mb at all three stations. The simulated wind and atmospheric pressure forcing are from the near field of the hurricane.

Snapshots of the simulated atmospheric pressure fields using a 24 hour increment are shown in Figures 7.33-7.34, respectively, and indicate the radial structure of the hurricane atmospheric pressure field. Snapshots of the simulated windfields at the same times are shown in Figures 7.35-7.36, respectively and show a difference in wind direction over the Port of Houston and near the barrier islands. This result needs further investigation.

In experiment two, simulated significant wave heights follow the same general pattern as in experiment one and are largely determined by the GBM offshore wave conditions. Wind generation increases wave heights by order 0.60 m at Galveston Pleasure Pier and at Port Bolivar and by order 0.25 m at Eagle and Morgans Point. Simulated wave directions are in the direction of the wind and move from near 270 deg T to 45 deg T at all stations during hindcast two.

In contrast to experiment one results, simulated significant wave periods are reduced at Galveston Pleasure Pier from 7s to 5s during hindcast one and are slightly increased at the Bay by less than 1s. During hindcast two, wave periods are reduced at Galveston Pleasure Pier from 8 to 6s, while at all Bay stations the differences in wave periods are less than 1s. The wave period is computed directly from the wind wave and the offshore swell period is not used in the wave period computations.

7.6. Wind and Water Surface Elevation Validation

In Table 7.2 peak simulated windspeeds over the GBM grid are compared with fastest mile observations reported by Case and Gerrish (1984). Simulated wind speeds computed

used the parametric hurricane model are in general agreement with these observations.

Table 7.2. Hurricane Alicia (1983) Wind speed Validation. Note simulated GBM peak corresponds to results obtained in Experiment Two with parametric hurricane model wind and atmospheric pressure forcing.

Station Location	ID	Simulated GBM Peak (m/s)	Observed Fastest Mile (m/s)
Galveston	12923	41.8	27.-35.
Ellington AFB	12906	38.5	25.
Hobby Airport	12918	38.1	42.

In Table 7.3, GBM peak simulated water levels and simulated significant wave heights are compared with observed peak water levels reported by Case and Gerrish (1984). The observed peak water levels are reported with respect to MSL whereas the GBM simulated water levels are with respect to the MTL model datum. As noted previously, MSL and MTL in Galveston Bay maximum differences are order 1 cm and therefore these two vertical datums are nearly equivalent. Peak water levels from high water marks, particularly at Seabrook and Baytown may include surface gravity wave effects making direct comparison more problematical. One should note that at the two Galveston water level gauges, the comparisons with simulation results shown in Figures 7.2-7.3 for experiment one and in Figures 7.27-7.28 for experiment two are made with respect to MLLW.

Table 7.3. Hurricane Alicia (1983) GBM Storm Surge Validation. Note + indicates high water mark. Exp1==Experiment One with no wind and atmospheric forcing, while Exp 2==Experiment Two with parametric hurricane model wind and atmospheric pressure forcing. Note *==Morgans Point value and #==Christmas Bay value.

Station Location	Simulated Peak Water Level (m-MTL)		Simulated Peak Wave Height (m)		Observed Peak Water Level (m-MSL)
	Exp 1	Exp 2	Exp 1	Exp2	
Galveston Pl. Pier	2.20	3.27	4.93	5.65	2.64
Galveston Pier 21	1.77	2.75	2.96	2.96	1.71
Seabrook	1.57*	3.85*	1.97*	2.72*	3.45+
Baytown	1.57*	3.85*	1.97 *	2.72*	3.24+
San Luis Pass	1.87#	2.23#	1.97#	1.97#	3.85+

7.7. Surface Salinity, Surface Current, and Inundation Statistics

In Table 7.4, GBM simulated surface minimum salinity and simulated maximum surface current strengths for stations proceeding northward up Galveston Bay are compared between experiment one and two. The added wind forcing significantly adjust the salinity structure and increase the maximum currents, due to the proximity of the center of the storm.

Inundation statistics for both experiments are presented in Table 7.5 in terms of the time and areal extent of the maximum flooding. Average and maximum flood depths are also determined. Experiment two values are significantly elevated over those of experiment one due the influence of the strong wind and atmospheric pressure forcing.

Table 7.4. Hurricane Alicia (1983) GBM Minimum Surface Salinity and Maximum Current Speeds. Exp1==Experiment One with no wind and atmospheric forcing, while Exp 2==Experiment Two with parametric hurricane model wind and atmospheric pressure forcing.

Station Location	Minimum Salinity (PSU)		Maximum Current (m/s)	
	Exp 1	Exp 2	Exp 1	Exp 2
Galveston Pleasure Pier	33.4	34.6	0.55	1.62
Galveston Pier 21	31.7	32.7	1.46	1.95
Eagle Point	19.9	29.8	0.71	0.56
Smith Point	24.6	13.0	0.67	1.94
Morgans Point	19.4	18.4	0.33	1.19
Round Point	10.8	7.9	0.14	0.57

Table 7.5. Hurricane Alicia (1983) Inundation Statistics. Note the first line corresponds to results from Experiment 1 with no wind and atmospheric pressure forcing. The second line presents results from Experiment 2 with parametric hurricane wind and atmospheric pressure forcing.

Hindcast No.	Simulation Dates	Time of Maximum Flood (JD)	Maximum Flooded Area (km ²)	Average Flood Depth (m)	Maximum Flood Depth (m)
1	8/16-8/17	-	-	-	-
		229.746	180	0.440	0.775
2	8/17-8/18	230.413	980	0.324	1.251
		230.704	1476	0.590	3.612

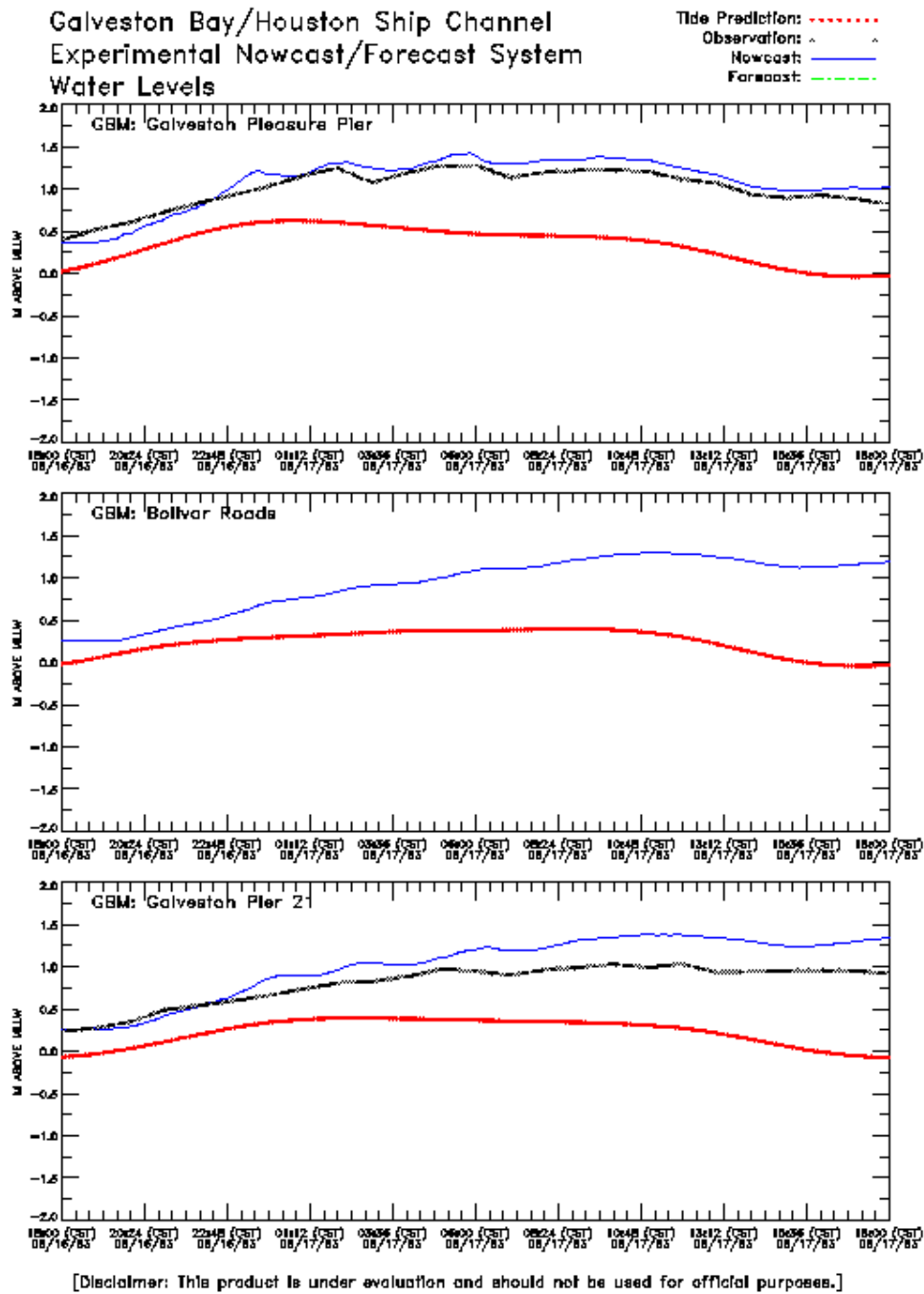


Figure 7.27. Hurricane Alicia GBM Water Levels Experiment Two:
16-17 August 1983

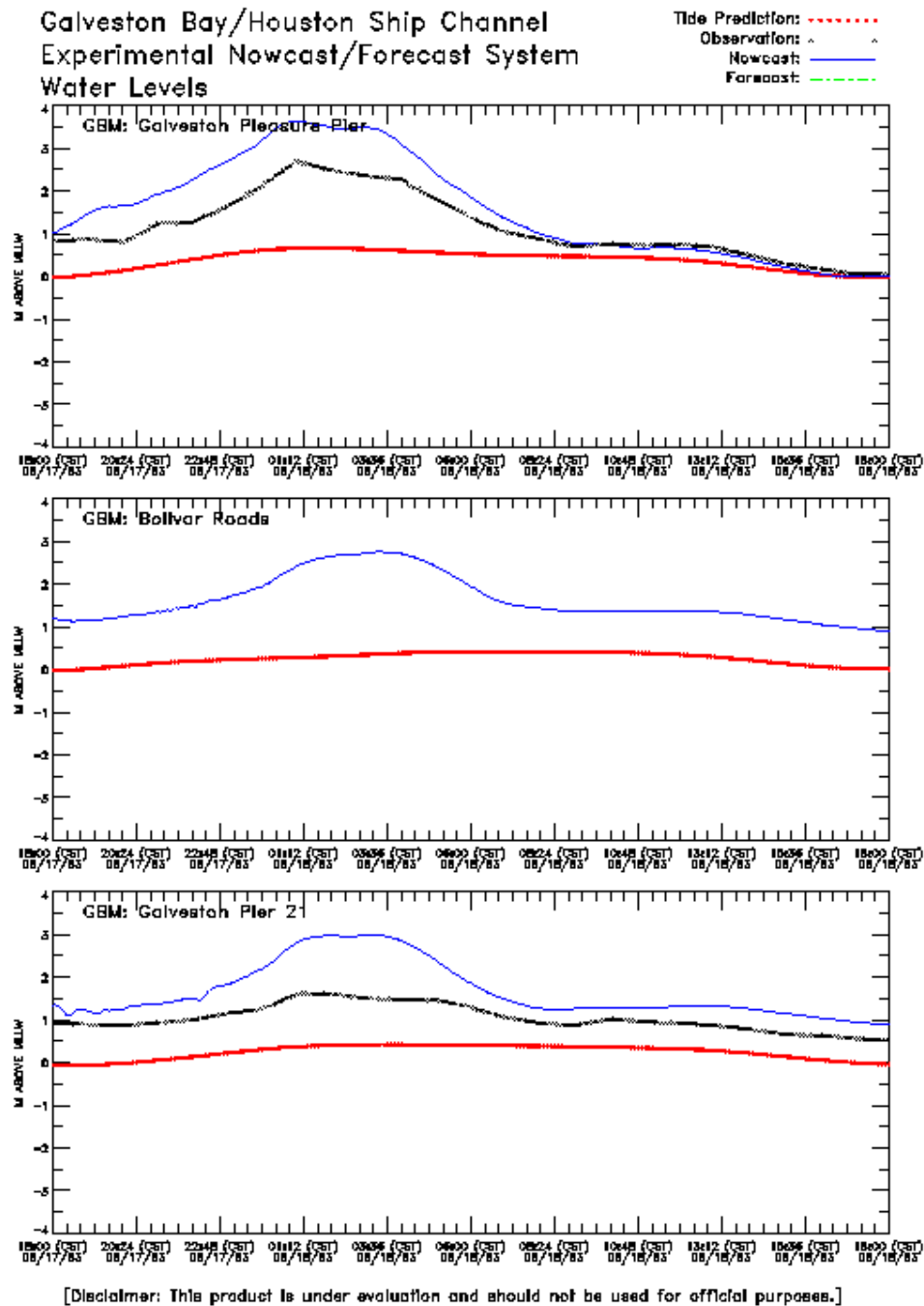


Figure 7.28. Hurricane Alicia GBM Water Levels Experiment Two:
17-18 August 1983

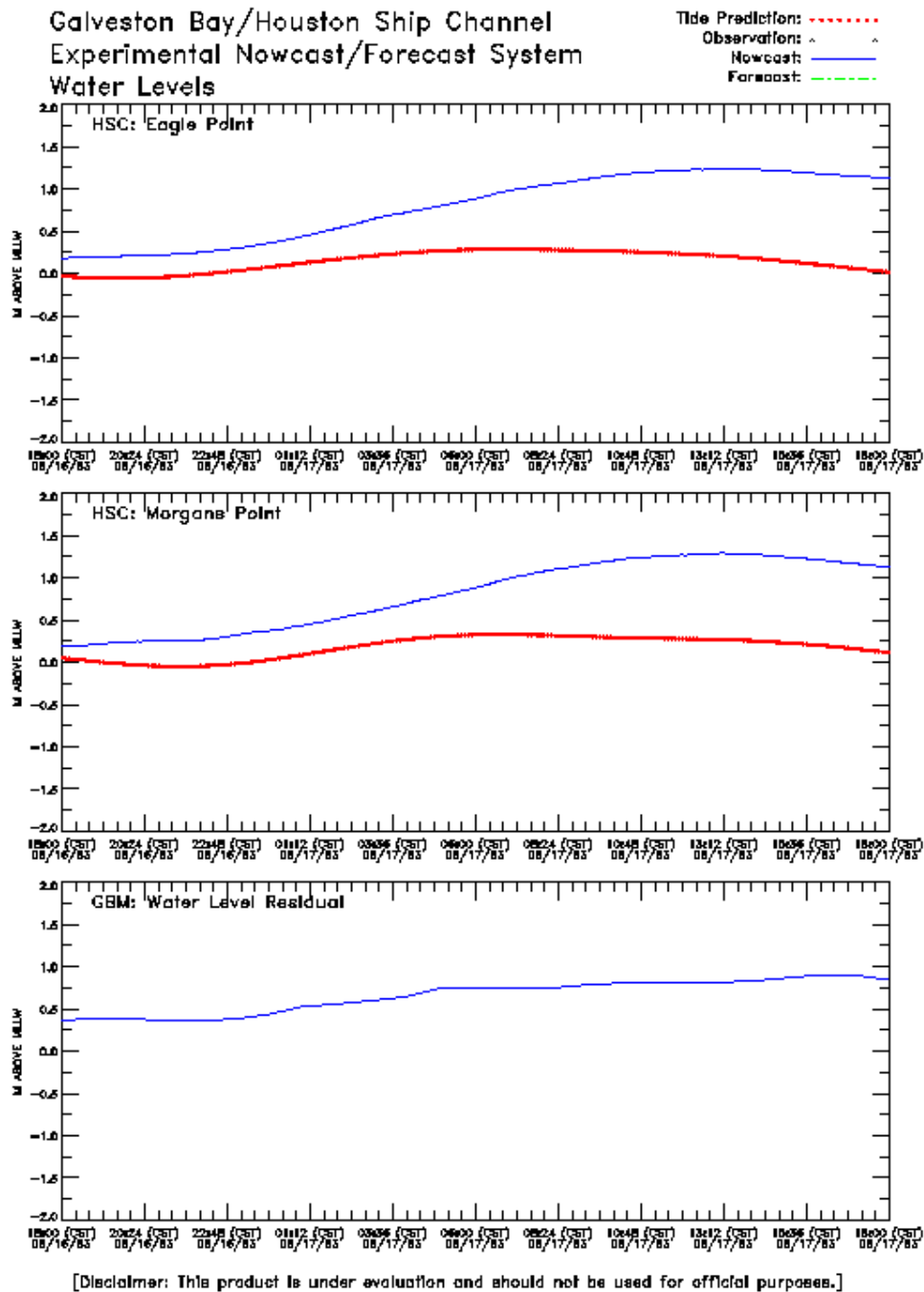


Figure 7.29. Hurricane Alicia HSCM Water Levels and GBM Water Level Residual Experiment Two: 16-17 August 1983

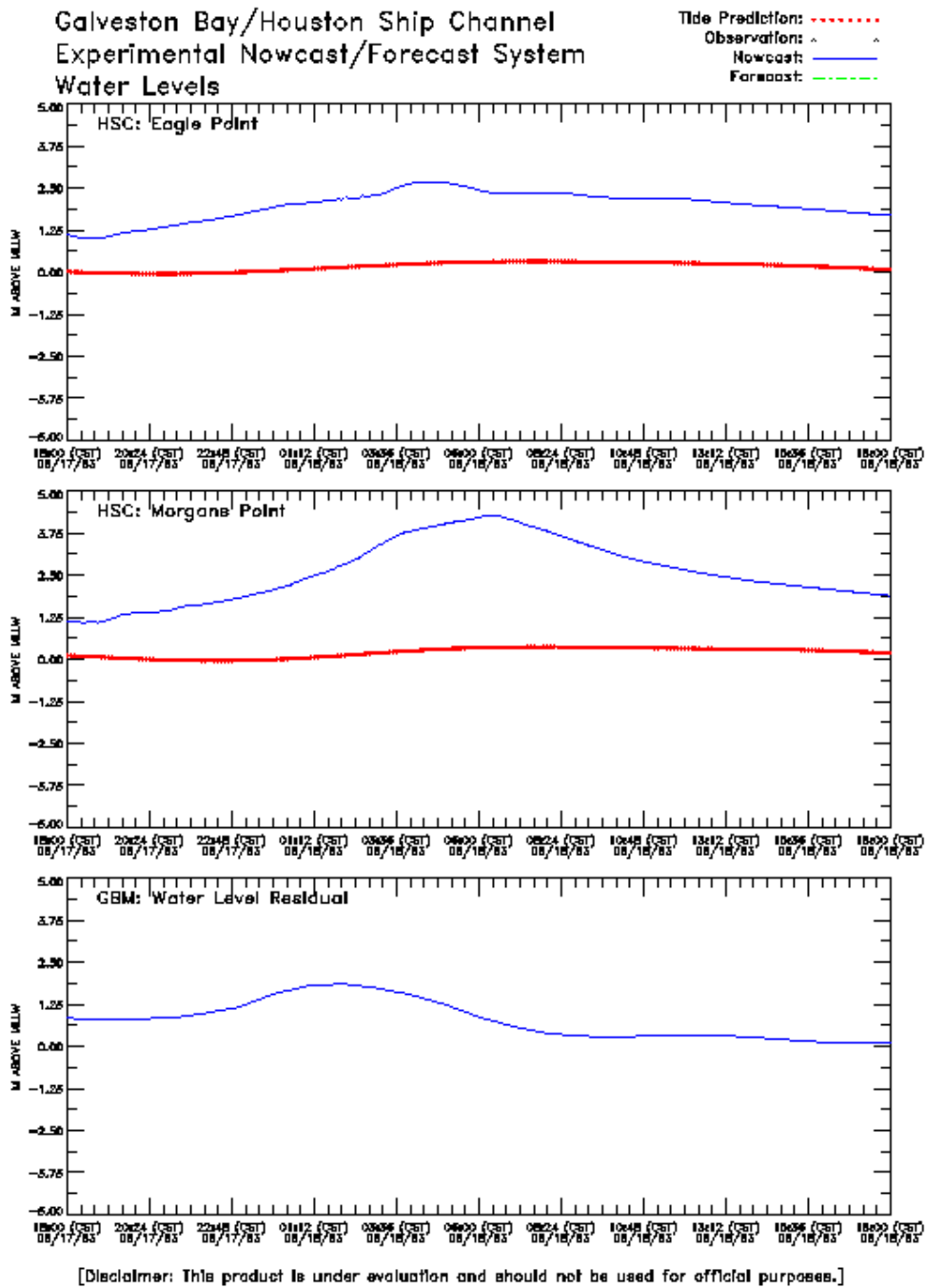


Figure 7.30. Hurricane Alicia HSCM Water Levels and GBM Water Level Residual Experiment Two: 17-18 August 1983

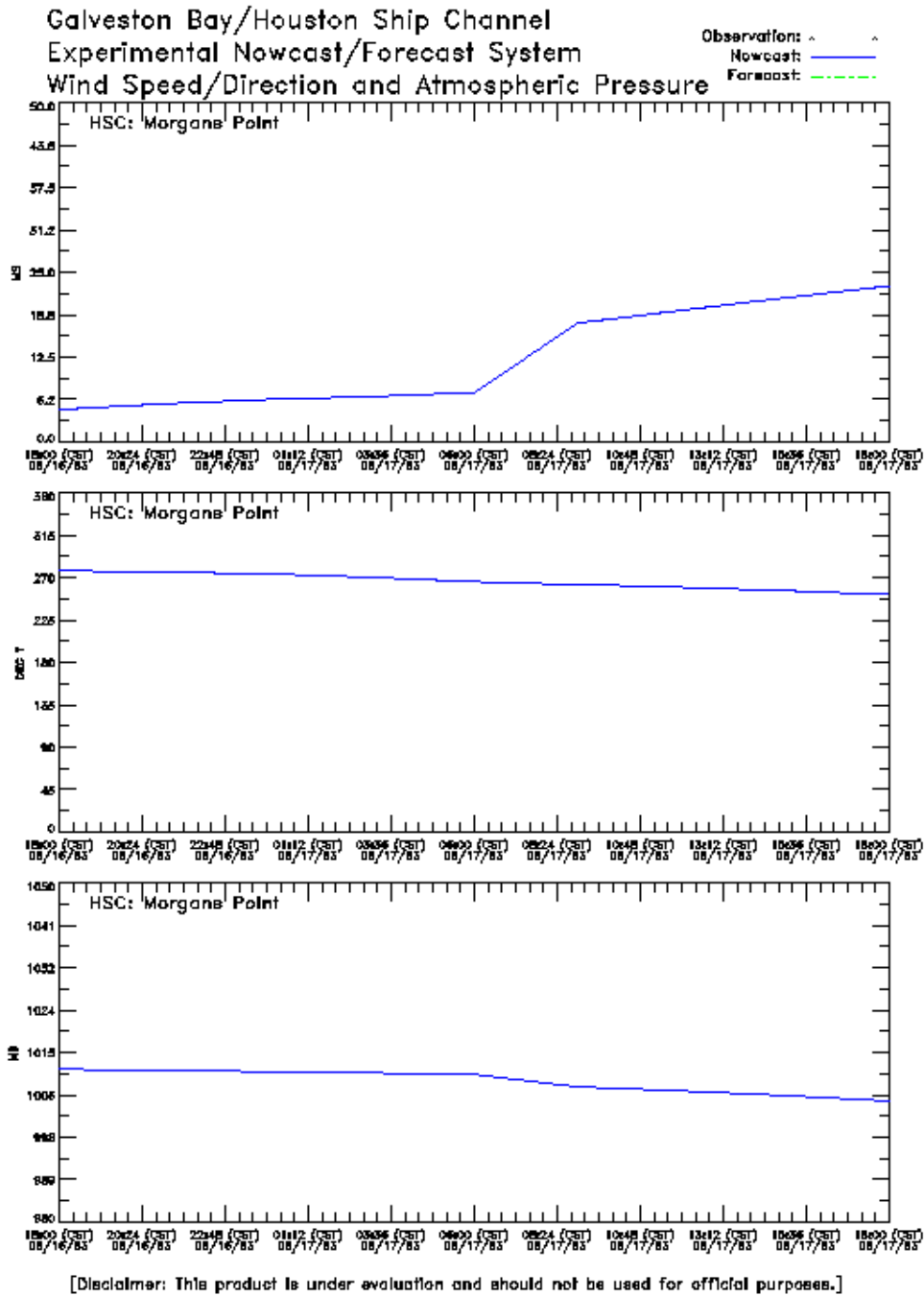


Figure 7.31. Hurricane Alicia Wind and Atmospheric Pressure at Morgans Point Experiment Two: 16-17 August 1983

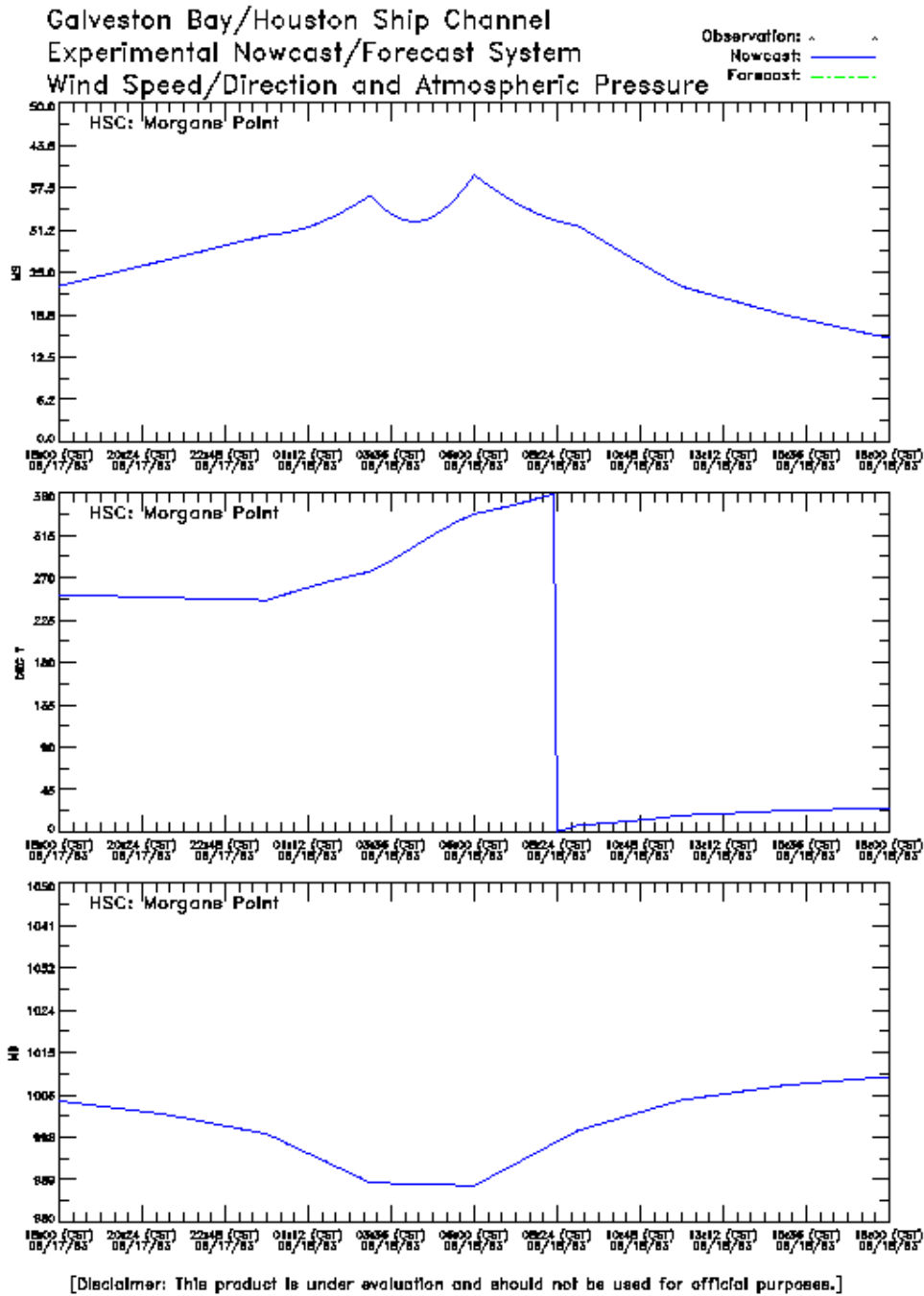


Figure 7.32. Hurricane Alicia Wind and Atmospheric Pressure at Morgans Point Experiment Two: 17-18 August 1983

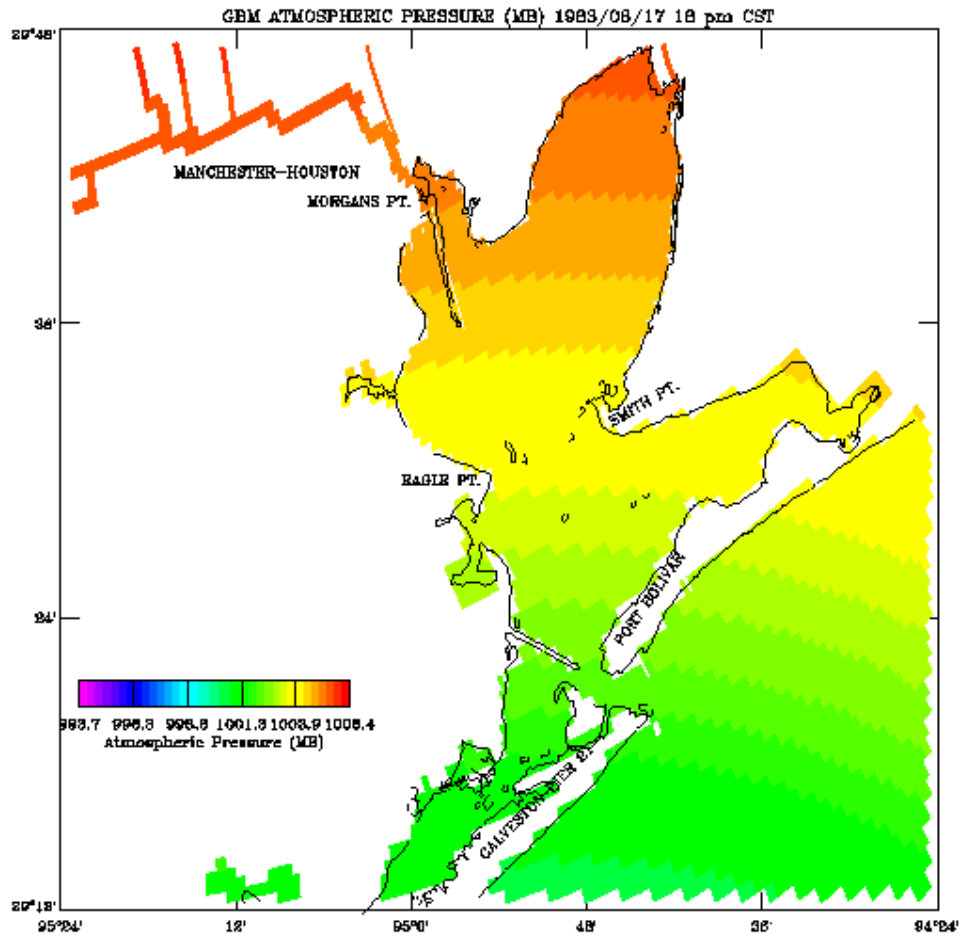


Figure 7.33. Hurricane Alicia GBM Atmospheric Pressure Field Experiment Two: 17 August 1983 18:00 CST

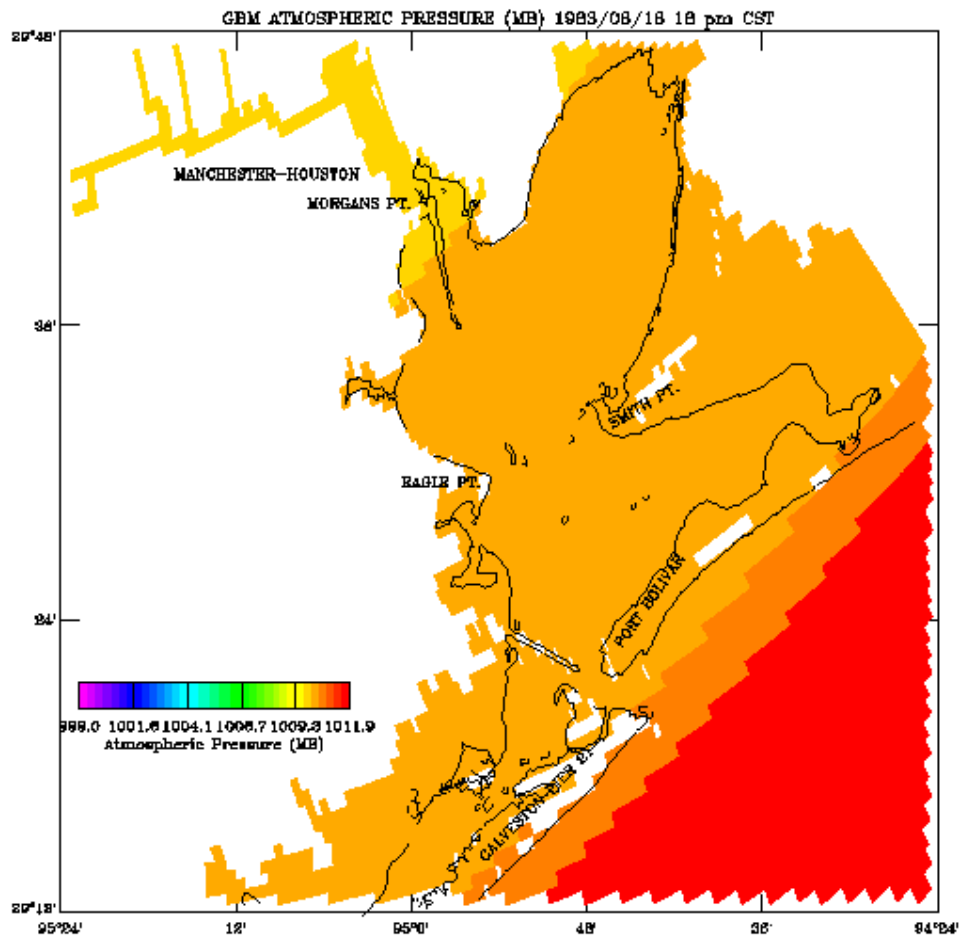


Figure 7.34. Hurricane Alicia GBM Atmospheric Pressure Field Experiment Two: 18 August 1983 18:00 CST

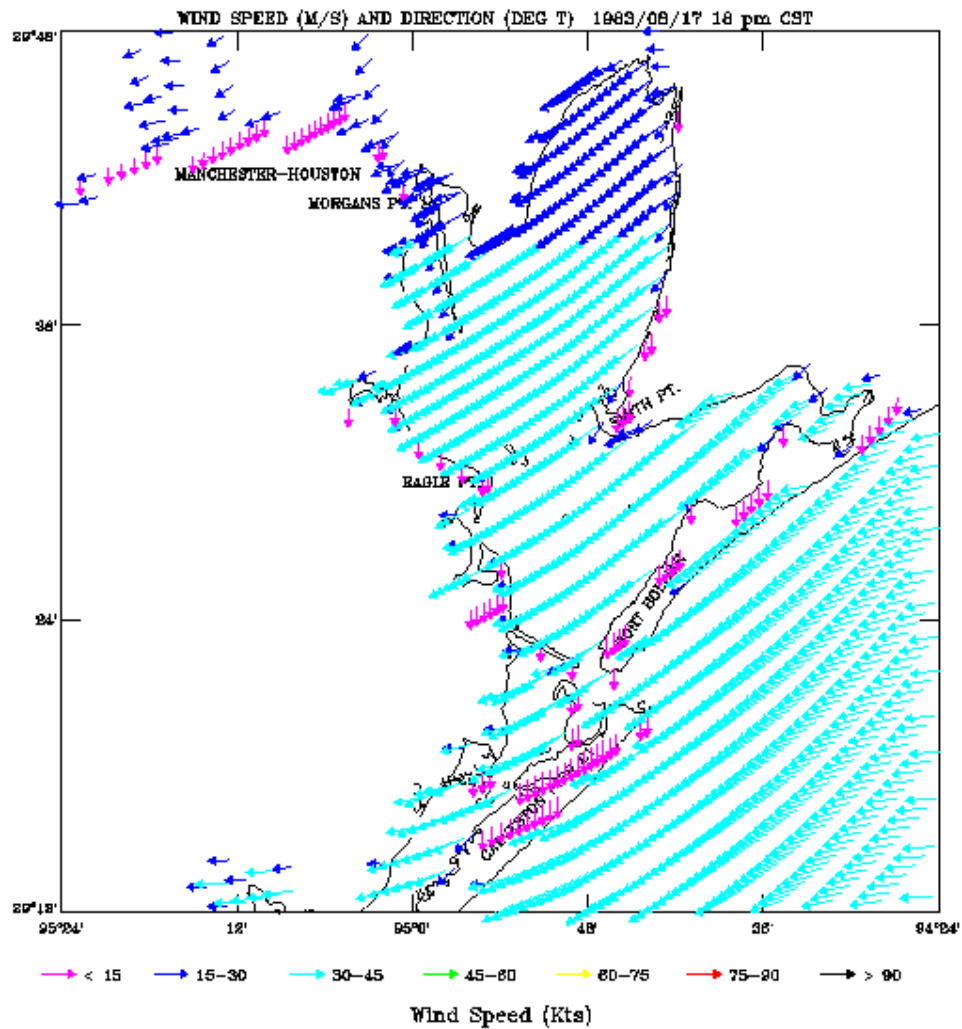


Figure 7.35. Hurricane Alicia GBM Wind Field Experiment Two:
17 August 1983 18:00 CST

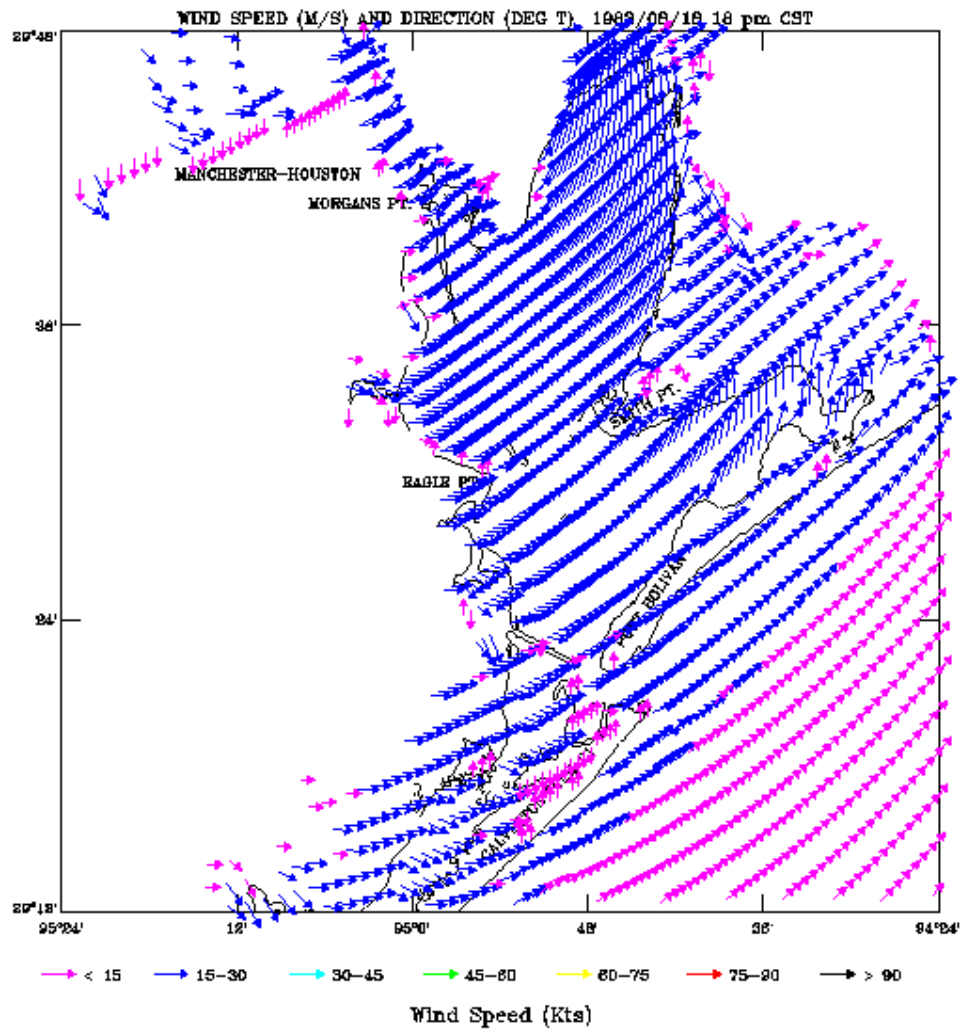


Figure 7.36. Hurricane Alicia GBM Wind Field Experiment Two: 18 August 1983 18:00 CST

8. TROPICAL STORM ALLISON (2001) SIMULATIONS

The complete All-Weather Nowcast/Forecast System is exercised for two separate events during Tropical Storm Allison: the surge event of 5-6 June 2001 and the rainfall/runoff event of 10-11 June. Nowcast/forecast cycle results are presented separately for each of these two events. The nowcast/forecast cycle consists of a 24-hour nowcast followed by a 36-hour forecast. On the nowcast, PORTS met stations are used via Barnes interpolation to provide the meteorological forcing, while the open boundary storm surge was based on the nontidal water level at Galveston Pleasure Pier. River flows are based on USGS average daily flows. On the forecast, NWS/WGRFC flows for the San Jacinto and Trinity Rivers and a persisted USGS daily flow for Buffalo Bayou are used. NWS/GFS (formerly AVN) atmospheric model winds and sea level pressure and NWS/ETSS storm surge levels at Galveston Pleasure Pier are used for meteorological forcing and nontidal water level, respectively.

For the surge event, two complete nowcast/forecast cycles for June 5 and 6 were performed with the calculations restarted for the second nowcast from results at the end of the first nowcast. Long wave results are given in terms of water surface elevation, current, salinity, and temperature time series. River flows and meteorological forcing are also shown. Short wave results are given in terms of significant wave height, period, and direction time series. No overland flooding occurred during the simulations and inundation statistics are not necessary.

For the rainfall/runoff event, two complete nowcast/forecast cycles for June 10 and 11 were performed with the calculations restarted for the second nowcast from results at the end of the first nowcast. Two separate experiments were performed. In experiment one, the standard inflows for the Trinity and San Jacinto Rivers and Buffalo Bayou are considered, while in experiment two additional inflows from Sims, Brays, Green, and Hunting Bayous within the City of Houston are also input. Long wave results are given in terms of water surface elevation, current, salinity, and temperature time series. River flows and meteorological forcing are also shown. Short wave results are given in terms of significant wave height, period, and direction time series. Salinity response is presented in terms of near surface and near bottom contour plots. No overland flooding occurred during the simulations and no inundation statistics are required.

8.1. Coastal Surge Propagation Event Characteristics

The track of Tropical Storm Allison is shown in Figure 8.1 with storm parameters given in Table 8.1. The storm made landfall along the Texas coast 50 km southwest of Galveston near Freeport, Texas at 1400 CST on the afternoon of June 5.

In the simulations, the radius to maximum winds was estimated at approximately 30 nm around the time of landfall based on Stewart (email, 20 March 2003) and was held at this value. Stewart (2002) notes that the peak storm surges were mild ranging from 0.64 m at Galveston Pleasure Pier to only 0.37 m at Morgans Point. At the west end of Galveston Island, wave heights of up to 2.4 m were reported with order 1 m of surge.

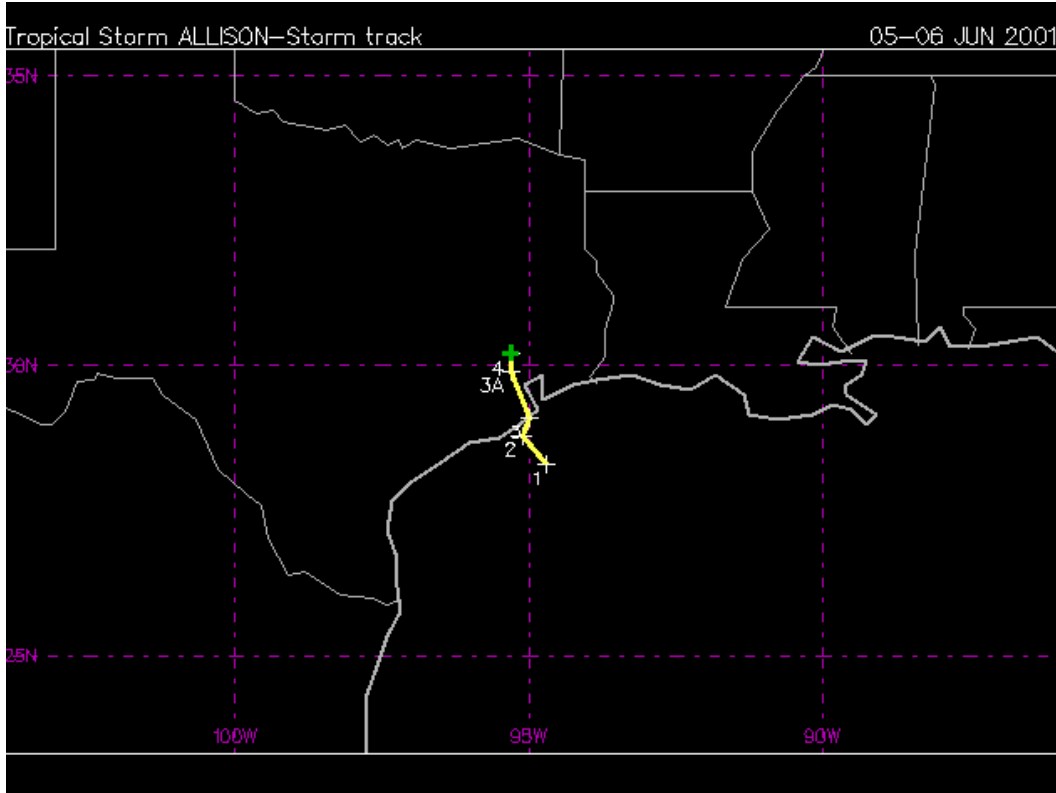


Figure 8.1. Tropical Storm Allison (2001) Storm Track 5-6 June.

Table 8.1. Tropical Storm Allison Storm Characteristics: 5-6 June 2001.

ADV	LAT	LON	TIME	WIND	PR	STAT
1	29.30	-94.70	06/05/19Z	50	1004	TROPICAL STORM
2	29.80	-95.10	06/05/21Z	50	1002	TROPICAL STORM--Landfall 21 GMT
3	29.10	-95.00	06/06/03Z	40	1003	TROPICAL STORM
3A	29.90	-95.30	06/06/06Z	35	1004	TROPICAL STORM
4	30.20	-95.30	06/06/09Z	30	1004	TROPICAL DEPRESSION

8.2. Rainfall/Runoff Event Characteristics

The track of Tropical Storm Allison shown in Figure 8.1 is only for the surge event portion of the storm. The storm then became stationary near Lufkin, Texas. On June 8 the storm proceeded southward entering the Gulf of Mexico on 17:00 CST on the afternoon of June 10 at nearly the same location that it had made landfall five days earlier. In the simulations, the radius to maximum winds was estimated at approximately 30 nm. Hourly rainfall information was obtained at Harris County Flood Control Station rain gages 1620 for Greens Bayou, 0410 for Brays Bayou, 0370 for Sims Bayou, and 0830 for Hunting Bayou, respectively, for use in the rainfall/runoff computations. Rainfall totals exceeded over 35 inches for Greens Bayou. Average daily flows on the San Jacinto River exceeded

100,000 cfs and even on Greens Bayou, a peak average daily flow of over 50,000 cfs was recorded.

8.3. Coastal Surge Propagation Event Simulation Set-up Procedures

The first nowcast covers the period June 3 18:00 CST to June 4 18:00 CST. Water surface elevations and velocities are started from rest. The initial salinity and temperature fields are determined based on climatology. PORTS data were used in the adjustment of these fields. Open boundary conditions for the GBM for water surface elevation are computed based on adding the observed nontidal water level at Galveston Pleasure Pier to the predicted astronomical tide. Salinity and temperature values along the open boundary are based on climatology. Sea surface temperature is specified by using the top level of the initial temperature field and is held constant in time. River inflows for the San Jacinto, Buffalo Bayou, and Trinity Rivers are based on USGS daily averaged values. During the 36 hour forecast out to June 6 06:00 CST, NWS GFS atmospheric model wind and sea level atmospheric pressure were used along with the NWS/ETSS storm surge forecast at Galveston Pleasure Pier. Wave data from NBDC 42035 buoy were used to specify the wave conditions along the GBM open boundary during both the nowcast and forecast period.

For the subsequent daily nowcast over the period June 4 18:00 CST to June 5 18:00 CST, conditions are restarted from the end of the previous nowcast. PORTS data based adjustments of the salinity and temperature fields were made. Open boundary conditions for water surface elevation, salinity, and temperature are specified using the same technique as described above for the first nowcast. Similarly, sea surface temperature, river inflows for the San Jacinto, Buffalo Bayou, and Trinity Rivers, and the wave conditions along the open boundary are specified as above. During the 36 hour forecast out to June 7 06:00 CST, NWS GFS atmospheric model wind and sea level atmospheric pressure were used along with the NWS/ETSS storm surge forecast at Galveston Pleasure Pier.

8.4. Rainfall/Runoff Event Simulation Set-up Procedures

The first nowcast covers the period June 8 18:00 CST to June 9 18:00 CST. Water surface elevations and velocities are started from rest. The initial salinity and temperature fields are determined based on climatology. PORTS data were used in the adjustment of these fields. Open boundary conditions for the GBM for water surface elevation are computed based on adding the observed nontidal water level at Galveston Pleasure Pier to the predicted astronomical tide. Salinity and temperature values along the open boundary are based on climatology. Sea surface temperature is specified by using the top level of the initial temperature field and is held constant in time. River inflows for the San Jacinto, Buffalo Bayou, and Trinity Rivers are based on USGS daily averaged values. During the 36 hour forecast out to June 11 06:00 CST, NWS GFS atmospheric model wind and sea level atmospheric pressure were used along with the NWS/ETSS storm surge forecast at Galveston Pleasure Pier. NBDC 42035 buoy data were used to specify representative wave conditions along the GBM open boundary during both the nowcast and forecast period.

For the subsequent daily nowcast over the period June 9 18:00 CST to June 10 18:00 CST, conditions are restarted from the end of the previous nowcast. PORTS data based adjustments of the salinity and temperature fields were made. Open boundary conditions for water surface elevation, salinity, and temperature are specified using the same technique as described above for the first nowcast. Similarly, sea surface temperature, river inflows for the San Jacinto, Buffalo Bayou, and Trinity Rivers, and the wave conditions along the open boundary are specified as above. During the 36 hour forecast out to June 12 06:00 CST, NWS GFS atmospheric model wind and sea level atmospheric pressure were used along with the NWS/ETSS storm surge forecast at Galveston Pleasure Pier.

Two experiments are run using the above conditions but with different freshwater inflows. In experiment one, the standard three inflows were used, while in the second experiment, four additional inflows from the City of Houston were included. Results are presented in separate sections for both experiments for the long wave computations with a particular emphasis on the comparison of the salinity decrease and water surface elevation increase at Morgans Point due to the additional inflows. Short period gravity wave results are shown for experiment one only, since results from experiment two with the additional inflows were nearly the same.

8.5. Coastal Surge Propagation Event Long Wave Results

Water surface elevations for each of the two nowcast/forecast cycles are shown at Galveston Pleasure Pier, Bolivar Roads, and Galveston Pier 21 in Figures 8.2 – 8.3. GBM simulated water levels are in excellent agreement with the observations at Galveston Pleasure Pier and at Galveston Pier 21. In Figures 8.4 – 8.5, HSCM simulated water surface elevations are shown for each nowcast/forecast cycle at Eagle Point and Morgans Point. HSCM simulated water levels are in excellent agreement with the observations at Eagle and Morgans Point. In the third panel of these figures, the water level residual (surge at Galveston Pleasure Pier) is given. This water level residual is applied uniformly in space over the entire GBM open water boundary.

Simulated Bolivar Roads currents demonstrate no strong persistent of flood or ebb flow with maximum current strengths of 80 cm/s with the exception of a peak ebb flow of 125 cm/s at the end of the first nowcast. Simulated currents at Redfish Bar, mid-way up the Bay have a similar behavior in their ebb-flood structure to simulated currents at Bolivar Roads; however, the peak ebb current strength at the end of the first nowcast is reduced to order 50 cm/s. At Morgans Point, the simulated currents exhibit a similar ebb-flood structure. The peak current strengths on ebb and flood are on the order of 35 cm/s with the exception of a peak ebb current of order 75 cm/s near the end of the first forecast. Additional rainfall/runoff flows have not been included and inflows from the Buffalo Bayou, San Jacinto River, and Trinity River were small.

Simulated surface temperature, temperature stratification (absolute difference between

simulated surface and bottom temperatures) and surface salinity are examined in three panels at Morgans Point in Figures 8.6-8.7. One notes the increase in simulated salinity at Bolivar Roads from 30 to 34 psu during the surge propagation phase. While the simulated surface temperature remains constant, there is mild stratification to order 0.75 °C as the cooler shelf water moves in over the bottom layers during the surge propagation phase of the storm. No PORTS data were available at this station. At Eagle Point the simulated surface salinity increases from 22.5 psu to a maximum of 27 psu at the end of the first nowcast in general agreement with the PORTS data, but the large dip and rapid increase in observed salinity is not replicated in the simulation. The same behavior is observed during the second nowcast period. The maximum simulated temperature stratification is only 0.5 °C. At Morgans Point the simulated surface salinity remains nearly constant at 17.5 psu with a maximum simulated temperature stratification of order 0.5 °C during the first nowcast with a similar behavior noted during the second nowcast. The large observed dip and increase in observed salinity at Morgans Point is not captured. This suggests that there are additional freshwater inflows effects which have not been accounted for in the simulation.

Simulated wind speed and direction and atmospheric pressure are shown in Figures 8.8-8.9 at Morgans Point. Maximum nowcast windspeeds at Bolivar Roads and Eagle Point are 12.5 m/s while at Morgans Point they are reduced to 6.3 m/s. Maximum forecast windspeeds are near 20 m/s at Bolivar Roads and Eagle Point. Nowcast and forecast atmospheric pressure is near 1010 mb at all stations.

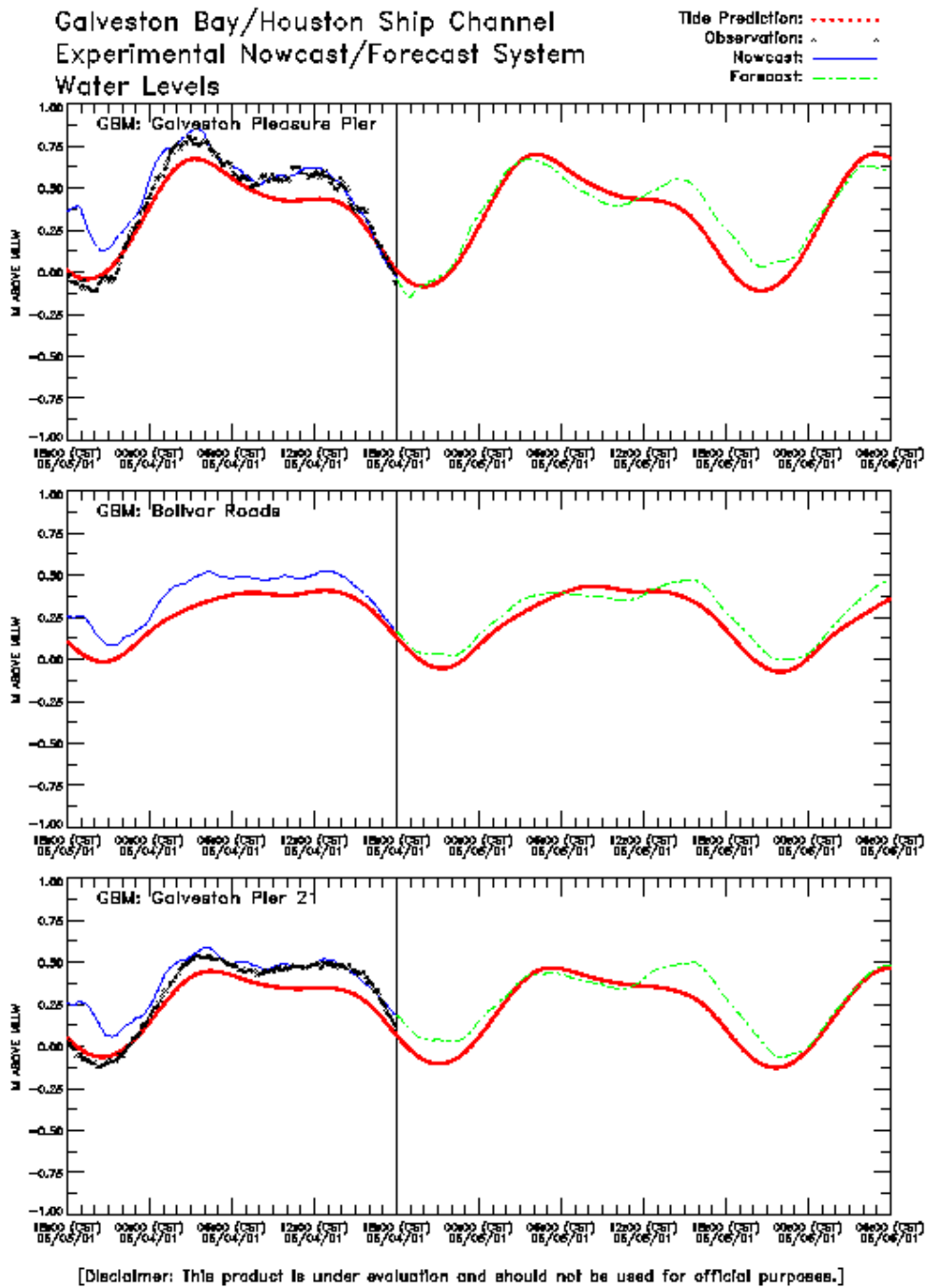


Figure 8.2. Tropical Storm Allison GBM Water Levels: 5 June 2001 Nowcast/Forecast Cycle

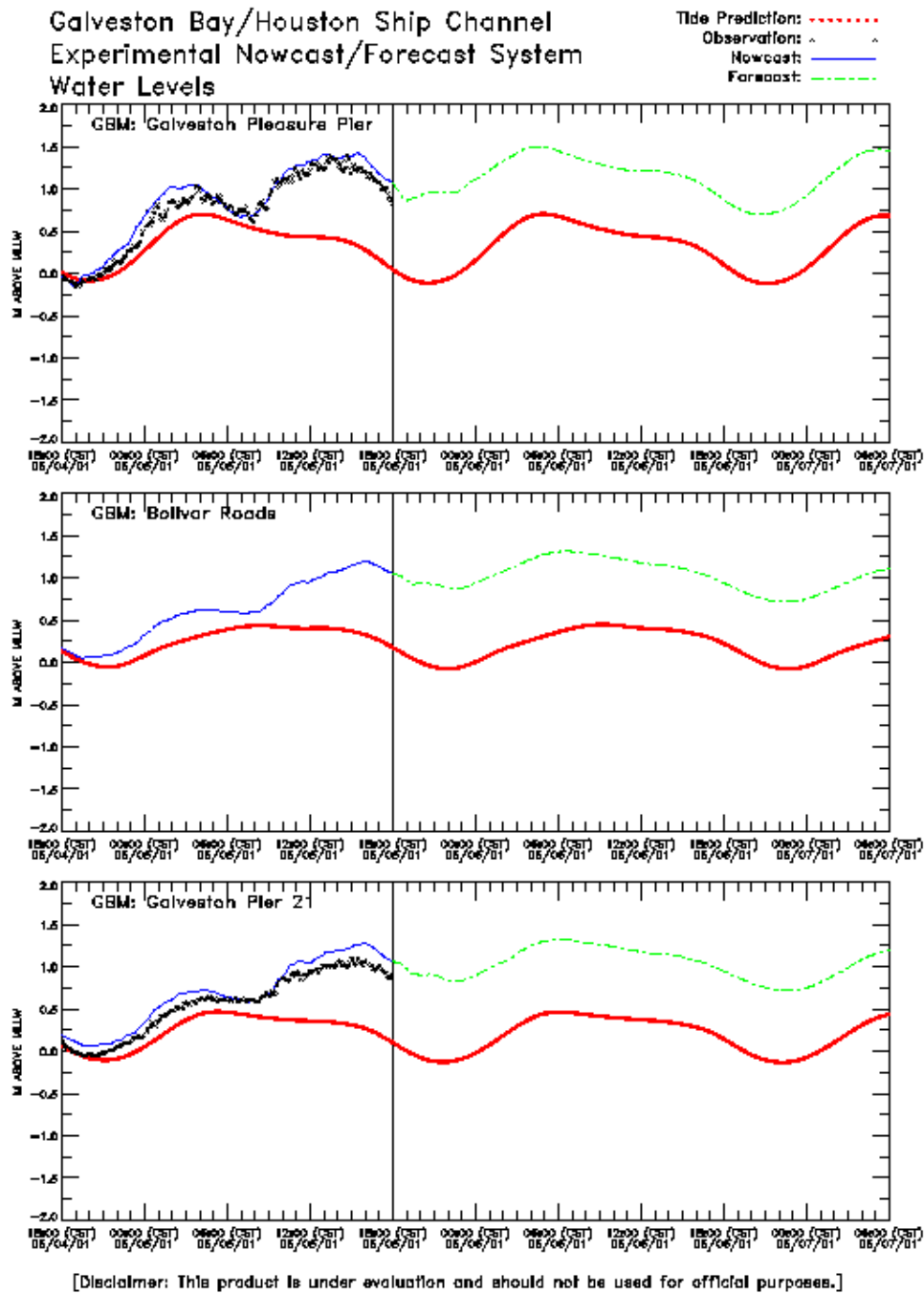


Figure 8.3. Tropical Storm Allison GBM Water Levels: 6 June 2001 Nowcast/Forecast Cycle

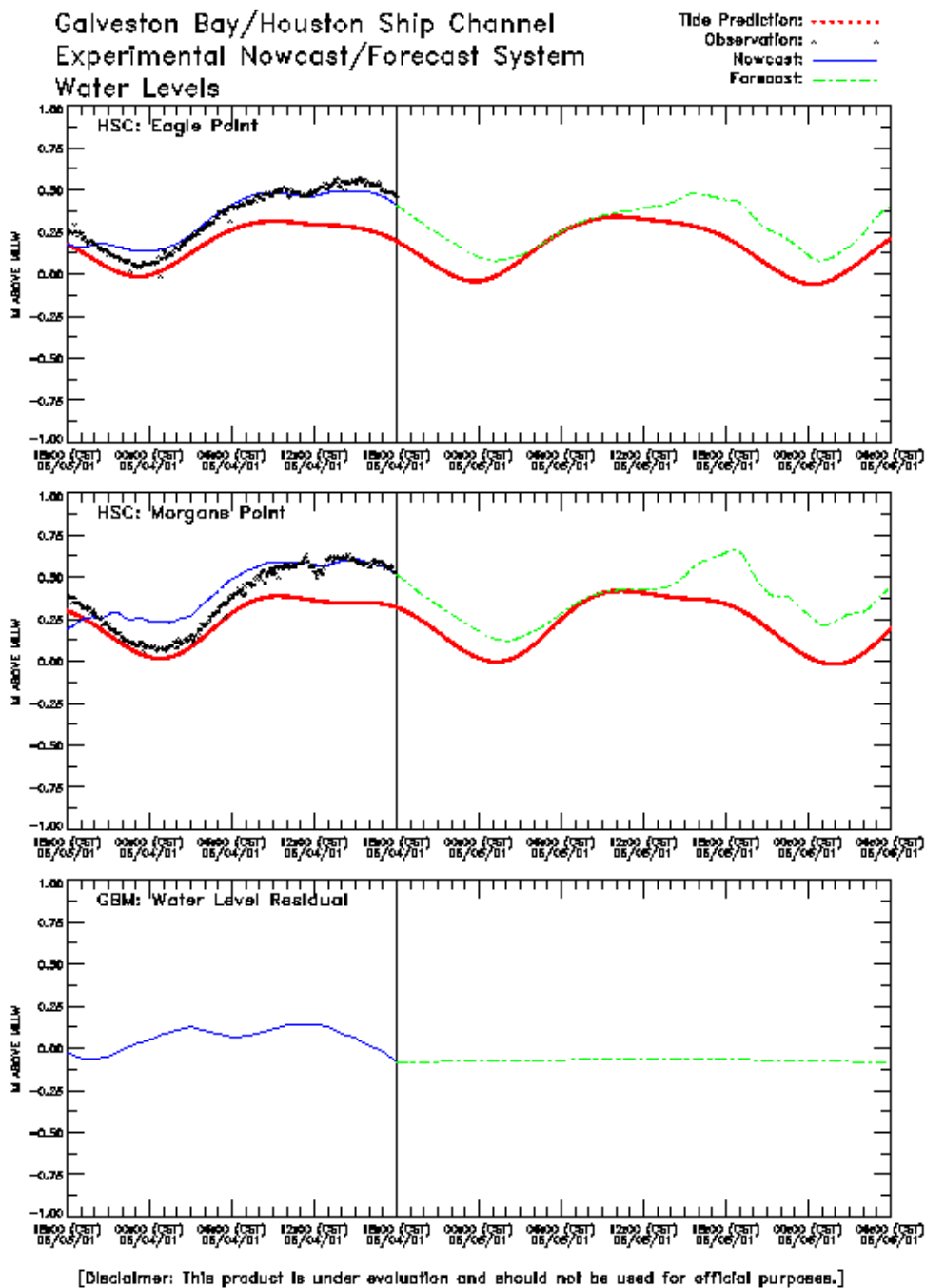


Figure 8.4. Tropical Storm Allison HSCM Water Levels and GBM Water Level Residual: 5 June 2001 Nowcast/Forecast Cycle

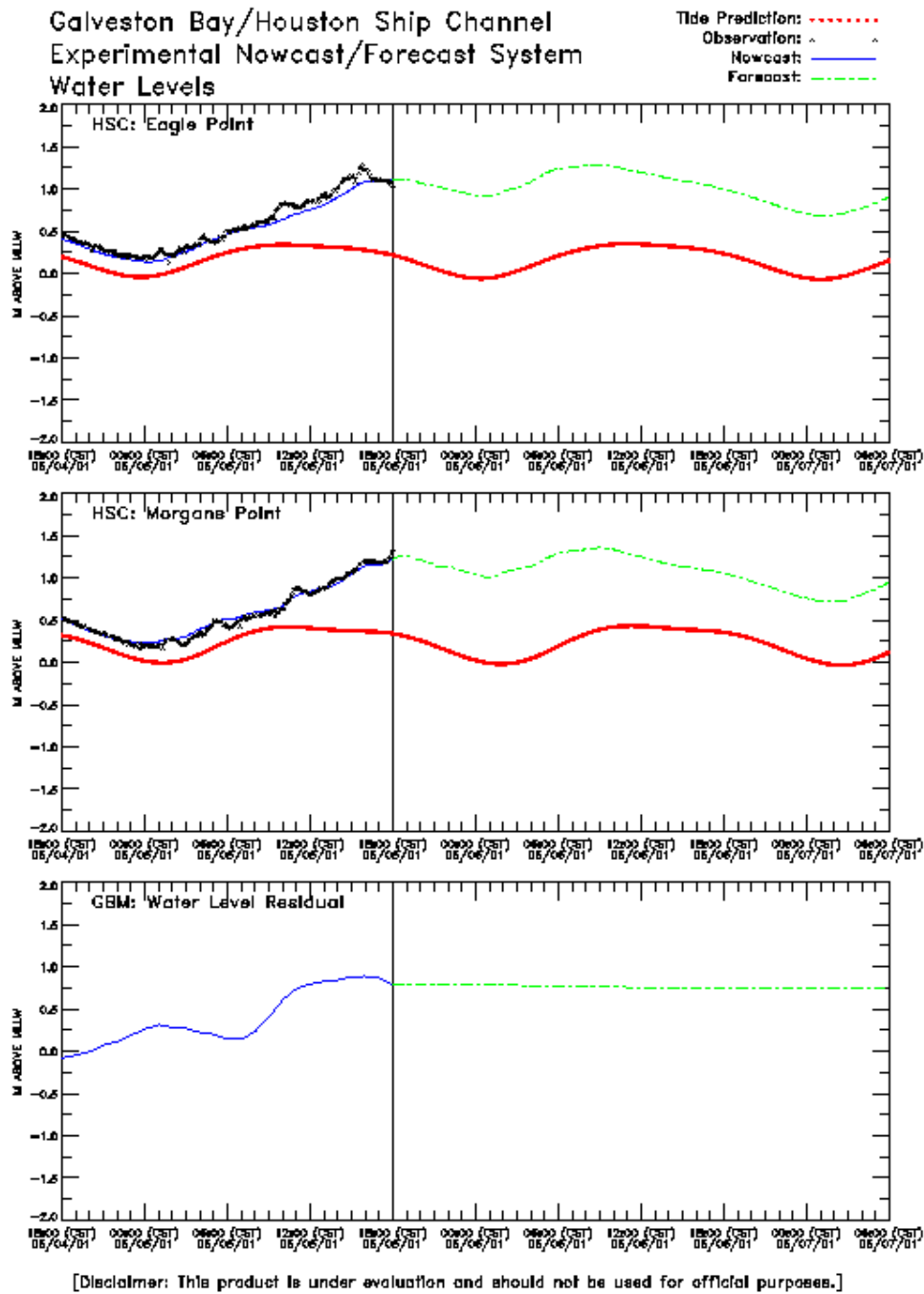


Figure 8.5. Tropical Storm Allison HSCM Water Levels and GBM Water Level Residual: 6 June 2001 Nowcast/Forecast Cycle

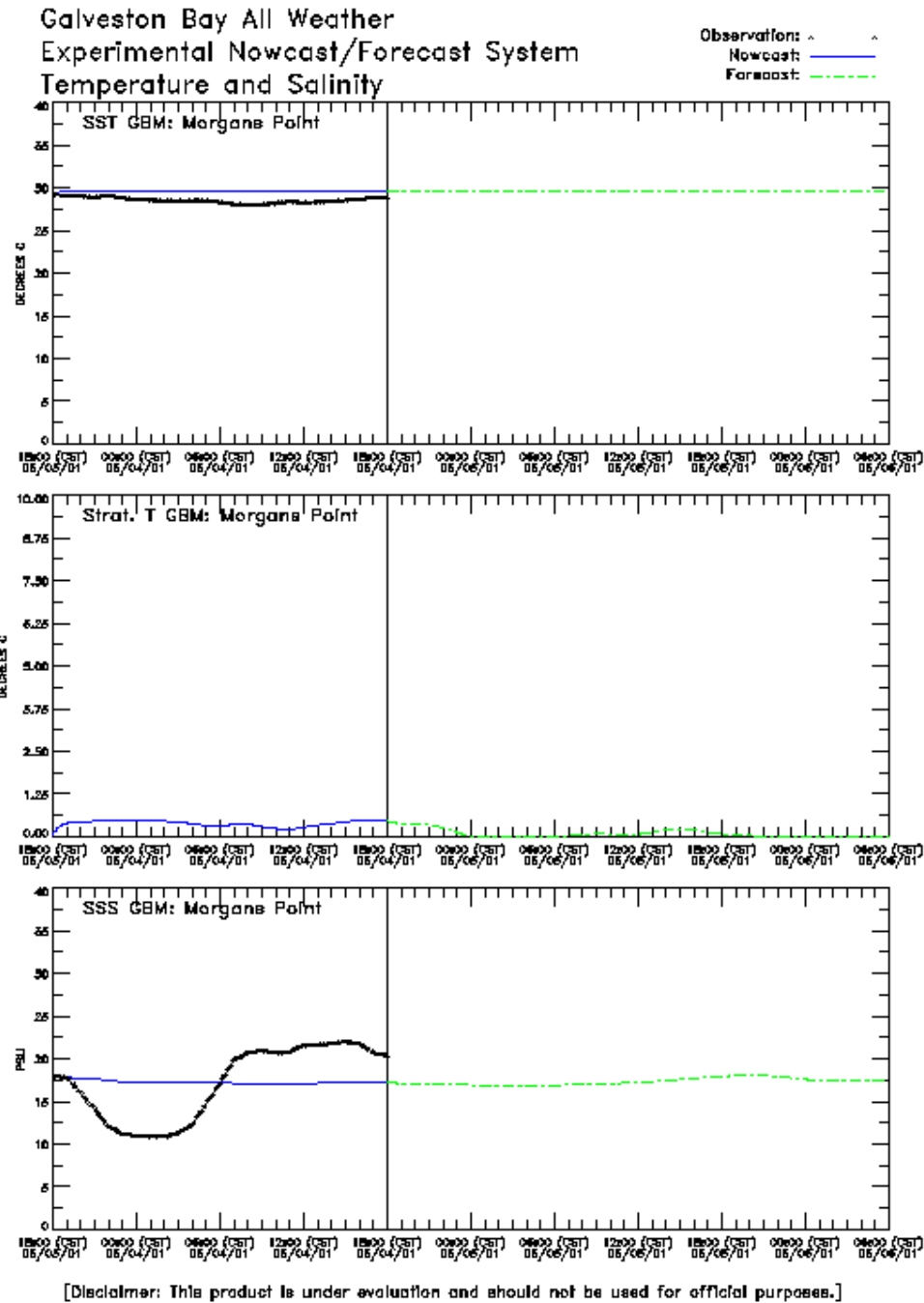


Figure 8. 6. Tropical Storm Allison HSCM Morgan's Point Temperature and Salinity: 5 June 2001 Nowcast/Forecast Cycle

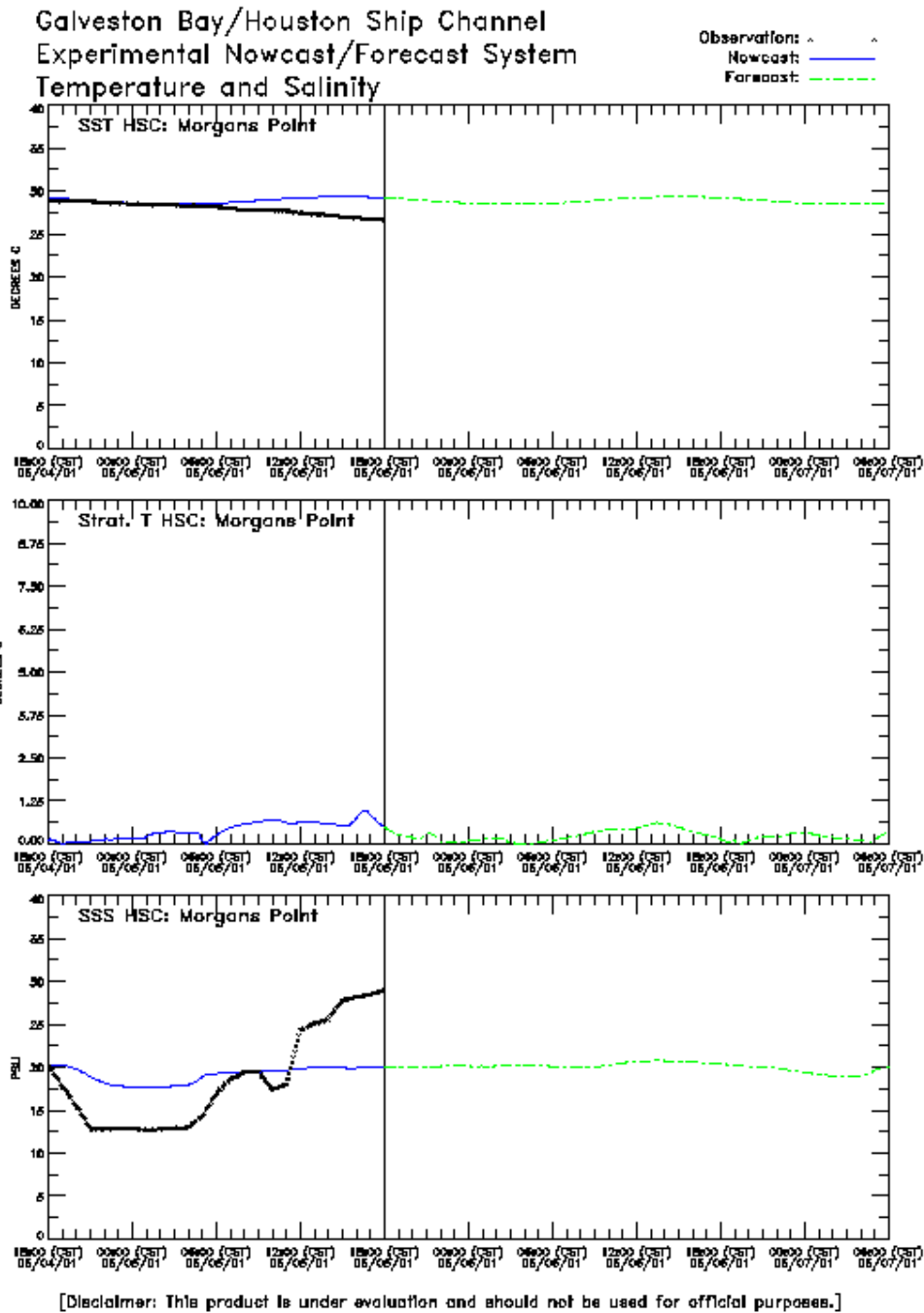


Figure 8.7. Tropical Storm Allison HSCM Morgans Point Temperature and Salinity: 6 June 2001 Nowcast/Forecast Cycle

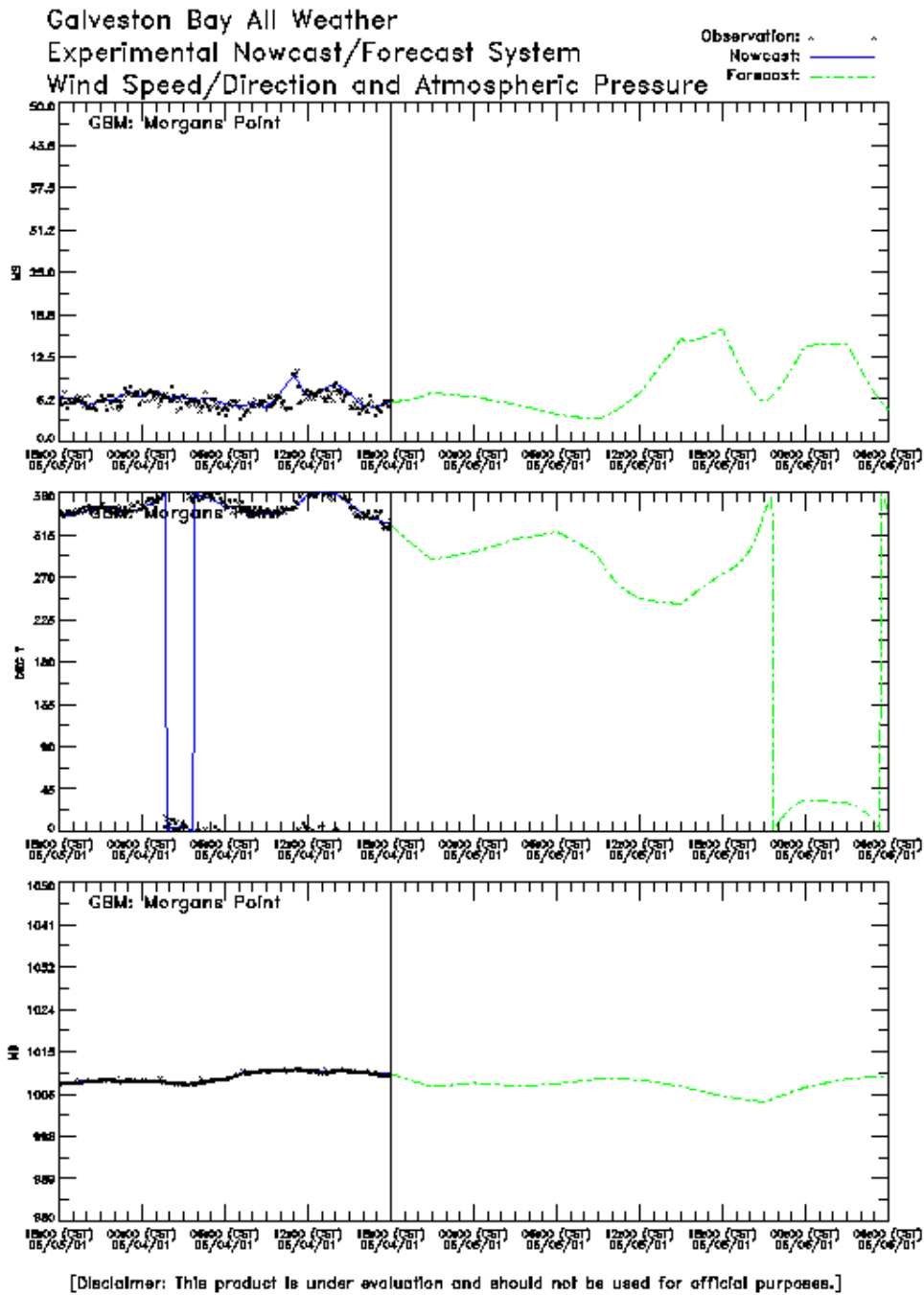


Figure 8.8. Tropical Storm Allison HSCM Morgans Point Wind and Atmospheric Pressure: 5 June 2001 Nowcast/Forecast Cycle

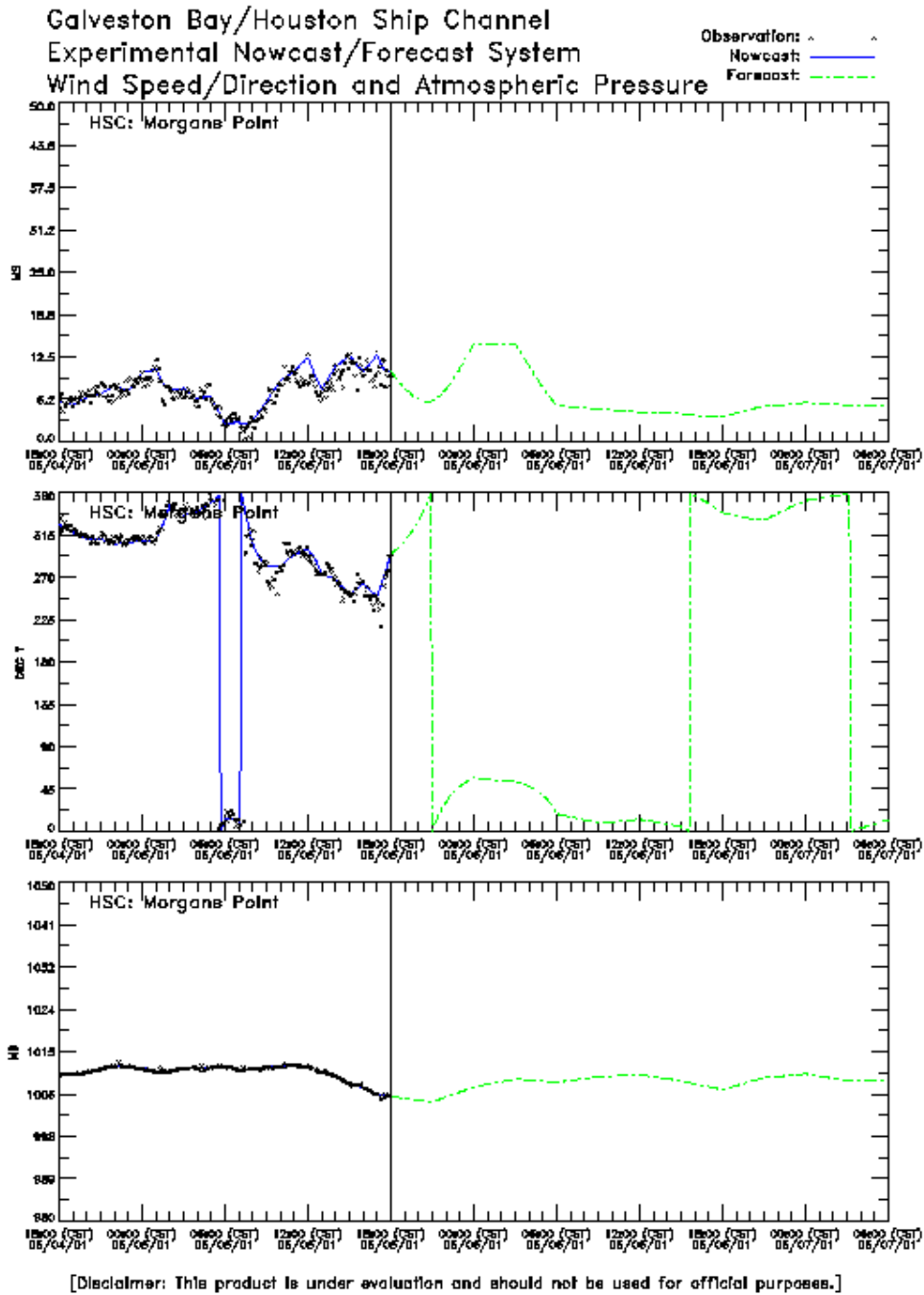


Figure 8.9. Tropical Storm Allison HSCM Morgans Point Wind and Atmospheric Pressure: 6 June 2001 Nowcast/Forecast Cycle

8.6. Coastal Surge Propagation Event Short Wave Results

Unfortunately, no wave information was available within the Bay for comparison. NDBC 42035 buoy data were used to specify the offshore boundary wave condition during both nowcast and forecast, since the forecasts were run after the fact.

Simulated significant wave height for each of the two nowcast/forecast cycles is shown at Galveston Pleasure Pier, Bolivar Roads, and Galveston Pier 21 in Figures 8.10-8.11. Maximum simulated wave heights are of order 2.6 m at Galveston Pleasure Pier, 2.0m at Bolivar Roads, and 1.2m at Galveston Pier 21. HSCM simulated significant wave heights at Eagle Point and Morgans Point are order 1.25 m. The maximum simulated significant wave height at NDBC buoy 42035, which represents the GBM open boundary wave condition, exceeds 4m. Note in this experiment with wind generation, the significant wave direction is equal to the wind direction, which is near 315 deg T.

GBM simulated significant wave periods for each of the nowcast/forecast cycles at Galveston Pleasure Pier, Bolivar Roads, and Galveston Pier 21 are order 4s. HSCM simulated significant wave periods for each nowcast/forecast cycle at Eagle Point and Morgans Point are also order 2s. The simulated significant wave period ranges from 5 to 7s at NDBC buoy 42035, which represents the GBM open boundary wave condition. This significant wave period is applied uniformly in space over the entire GBM open water boundary.

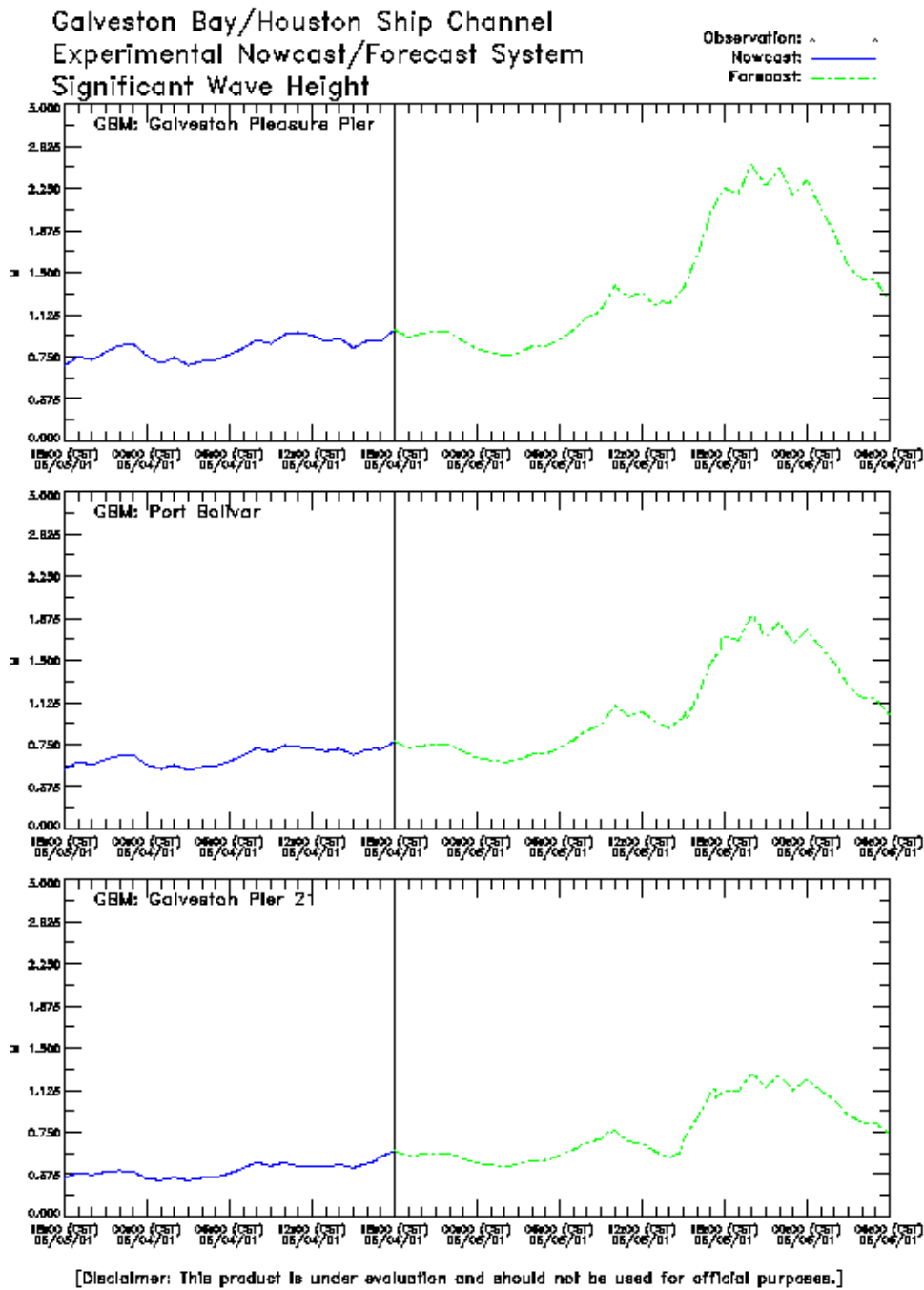


Figure 8.10. Tropical Storm Allison GBM Significant Wave Height:
5 June 2001 Nowcast/Forecast Cycle

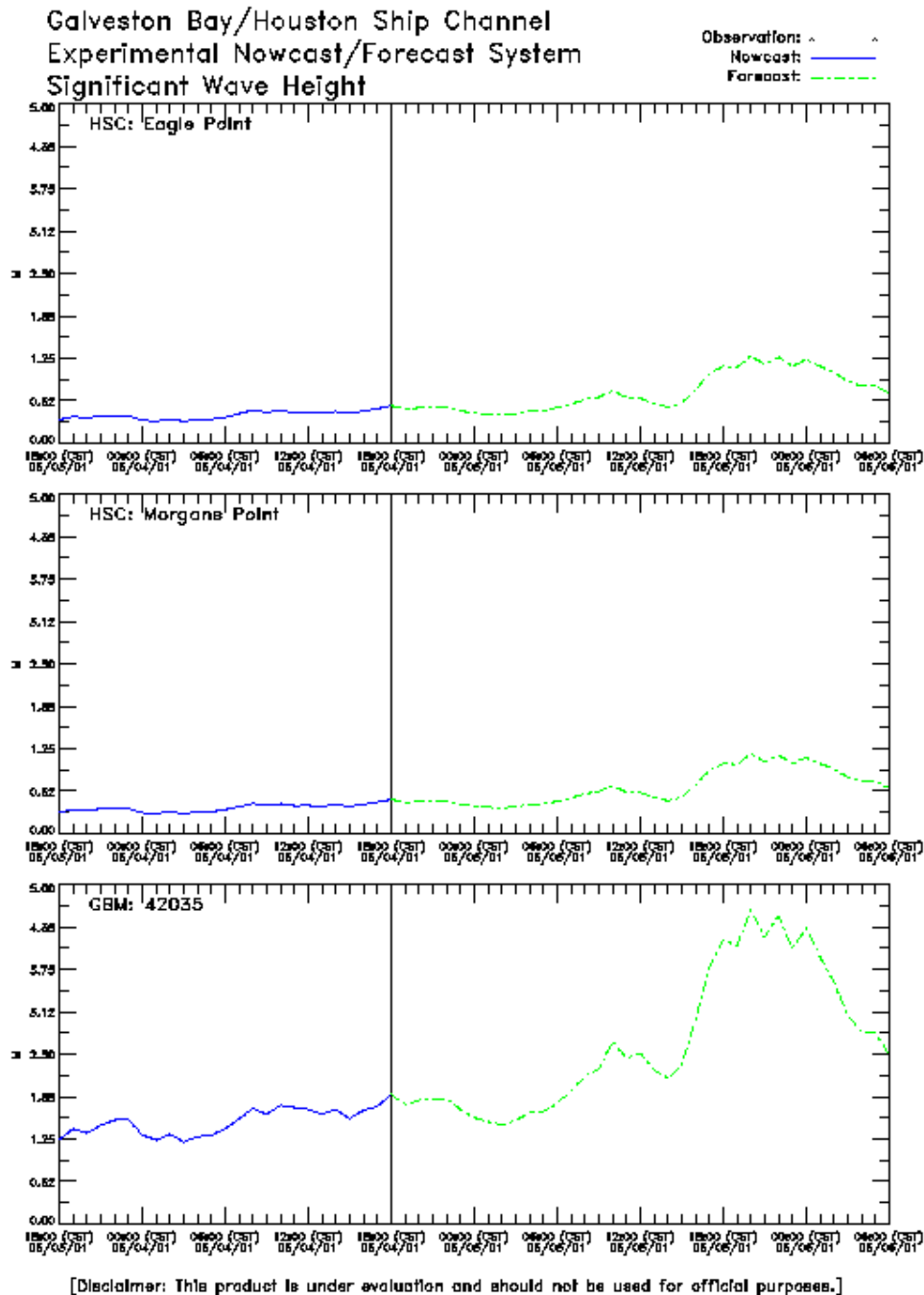


Figure 8.11. Tropical Storm Allison HSCM and GBM 42035 Significant Wave Height: 5 June 2001 Nowcast/Forecast Cycle

8.7. Rainfall/Runoff Event Experiment One Long Wave Results

Tropical Storm Allison standard inflows for the Trinity, San Jacinto, and Buffalo Bayou inflows are shown for both nowcast/forecast cycles in Figures 8.12 and 8.13. Note the forecast and subsequent nowcast flow of over 100000 cfs for the San Jacinto River. Trinity and Buffalo Bayou inflows are order 35,000 cfs and less than 8000 cfs, respectively.

Water surface elevations for each of the two nowcast/forecast cycles are shown for Galveston Pleasure Pier, Bolivar Roads, and Galveston Pier 21 in Figures 8.14-8.15. GBM simulated water levels are in excellent agreement with the observations at Galveston Pleasure Pier and at Galveston Pier 21. In Figures 8.16-8.17, HSCM simulated water surface elevations are shown for each nowcast/forecast cycle at Eagle Point and Morgans Point. HSCM simulated water levels are below the observations at Eagle and Morgans Point during the second nowcast by order 25 cm. In the third panel of these figures, the water level residual (surge at Galveston Pleasure Pier) is given. This water level residual is applied uniformly in space over the entire GBM open water boundary.

Simulated currents are examined in three panel figures for current speed, current direction, and principal component direction with flood considered positive. Simulated Bolivar Roads currents are shown in Figures 8.18-8.19 for each nowcast/forecast cycle. One notes no strong persistent flood or ebb flow with peak current strengths of order 100 cm/s during both nowcast/forecast cycles. Simulated currents at Redfish Bar, mid-way up the Bay, are shown in Figures 8.20-8.21 for each nowcast/forecast cycle. One notes a similar behavior in the ebb-flood structure to simulated currents at Bolivar Roads; however, the peak flood current strengths are reduced to order 50 cm/s. At Morgans Point, the simulated currents in Figures 8.22-8.23, exhibit a much different ebb-flood structure, with ebb dominance occurring during the first forecast and throughout both the second nowcast/forecast cycle. Ebb current strengths are in the range of 70-100 cm/s.

Simulated surface temperature, temperature stratification (absolute difference between surface and bottom temperatures) and surface salinity are examined in three panels at Bolivar Roads in Figures 8.24-8.25, at Eagle Point in Figures 8.26-8.27, and at Morgans Point in Figures 8.28-8.29, respectively. One notes the sinusoidal character of the simulated salinity at Bolivar Roads with amplitude order 2.5 psu. While the simulated surface temperature remains constant, there is a mild simulated stratification to order 0.5 °C. At Eagle Point the simulated surface salinity remains constant near 15 psu and does not follow the decrease in observed salinity from 15 to 5 psu during the first nowcast. The maximum simulated temperature stratification is only 0.5 °C. At Morgans Point the surface salinity remains nearly constant at 12 psu and does not follow the decrease from 12 to 4 psu during the first nowcast. During the second nowcast, the simulated salinity is in closer agreement with the observations. The maximum simulated temperature stratification is 1.5 °C.

Wind speed and direction and atmospheric pressure are in Figures 8.30-8.31 at Morgans Point. Maximum nowcast windspeeds at Bolivar Roads and Eagle Point are 12.5 m/s at all three stations. Maximum forecast windspeeds are less than maximum nowcast windspeeds. Nowcast and forecast atmospheric pressure is near 1010 mb at all stations.

HSCM simulated near surface and near bottom salinity contours are shown at the end of the second nowcast and forecast in Figures 8.32-8.33 and in Figures 8.34-8.35, respectively. One notes the propagation of the freshwater effects on salinity down the estuary in both the surface and bottom waters due to the large flows in the San Jacinto River.

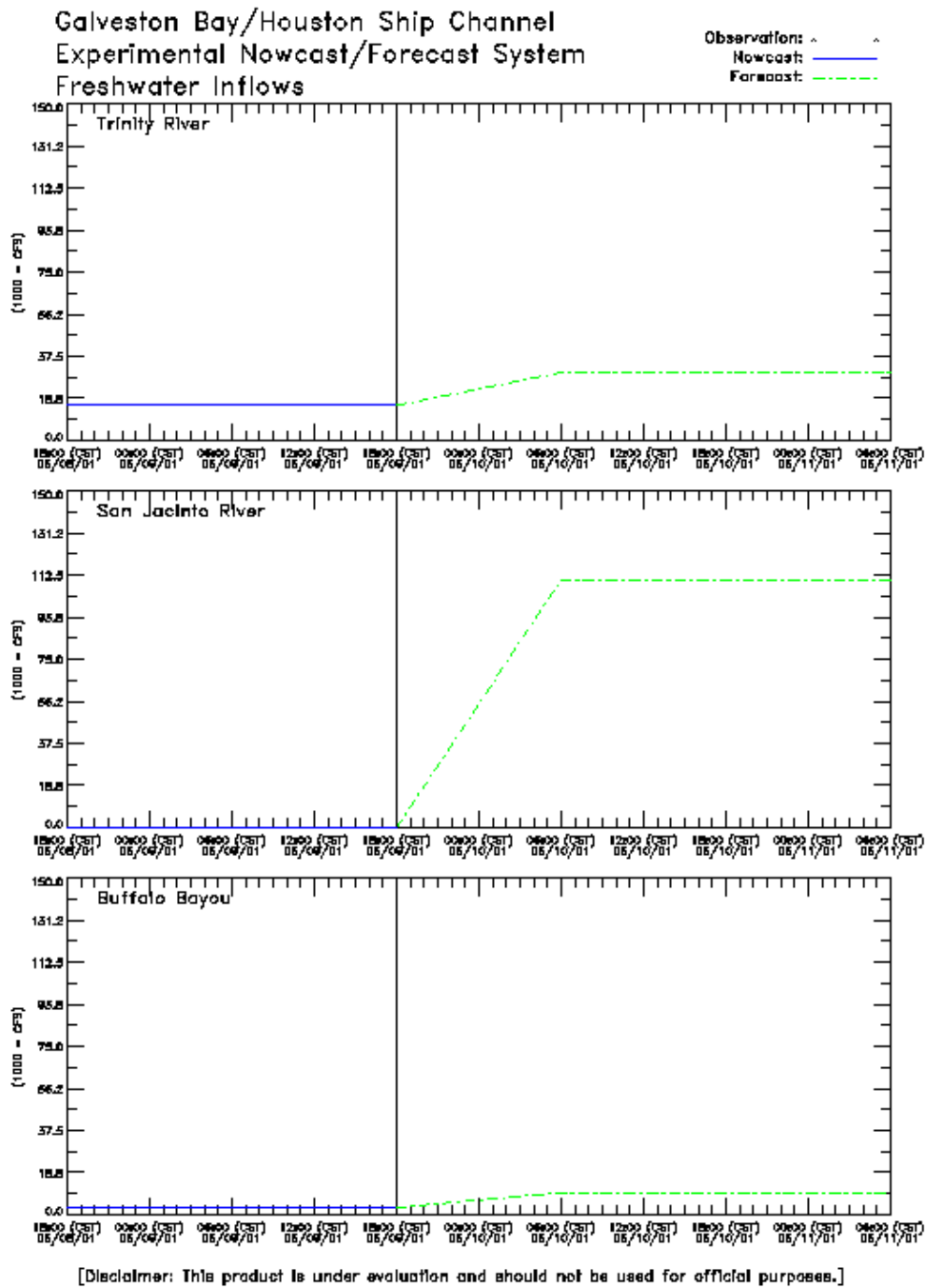


Figure 8.12. Tropical Storm Allison Standard Inflows
Experiment One: 10 June 2001 Nowcast/Forecast Cycle

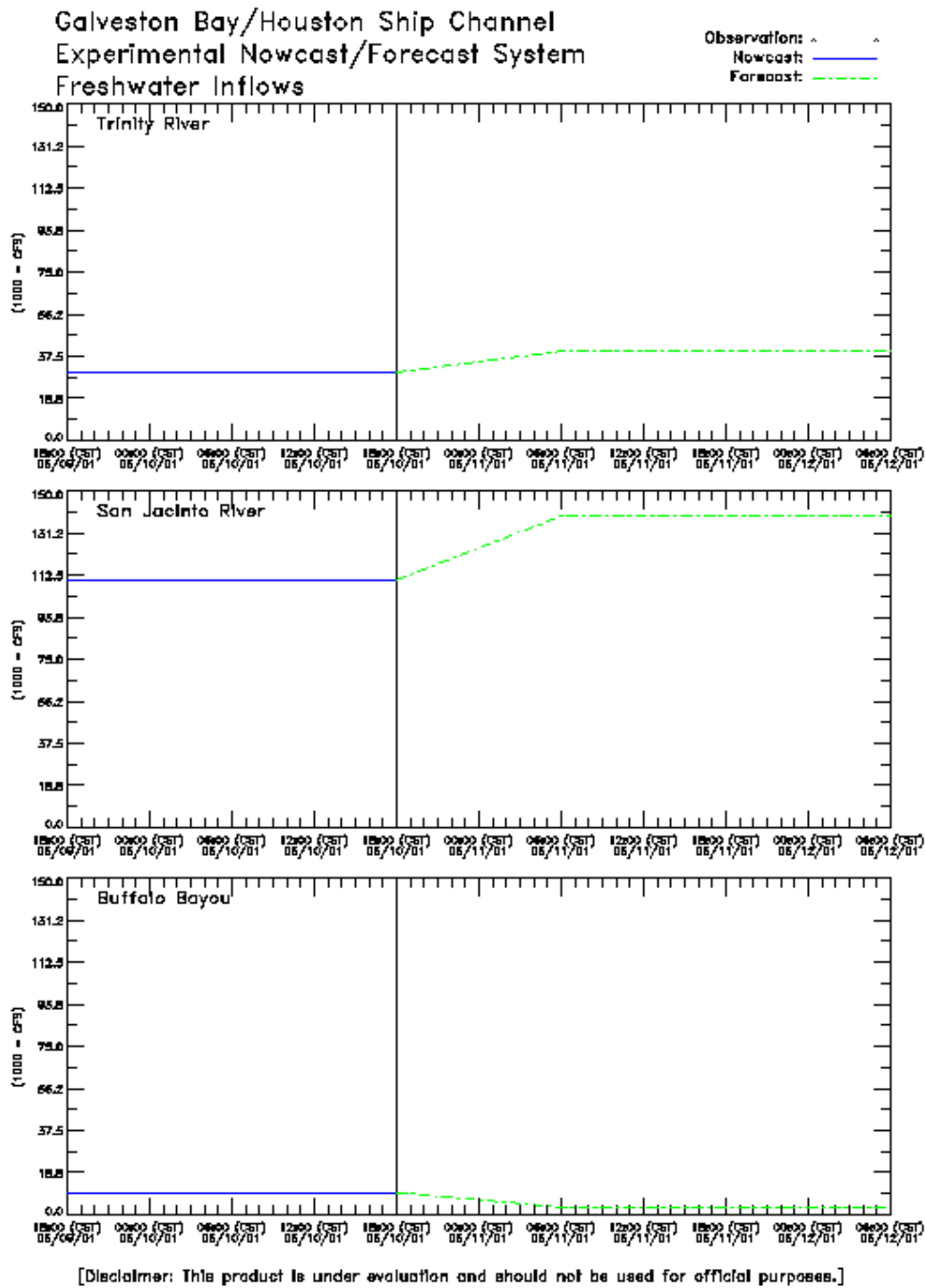


Figure 8.13. Tropical Storm Allison Standard Inflows Experiment One: 11 June 2001
Nowcast/Forecast Cycle

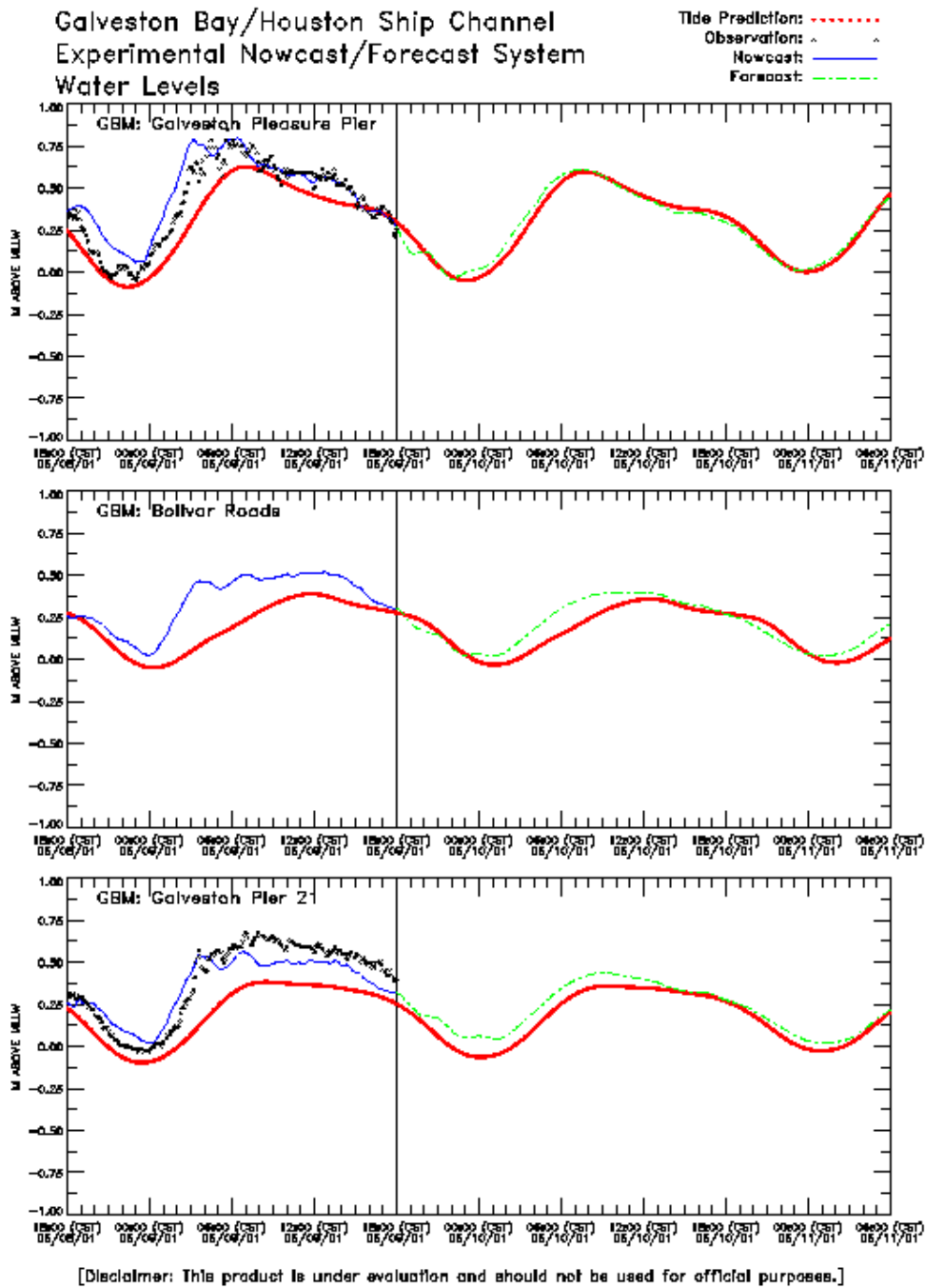


Figure 8.14. Tropical Storm Allison GBM Water Levels Experiment One: 10 June 2001
Nowcast/Forecast Cycle

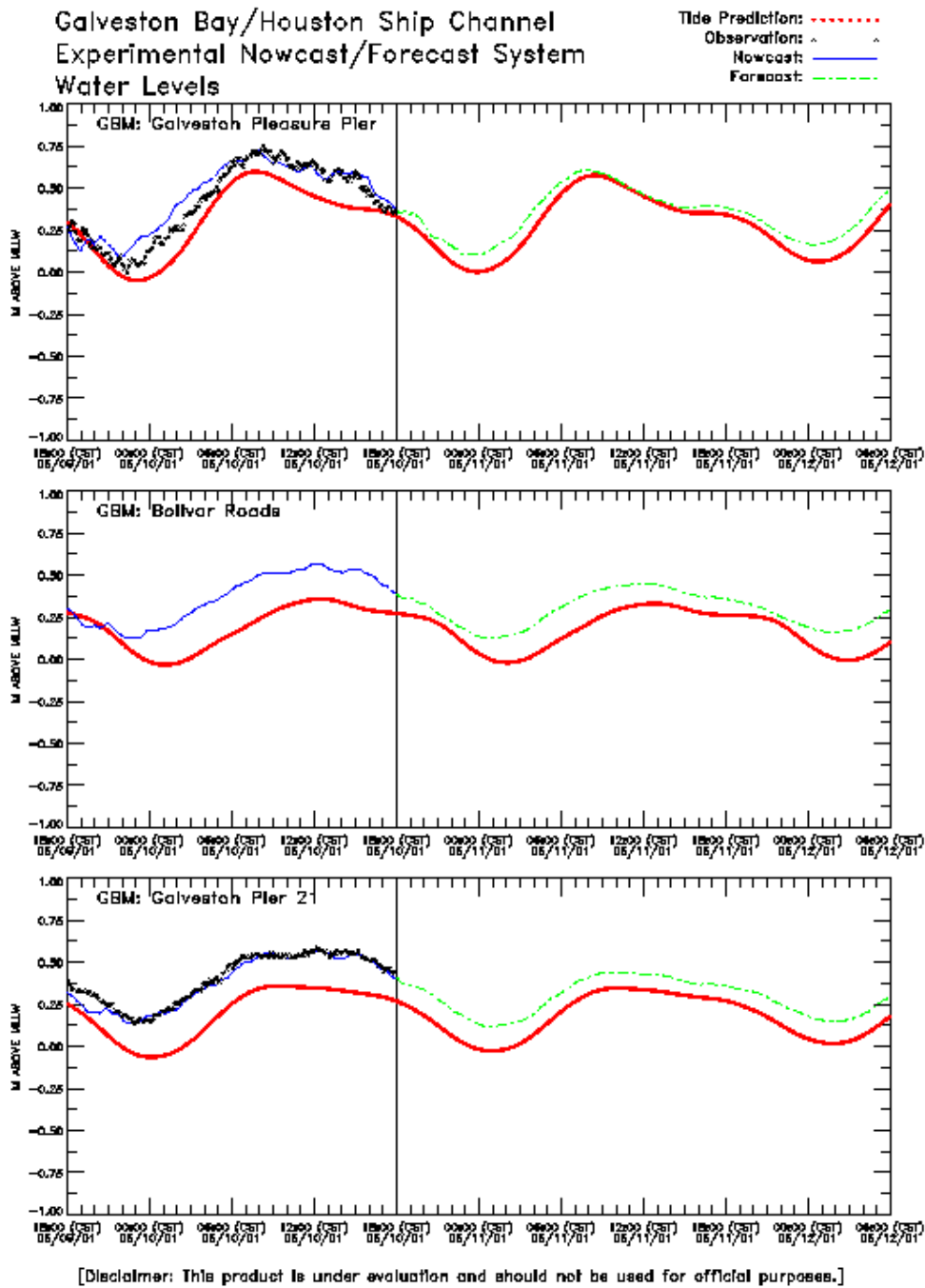


Figure 8.15. Tropical Storm Allison GBM Water Levels Experiment One: 11 June 2001
Nowcast/Forecast Cycle

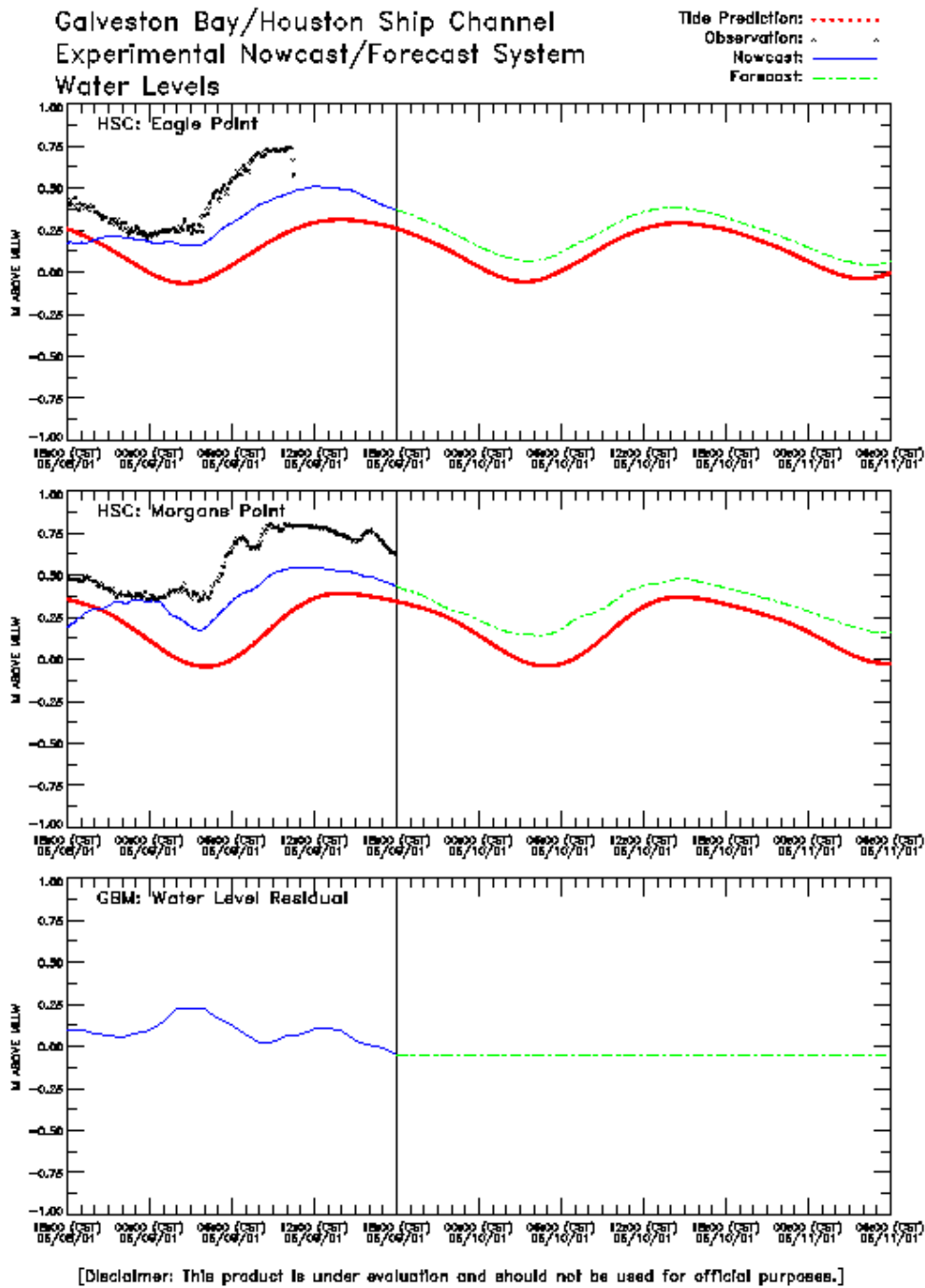


Figure 8.16. Tropical Storm Allison HSCM Water Levels and GBM Water Level Residual Experiment One: 10 June 2001 Nowcast/Forecast Cycle

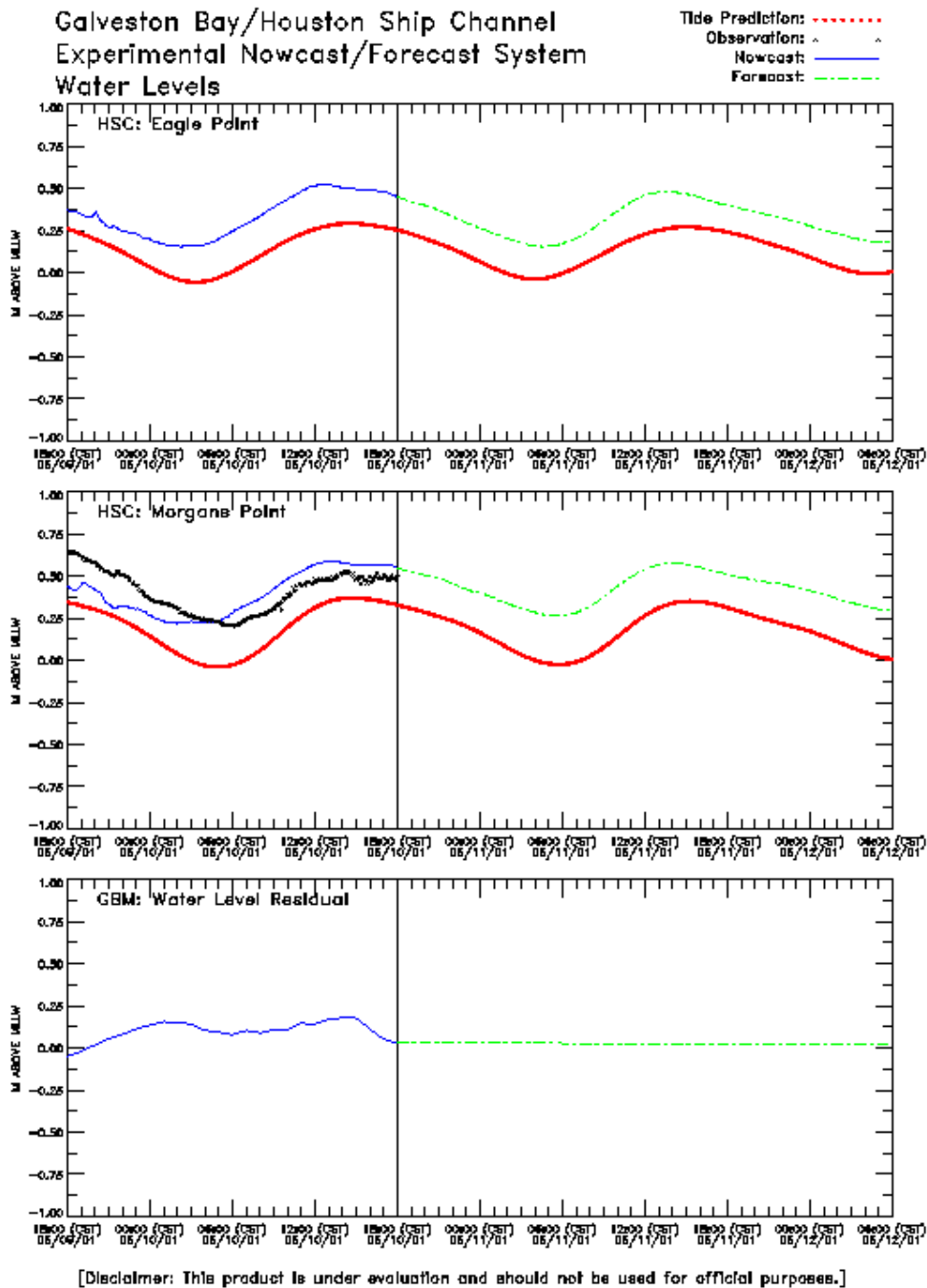


Figure 8.17. Tropical Storm Allison HSCM Water Levels and GBM Water Level Residual Experiment One: 11 June 2001 Nowcast/Forecast Cycle

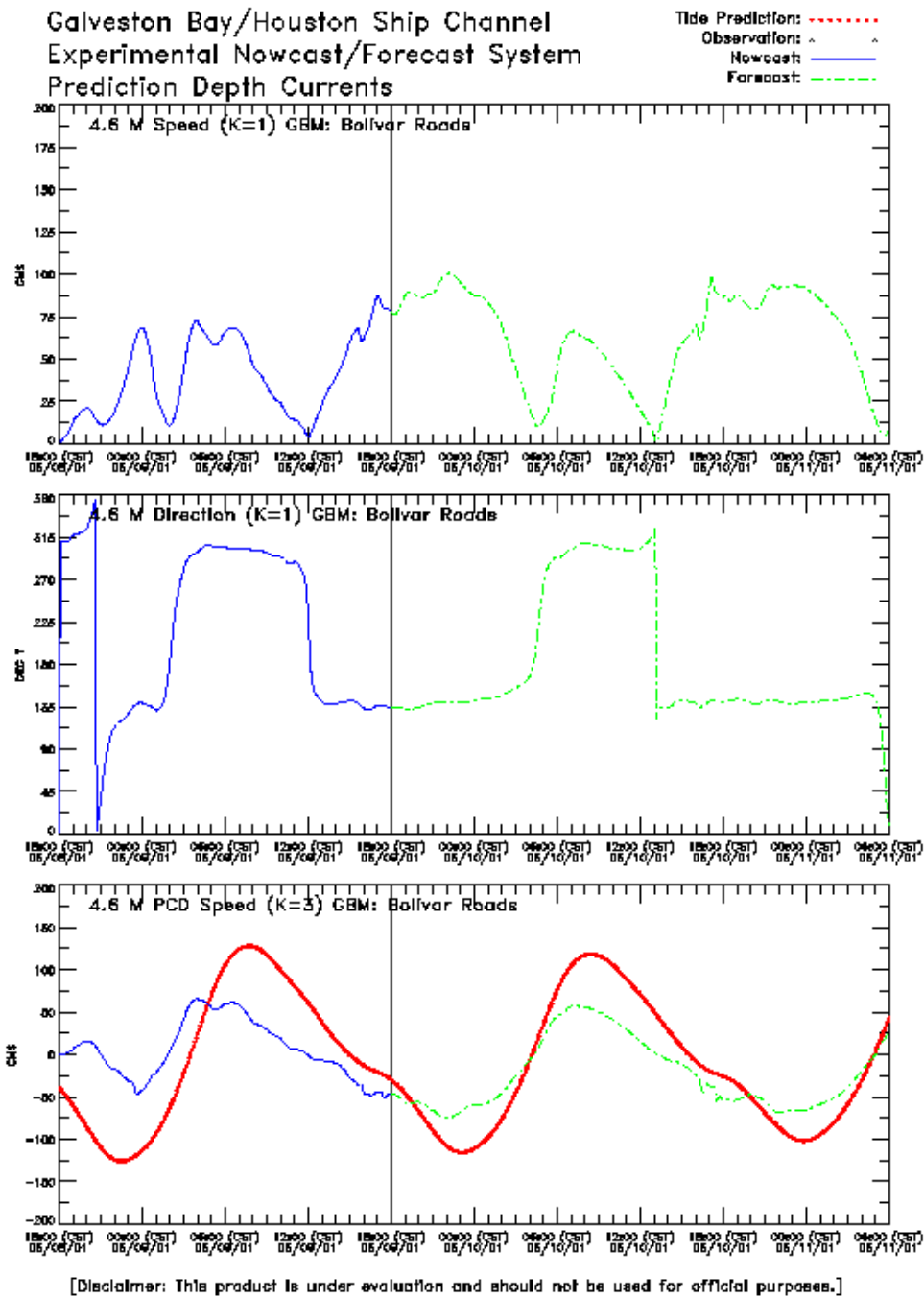


Figure 8.18. Tropical Storm Allison GBM Bolivar Roads Currents Experiment One: 10 June 2001 Nowcast/Forecast Cycle

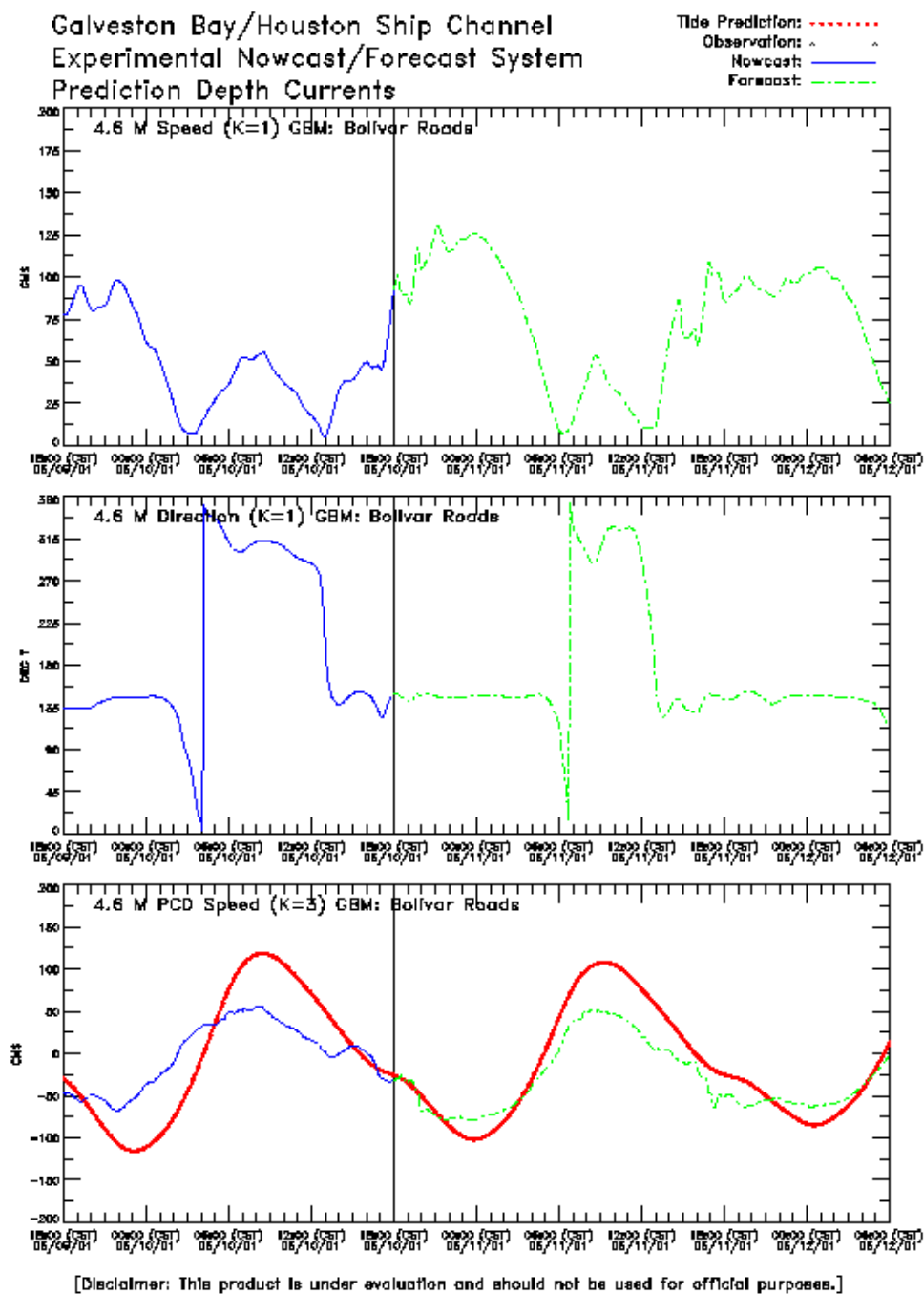


Figure 8.19. Tropical Storm Allison GBM Bolivar Roads Currents Experiment One: 11 June 2001 Nowcast/Forecast Cycle

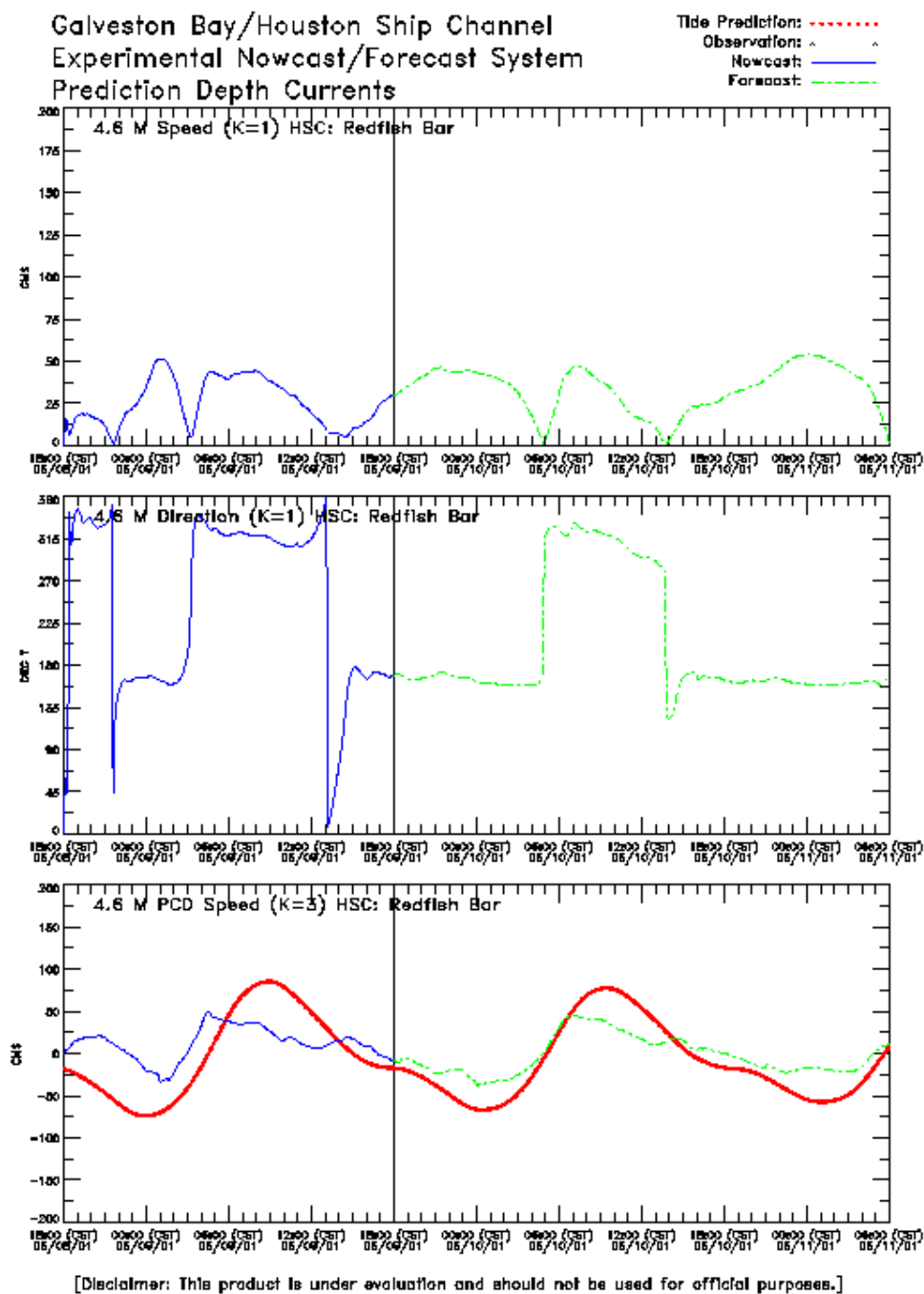


Figure 8.20. Tropical Storm Allison GBM Redfish Bar Currents Experiment One: 10 June 2001 Nowcast/Forecast Cycle

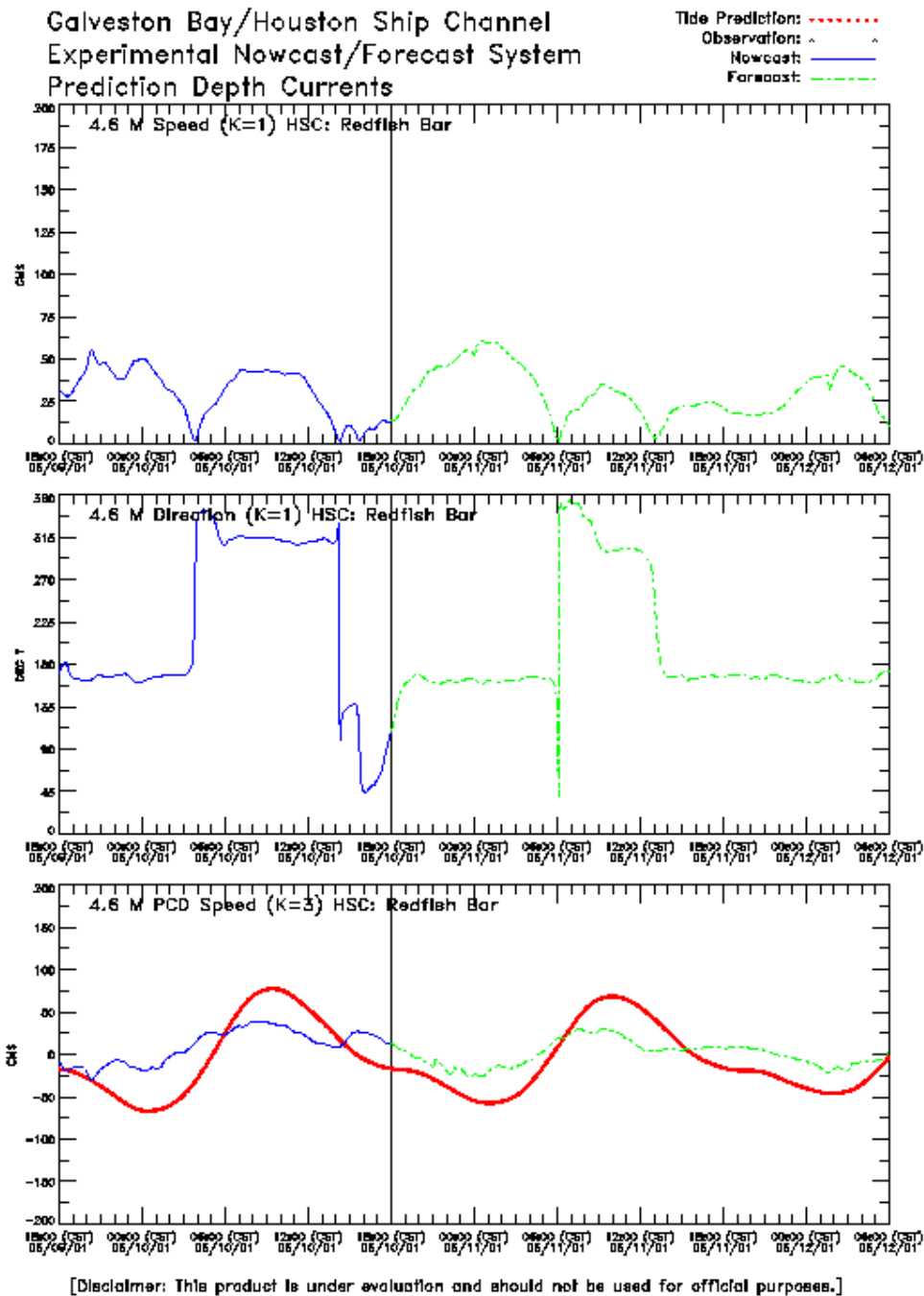


Figure 8.21. Tropical Storm Allison GBM Redfish Bar Currents Experiment One: 11 June 2001 Nowcast/Forecast Cycle

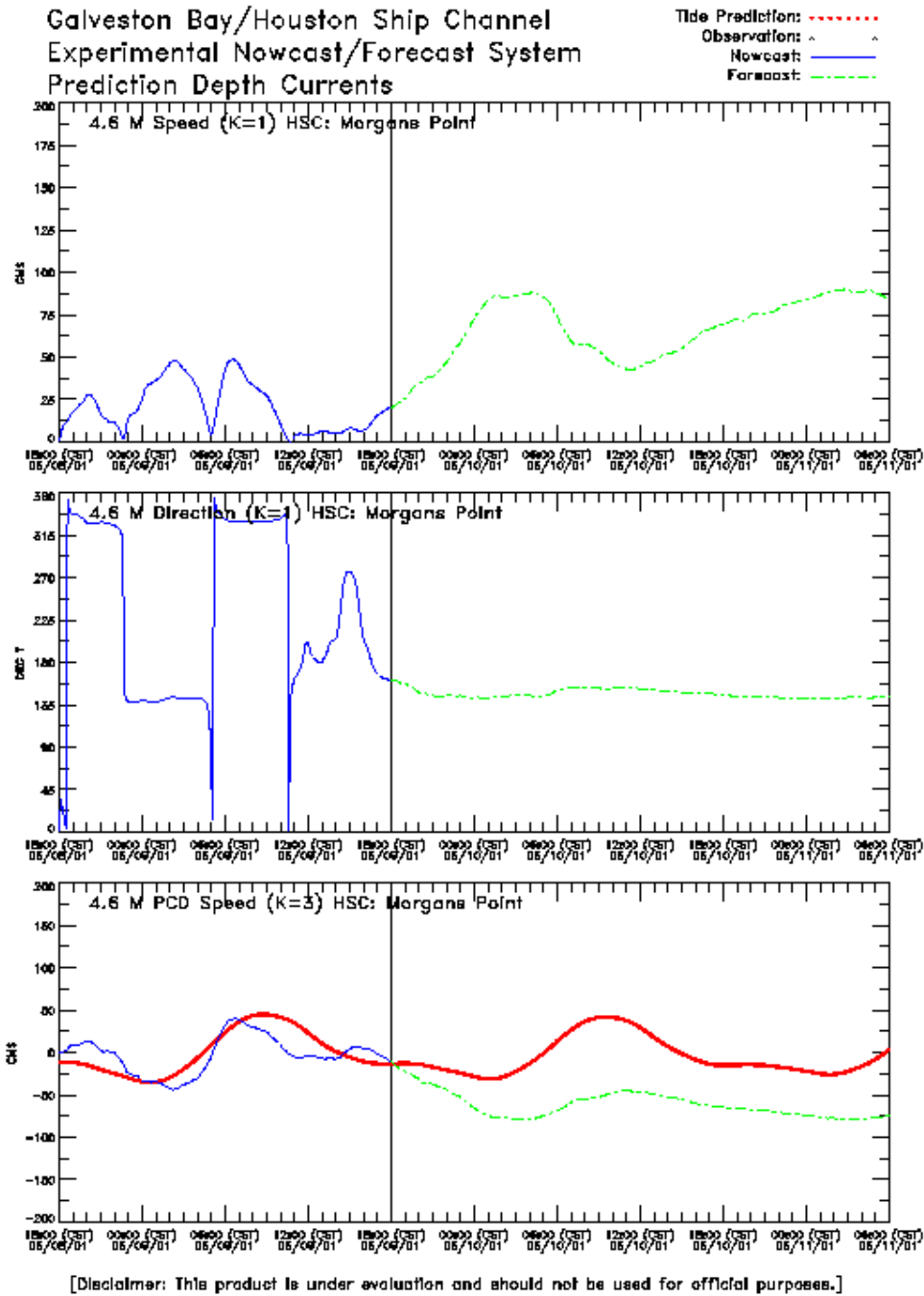


Figure 8.22. Tropical Storm Allison GBM Morgans Point Currents Experiment One: 10 June 2001 Nowcast/Forecast Cycle

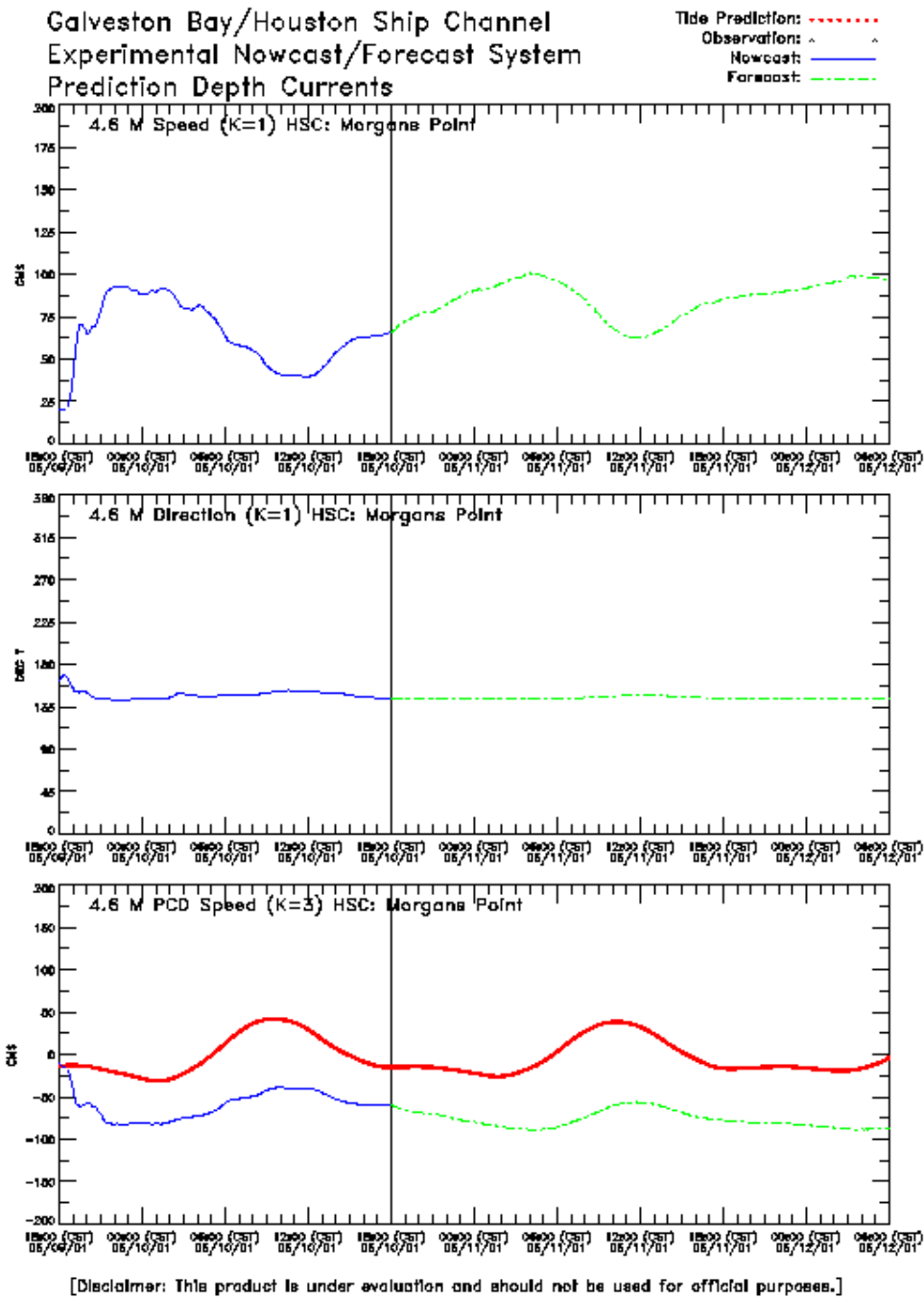


Figure 8.23. Tropical Storm Allison GBM Morgans Point Currents Experiment One: 11 June 2001 Nowcast/Forecast Cycle

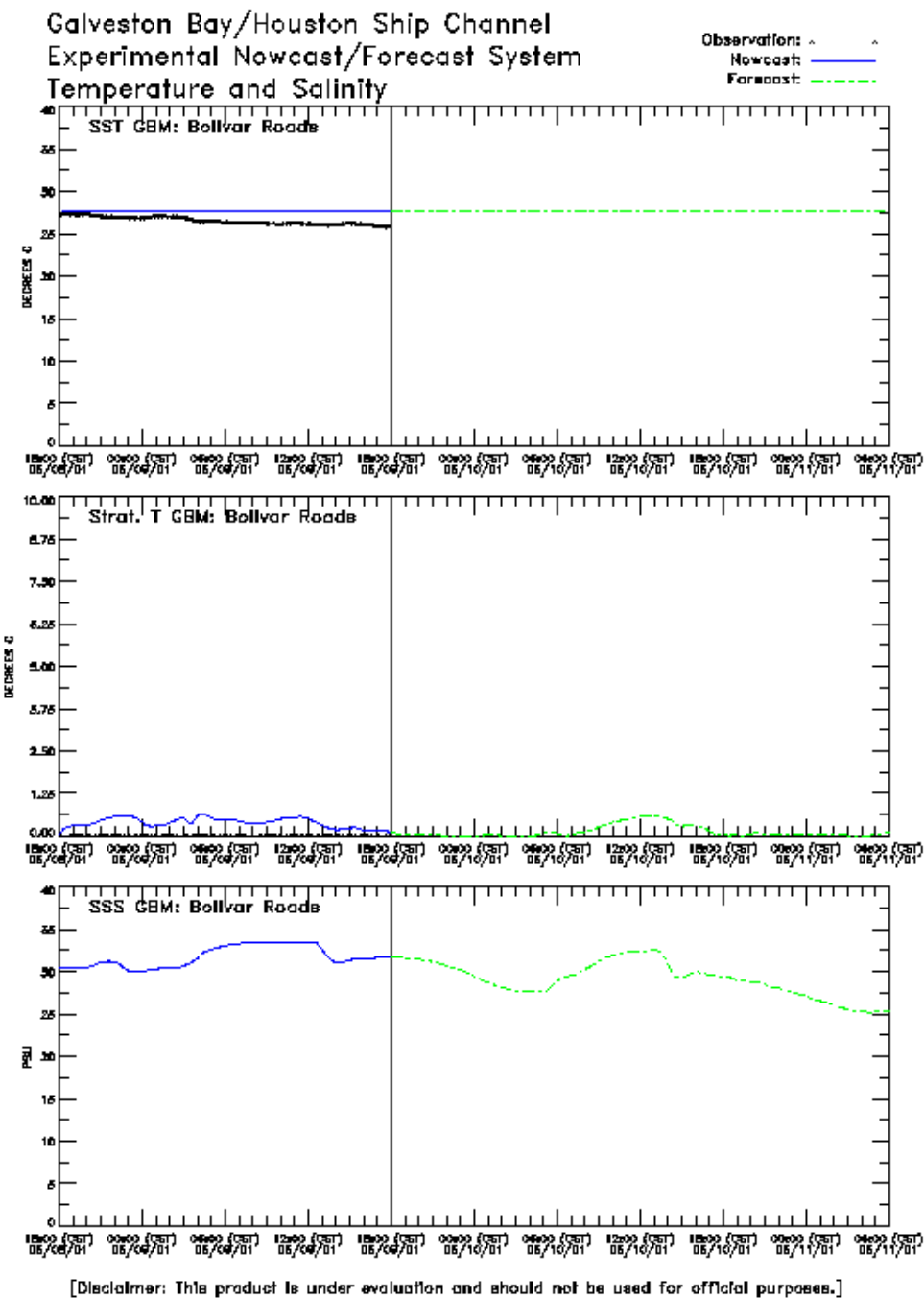


Figure 8.24. Tropical Storm Allison GBM Bolivar Roads Temperature and Salinity Experiment One: 10 June 2001 Nowcast/Forecast Cycle

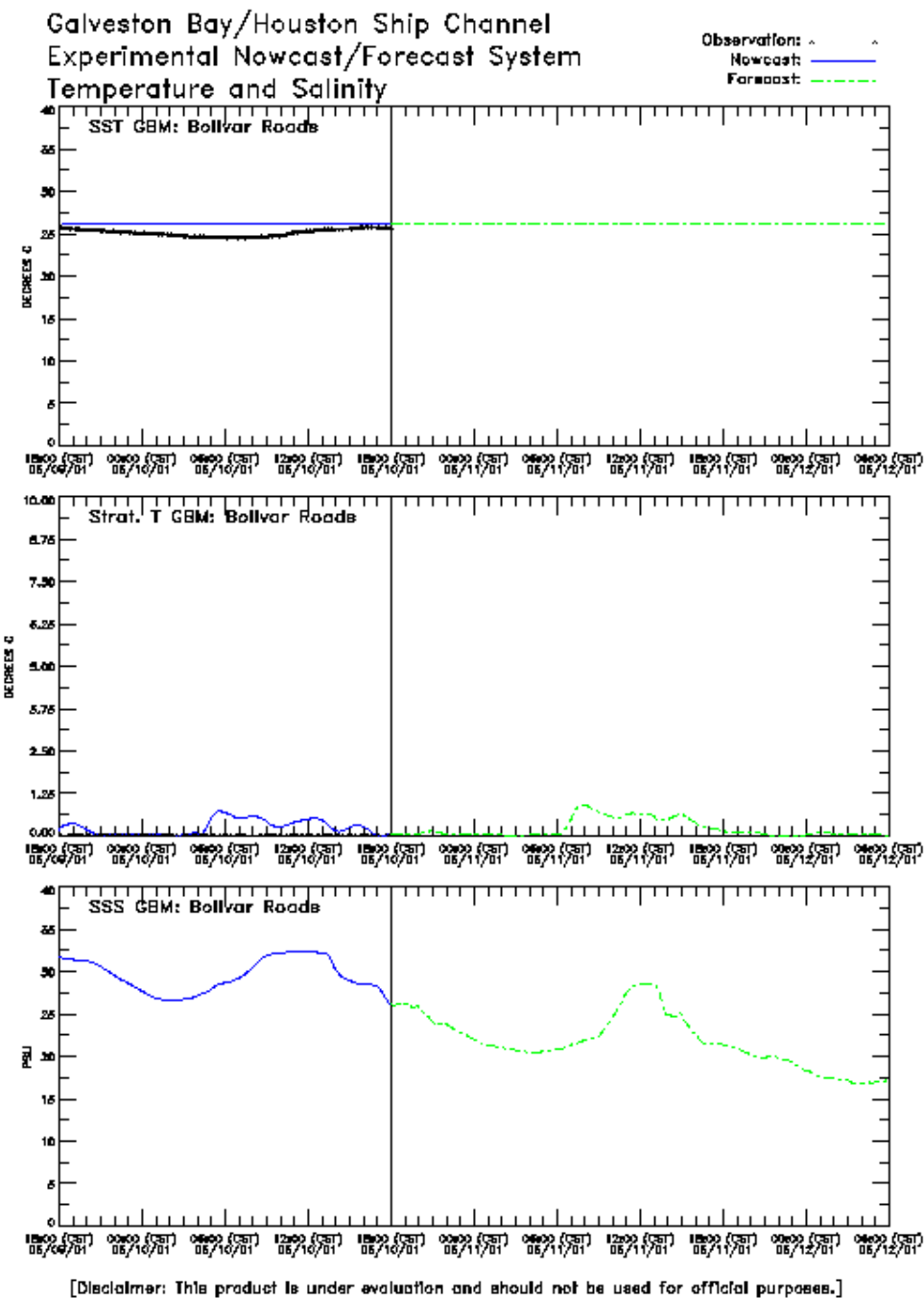


Figure 8.25. Tropical Storm Allison GBM Bolivar Roads Temperature and Salinity Experiment One: 11 June 2001 Nowcast/Forecast Cycle

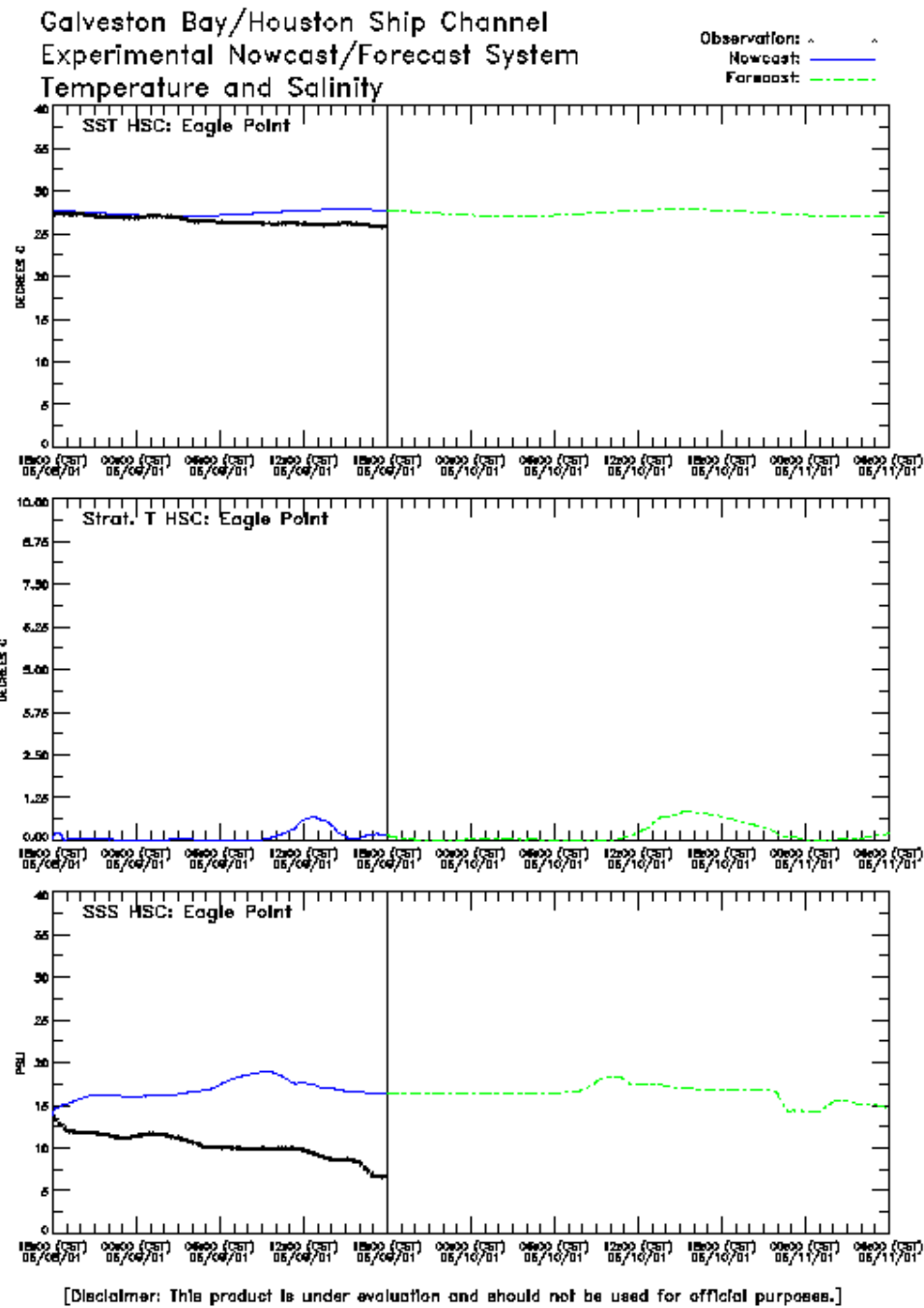


Figure 8.26. Tropical Storm Allison HSCM Eagle Point Temperature and Salinity Experiment One: 10 June 2001 Nowcast/Forecast Cycle

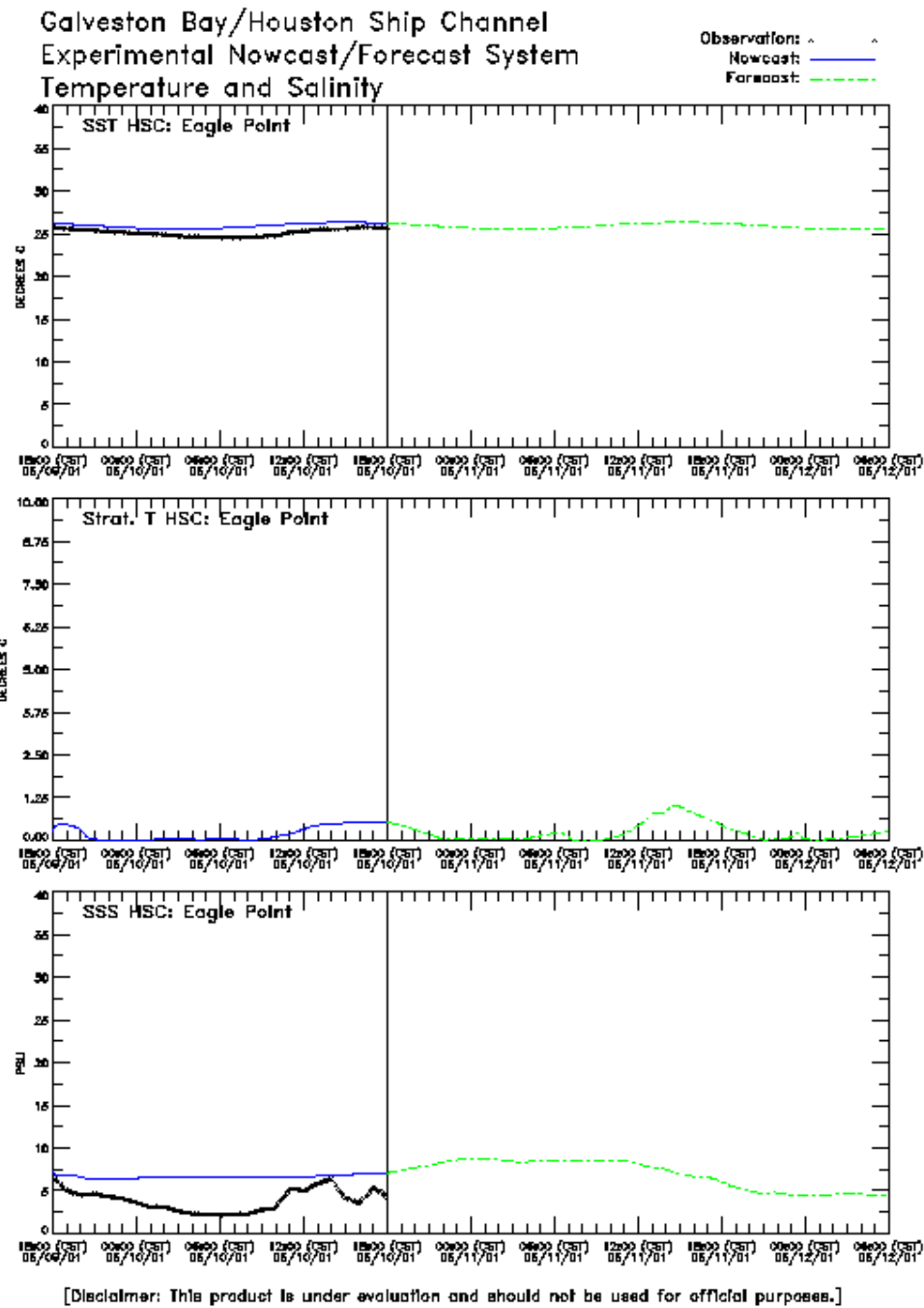


Figure 8.27. Tropical Storm Allison HSCM Eagle Point Temperature and Salinity Experiment One: 11 June 2001 Nowcast/Forecast Cycle

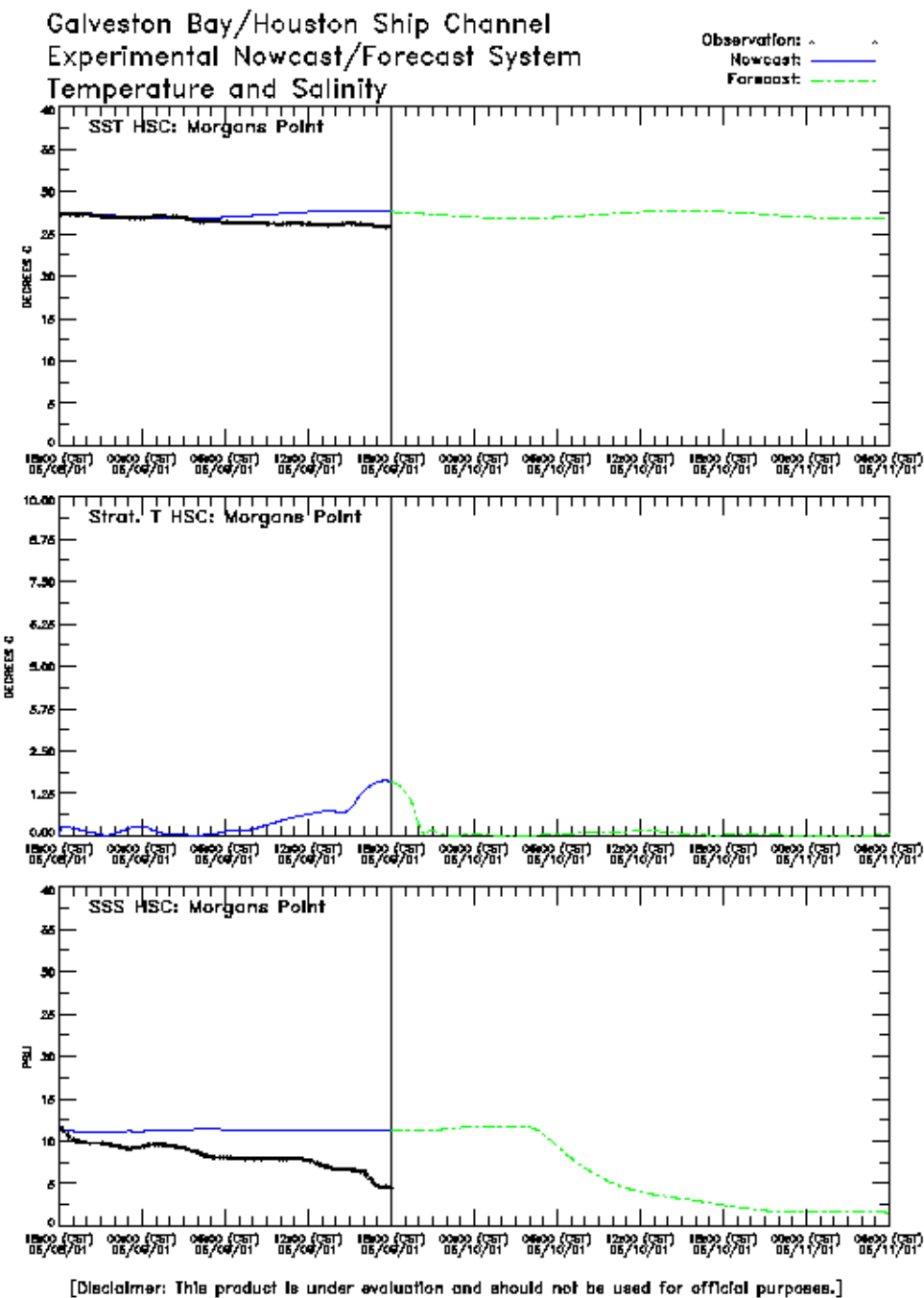


Figure 8.28. Tropical Storm Allison HSCM Morgans Point Temperature and Salinity Experiment One: 10 June 2001 Nowcast/Forecast Cycle

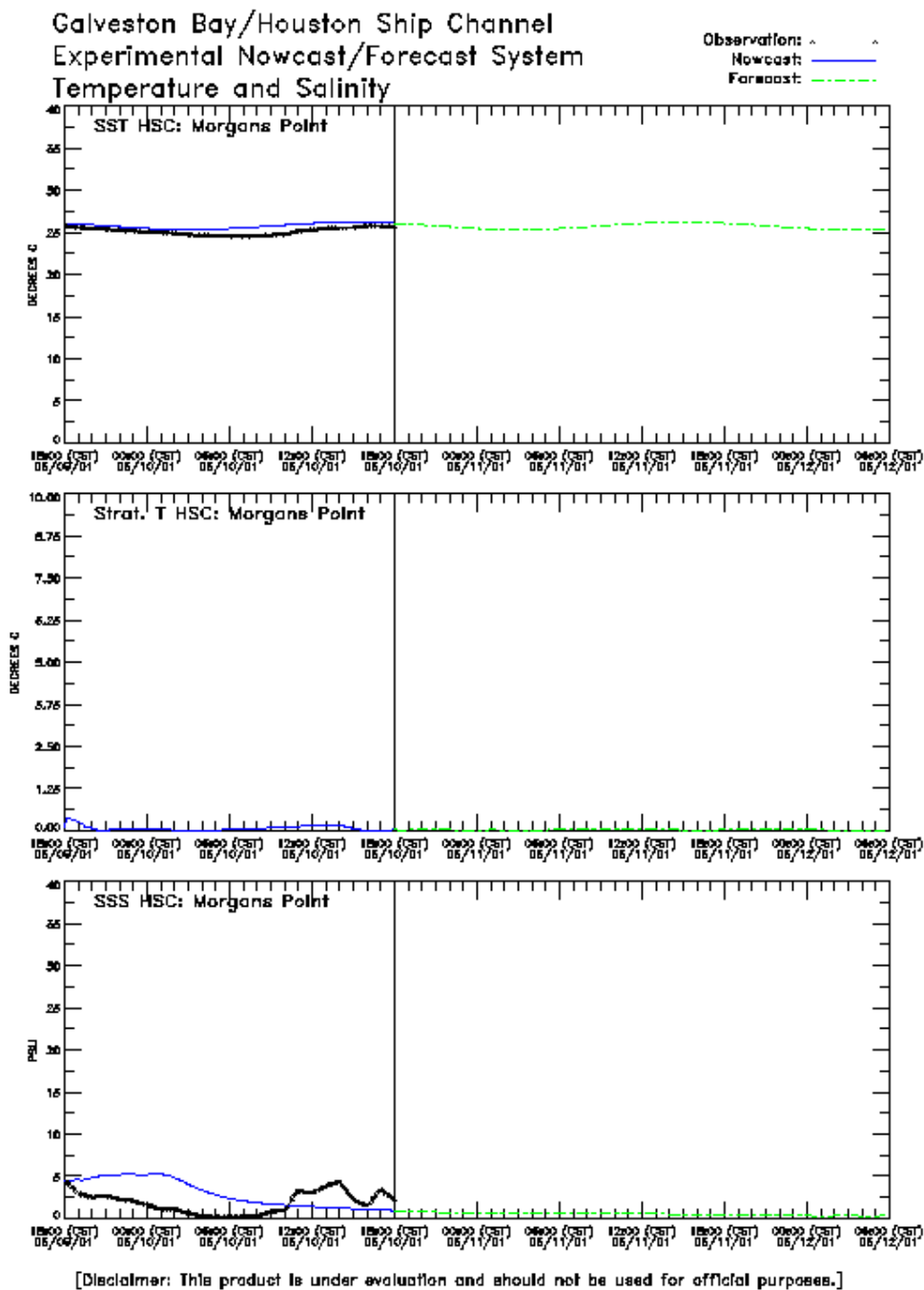


Figure 8.29. Tropical Storm Allison HSCM Morgans Point Temperature and Salinity Experiment One: 11 June 2001 Nowcast/Forecast Cycle

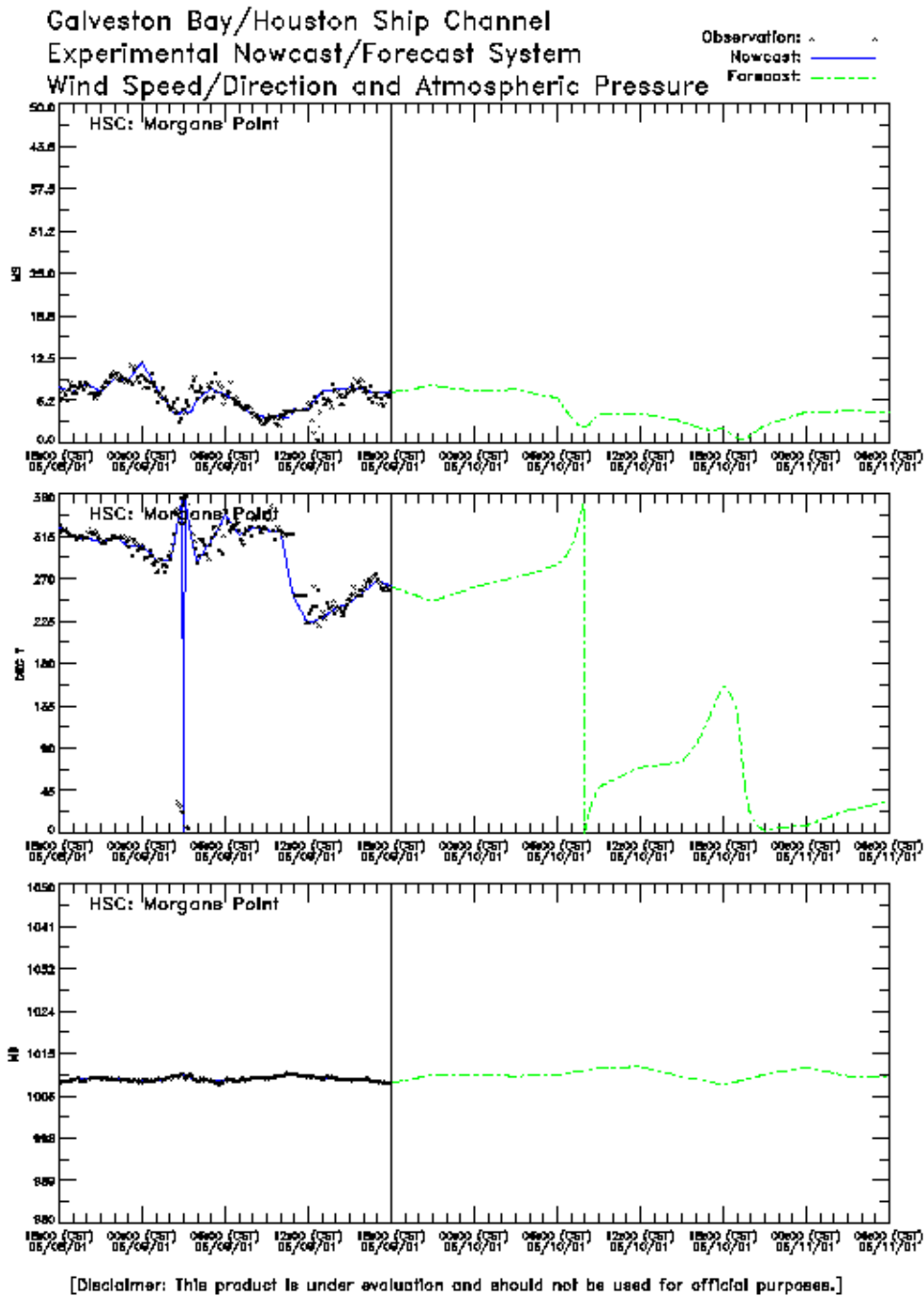


Figure 8.30. Tropical Storm Allison Wind and Atmospheric Pressure at Morgans Point Experiment One: 10 June 2001 Nowcast/Forecast Cycle

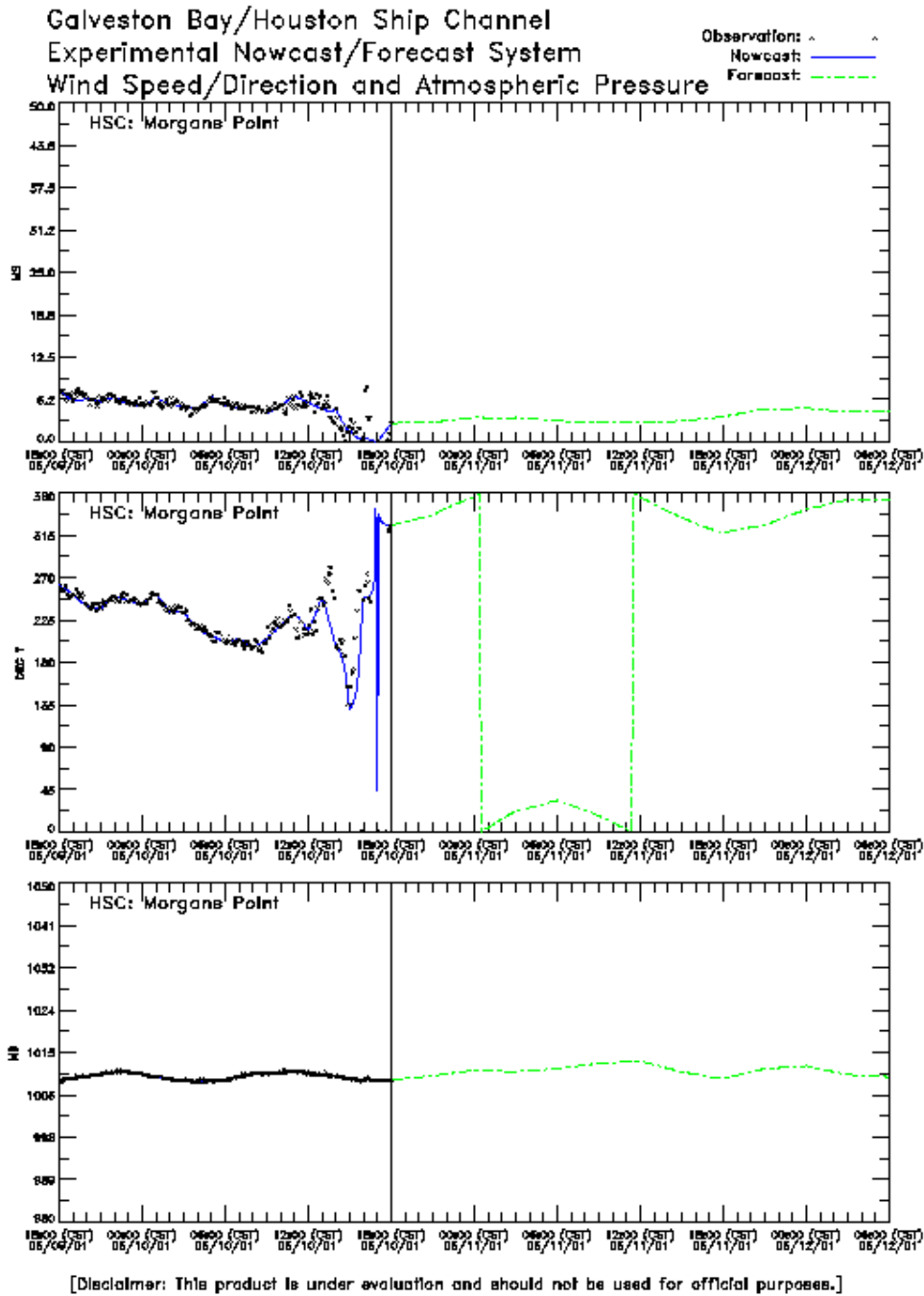


Figure 8.31. Tropical Storm Allison Wind and Atmospheric Pressure at Morgans Point Experiment One: 11 June 2001 Nowcast/Forecast Cycle

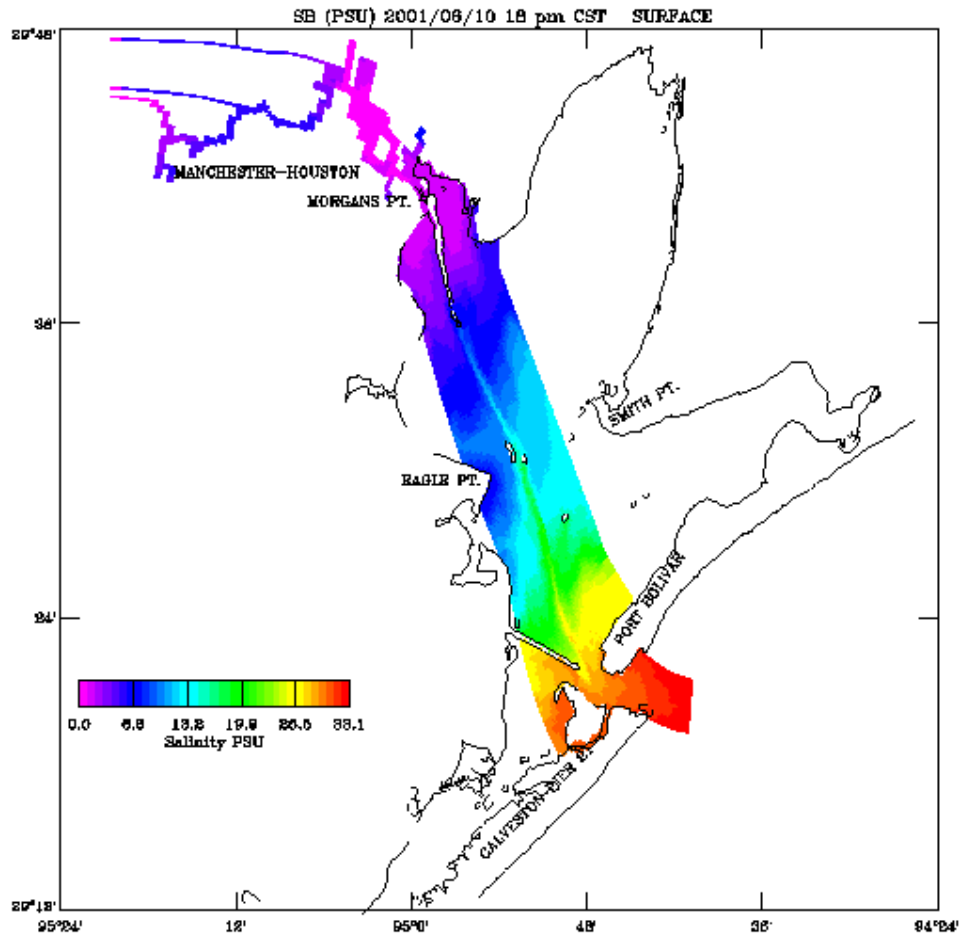


Figure 8.32. Tropical Storm Allison HSCM Near Surface Salinity Field
Experiment One: 11 June 2001 Nowcast End

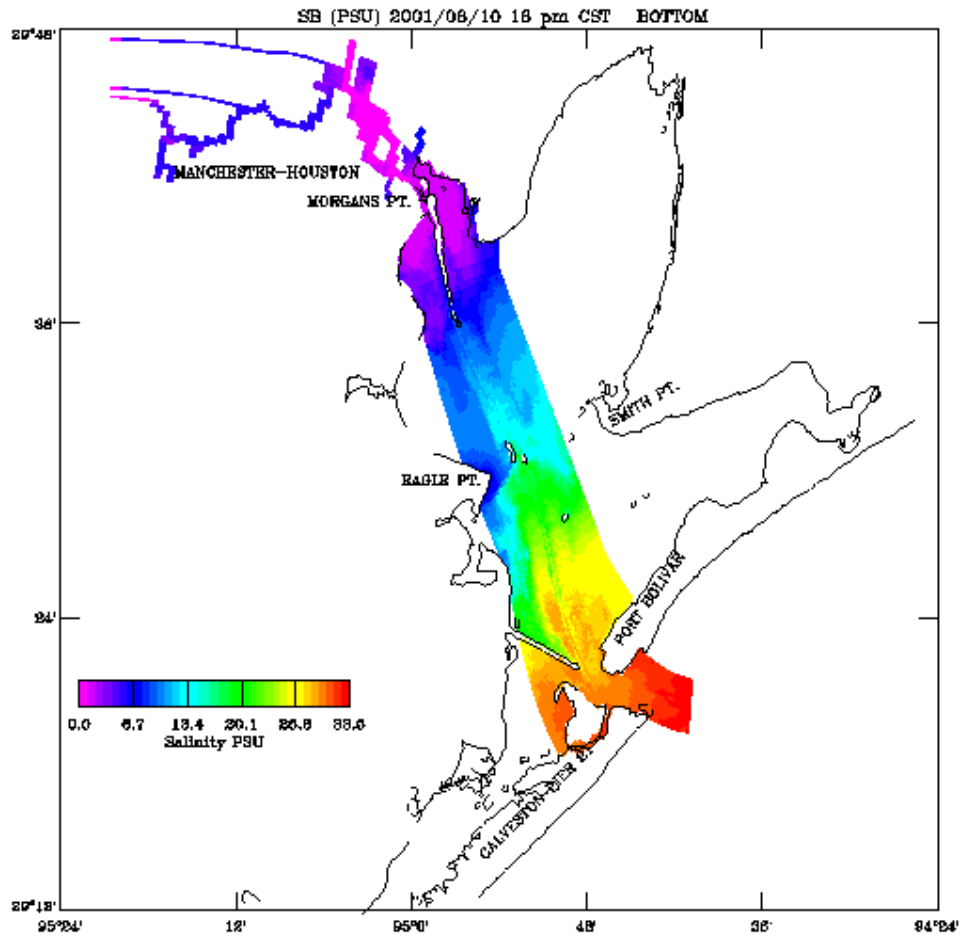


Figure 8.33. Tropical Storm Allison GBM Near Bottom Salinity Field
Experiment One: 11 June 2001 Nowcast End

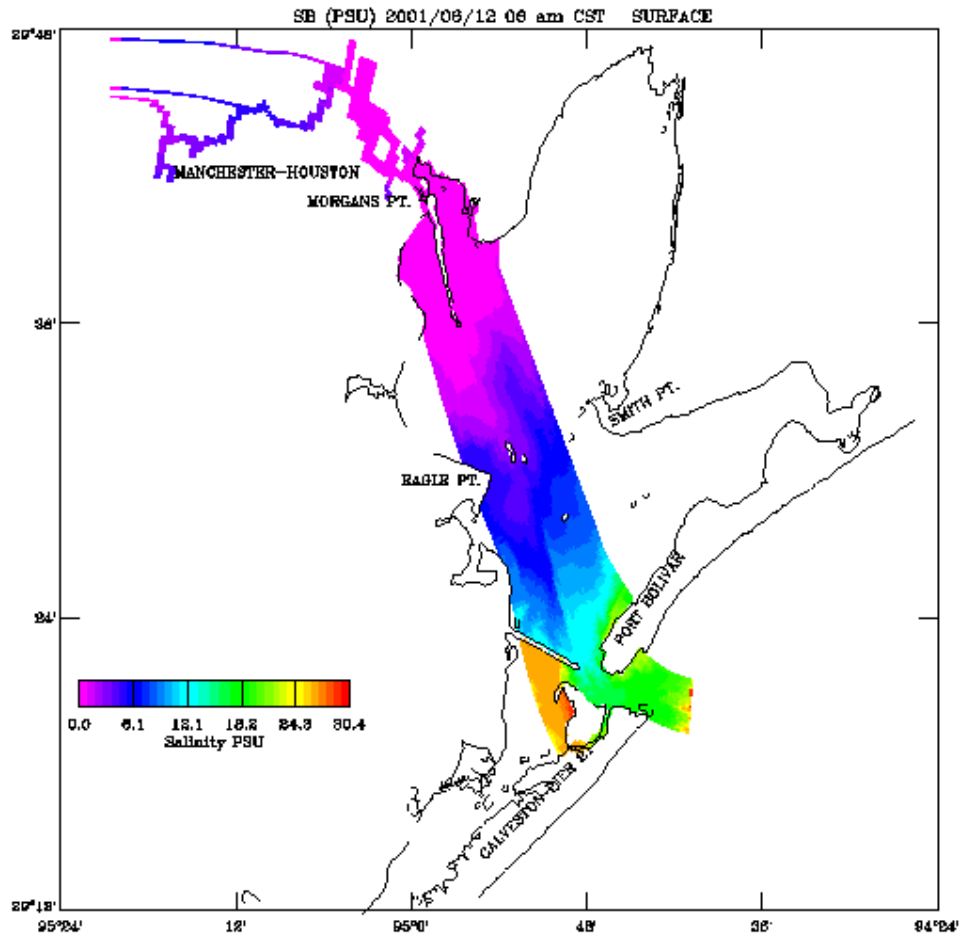


Figure 8.34. Tropical Storm Allison HSCM Near Surface Salinity Field
Experiment One: 11 June 2001 Forecast End

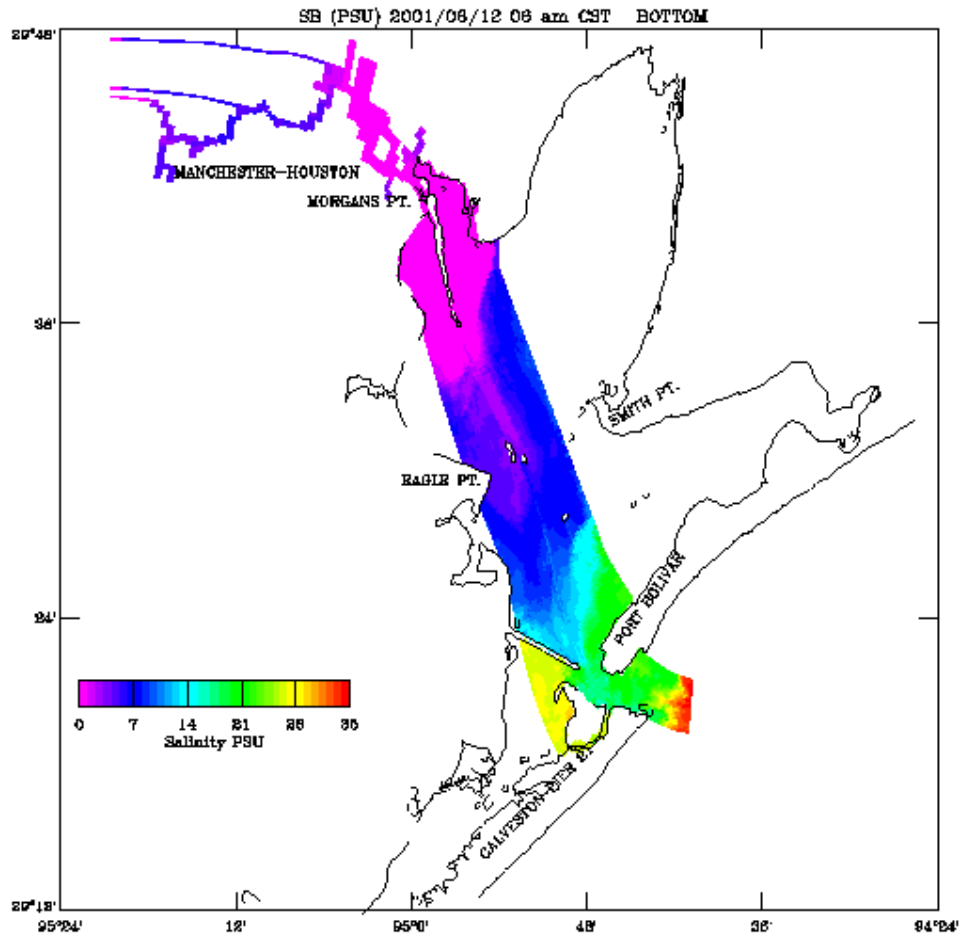


Figure 8.35. Tropical Storm Allison HSCM Near Bottom Salinity Field
Experiment One: 11 June 2001 Forecast End

8.8. Rainfall/Runoff Event Experiment Two Long Wave Results

Tropical Storm Allison standard inflows for the Trinity, San Jacinto, and Buffalo Bayou inflows were shown for both nowcast/forecast cycles in Figures 8.12 and 8.13, where we noted the forecast and subsequent nowcast flow of over 100000 cfs for the San Jacinto River. Here additional inflows are shown for flow set one in Figures 8.36-8.37, and in Figures 8.38-8.39 for flow set two. Note in the third panel of these figures, the Buffalo Bayou inflow is shown as a reference comparison flow. One notes the Greens Bayou forecast and nowcast flows exceed 50,000 cfs, while the other inflows are order those of Buffalo Bayou inflow.

In response to this additional inflow, the HSCM simulated water surface elevations are shown in Figures 8.40-8.41 for each nowcast/forecast cycle at Eagle Point and Morgans Point. These results are to be compared with experiment one HSCM simulated water levels shown in Figures 8.16-8.17. One notes similar results except at Morgans Point where water surface elevations in experiment two are elevated by order 10-15 cm above experiment one levels during the second nowcast/forecast cycle.

HSCM simulated currents are examined in three panel figures for current speed, current direction, and principal component direction with flood considered positive at Morgans Point in Figures 8.42-8.43, and exhibit peak current speeds of 125 cm/s. These results are to be compared with the experiment one results given in Figures 8.22-8.23. One notes a similar ebb dominance but with current strengths reduced by 25 cm/s in experiment one.

HSCM simulated surface temperature, temperature stratification (absolute difference between surface and bottom temperatures) and surface salinity are examined in three panels at Eagle Point in Figures 8.44-8.45, and at Morgans Point in Figures 8.46-8.47, respectively. From experiment one results at Eagle Point both the salinity and temperature responses are nearly identical for both experiments. From experiment one results at Morgans Point the simulated surface salinity and temperature responses are nearly the same but with the degree of temperature stratification reduced by 0.6 °C.

HSCM simulated near surface and near bottom salinity contours are shown at the end of the second nowcast and forecast are shown in Figures 8.48-8.49 (see experiment one results in Figures 8.32-8.33) and in Figures 8.50-8.51 (see experiment one results in Figures 8.34-8.35), respectively. Via the figure comparisons, one notes the greater area of propagation of the freshwater effects on salinity down the estuary in both the surface and bottom waters in experiment two relative to experiment one due to the additional Greens Bayou inflows of experiment two.

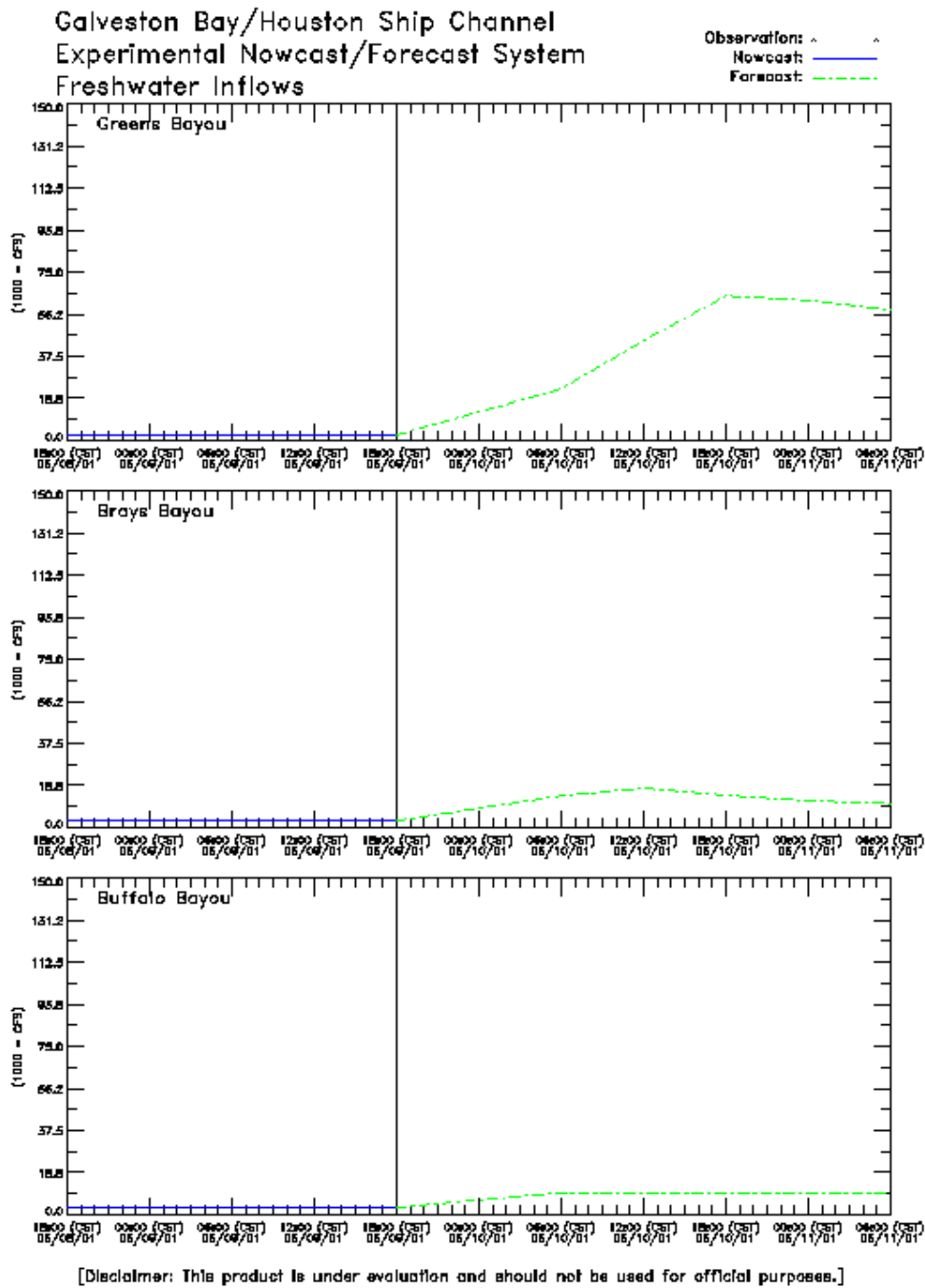


Figure 8.36. Tropical Storm Allison City of Houston Inflow Set One
Experiment Two: 10 June 2001 Nowcast/Forecast Cycle

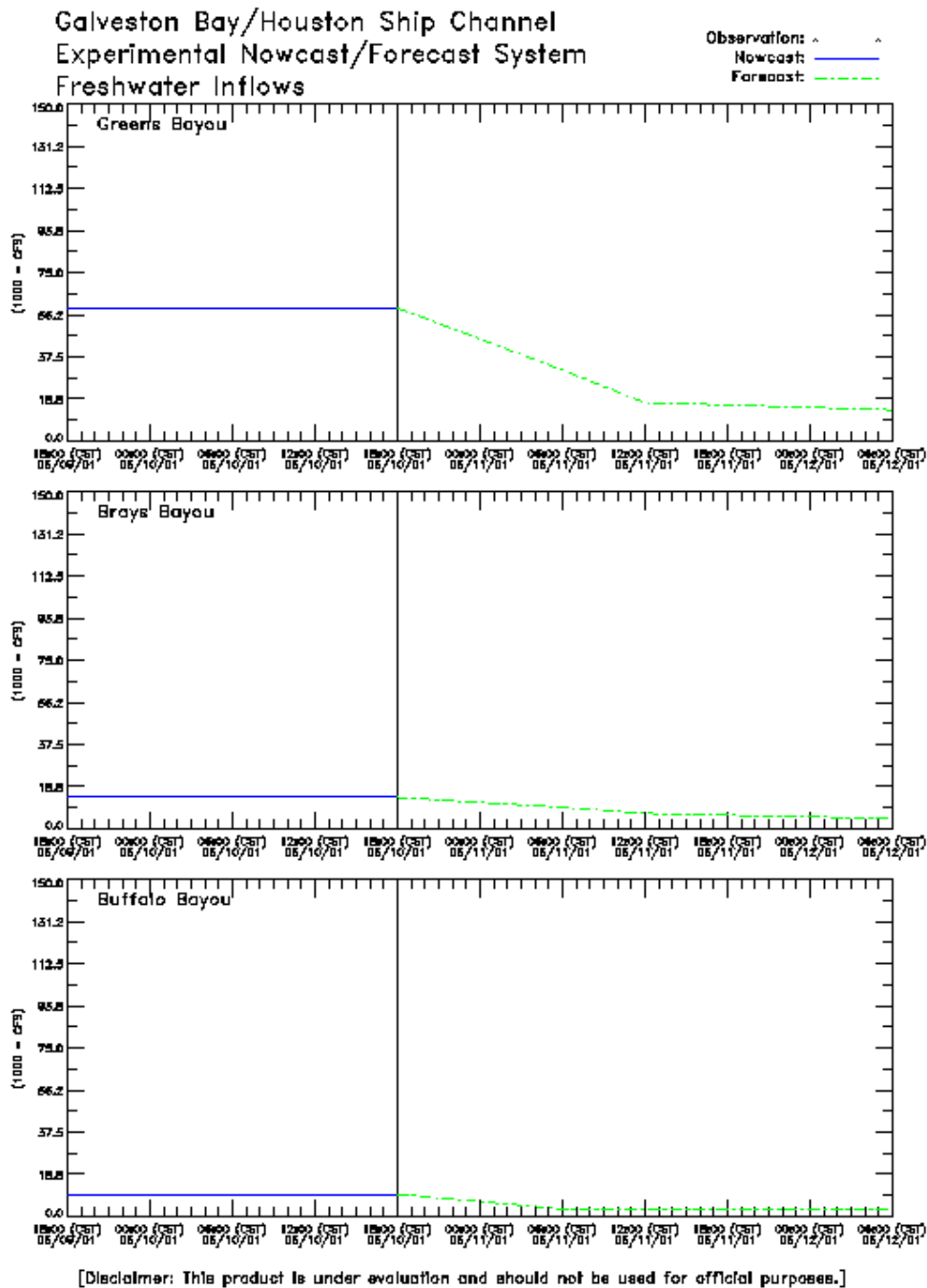


Figure 8.37. Tropical Storm Allison City of Houston Inflow Set One
Experiment Two: 11 June 2001 Nowcast/Forecast Cycle

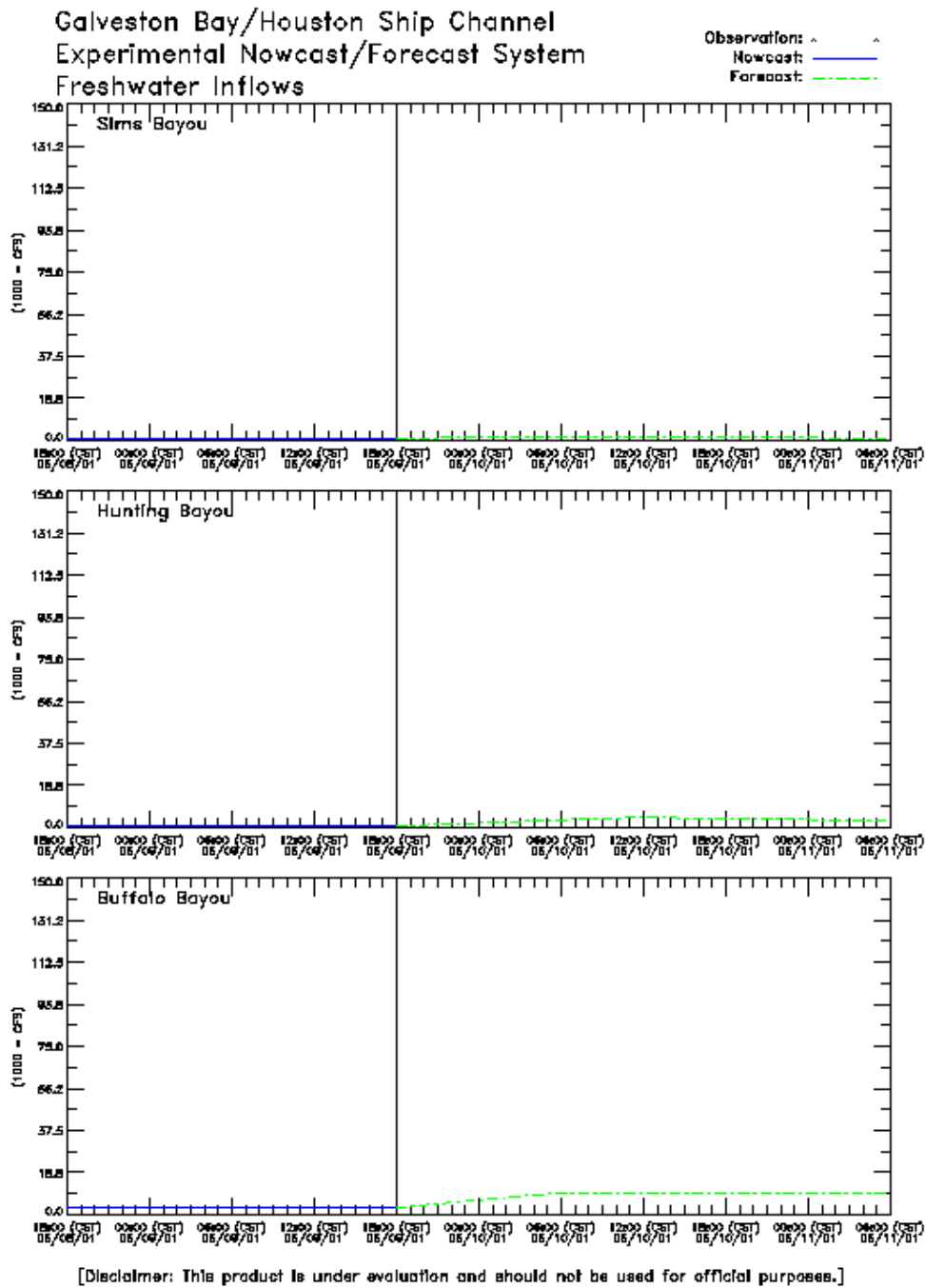


Figure 8.38. Tropical Storm Allison City of Houston Inflow Set Two
Experiment Two: 10 June 2001 Nowcast/Forecast Cycle

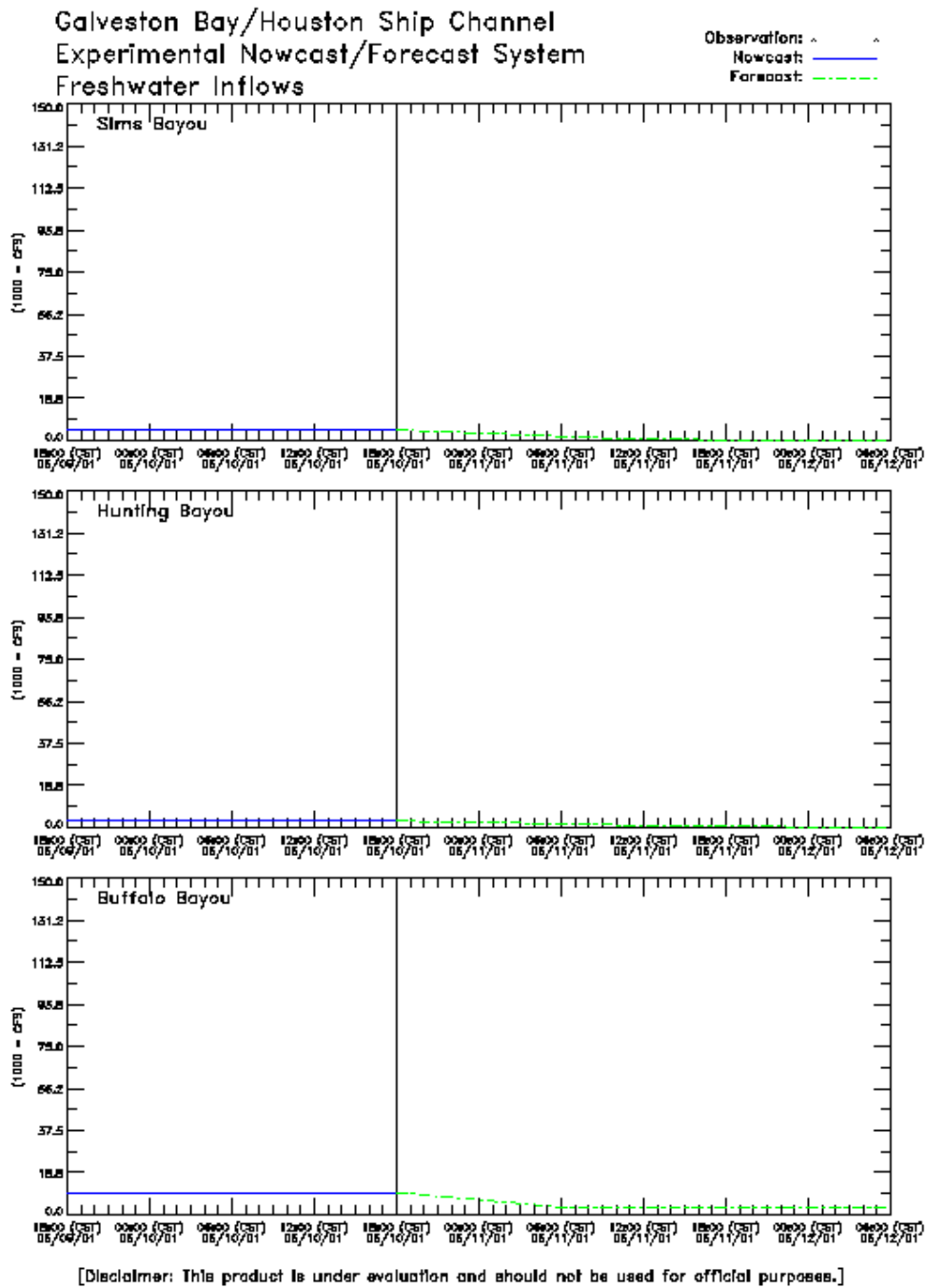


Figure 8.39. Tropical Storm Allison City of Houston Inflow Set Two
Experiment Two: 11 June 2001 Nowcast/Forecast Cycle

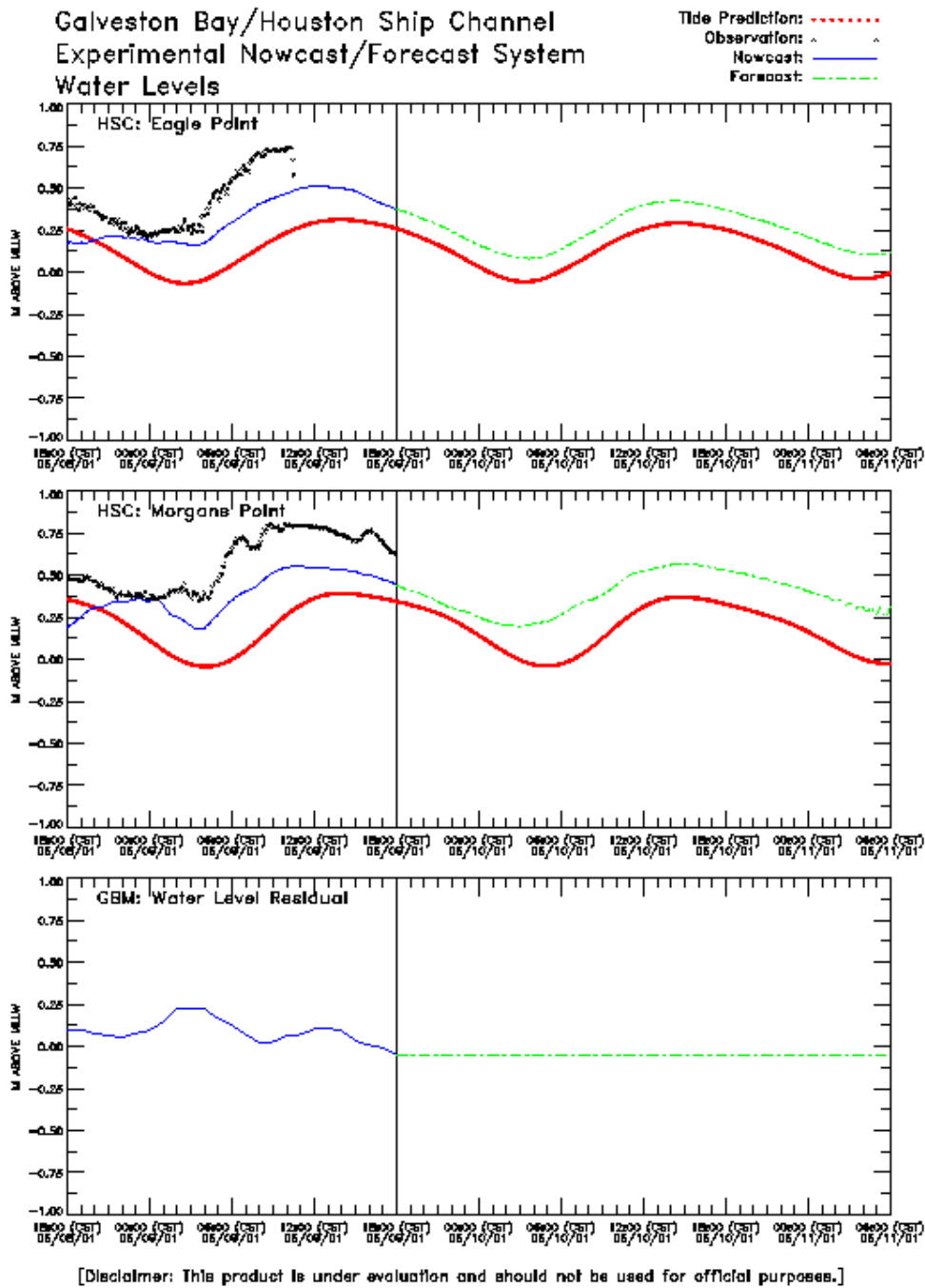


Figure 8.40. Tropical Storm Allison HSCM Water Levels and GBM Water Level Residual Experiment Two: 10 June 2001 Nowcast/Forecast Cycle

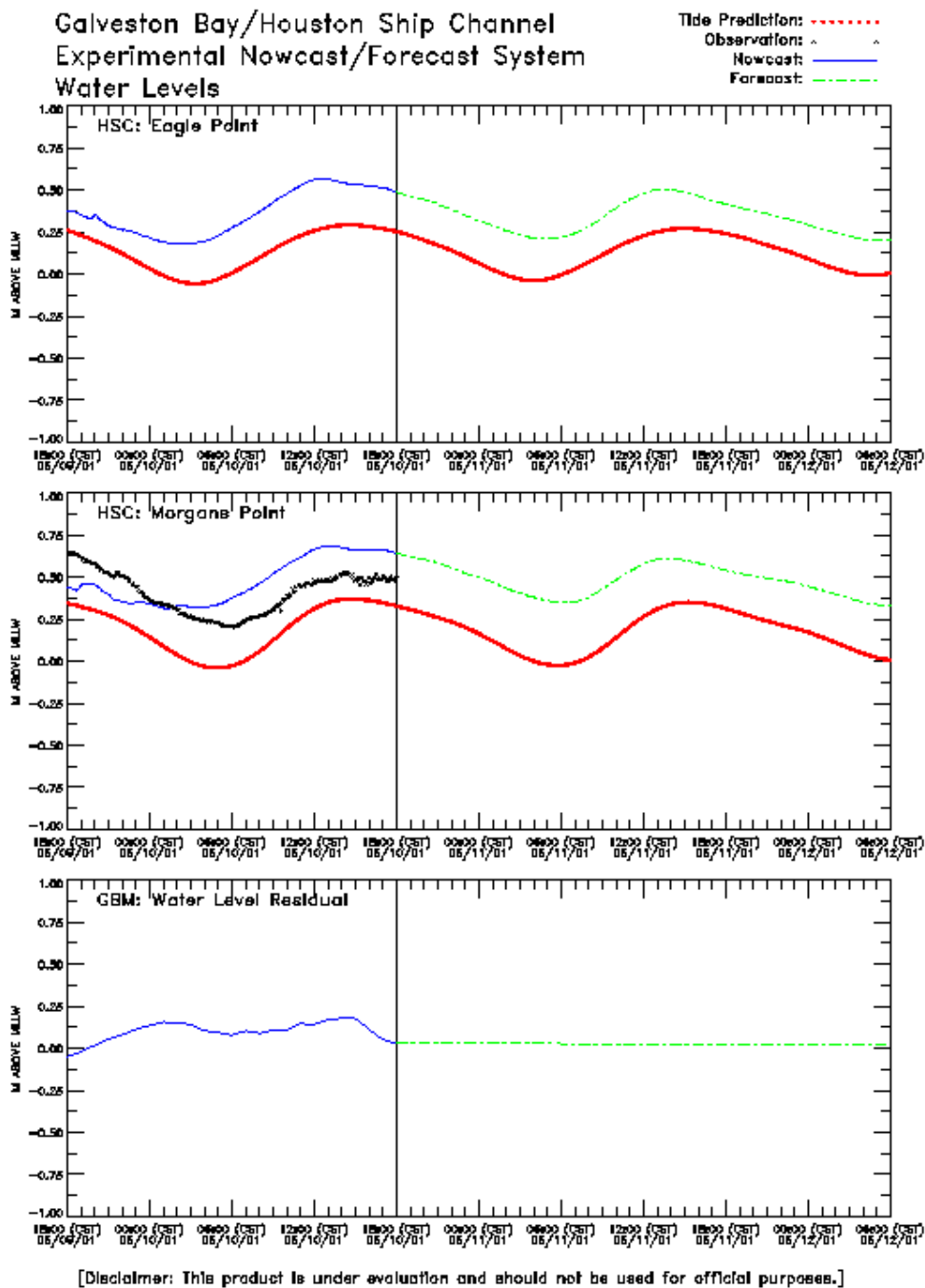


Figure 8.41. Tropical Storm Allison HSCM Water Levels and GBM Water Level Residual Experiment Two: 11 June 2001 Nowcast/Forecast Cycle

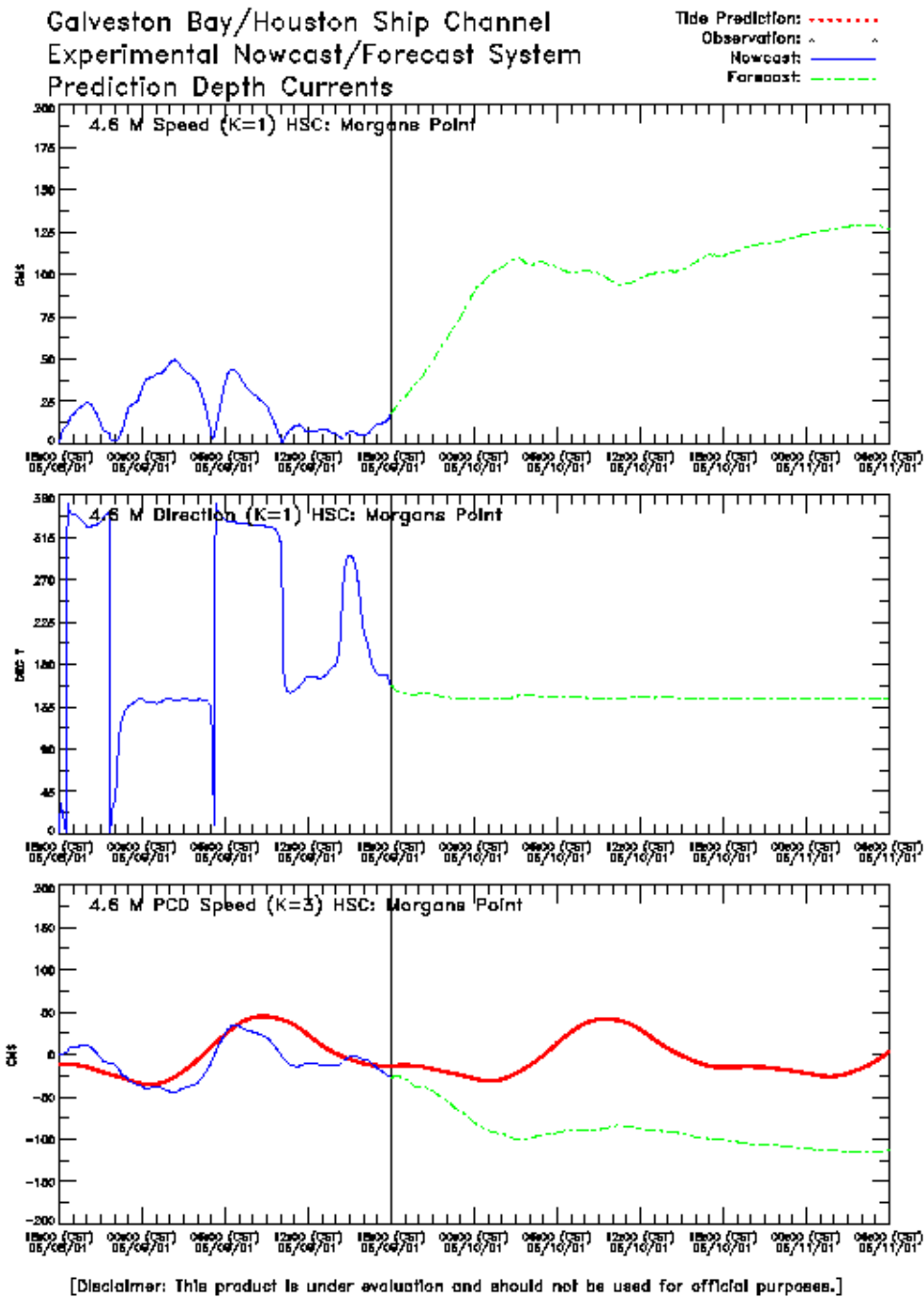


Figure 8.42. Tropical Storm Allison HSCM Morgans Point Currents Experiment Two: 10 June 2001 Nowcast/Forecast Cycle

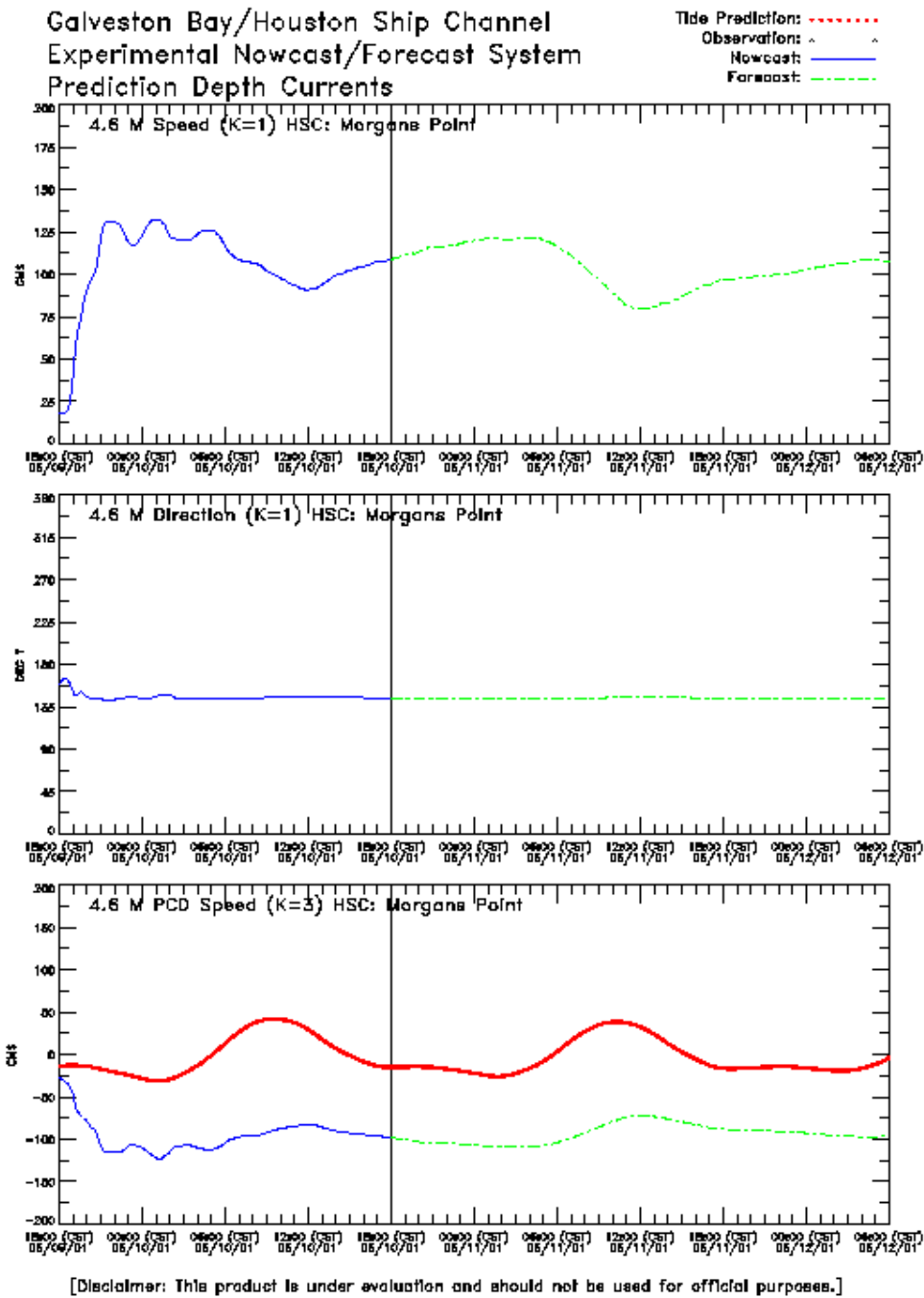


Figure 8.43. Tropical Storm Allison HSCM Morgans Point Currents Experiment Two: 11 June 2001 Nowcast/Forecast Cycle

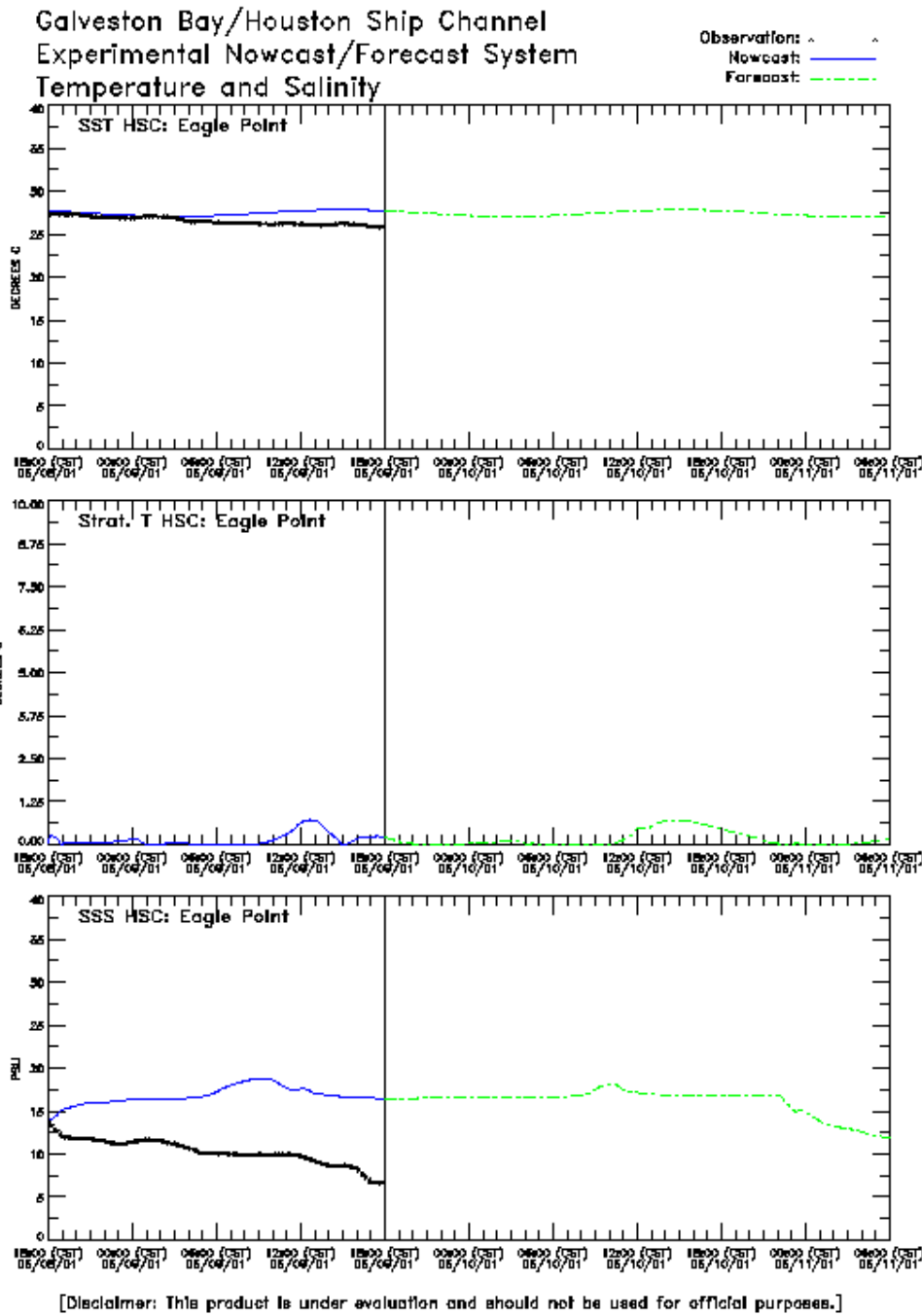


Figure 8.44. Tropical Storm Allison HSCM Eagle Point Temperature and Salinity Experiment Two: 10 June 2001 Nowcast/Forecast Cycle

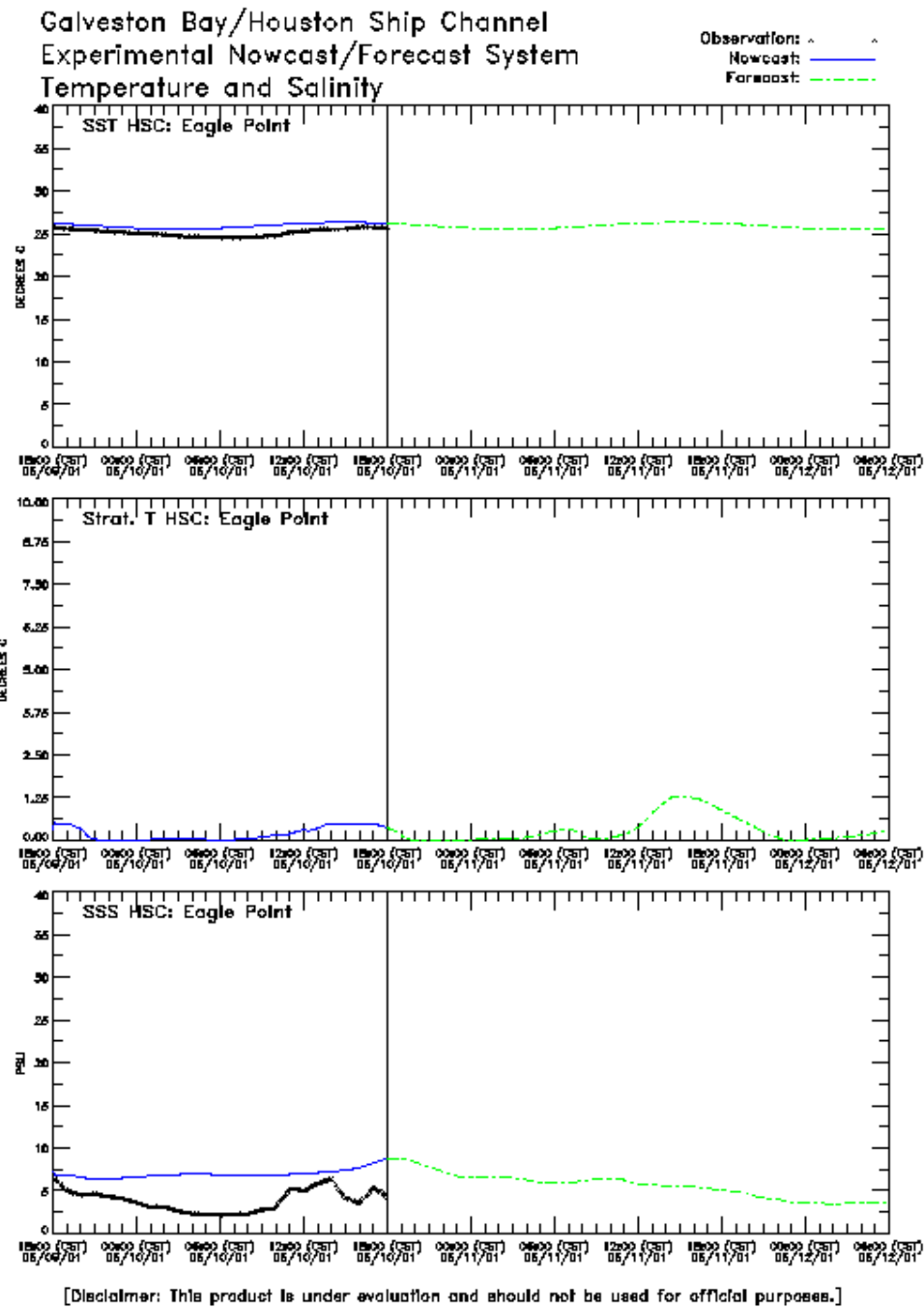


Figure 8.45. Tropical Storm Allison HSCM Eagle Point Temperature and Salinity Experiment Two: 11 June 2001 Nowcast/Forecast Cycle

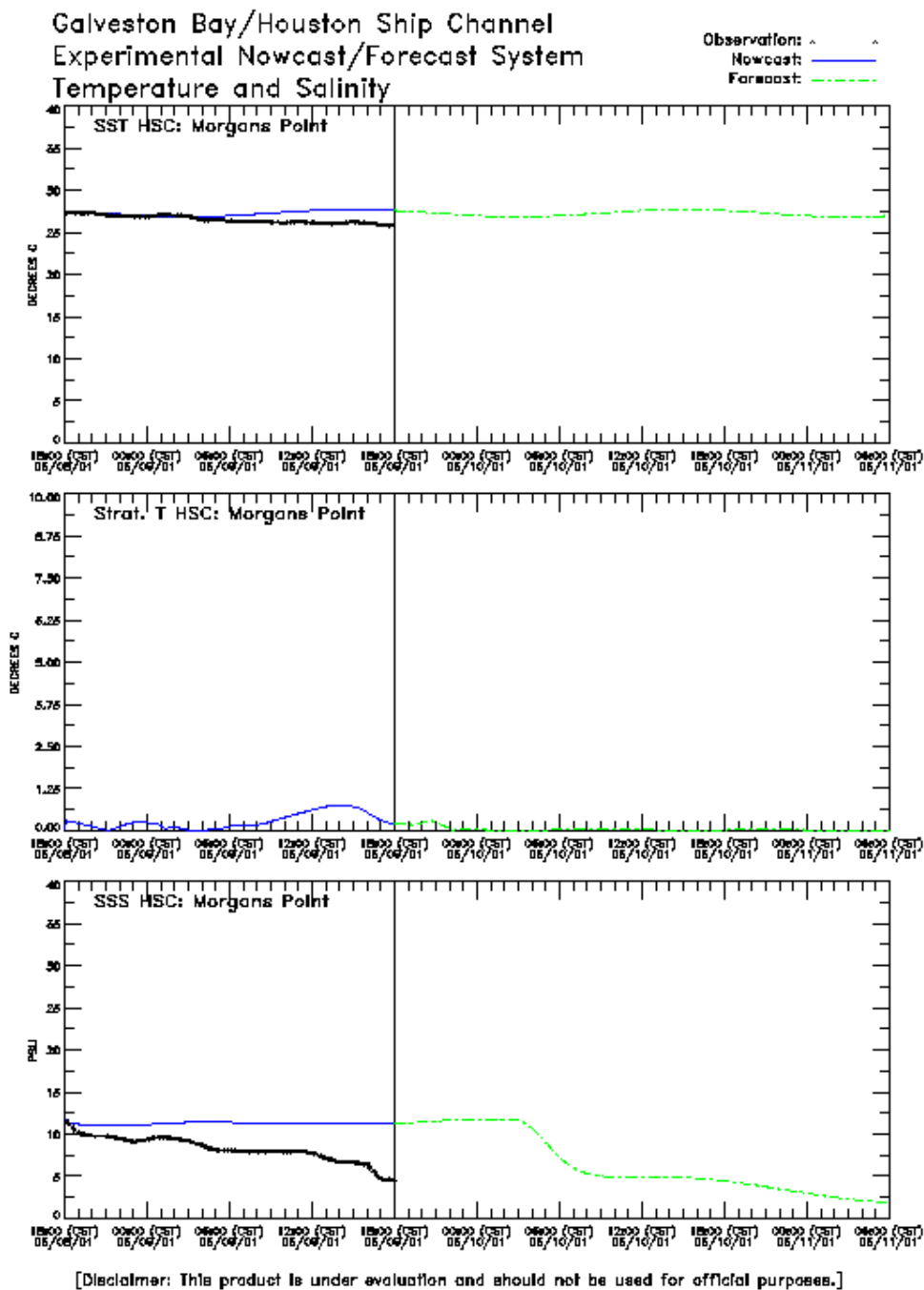


Figure 8.46. Tropical Storm Allison HSCM Morgans Point Temperature and Salinity Experiment Two: 10 June 2001 Nowcast/Forecast Cycle

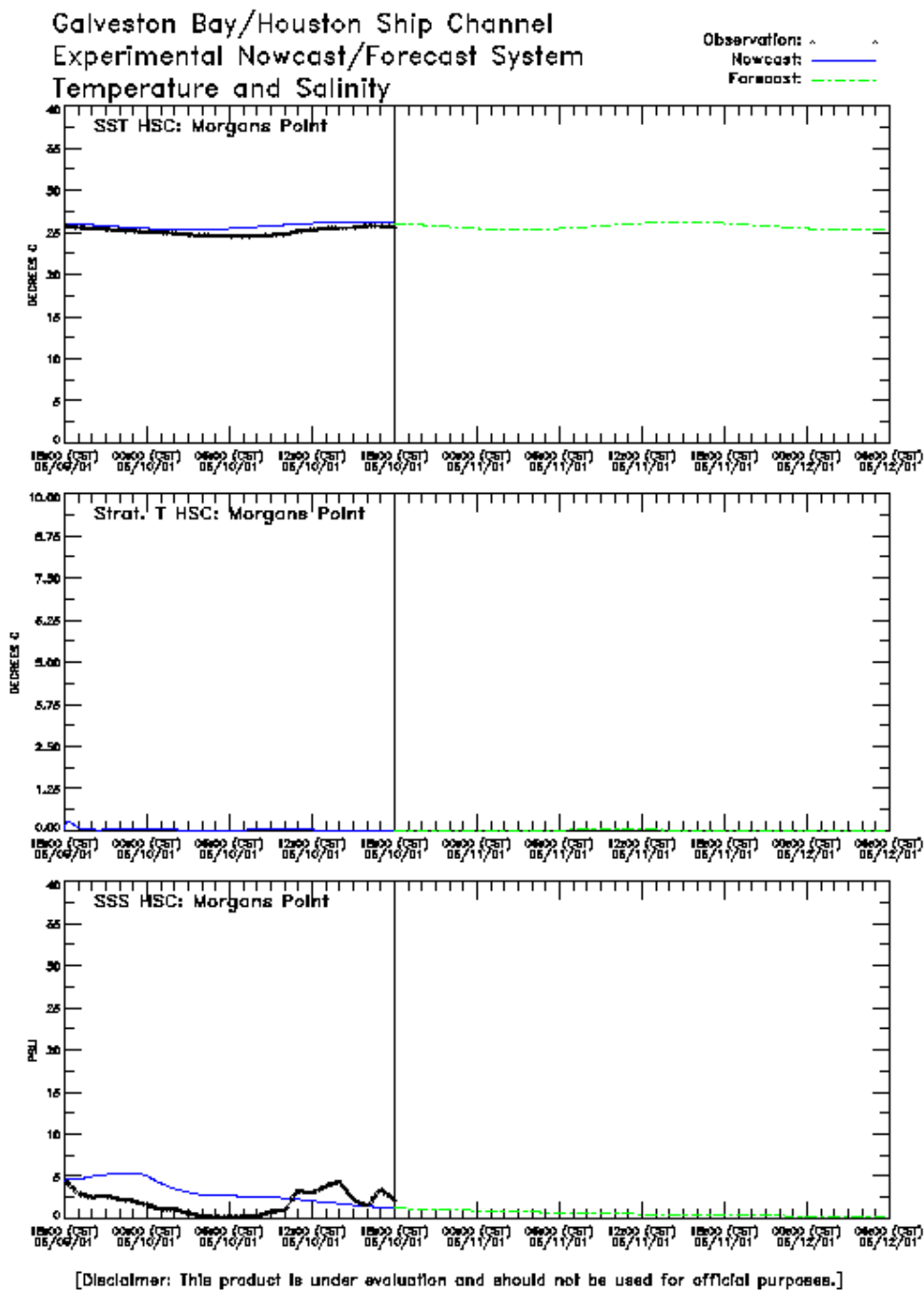


Figure 8.47. Tropical Storm Allison HSCM Morgans Point Temperature and Salinity Experiment Two: 11 June 2001 Nowcast/Forecast Cycle

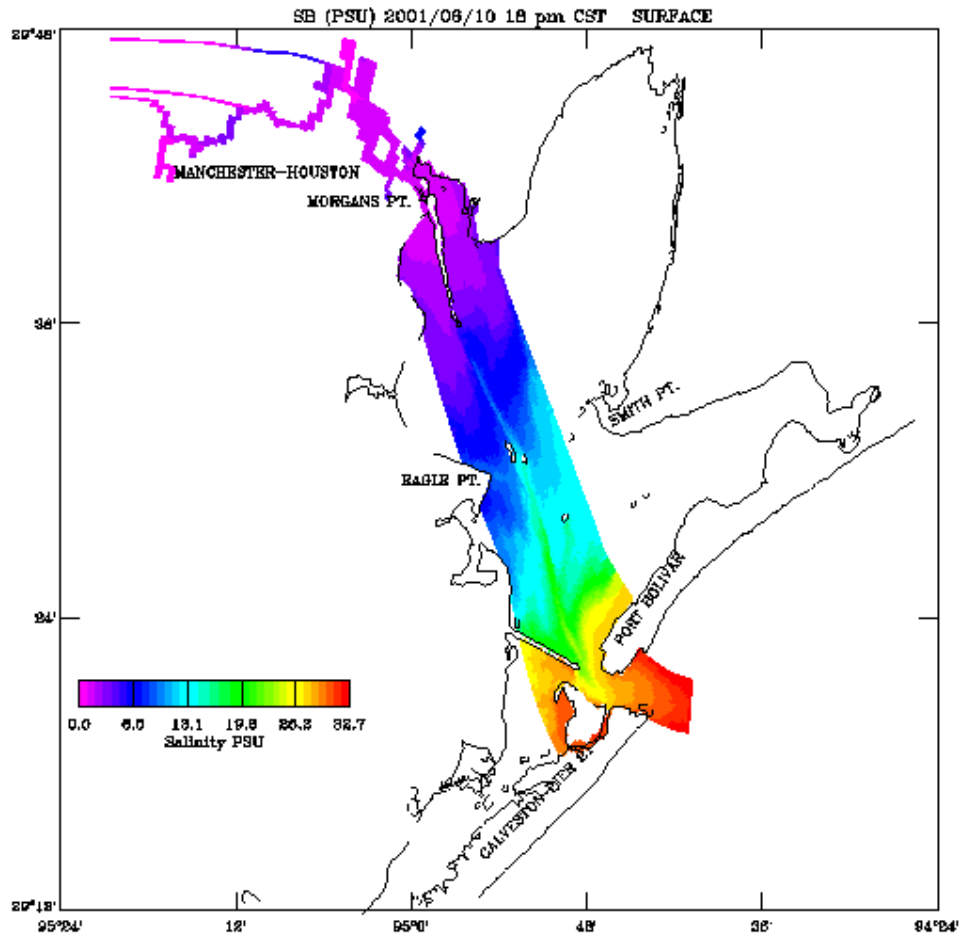


Figure 8.48. Tropical Storm Allison HSCM Near Surface Salinity Field
Experiment Two: 10 June 2001 Nowcast End

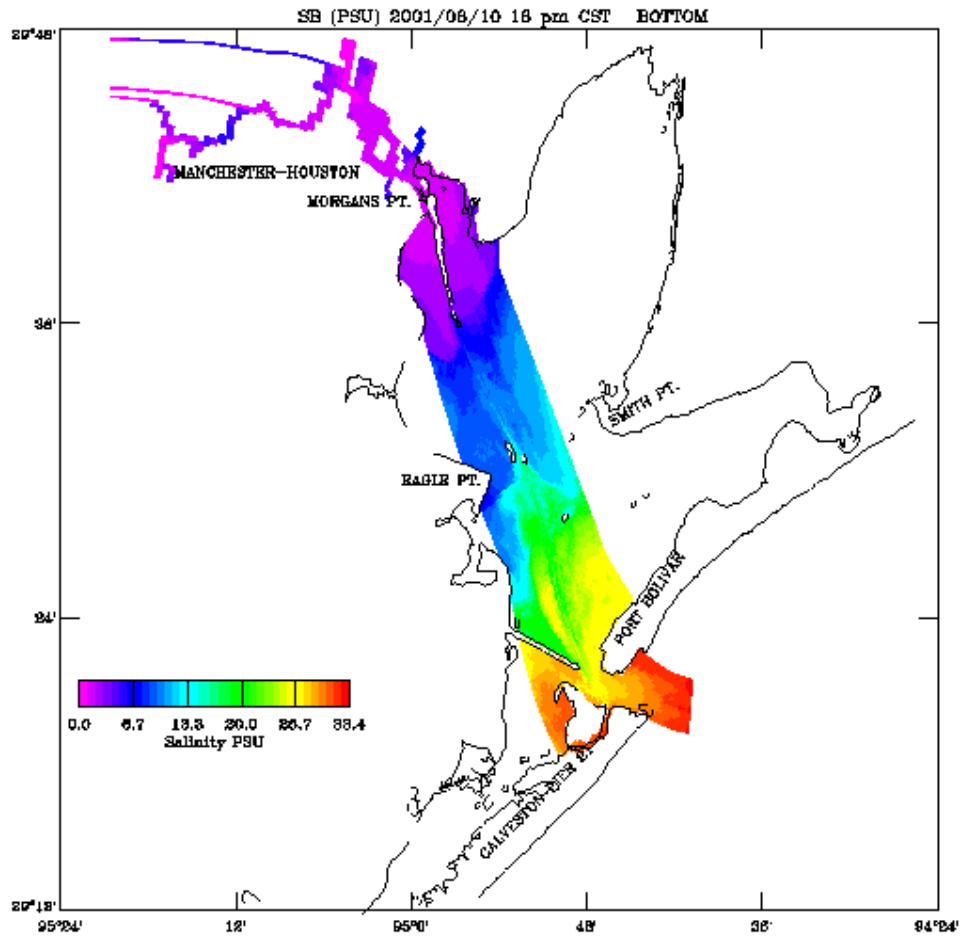
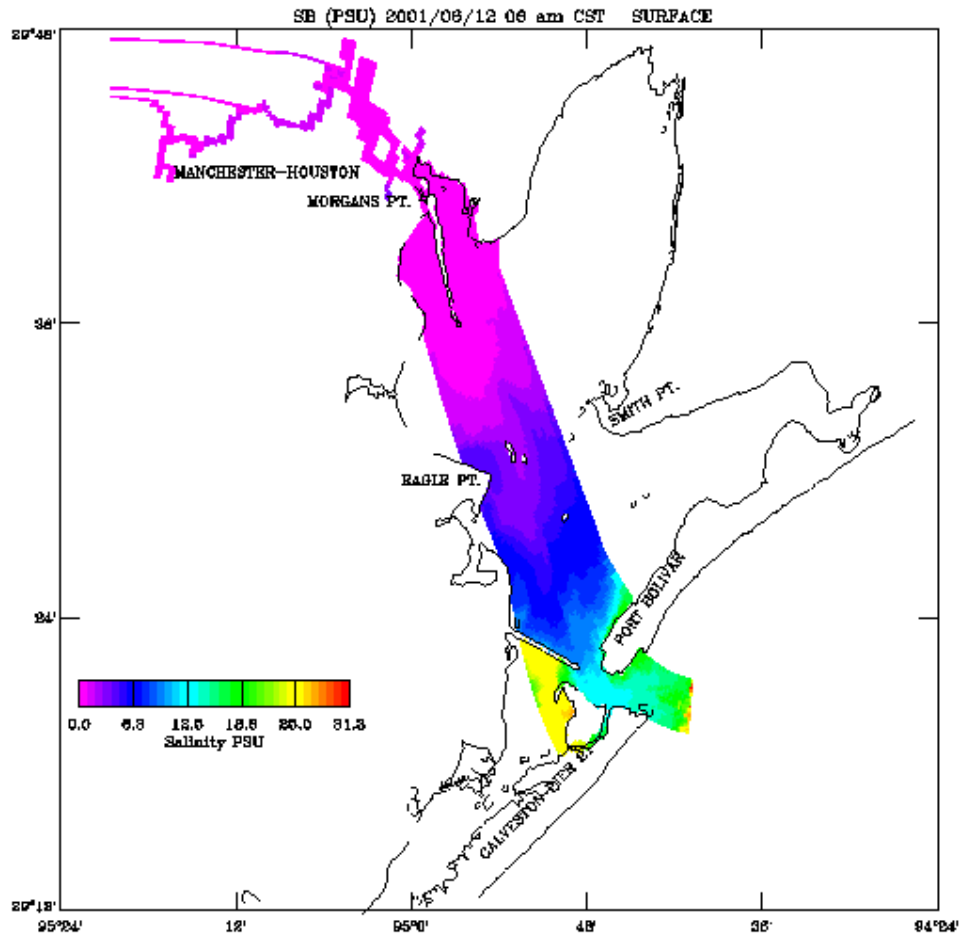


Figure 8.49. Tropical Storm Allison HSCM Near Bottom Salinity Field
Experiment Two: 10 June 2001 Nowcast End



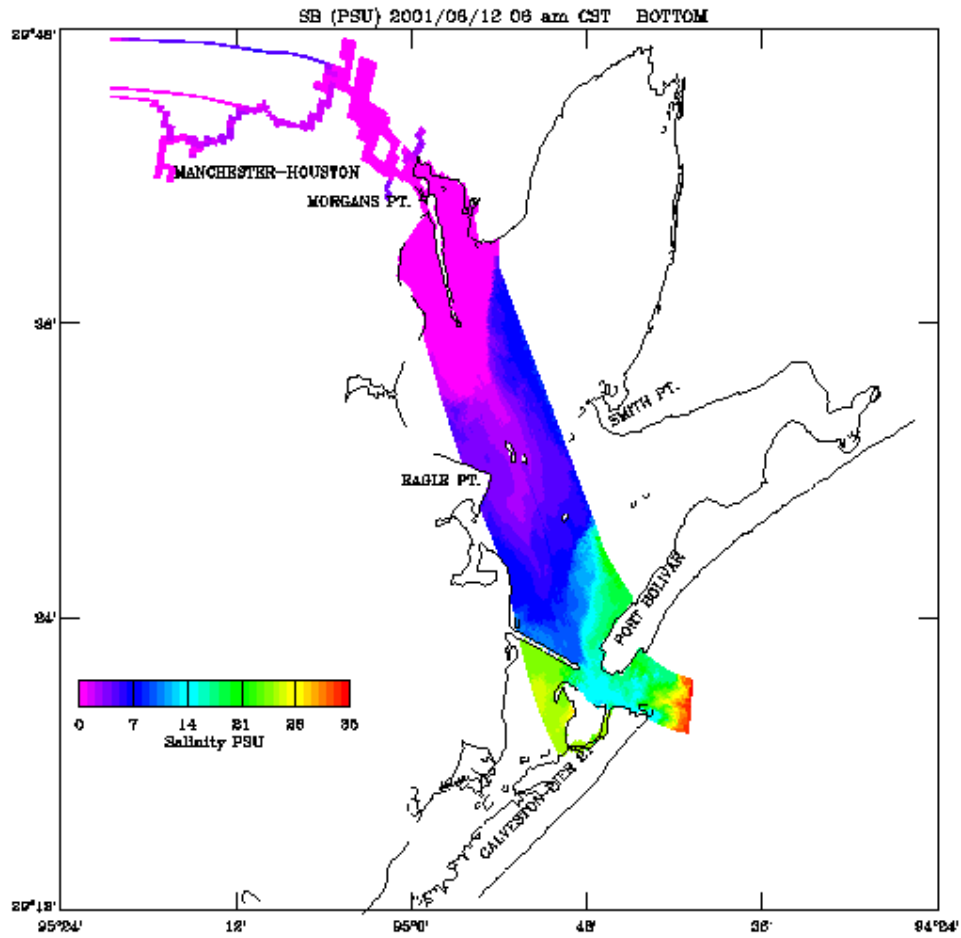


Figure 8.51. Tropical Storm Allison GBM Near Bottom Salinity Field
Experiment Two: 11 June 2001 Forecast End

8.9. Rainfall/Runoff Event Short Wave Results

Unfortunately, no wave information was available within the Bay for comparison. NDBC 42035 buoy data were used to specify the offshore boundary wave condition during both nowcast and forecast, since the forecasts were run after the fact. Results are given for experiment one, since the results for experiment two are nearly identical.

Maximum simulated wave heights are of order 1.0 m at Galveston Pleasure Pier, 0.75m at Bolivar Roads, and 0.5 m at Galveston Pier 21. HSCM simulated significant wave heights at Eagle Point and Morgans Point are order 0.5 m. The simulated significant wave height at NDBC buoy 42035, which represents the GBM open boundary wave condition, exceeds 1.75 m.

GBM simulated significant wave periods for each of the nowcast/forecast cycles at Galveston Pleasure Pier, Bolivar Roads, and Galveston Pier 21 are order 4s. HSCM simulated significant wave periods at Eagle Point and Morgans Point are order 2s. The simulated significant wave period ranges from 5 to 7s at NDBC buoy 42035, which represents the GBM open boundary wave condition. Note in this experiment with wind generation, the significant wave direction is equal to the wind direction, which ranges from 135 to 315 deg T.

9. OPERATIONAL CONSIDERATIONS

Prior to implementation in the operational setting, it would be advantageous to implement the surface wave and all-weather algorithms in a quasi-operational setting with the NOS Galveston Bay Experimental Nowcast/Forecast System. Approaches towards achieving this goal are outlined.

The most immediate step would be to implement the surface gravity wave algorithms within the present experimental nowcast/forecast system. What is needed are the linkages from ODAAS for the wavewatch 3 wave model forecasts at Galveston Pleasure Pier and the real-time acquisition of NBDC 42035 buoy wave and wind conditions. The present CSDL website would then be updated to provide the wave products, which have been demonstrated in this work; e.g., time series of significant wave height, direction, and period as well as field plots of wave height and direction.

An all-weather capability has been demonstrated here and should be implemented in the experimental system to further gain insight on computational requirements. When a storm is predicted to influence the Galveston region, a storm track file is created defining the storm path and intensity. If the track file is present, the system operates in the all-weather mode. Note rainfall predictions are also necessary over the four major drainage areas within the City of Houston. Based on storm intensity it would be necessary to potentially modify hydrodynamic model time steps and the computational burdens would be accordingly increased. Some indication of these requirements is discernable in Tables 9.1-9.4, which present the computational requirements for the simulations reported.

Table 9.1. Hurricane Carla (1961) Long and Short Wave Computational Time. Note the computations were performed on a 4 CPU SGI Origin 3000. Note the two entries are for experiment one and two, respectively.

	GBM Real Time (min:sec)	HSCM Real Time (hr:min:sec)
Time Steps (External, Internal)	(5s,30s)	(0.5s,3s)
9/11 24 hr Hindcast	7:51.9 7:54.2	1:14:15.0 1:17:50.1
9/12 24 hr Hindcast	9:05.5 9:14.5	1:19:40.0 1:17:13.9
9/13 24 hr Hindcast	7:52.8 7:56.9	1:16:41.4 1:16:19.1

Table 9.2. Hurricane Alicia (1983) Long and Short Wave Computational Time. Note the computations were performed on a 4 CPU SGI Origin 3000. Note the two entries are for experiment one and two, respectively.

	GBM Real Time (min:sec)	HSCM Real Time (hr:min:sec)
Time Steps (External, Internal)	(5s,30s)	(0.5s,3s)
8/18 24 hr Hindcast	7:48.9 8:00.1	1:18:28.5 1:14:25.7
8/19 24 hr Hindcast	7:51.9 8:01.0	1:15:46.6 1:36:39.8

Table 9.3. Tropical Storm Allison (2001) Coastal Surge Propagation Event Long and Short Wave Computational Time. Note the computations were performed on a 4 CPU SGI Origin 3000. Note no experiment two was performed.

	GBM Real Time (min:sec)	HSCM Real Time (hr:min:sec)
Time Steps (External, Internal)	(10s,60s)	(2s,10s)
6/5 24 hr Hindcast/36 hr Forecast	9:51.1	1:00:26.6
6/6 24 hr Hindcast/36 hr Forecast	11:25.5	1:03:1.0

Table 9.4. Tropical Storm Allison (2001) Rainfall/Runoff Event Long and Short Wave Computational Time. Note the computations were performed on a 4 CPU SGI Origin 3000. Note the two entries are for experiment one and two, respectively. Note the third entry was used to achieve stability in the additional inflow case of experiment two.

	GBM Real Time (min:sec)		HSCM Real Time (hr:min:sec)		
Time Steps (External, Internal)	(10s,60s)	(5s,30s)	(2s,10s)	(0.5s,3s)	(0.2s,1s)
6/10 24 hr Hindcast/36 hr Forecast	9:46.9	19:44.4	1:03:45.1	3:18:55.6	-
6/11 24 hr Hindcast/36 hr Forecast	9:54.4	21:19.7	1:05:05.0	3:13:37.5	8:45:53.1

Note the computational requirements of each model for different time steps are given. While the computational times for the GBM are modest, the HSCM computational requirements for the high flow case are intensive.

For the present grids, an accurate prediction of coastal storm surge is required as the offshore boundary condition and this must be supplied from either NWS/ETSS or another basin scale model. It is possible to further explore the extension of the GBM to deeper waters and allow a direct computation of the storm surge over the extended grid. This would suggest a separate model grid for storm surge which would be run on a nowcast/forecast system basis by the National Hurricane Center (NHC). CO-OPS would provide the NHC with the latest nowcast/forecast cycle restart prior to the storm track input and the NHC would use the system to provide additional model guidance. The impacts on wetlands and the ecological response to the storm could be studied to allow for enhanced wetland and estuarine resource planning.

10. CONCLUSIONS AND FUTURE WORK

The algorithms developed for rainfall/runoff, overland flooding, surface gravity waves, and for the hurricane wind and atmospheric pressure fields, have been adopted within the NOS Galveston Bay Experimental Nowcast/Forecast System. Their effectiveness in replicating the storm surge has been demonstrated for Hurricanes Carla (1961) and Alicia (1983), and Tropical Storm Allison (2001). The effectiveness of a modular nested grid approach; e.g., the GBM to the HSCM one-way coupling has been demonstrated.

To further improve results during high flow events, hourly discharges should be used. Additional combined sewer overflows and municipal treatment plant flows should also be specified. While the effects of runoff from the Houston metroplex have been considered, the properties of the other drainage areas surrounding Galveston Bay need further consideration. In particular, marsh hydrodynamics should be considered. Within the present simulations, drainage and seepage of flooded areas is not considered. These might be used as inputs to marsh hydrodynamic simulations. More work on the wave-current interaction effects needs to be considered. The issues of sediment transport and morphological change prediction should also be considered. In this instance, it will be necessary to consider moveable bed hydrodynamics.

To further validate the algorithms developed additional field data are required. Detailed inundation mapping based on overflights of the flooded areas needs to be performed for each major hurricane. Post event high water marks are not sufficient. Improvements in wind and water level instrumentation to withstand hurricane conditions would enable additional validation data to be collected. Salinity, turbidity, and chlorophyll-a fields need to be measured on a daily basis over the next month following storm passage to assess storm ecological impacts.

ACKNOWLEDGMENTS

The storm surge model work has been carried out in the Coast Survey Development Laboratory (CSDL) of NOS's Office of Coast Survey with the encouragement from the Chief of CSDL's Marine Modeling and Analysis Programs, Dr. Frank Aikman. Dr. Frank Aikman also provided further information on the Coastal Storms Initiative. Philip H. Richardson assisted in a review of recent storm surge modeling and the application of the wave algorithms to the January 25-30, 1997 period.

REFERENCES

Appell, G. F., T. N. Mero, T. D. Bethem, and G. W. French, 1994. The development of a real-time port information system, *IEEE, Journal of Oceanic Engineering*, 19,149-157.

Blumberg, A. F., and G. L. Mellor, 1987. A description of a three-dimensional coastal ocean circulation model. *Three-Dimensional Coastal Ocean Models*, (ed. Heaps), American Geophysical Union, Washington, DC., 1 - 16.

Blumberg, A. F., and H.J. Herring, 1987. Circulation modeling using orthogonal curvilinear coordinates, in *Three-Dimensional Models of Marine and Estuarine Dynamics*, (ed. Nihoul and Jamart), Elsevier Oceanography Series, 45, 55-88.

Case, R.A. and H.P. Gerrish, 1984. Atlantic hurricane season of 1983, *Monthly Weather Review*, Vol. 112, 1083-1092.

Coastal Engineering Technical Note, CETN-I-6, 1981. Revised method for wave forecasting in shallow water, Coastal Engineering Research Center, Vicksburg, MS.

Collins, J.I. and Viehman, M.J., 1971. A simplified empirical model for hurricane wind fields, Offshore Technology Conference, Vol 1, Preprints, Houston, TX.

Cooperman, A.I. and H.C. Sumner, 1961. North Atlantic tropical cyclones, September 1961, *Climatological Data, National Summary*, Vol. 12, No. 9, 458-473.

Davies, A.M. and J. Lawrence, 1995. Modeling the effect of wave-current interaction on the three-dimensional wind-driven circulation of the Eastern Irish Sea, *Journal of Physical Oceanography*, 25, 29-45.

Donelan, M.A., 1977. A simple numerical model for wave and wind stress prediction, *Report, National Water Resources Institute*, Burlington, Ontario.

Drennan, W.M, H.C. Graber, D. Hauser, and C. Quentin, 2003. On the wave age dependence of wind stress over pure wind seas, *Journal of Geophysical Research*, 108, 8062.

Dunn, G.E. and staff, 1962. The hurricane season of 1961, *Monthly Weather Review*, Vol. 134, 107-119.

Graham, H.E. and Nunn, D.E., 1959. Meteorological considerations pertinent to the Standard Project Hurricane, Atlantic and Gulf Coasts of the United States, *NHRP No. 33*, National Weather Service, Silver Spring, MD.

Grant, W.D and O.S. Madsen, 1979. Combined wave and current interaction with a rough bottom, *Journal of Geophysical Research*, 84, 1797-1808.

Grant, W.D. and O.S. Madsen, 1982. Movable bed roughness in unsteady oscillatory flow, *Journal of Geophysical Research*, 87, 469-481.

Holland, G.J., 1980. An analytic model of the wind and pressure profiles in hurricanes, *Monthly Weather Review*, Vol 108, 1212-1218.

Johnson, H.K., and H.J. Vested, 1992. Effects of water waves on wind shear stress for current modeling, *Journal of Atmospheric and Oceanic Technology*, 9, 850-861.

Large, W.G. and Pond, S., 1981. Open ocean momentum flux measurements in moderate to strong winds, *Journal of Physical Oceanography*, 11, 324-336.

Linsley, R.K, M. A. Kohler, and J.L.H. Paulhus., 1982. *Hydrology for engineers*, New York, McGraw Hill.

Liscum, F., 2001. Effects of urban development on stormwater runoff characteristics for the Houston, Texas metropolitan area, *USGS, Water-Resources Investigations 01-4071*, Austin, TX.

Mastenbroek, C., G. Burgers, and P.A.E.M. Janssen, 1992. The dynamic coupling of a wave model and a storm surge model through the atmospheric boundary layer, *Journal of Physical Oceanography*, 23, 1856-1866.

Mellor, G.L., 2003a. The three-dimensional, current and surface wave equation, *Journal of Physical Oceanography*, 33, 1978-1989.

Mellor, G.L, 2003b. Users guide for a three-dimensional, primitive equation, numerical ocean model, *Progr Atmos and Ocean Sci*, Princeton University. (Available at www.aos.princeton.edu/WWWPUBLIC/htdocs.pom/publications.htm)

Mellor, G. L., 2005. Some consequences of the three-dimensional current and surface wave equations, *Journal of Physical. Oceanography*, 35, 2291-2298.

Mellor, G. L. and M. A. Donelan, 2006. A surface wave model for coupling with numerical ocean circulation models, submitted.

Monahan E. C., 2002. Oceanic whitecaps: Sea surface features detectable via satellite that are indicators of the magnitude of the air-sea gas transfer coefficient, *Proceedings Indian Academy of Sciences, Earth and Planetary Science*, 111, No 3, 315-319.

NOAA, 2002. Coastal Storms Initiative, Coastal Science Center, Charleston, SC. (Available at www.csc.noaa.gov/csi)

NOS, 1999. NOS procedures for developing and implementing operational nowcast and forecast systems for PORTS, *NOAA Technical Report NOS CO-OPS 0020*, Silver Spring, MD.

NWS, 2001. Service Assessment Tropical Storm Allison Heavy Rains and Floods Texas and Louisiana June 2001, National Weather Service, Silver Spring, MD

Project CW-167, 1955. Waves and wind tides in shallow lakes and reservoirs: summary report, U.S. Army Corps of Engineers, Jacksonville, FL.

Richardson, P. H. and R. A. Schmalz, 2002a. Water Level Event Analysis: Program Documentation, *CSDL Informal Technical Note 1*, Silver Spring, MD.

Richardson, P. H. and R. A. Schmalz, 2002b. Principal Component Direction Event Analysis: Program Documentation, *CSDL Informal Technical Note 2*, Silver Spring, MD.

Schmalz, R. A., 1986a. A numerical investigation of hurricane induced water level fluctuations in Lake Okeechobee, Report 1: Forecasting and Design, *Miscellaneous Paper CERC-86-12*, Coastal Engineering Research Center, Vicksburg, MS.

Schmalz, R. A., 1986b. A numerical investigation of hurricane induced water level fluctuations in Lake Okeechobee, Report 1: Forecasting and Design Appendices, *Miscellaneous Paper CERC-86-12*, Coastal Engineering Research Center, Vicksburg, MS.

Schmalz, R. A., 1986c. A numerical investigation of hurricane induced water level fluctuations in Lake Okeechobee, Report 2: Joint Probability Theoretics and Application, *Miscellaneous Paper CERC-86-12*, Coastal Engineering Research Center, Vicksburg, MS.

Schmalz, R.A., 1996. National Ocean Service Partnership: DGPS-supported hydrosurvey, water level measurement, and modeling of Galveston Bay: development and application of the numerical circulation model. NOAA, National Ocean Service, Office of Ocean and Earth Sciences, *NOAA Technical Report NOS OES 012*, Silver Spring, MD.

Schmalz, R.A., 1998a. Development of a Nowcast/Forecast System for Galveston Bay, *Proceedings of the 5th Estuarine and Coastal Modeling Conference*, ASCE, Alexandria, VA, 441-455.

Schmalz, R.A., 1998b. Design of a Nowcast/Forecast System for Galveston Bay, *Proceedings of the 2nd Conference on Coastal Atmospheric and Oceanic Prediction and Process*, AMS, Phoenix, AZ, 15-22.

Schmalz, R.A., 1998c. Initial Evaluation of a Nowcast/Forecast System for Galveston Bay during September 1997, *Proceedings of the Ocean Community Conference*, MTS, Baltimore, MD, 426-430.

Schmalz, R.A., 2000a. A Nowcast/Forecast System for Galveston Bay, *Proceedings of the 2000 Joint Conference on Water Resources Engineering and Water Resources Planning and Management*, ASCE, General Conference, Flood Hazard Modeling Applications, CDROM.

Schmalz, R.A., 2000b. Demonstration of a Nowcast/Forecast System for Galveston Bay, *Proceedings of the 6th Estuarine and Coastal Modeling Conference*, ASCE, New Orleans, LA, 868-883.

Schmalz, R.A., 2000c. High-Resolution Houston Ship Channel ADCP and CTD Survey: Model-Data Intercomparisons, *NOAA Technical Report NOS CS 6*, Silver Spring, MD.

Schmalz, R.A., 2001. Three-Dimensional Hydrodynamic Model Developments for a Galveston Bay Nowcast/Forecast System, *NOAA Technical Report NOS CS 9*, Silver Spring, MD.

Schmalz, R.A., 2003. Development of a Real Time Wave Model for Galveston Bay, *Proceedings of the World Water & Environmental Resources Congress*, ASCE, Philadelphia, PA, CDROM.

Schmalz, R.A., 2004. Development of the NOS Galveston Bay Operational Nowcast/Forecast System, *Proceedings of the 7th International Marine Environmental Modelling Seminar*, Washington, DC.

Schmalz, R.A. and P. H. Richardson, 2002. Evaluation of the NOS Experimental Nowcast/Forecast System for a Galveston Bay, *NOAA Technical Report NOS CS 14*, Silver Spring, MD.

Schwab, D. R., J.R. Bennett, P.C. Liu, and M.A. Donelan, 1984. Application of a Simple Numerical Wave Prediction Model to Lake Erie, *Journal of Geophysical Research*, Vol. 89, C3, 3586-3592.

Schwerdt, R. et al., 1979. Criteria for Standard Project Hurricane and probable maximum hurricane wind field, Gulf and East Coast United States, *NOAA Technical Report NWS-23*, Silver Spring, MD.

Signell, R.P., R.C. Beardsley, H.C. Graber, and A. Capotondi, 1990. Effect of wave-current interaction on wind-driven circulation in narrow, shallow embayments. *Journal of Geophysical Research*, 95, 9671-9678.

Sinha, J. and G.S. Mandal, 1999. An analytical model of over-land surface windfield in cyclone for the Indian coastal region, National Seminar on Wind Engineering-01, IIT, Kharagpur.

Smith, S.D. 1980. Wind stress and heat flux over the ocean in gale force winds, *Journal of Physical Oceanography*, 10, 709-726.

Stewart, S.R., 2002. Tropical Storm Allison, 5-17 June 2001, National Hurricane Center Tropical Storm Report, (<http://www.nhc.noaa.gov/2001/allison.html>), Miami, FL.

Stewart, S. R., 2003. Personal email to Richard.Schmalz@noaa.gov, March 20th, NOS, NOAA, Silver Spring, MD.

Stewart, S. R., 2002. Tropical Storm Allison, 5-17 June 2001, *Tropical Cyclone Report*, NHC, NOAA, Miami, FL.

Tetra Tech, Inc., 1979. Coastal Flooding Storm Surge Model Part I: Methodology, Part II: Codes and User's Guide, Federal Emergency Management Agency, Washington, DC.